INSTITUTO DE HIGIENE E
MEDICINA TROPICAL
DESDE 1902

Universidade Nova de Lisboa

Instituto de Higiene e Medicina Tropical

TickProVac: An insight into the *Rhipicephalus sanguineus* tick salivary gland proteome during *Ehrlichia canis* infection towards vaccine development

Joana Isabel Figueira Ferrolho Gibson

DISSERTAÇÃO PARA A OBTENÇÃO DO GRAU DE DOUTOR EM CIÊNCIAS BIOMÉDICAS

ESPECIALIDADE EM PARASITOLOGIA

(MARÇO, 2023)

Universidade Nova de Lisboa

Instituto de Higiene e Medicina Tropical

TickProVac: An insight into the *Rhipicephalus sanguineus* tick salivary gland proteome during *Ehrlichia canis* infection towards vaccine development

Autor: Joana Isabel Figueira Ferrolho Gibson

Orientador: Doutora Ana Domingos

Coorientadores: Professor Doutor José de La Fuente

Professor Doutor Gervásio Bechara

Dissertação apresentada para cumprimento dos requisitos necessários à obtenção do grau de Doutor em Ciências Biomédicas – Especialidade em Parasitologia

Estudo financiado pela Fundação para a Ciência e Tecnologia (FCT) com a Referência **SFRH/122894/2016**

Declaration

I declare that this thesis has been composed by myself and all the work included in this thesis is my own except where otherwise stated. No part of this work has been or will be submitted for any other degree or professional qualification.

Joana Ferrolho Gibson

2022

Published Articles

Ferrolho J., Antunes S., Sanches G., Couto J., Évora P., Rosa C., André M., Machado R., Bechara G., Domingos A. **"*Ferritin 1* silencing effect in *Rhipicephalus sanguineus sensu lato* (Acari: Ixodidae) during experimental infection with *Ehrlichia canis*."** in Ticks and Tick-borne Diseases, 8 (1): 174-184, 2017.
doi: 10.1016/j.ttbdis.2016.10.015.

Oral Communications

Ferrolho J., Bechara G., Antunes S., Domingos A. **"Genómica funcional em interações entre *Rhipicephalus sanguineus* e *Ehrlichia canis* para o desenvolvimento de vacinas."** presented at the V Jornadas Científicas do Instituto de Higiene e Medicina Tropical – Universidade Nova de Lisboa (IHMT-UNL); Lisbon, Portugal (2014).

Bell-Sakyi L., **Ferrolho J.** and Zweygarth E. **"*Ehrlichia canis* grows in some, but not all cell lines derived from vector and non-vector tick species."** presented at the 12th Biennial Conference of the Society for Tropical Veterinary Medicine (STVM) and the VIII International Conference on Ticks and Tick-borne Pathogens (TTP-8); Cape Town, South Africa (2014).

Ferrolho J., Bechara G., Antunes S., Domingos A. **"Genómica funcional em interações entre *Rhipicephalus sanguineus* e *Ehrlichia canis* para o desenvolvimento de vacinas."** presented at the V Jornadas Científicas do Instituto de Higiene e Medicina Tropical – Universidade Nova de Lisboa (IHMT-UNL); Lisbon, Portugal (2014).

Ferrolho J., Antunes S., Sanches G., Couto J., Évora P., Rosa C., André M., Machado R., Bechara G., Domingos A. **"Avaliação do efeito do silenciamento do gene *ferritina 1* na alimentação, no desenvolvimento dos ovários e na oogénese da carraça *Rhipicephalus sanguineus* durante a infeção experimental por *Ehrlichia canis*"** presented at the II Workshop NOVA/INSA de Doenças Transmitidas por Vetores at Instituto de Higiene e Medicina Tropical (IHMT); Lisbon, Portugal (2016).

Ferrolho J., Antunes S., Sanches G., Couto J., Évora P., Rosa C., André M., Machado R., Bechara G., Domingos A. **"*Ferritin* and *64P* gene silencing in *Rhipicephalus sanguineus* ticks infected with *Ehrlichia canis*"** presented at the First Joint International Conference of the Association of Institutions for Tropical Veterinary Medicine (AITVM) and the Society of Tropical Veterinary Medicine (STVM); Berlin, Germany (2016).

Ferrolho J., Antunes S., Sanches G., Couto J., André M., Machado R., Bechara G., de La Fuente J., Domingos A. **"Estudos de genómica funcional na carraça *Rhipicephalus sanguineus* durante a infeção experimental por *Ehrlichia canis* para o desenvolvimento de vacinas."** presented at the VIII Jornadas Científicas do Instituto de Higiene e Medicina Tropical – Universidade Nova de Lisboa (IHMT-UNL); Lisbon, Portugal (2014).

Ferrolho J., Antunes S., Sanches G., Couto J., de La Fuente J., Bell-Sakyi L., Domingos A. **"Small heat shock protein knockdown affects *Ehrlichia canis* infection and multiplication in cultured tick cells"** presented at the 14th Society for Tropical Veterinary Medicine (STVM) and the 16th Association of Institutions for Tropical Veterinary Medicine – 2nd Joint Conference; Buenos Aires, Argentina (2018).

Dedication

In memory of my mother.

Acknowledgements

The completion of this thesis would not have been possible without the help, assistance and guidance of my main Supervisor, Doctor Ana Domingos and Coosupervisors Professor José de La Fuente and Professor Gervásio Bechara. Therefore, I would like to thank them for giving me the opportunity, advice and support over the past years and for the way that each consultation made me more enthusiastic and willing to finish my studies.

I appreciate the financial support from Fundação para a Ciência e Tecnologia (FCT), Grant number **SFRH/122894/2016.**

I would like to thank my group members Sandra Antunes, Joana Couto, Gustavo Sanches, Filipa Dias and Gonçalo Seixas for their assistance and technical guidance in molecular biology techniques.

I would also like to thank Doctor Lesley Bell-Sakyi, Doctor Marcos André and Professor Rozângela Machado for their hospitality during my stay in Liverpool and Jaboticabal and for all the training provided in *Ehrlichia canis* cultivation and experimental infections.

Finally, thanks to my family and friends, especially to my husband Mark, my children Manuel and Maria, and my parents in law, Isabel and Geoff, for all their support and for forgiving my unavailability.

Resumo

As carraças são reconhecidas como vectores de diversos agentes patogénicos responsáveis por doenças relevantes na medicina humana e animal. Erliquiose monocítica canina (EMC), causada pela bactéria *Ehrlichia canis*, é transmitida pela carraça *Rhipicephalus sanguineus*. O potencial zoonótico da EMC está bem documentado com relatos de infecções humanas em aumento permanente. A infestação por carraças e as doenças por elas transmitidas (DTCs) continuam a representar um sério problema devido à falta de profilaxias eficazes. É, portanto, imperativo adotar novas abordagens, nomeadamente a utilização de vacinas, para a redução de infestações por carraças e DTCs. Actualmente não existe vacina anti-*R. sanguineus* comercialmente disponível. De forma a solucionar esta lacuna, o objetivo principal do presente trabalho foi a caracterização de genes e proteínas que atuam na interface vector-agente patogénico na presença de infeção para compreender os mecanismos associados à transmissão de DTCs. Neste trabalho estão reportados genes e proteínas diferencialmente expressos obtidos a partir da análise transcriptómica e proteómica das glândulas salivares (GSs) de *R. sanguineus* durante a infeção com *E. canis*. Os níveis de expressão dos genes que codificam as proteínas serina carboxipeptidase (*psc*), proteína de choque térmico (*phsrp20*) e proibitina (*prohib*) foram investigados *in vitro* e *in vivo*, em amostras infectadas e não infectadas. Posteriormente, o silenciamento de genes foi realizado através de RNA de interferência (RNAi) para avaliar o efeito da sub-expressão de *ferritina 1* na alimentação, desenvolvimento ovárico, oogénese e aquisição *E. canis* pela carraça. O mesmo foi efetuado para determinar o efeito da sub-expressão de *psc*, *prohib* e *phsrp20* na invasão e multiplicação desta bactéria na linha celular IDE8 e em *R. sanguineus*. O péptido pPHSRP20, relacionado com o choque térmico, foi sintetizado para avaliar a sua imunogenicidade em ratos CD1. Os resultados mostraram que o silenciamento de *ferritina 1* compromete a competência da carraça em se alimentar e provoca alterações morfológicas e histoquímicas nos ovários e oócitos. Os dados transcriptómicos e proteómicos demonstraram que as alterações da expressão génica e proteica estão principalmente relacionadas com processos proteicos celulares e metabólicos e com atividades catalíticas, muito provavelmente um reflexo de alterações de transcrição e tradução em resposta à presença de infecção. Em amostras infectadas verificou-se uma sub-expressão de *phsrp20* e *prohib* em células IDE8 e de *phsrp20* e *psc* nas GSs. Inversamente, os genes *psc* nas células IDE8 e *prohib* nas GSs estavam sobre-expressos. Apesar de se terem atingido níveis elevados de silenciamento, o seu efeito na biologia de *E. canis* não foi determinado devido a limitações moleculares. pPHSRP20 desencadeou uma resposta imunitária detectável e específica nos ratos CD1. Em geral, os resultados demonstraram que a presença de *E. canis* nas GSs desencadeia respostas celulares para regulação do *stress*, inflamação e rearranjo do citoesqueleto. A modulação desta maquinaria molecular pela bactéria poderá ser uma estratégia para lidar e escapar à resposta imunitária e para utilizar proteínas do vector necessárias à virulência. Através destes resultados esperou identificar-se potenciais antigénios de carraça que contribuam para o desenvolvimento de uma vacina anti-*R. sanguineus* e/ou bloqueadora da transmissão de agentes patogénicos.

Palavras-chave: *Rhipicephalus sanguineus*; *Ehrlichia canis*; transcriptoma; proteoma; silenciamento genético.

Abstract

Ticks are recognised as potent vectors of disease-causing pathogens of medical and veterinary importance. *Ehrlichia canis,* the causative agent of canine monocytic ehrlichiosis (CME), is transmitted by the brown dog tick *Rhipicephalus sanguineus* and is acknowledged as a highly infectious disease. The zoonotic potential of CME is widely recognised with reports of human infections steadily increasing. Tick infestation and tick-borne diseases (TBDs) remain a serious and persistent veterinary health problem, due to the lack of efficient control measures. It is therefore vital that novel approaches to tackle TBDs are pursued. Although vaccination to reduce tick infestation is recognised, no anti- *R. sanguineus* vaccine exists. To address this, we aimed to characterise the crucial gene and protein interactions at the vector-pathogen interface to gain a fundamental understanding of the interactions underpinning disease transmission. Here we report differentially expressed genes and proteins found either in the literature or found in our transcriptomic and proteomic data from *R. sanguineus* salivary glands (SGs) during *E. canis* infection. The mRNA expression levels of the *putative serine carboxypeptidase* (*psc*), *heat-shock related protein* (*phsrp20*) and *prohibitin-like protein* genes were investigated *in vitro* and *in vivo*, in infected and uninfected samples. RNA interference (RNAi) was carried out to determine the effect of *ferritin 1* in tick feeding, ovary (OV) development, oogenesis, and pathogen acquisition. We also determined the effect of a downregulation of three selected genes or proteins from our omics data on *E. canis* invasion and multiplication in the IDE8 tick cell line and *R. sanguineus* ticks. We synthesised a heat-shock related protein (pPHSRP20) peptide to evaluate its immunogenicity in CD1 mice. Our results have shown that silencing *ferritin 1* alters tick competence to normally engorge and causes morphological and histochemical changes in the OV and oocytes. Our transcriptomic and proteomic data has revealed alterations in gene and protein expression, mostly concerning protein cellular and metabolic processes and catalytic activities, perhaps related with transcriptional and translational responses to *E. canis* infection. When analysing the transcription levels in *E. canis*-infected samples, a downregulation was verified for *phsrp20* and *prohib* in IDE8 cells and *phsrp20* and *psc* in the SGs, whereas an upregulation was observed for *psc* in IDE8 cells and *prohib* for the SGs. Even with high levels of gene silencing, the effect of gene silencing in *E. canis* biology was not determined due to molecular limitations. pPHSRP20 triggered a detectable and specific immune response in mice. Overall, results show that the presence of *E. canis* in the SGs leads to regulation of stress response, inflammation and cytoskeletal rearrangement molecules. Modulation of tick molecular machinery is a coping strategy to evade the host immune response and to utilise its proteins for infectivity. From this, we expected to identify tick antigens that will direct the development of an anti-*R. sanguineus* and/or transmission-blocking vaccine.

Keywords: *Rhipicephalus sanguineus*; *Ehrlichia canis*; transcriptome; proteome; gene silencing.

Table of Contents

List of Figures

List of Tables

List of Supplementary Tables

Abbreviations

a.a.	amino acid
ACN	acetronile
AGO	argonaute
AP	alkaline phosphatase
APK-C2	cAMP-dependent protein kinase catalytic subunit isoform 2
APP	acute phase proteins
APS	adenosine 5'-phosphosulfate kinase
ARG	Argentina
BLAST	basic local alignment search tool
bp	base pair
BP	biological process
BRS	Rio Grande do Sul state, southern Brazil tick population
BSP	São Paulo state, south-eastern Brazil tick population
CC	cellular component
cDNA	complementary DNA
CEUA	Comissão de Ética no Uso de Animais
CME	canine monocytic ehrlichiosis
CONCEA	Conselho Nacional de Controle da Experimentação Animal
COVID-19	coronavirus disease 2019
cps	counts for second
CRP	C-reactive protein
CRT	capillary repletion time
CW	critical weight
DGAV	Divisão Geral de Alimentação e Veterinária
DH82	canine monocyte-macrophage cell line
DMEM	Dulbecco’s modified Eagle’s medium
DNA	Deoxyribonucleic acid
dsb	disulphide bond formation protein gene

dsDNA	double-stranded DNA
dsRNA	double-stranded RNA
DTC	doenças transmitidas por carraças
DTT	dithiothreitol
ECM	*Ehrlichia canis* medium
ELISA	enzyme-linked immunosorbent assay
EMC	erliquiose monocítica canina
ER	endoplasmic reticulum
EV	extracellular vesicles
FA	formic acid
FBS	fetal bovine serum
FCAV-UNESP	Faculdade de Ciências Agrárias e Veterinárias – Campus de Jaboticabal, Universidade Estadual Paulista
FDR	false discovery rate
Fe^{2+}	ferrous iron
Fe^{3+}	ferric ion
fer 1 or FER 1	ferritin 1 protein gene
fer 2 or FER 2	ferritin 2 protein gene
FER1	intracellular ferritin 1 protein
FER2	secretory ferritin 2 protein
gDNA	genomic DNA
GO	gene ontology
GS	glândulas salivares
GST	glutathione S-transferase protein
gst or GST	glutathione S-transferase protein gene
H&E	haematoxylin and eosin
H_2O_2	hydrogen peroxide
HEPES	4-(2-hydroxyethyl)-1-piperazineethanesulfonic acid
HSP	heat shock protein
HTC	haematocrit
IDA	information-dependent acquisition
IDE8	*Ixodes scapularis* embryo-derived cell line

IEDB	immune epitope database and analysis resource
IFAT	indirect fluorescent antibody test
Ig	immunoglobulin
IgA	immunoglobulin A
IgG	immunoglobulin G
IgM	immunoglobulin M
IHMT-UNL	Instituto de Higiene e Medicina Tropical - Universidade Nova de Lisboa
imp	importin subunit α protein gene
IMP	importin subunit α protein
IRE	iron-responsive element
IRP	iron regulatory proteins
ISE6	*Ixodes scapularis* cell line
LC	liquid chromatography
LC-MS	liquid chromatography - mass spectrometry
LC-MS/MS	liquid chromatography with tandem mass spectrometry
LNP	lipid nanoparticles
M-value	gene expression stability value
MBP-GFP	maltose-binding periplasmic protein with green fluorescent protein
MDH2	malate dehydrogenase protein
MF	molecular function
MG	midgut
MHC	major histocompatibility complex
MIQE	minimum information for publication of qPCR experiments
mRNA	messenger RNA
MS	mass spectrometry
MTA	material transfer agreement
$NaHCO_3$	sodium bicarbonate
NaOH	sodium hydroxide
NCBI	national centre for biotechnology information

NLS	nuclear localisation signal
OD	optical density
Omp-1	outer membrane protein 1 gene
OspA	outer surface protein A
OV	ovaries
p28	outer membrane multigene 28 protein gene
p30	outer membrane multigene 30 protein gene
PBS	phosphate buffered saline
PBS-T	PBS containing 0.05% (v/v) Tween 20
PCR	polymerase chain reaction
PCV	packed cell volume
phsrp20	gene da proteína de choque térmico or putative heat-shock related protein gene
PHSRP20	putative heat shock-related protein
PLT	platelets
pPHSRP20	synthesised peptide based on the heat-shock related protein
prohib	gene da proibitina or putative prohibitin-like protein gene
PROHIB	putative prohibitin-like protein
psc	gene da serina carboxipeptidase or putative serine carboxypeptidase protein gene
PSC	putative serine carboxypeptidase protein
qPCR	quantitative real-time PCR
RBC	red blood cells
rGST-Hl	*Haemaphysalis longicornis* recombinant GST
RISC	RNA-induced silencing complex
RNA	ribonucleic acid
RNA-seq	RNA-sequencing
RNAi	RNA de interferência or RNA interference
ROS	reactive oxygen species
RSE8	*Rhipicephalus sanguineus* cell line

RT	room temperature
RTr	reverse transcription
s.l.	*sensu lato*
s.s.	*sensu stricto*
SAA	serum amyloid A
SARS CoV-2	severe acute respiratory syndrome coronavirus 2
SAT	saliva-activated transmission
SDS	sodium dodecyl sulphate
SDS-PAGE	sodium dodecyl sulphate–polyacrylamide gel electrophoresis
SEM	standard error of the mean
SG	salivary glands
siRNA	small interfering RNA
SPI	serine protease inhibitor
SRA	sequence read archives
ssDNA	single-stranded DNA
SWATH™-MS	sequential window acquisition of all theoretical mass spectra
TAE	tris-acetate-EDTA
TBD	tick-borne diseases
TBP	tick-borne pathogens
TBS-T	tris-buffered saline with 0.05% (v/v) Tween 20
TEMED	tetramethylethylenediamine
TFSS	type IV secretion system
TIM	translocases of the inner membrane proteins
TIM	inner membrane translocases
T_m	Melting temperature
TNF-α	tumour necrosis factor-α
TPB	tryptose phosphate broth
Treg	regulatory T cells
TROSPA	tick receptor for outer surface protein A
UCH	ubiquitin carboxyl-terminal hydrolase protein

uch	ubiquitin carboxyl-terminal hydrolase protein gene
UK	United Kingdom
URU	Uruguay
USA	United States of America
UTR	untranslated region
Vg	vitellogenin
Vn	vitellin
WBC	white blood cells
X^2	chi-square
XIC	extracted-ion chromatogram
β2m	β-2-microglobulin protein gene
β2m	β-2-microglobulin protein

Chapter 1: Introduction

Over the past decade, tick-borne diseases (TBDs) caused by Ehrlichiae have garnered increasing attention from the veterinary, medical, and biological fields (1). The importance of ticks (Arachnida: Ixodida) as vectors of human and animal infectious diseases makes them second only to mosquitoes (Insecta: Diptera) in this regard and tick-borne ehrlichial diseases are important emerging infections with a global prevalence (2, 3).

Canine monocytic ehrlichiosis (CME) is a potentially fatal tick-borne infectious disease transmitted by the brown dog tick *Rhipicephalus sanguineus*. The etiological agent is the obligate intracellular rickettsia *Ehrlichia canis* that invades and develops in canine monocytes, eventually leading to death (2). In addition to CME, *R. sanguineus* is also known to act as the vector of several other infectious diseases, underlining its efficiency at transmitting disease (4).

Human ehrlichiosis is a newly recognised disease and human infection with *E. canis* has been reported with increasing frequency since its discovery in 1987 (5-9). This suggests its zoonotic potential is either greatly underappreciated or steadily increasing. Such reports combined with changing environmental conditions and the increasing distribution of several tick species, firmly aligns the control of CME with the aim of the "One Health" concept that emphasises the importance of improving healthcare for humans, animals and the environment.

Current methods of controlling ticks and TBDs rely heavily on chemical acaricides; however, their continued use is unsustainable due to widespread cross-species resistance and growing environmental concerns (10, 11). Alternative cost-effective and environmental-friendly control measures such as anti-tick vaccines are urgently needed. The use of vaccines poses minimal risk of selecting acaricide-resistant ticks, since point mutations that render acaricides ineffective are less likely to alter epitopes on target proteins (12, 13). Although several attempts have been made towards developing anti-tick vaccines, no commercial anti-*R. sanguineus* vaccine exists. We, therefore, intend to identify novel immunogenic proteins that will form the basis of a safe and effective

vaccine to control *R. sanguineus*-mediated disease. We will employ cutting edge molecular techniques such as ribonucleic acid (RNA)-sequencing (RNA-seq) and quantitative proteomics (14-18) to select and characterise only the relevant genes and proteins underpinning disease transmission. Once identified, the functional importance of these candidate proteins will be confirmed using RNA interference (RNAi) (19). To date, several anti-tick vaccine development studies have used a transcriptomic and proteomic-based approach (14, 15, 20, 21), however, none has used the model *R. sanguineus- E. canis* we want to investigate.

Despite the potential of tick salivary glands (SGs) proteins to be used as target vaccine antigens, the molecular identity and function of most of these molecules remains unknown. Thus, screening differentially expressed SGs genes and proteins can reveal the dynamic changes occurring at the molecular level during tick infection and pathogen transmission (22). Our working hypothesis is that SGs genes and proteins directly influence disease transmission at the vector-pathogen interface and are differentially expressed in response to pathogen infection. Therefore, our study aims to identify and characterise the crucial host and vector protein interactions at this interface.

With that aim, we have designed four main objectives:

1. Identify the SGs genes and proteins differentially expressed in response to *E. canis* infection conducting transcriptomic and proteomics data analysis. To accomplish this objective *R. sanguineus* ticks were infected with the *E. canis* Jaboticabal strain to obtain biological samples from the SGs.
2. Obtain, after transcriptomic and proteomic data analysis, a catalogue of tick SGs proteins differentially represented during *E. canis* infection, further available online to all the scientific community. The data sets were then used to construct a catalogue of up-, down- or newly expressed genes and proteins during infection.
3. Conduct functional analysis and validation of the genes encoding the differentially represented SGs proteins during infection by RNAi mediated gene silencing. Here double-stranded RNA (dsRNA) corresponding to the selected genes was synthesised to perform messenger RNA (mRNA) disruption of gene expression and confirm their involvement in pathogen infection and transmission by *in vivo* and *in vitro* parameters.

4. Isolation and characterisation of the identified antigens for inclusion in a multi-recombinant antigen vaccine for vaccination trials in the natural host. A selected antigen was synthesised and used to evaluate its immunogenicity in CD1 mice.

Ultimately, our findings will directly contribute to the improvement of current and future control measures aimed at reducing environmental tick populations, host tick infestations and zoonotic TBDs and to generate a broadly applicable model system for other arthropod-borne diseases.

1.1. Canine monocytic ehrlichiosis

1.1.1. Background

CME is a tick-borne infectious disease of dogs, which has the potential to be fatal, but is not contagious. In the past, it has also been referred to as canine rickettsiosis or canine haemorrhagic fever (3, 23). A gram-negative bacterium, the obligate intracellular rickettsia *E. canis* (family Anaplasmataceae, order Rickettsiales), is the aetiological agent (24). It becomes manifested in canine hosts by invading then replicating in monocytes and macrophages. A range of clinical signs have been observed in infected animals, such as depression, fever, leukopenia, thrombocytopaenia, sometimes resulting in death. The brown dog tick, *R. sanguineus*, is the principal vector that transmits the *E. canis* parasite (1, 25, 26). The first recognised incidence of CME occurred in 1935, when veterinarians at the Pasteur Institute (Algeria), described a disease in dogs that causes acute fever and conspicuous anaemia (25). Numerous dogs used by the United States of America (USA) military during the Vietnam War also succumbed to what was later identified as tropical canine pancytopenia, an older name given to CME (27). Reports of the disease also emanated from parts of Africa, the Middle East, and the Orient some years later (23). CME is now a disease prevalent worldwide, responsible for extensive morbidity and mortality in domestic and wild canid populations (26).

1.1.2. Hosts

E. canis predominantly infects dogs as well as other members of the family *Canidae*. From an outbreak in a Florida zoo, significant mortality amongst species of wild canids,

including wolves and wolf-dog crosses, as well as many dogs, occurred in response to *E. canis* infection and CME (28). Coyotes, red foxes and grey foxes were shown to be susceptible to infection after inoculating them with blood from dogs. Furthermore, *R. sanguineus* larvae received an infected blood meal after feeding on a grey fox (29, 30). More recently, *E. canis* has also been detected in a small number of red foxes in Portugal (31). Though less common than in dogs, *E. canis* can also infect cats, leading to feline ehrlichiosis, which was first reported through a natural infection in France in 1986. It has subsequently been recognised worldwide with increasing frequency (32, 33). There are two recognised forms of feline ehrlichiosis, but only one is caused by *E. canis*, and infects mononuclear cells. Immune responses have also been demonstrated to *E. canis*, through seroconversion, in jackals, a raccoon and a puma, but not in capybara, deer or lemurs as reviewed by Stich et al, (2008) (34). Though only a low percentage of raccoons were positive for antibodies reactive to *E. canis* in another study, suggesting they are unlikely to be important in transmission (35).

1.1.3. *Ehrlichia canis* development in the host

E. canis is an obligate intracellular bacterium, small (0.5 – to 1.5 µm) and gram-negative. It has selective tropism for peripheral blood monocytes and macrophages in dogs and other mammalian hosts. It is also deposited in target organs, invading the bone marrow, liver, spleen, and lymph nodes (36-38). The development of *E. canis* in the host remains incompletely understood, though it follows a sequential three step transition of acute, subclinical, and chronic phases after the initial incubation period. When an infected tick is feeding on the host, mononuclear cells are attracted to the inflamed site where a tick is attached. Salivary secretions from the tick may support the development of *E. canis* infection in monocytes by modulating host immunity (26). This is the acute phase of the disease and is characterised by *E. canis* bacteria infecting and multiplying in granular lymphocytes and monocytes. Bacteria reside inside these cells in membrane-bound cytoplasmic vacuoles or modified parasitophorous endosomes known as morulae (36, 39, 40) (Figure 1).

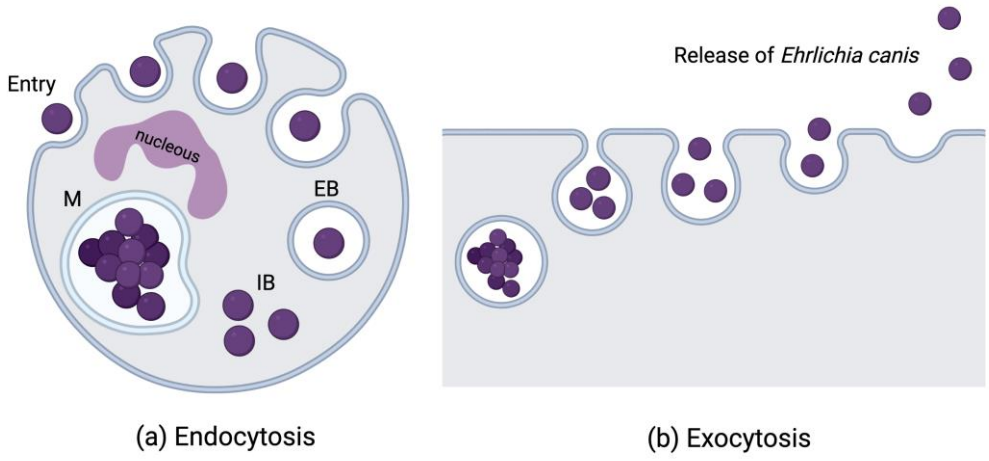

Figure 1. *Ehrlichia canis* life cycle in mononuclear cells.

The host gets infected through the tick bite and, once in the perivascular area, *E. canis* adheres to the membrane of mononuclear cells. Through endocytosis **(a)** enters the cell and forms pleomorphic elementary bodies **(EB)** in phagosomes for 2 or 3 days. Elementary bodies grow and divide by binary fission and exit the phagosome as initial bodies **(IB)**, that in turn continue to multiply and maturate into morulae **(M)**. Bacteria exit the cells by exocytosis **(b),** after morulae rupture, and enter in the host circulation to be phagocytised by other leucocytes (Image created with BioRender.com).

1.1.4. Vectors

Ticks are arthropods (phylum Arthropoda) that have a significant impact on medical and veterinary fields, despite being generally underappreciated. They can cause direct damage to the physiology of the species they feed off, as well as existing as vectors of numerous different pathogens. These include bacteria, protozoa, helminths, and viruses (41, 42). Currently, all of the known *Ehrlichia* species are transmitted by different hard-bodied ticks within the Ixodidae family (34). The principal vector of CME, in both experimental and biological settings, is the brown dog tick *R. sanguineus* (23, 26, 28). It has also been described as the "kennel tick" and was first distinguished taxonomically as *Ixodes sanguineus* in 1806 by Latreille (1, 4, 25, 26). Prior to 1998, there were no reports of experimental transmission of *E. canis* by any ixodid ticks other than *R. sanguineus*. Eight years before this an experiment was attempted to transmit the pathogen with the argasid tick *Otobius megini*, but it was not successful (43). The transstadial transmission of *E.*

canis was eventually demonstrated in the American dog tick *Dermacentor variabilis* (44).

During the past years, the taxonomic classification of *R. sanguineus sensu stricto* (*s.s.*) has been under ongoing debate and some genetic findings strongly suggest the existence of different identities under the same name (45). According to multiple biological parameters, phylogenetic analysis, and reproductive compatibility, at least two distinct populations were reported in the Americas and named as *R. sanguineus sensu lato* (*s.l.*) tropical lineage and *R. sanguineus s.l.* temperate lineage (46-55). Morphologically, the two lineages are very similar (51, 56). Some reports suggest that the absence of established temperate lineage ticks in tropical climates is because adults would become inactive i.e., in diapause, immediately after moulting throughout the year. Likewise, the absence of established tropical lineage ticks in temperate climates is because they would not start diapause to avoid the fatal consequences of adverse winters (54, 57).

The vector competence for *E. canis* was investigated by Moraes-Filho et al. (2015) in larvae and nymphs exposed to infection by feeding on an infected host. After moulting into nymphs and adults, respectively, the *E. canis* polymerase chain reaction (PCR)-positive ticks were allowed to feed on a naïve dog. For this study four populations of ticks were used: São Paulo state, south-eastern Brazil (BSP), Rio Grande do Sul state, southern Brazil (BRS), Argentina (ARG), and Uruguay (URU). Only dogs infested with BSP adult ticks became clinically ill, presented *E. canis* seroconversion and were *E. canis*-PCR positive in the blood. Furthermore, only the population of unfed BSP nymphs and adults were positive for *E. canis* deoxyribonucleic acid (DNA) 30 days after moulting. Accordingly, the BSP population was shown to be a competent vector for this bacterium, contrary to BRS, ARG and URU tick populations (58). Likewise, the presence of *E. canis* infection in the tropical lineage was reported in Argentina (59), tropical areas of Brazil (60, 61), but not in ticks collected from dogs temperate areas of Uruguay (62). The specific reason why the tropical lineage is a competent vector, whereas the temperate lineage is not still unclear. A recent study suggested that *Coxiella* species, part of the tick prokaryotic microbiome composition, may be different in both lineages, influencing the interaction between the vector and the harboured pathogens (63).

In domestic dogs, *R. sanguineus* is a very common ectoparasite i.e. lives on the outside of its host (4); resulting in the distribution of CME being directly proportional to the prevalence of the vector (64). *R. sanguineus* is the most widely distributed tick in the world, being especially prevalent in tropical and subtropical areas (3, 37, 65-68). In regions with a moderate climate, *R. sanguineus* tick activity is increased from late spring to early autumn, however, they are continually active in tropical and subtropical regions (3). As *R. sanguineus* are a monotropic tick, all life cycle stages favour dogs as the principal hosts regardless of geographical area, despite their ability to feed on other domestic and wild and animals (3). Ticks in immature life stages can sometimes be found on various mammals, such as rabbits, cats, rodents, wild canids, and humans, as well as pigeons; however, adults prefer larger mammals (32, 33, 69).

Morphological features of *R. sanguineus* ticks include a small, elongated body free of any ornamentation, which is red brown in colour. They have short palps, which are sensory structures that resemble a pair of legs, and a distinguishing feature known as the *basis capituli*, which is a flat hexagonal surface, where the mouthparts are attached (4). All ixodid ticks, including *R. sanguineus* undergo four developmental stages: egg, larva, nymph, and adult. To complete their development, a blood meal is required at each of the three stages after the egg (70). A different host is required by *R. sanguineus* at each active developmental phase. After feeding on one host, the tick leaves that host to develop and moult and this happens twice: between larval and nymphal, and nymphal and adult stages (4, 71). *R. sanguineus* spend most of their life off-host, but they only mate when on a host (71, 72). When seeking a new host, they exhibit hunter behaviour, and, on occasion, can also outstretch their first pair of legs, which is a positioning known as questing (3). After feeding on a host, which can last for 5 to 21 days, engorged adult females seek out sheltered places like cracks or crevices indoors to lay a large batch of eggs (4, 71). For each female, egg laying represents the end of their life - they lay around 4000 eggs and then die (4, 73). After a gestation period lasting 1 to 3 weeks, the larvae hatch and seek out a host. Larvae take a blood meal over the course of 3 to 10 days, then drop off the host and moult into nymphs. As nymphs, they follow the same cycle again for around 3 days to 2 weeks, before moulting into adults. Male and female adult ticks both feed off

the hosts. The entire life cycle lasts for just over two months when conditions are favourable. Contrary to many other tick species, *R. sanguineus* are endophilic, meaning they are frequently found indoors (4). Life cycle is represented in Figure 2.

In addition to their role in *E. canis* transmission, *R. sanguineus* ticks act as vectors for other pathogens including the etiological agents of canine babesiosis, *Babesia canis* (74) and *Babesia gibsoni* (75); the agent of Q fever *Coxiella burnetii* (76); the agent of canine hepatozoonosis *Hepatozoon canis* (77), *Rickettsia conorii*, which causes Mediterranean spotted fever (78) and the bacterium that causes Rocky Mountain spotted fever, *Rickettsia rickettsii* (79). Visceral leishmaniasis, caused by the transmission of *Leishmania infantum*, may be yet another pathogen for which *R. sanguineus* ticks act as a vector (80).

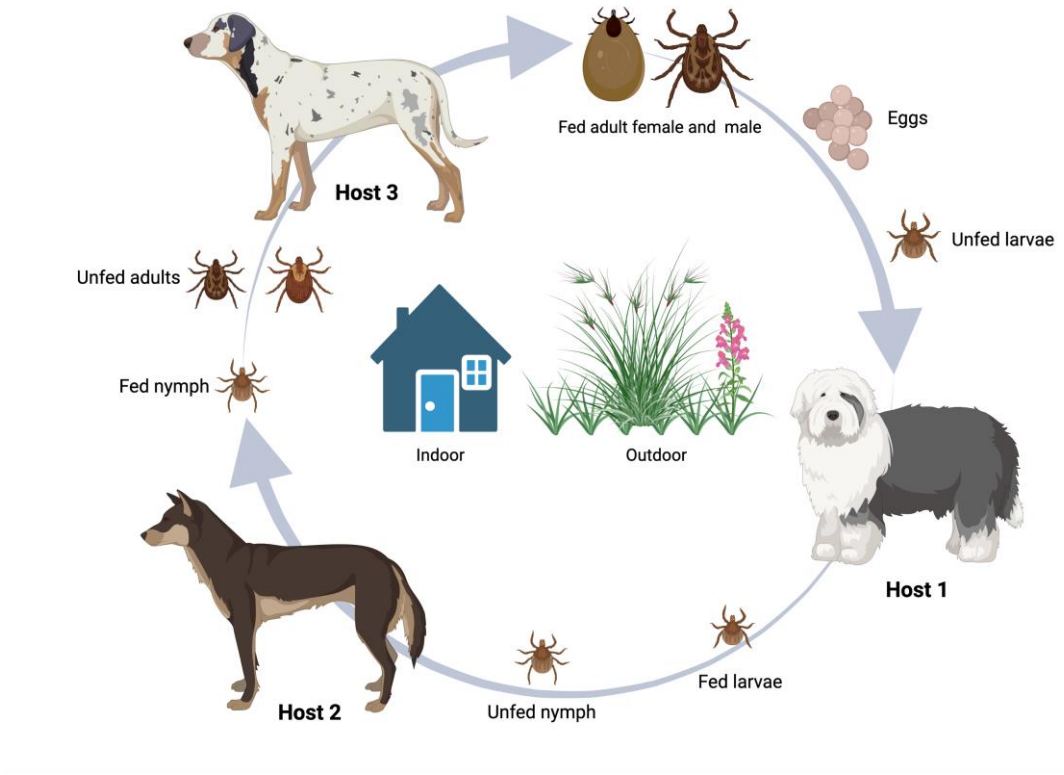

Figure 2. *Rhipicephalus sanguineus* life cycle.
After the blood meal, engorged females drop-off and lay eggs in the environment, normally in sheltered places with easy acccess to a vertebrate host. Unfed larvae hatch from these eggs, attach to a host to feed for about 4 days and drop-off to mould into nymphs. Nymphs will attach and feed on a dog for another 4 days, drop-off and moult into adults. Unfed adults will also attach and feed on a host, for about a week, mate, drop-off and lay eggs to restart the life cycle. In perfect conditions, the entire cycle can be completed in 2 months (Image created with BioRender.com).

1.1.5. *Ehrlichia canis* development in the vector

There are important epidemiological implications associated with pathogen acquisition and transmission at the different tick developmental stages (1). After feeding on dogs infected with *E. canis*, *R. sanguineus* ticks take up the bacterium and become infectious (34). After multiplying within the digestive tract of engorged larvae, nymphs and adults, *E. canis* then infects the midgut (MG) epithelium cells, haemocytes and SGs cells (81). Transstadial transmission, which occurs during "moulting" is where a pathogen needs to survive in the vector from one stage of the life cycle to the next. *E. canis* must do this to

be able to transmit infection between two hosts. Ticks facilitate transstadial transmission between canine hosts through salivary secretions whilst ingesting a blood meal at the attachment site (26). Male *R. sanguineus* ticks were shown to be capable of intrastadial transmission i.e., within the same developmental stage and transstadial acquisition and transmission of *E. canis* to susceptible dogs under experimental conditions. This was possible without the presence of female ticks (1). Since 1975, transovarial transmission, which is the vertical passage of parasites from an adult tick to its offspring by infecting developing eggs, has not been demonstrated with *E. canis* in *R. sanguineus* ticks (26).

1.1.6. Pathogenesis

Once a host animal has become infected with *E. canis*, either from an infected tick, the transfusion of infected blood, or the transfer of infected leukocytes (44), CME pathogenesis begins with an incubation period of 8 to 20 days followed by three sequential phases: acute, subclinical, and chronic, though not all dogs advance to the latter (37).

At around day 10 after the initial infection, a collection of mild and non-specific clinical signs defines the acute phase. These include anorexia fever, depression, dyspnoea, haemorrhaging, lethargy, lymphadenopathy, splenomegaly and weight loss, which can progress to death (28, 34, 82-84). Furthermore, anterior uveitis and retinal lesions are frequently observed in dogs with CME at each of the three phases (85). The duration of the acute phase is typically 1 to 3 weeks (40), after which, *E. canis* infection perpetuates due to either inadequate treatment or spontaneous (clinical) resolution. Consequently, these animals can appear to be disease-free but may advance to the subclinical phase of CME (34, 84, 86). Therefore, clinically healthy dogs in this CME phase harbour rickettsia for years without advancing to clinical disease. These dogs act as conduits for CME as ticks can continue to acquire and spread *E. canis* to other hosts (1, 86).

It remains uncertain why some dogs then progress to the chronic phase of CME (84). This phase is characterised by a spectrum of symptoms, which may be mild or severe and include emaciation, epistaxis, haemorrhages, peripheral oedema, ocular problems, and hypotensive shock, which can result in death (34, 87, 88). Dogs that only experience the

milder form of chronic CME can carry an infection devoid of clinical signs for several years, in effect, making them the natural reservoir of *E. canis* (26).

The severity of CME is a multifactorial problem and includes *E. canis* strain pathogenicity, host immunocompetence, canine breed, dose of the disease received, and the impact of co-infections. Two known pathogens that can also be transmitted by *R. sanguineus* to co-infect dogs and influence CME severity are *Babesia canis vogeli* and *H. canis* (36, 89). Though all dogs can be infected, German shepherds seem to be the breed most susceptible to *E. canis*. They often develop a chronic haemorrhagic syndrome, coupled with higher rates of morbidity and mortality (90, 91). Currently, there is no established link between CME disease susceptibility and age or gender (84).

Haematological irregularities associated with the acute phase include anaemia and leukopenia, both mild as well as thrombocytopaenia (92). In the subclinical phase, which follows the acute, dogs typically lack clinical signs; haematological parameters are generally normal, though platelet (PLTs) count can be low (93). It has been suggested *E. canis* organisms are located in the spleen during this phase (86). The spleen is known to be the major reservoir of monocytes in mammals (94) and splenic macrophages are also well described, which would support this suggestion. In the chronic phase, pancytopenia is highly prevalent. The most common clinical signs of the disease in this stage are anorexia, bleeding diathesis, depression, lethargy, lymphadenomegaly, pyrexia, splenomegaly, and weight loss (92).

Different aspects of the canine immune response to *E. canis* infection have been investigated to varying degrees. Numerous studies have been carried out in experimentally infected dogs, though far fewer exist in animals that were naturally infected. Comparing two groups of dogs with either clinical or subclinical infection, a study found the former to present lower numbers for eosinophils, red blood cells (RBCs), packed cell volume (PCV), haemoglobin, and albumin, and a reduced albumin/globulins ratio (95). Dogs with clinical infection also had higher **γ**-globulin levels. There was nothing statistically significant between the groups following analysis of total $CD3^+$ T cells, $CD4^+$ helper T cells, $CD8^+$ cytotoxic T cells, B cells or major histocompatibility

complex (MHC) II+ lymphocytes. Though $CD21^+$ B cell numbers, both relative and absolute, were lower in dogs with clinical infection. This may be due to these cells moving out of the blood into specific organs (95).

Other studies have sought to directly compare experimentally and naturally infected dogs. For instance, one relatively recent study examined leukocyte abnormalities in both groups of dogs experiencing acute CME. During the first 14 days of experimental infection, a clear decrease in nearly all leukocyte populations, including segmented neutrophils, lymphocytes, monocytes and eosinophils, was observed. By contrast, a statistically significant increase in band neutrophils was apparent. By day 28 after infection, cell counts had returned to at least, and in some cases slightly higher than, pre-infection levels (96). Neutropenia was the most striking leukocyte anomaly in this group, which may be due to impaired granulopoiesis, a more rapid egress of these cells from bone marrow or destruction caused by anti-neutrophil antibodies. Though neutrophil levels did increase again from 28 after infection, making this less likely. Data in naturally infected dogs was far more variable with both neutropenia and neutrophilia found with similar frequency. Though this discrepancy may be due to the small and heterogenous population of naturally infected dogs that were sampled. Neutrophils are the first immune cell population to respond to infections and tissue damage (97). Although several studies have reported neutropenia in dogs infected with CME, neutrophil function during the acute phase of the disease has been largely, though not completely, ignored. One study has quantified oxidative metabolism in neutrophils isolated from the peripheral blood of dogs during the first six weeks of infection. It found that there were no significant differences in oxidative metabolism between cells from infected and uninfected dogs. From 2 weeks post-infection, however, infected neutrophils that were re-stimulated with an inactivated bacterial extract, were much more reactive than those from uninfected dogs receiving the same treatment. This response was sustained until the end of the 6-week experiment. This is a particularly interesting observation and may be an example of trained immunity in these cells. This mechanism was not formally characterised until 2011 (98), six years after the CME study in question. More recently, it has been shown to occur in neutrophils (99).

The acute phase response, which forms part of the innate immune response to pathogen challenge, involves the production of several acute phase proteins (APP). In response to stimulation by pro-inflammatory cytokines released by monocytes and macrophages, the liver synthesizes these proteins. In dogs, the assessment of innate inflammatory responses after vaccination against CME are not common. In one study, the production kinetics of a selection of APPs was compared in unvaccinated and attenuated *E. canis* strain-vaccinated dogs that were subsequently challenged with a wild strain. In vaccinated dogs, levels of C-reactive protein (CRP), serum amyloid A (SAA), haptoglobin, albumin, paraoxonase-1 and total antioxidant capacity were significantly lower than in unvaccinated dogs. *Post*-challenge increases in these markers were also more delayed in the vaccinated dogs than those lacking protection. A strong positive correlation was apparent between rickettsial load and APPs such as CRP and SAA, indicative of a direct impact by the pathogen on these inflammatory markers, as would be expected. These findings fit with those from an earlier study examining naturally infected dogs (100).

As previously discussed, *E. canis* has tropism for and invades canine monocytes and macrophages. Insights into the intercellular spreading process between macrophages were gained through use of a panel of drugs on the *E. canis*-infected canine monocyte-macrophage cell line, DH82 cells (101). A reduced infection rate was observed in cytochalasin D-treated cells, identifying the actin cytoskeleton as crucial. This compound inhibits actin polymerisation, which is known to be important for pathogen spreading. Bacterial growth was also decreased in cells exposed to deferoxamine, which chelates iron. Earlier studies had revealed iron influx as crucial for the proliferation and spreading of other bacterial species. This study confirmed it is also relevant for *E. canis* spreading. Finally, the most significant impact on bacterial spreading was observed when verapamil, a cell membrane and endoplasmic reticulum calcium channel blocker, was used. It completely inhibited the spread of *E. canis* to adjacent cells. Analysis of acid phosphatase labelling to observe phagosome-lysosome fusion indicated *E. canis* also evades lysosomal fusion to survive and replicate (101). This could be due to an active type IV secretion system (TFSS), which is known to inhibit the transport of bacteria to lysosomes and is conserved (102) and expressed (103) in *E. canis*. As is often the case with successful pathogens, *E. canis* can evade elimination by host cells through more than one

strategy. Evidence of its capacity to modulate host immune responses was shown in DH82 cells. Using two different antibodies, MHC class II molecules were expressed on 46.9% of uninfected cells. By contrast, *E. canis* completely abrogated surface expression, identifying a mechanism used by the bacterium to subvert the host immune response (104).

To better understand the pathogenesis of canine ehrlichiosis as well as the host response to the pathogen, the *E. canis* genome was sequenced for the first time in 2006 (102). Of particular interest was a conserved group of twelve cell wall proteins that contain tandem repeats. Prior studies had shown this family are involved in host-pathogen interactions and pathogenicity. All twelve of these *E. canis* proteins have identifiable tandem repeat-containing orthologues in other *Rickettsiales* genomes. Another group of genes engaged in host-pathogen interactions and pathogenicity are the Vir proteins. The *E. canis* genome build shows they are arranged in two clusters: *virB8/virB9/ virB10/virB11/virD4*, and *virB3/virB4/ virB6* plus three *virB6*-related genes. Earlier work revealed *virB/D* operons drive expression of the TFSS, which is used to deliver virulence factors from bacteria to host cell cytoplasm (105). Of interest, the *E. canis VirB9* is expressed in canine and tick hosts, with modelling identifying several antigenic epitopes (103). Added to the fact that *virB/D* operons needed to express TFSS components were identified and functionally characterised in *Ehrlichia chaffeensis* (106); it is highly likely *E. canis* relies on its orthologous proteins for intracellular survival and replication. Further evidence of the ability of *E. canis* to evade the host immune response can be inferred from absent cell wall components. The genes required for the synthesis of both lipopolysaccharide and peptidoglycan are lacking in the *E. canis* genome (as well as other *Ehrlichia*). This makes its recognition by Toll-like receptors 2 and 4 highly unlikely, limiting the innate immune response (102).

The ongoing "success" of *E. canis* to invade and persist in hosts can be partially attributed to our limited understanding of its functional genes and proteins. In fact, it has been suggested the lack of a vaccine is hindered by its arsenal of protective, immunoreactive proteins that elicit strong antibody responses in infected dogs (107). The known repertoire of these proteins is also believed to be a fraction of the true total, with many undefined.

With that in mind, two recent studies have offered a significant advance in this area through discovery of several novel immunoreactive proteins that may assist future vaccine development efforts (107, 108). In both studies, proteins with conformation-dependent antibody epitopes were identified using novel approaches. Previous efforts had revealed a small selection of proteins with only linear antibody epitopes, since experimental methods were limited. Notably, sixteen out of the thirty-four proteins identified in the two studies were predicted to be secreted as well as immunoreactive (107, 108). As they are probably targeted by the host immune response to neutralize their function, they may be responsible for subverting canonical host processes in order to promote infection.

1.1.7. Diagnosis

The different phases and multiple clinical manifestations of CME can make its diagnosis challenging (84). Typically, a combination of anamnesis i.e. residing in or travelling to an endemic region as well as previous exposure to ticks, characteristic clinical signs, as described previously, plus haematological and biochemical alterations leads to a diagnosis (84). To definitively confirm this, laboratory tests comprising of one or more of microscopy, serology, cell culture or PCR (84, 109) are carried out to directly or indirectly detect *E. canis*. Intracytoplasmic morula-like bodies, either single or multiple, observed in monocytes by microscopy during the acute phase, is conclusive (82, 84). Despite this, it is a method lacking in sensitivity, often reporting false negatives and false positives with other ehrlichiae of the *Anaplasmatacea* family. For example, canine monocytes may be infected with *E. chaffeensis*, *Ehrlichia ruminantium* or *Ehrlichia risticii* (110-112). This method is also less than ideal due to its time-consuming workflow, and low numbers of organisms make diagnosis difficult (34, 84, 109). Just 4% of blood smears from dogs with ehrlichiosis are sufficiently unambiguous to observe the presence of *E. canis* morulae (113).

There are now improved serological methods available to accurately screen and/or diagnose CME (84). One example is the use of indirect fluorescent antibody tests (IFAT) for anti-*E. canis* immunoglobulin (Ig) G (IgG), which were long considered to be the "*gold standard*" (84, 114, 115) . Enzyme-linked immunosorbent assays (ELISA) are also

used to diagnose *E. canis* infection (114-117). In the past, a problematic aspect of serological assays was the potential for cross-reactivity with other ehrlichial organisms. These were reported in endemic areas with other *Ehrlichia* species, for instance: *Ehrlichia ewingii, E. chaffeensis* and *E. risticii* (84, 115, 118). *Ehrlichia canis* antibodies may also cross react with *Anaplasma phagocytophilum* antigens (115). Improvements in the sensitivity and specificity of ELISAs have made them a more robust method for diagnosing *E. canis* infection. This is, in part, due to a deeper molecular characterization of *E. canis* proteins. For example, two conserved immunoreactive antigens, the glycoproteins gp19 and gp36, were identified as able to induce specific antibody responses to *E. canis* (119, 120). These antigens, as well as the glycoprotein gp200 were expressed as recombinant glycoproteins, and used to develop an ELISA that demonstrated 100% sensitivity and specificity compared to IFAT. This ELISA can also detect antibodies two weeks earlier than IFAT in samples from experimentally infected dogs. Furthermore, it is species-specific; there is no cross reactivity with antibodies in sera from dogs infected with *E. chaffeensis* (121). If strain-specific detection is needed, there are genotype-specific ELISAs now available that offer this degree of specificity. Taking advantage of a tandem repeat motif within the *TRP36*, an ELISA that can distinguish between Brazilian and American *E. canis* infections derived from these alternative genotypes, was developed (122).

In addition to serological assays, molecular detection methods also provide a definitive diagnosis. The PCR coupled with amplicon sequencing can sensitively detect and potentially reveal the genotype of *E. canis* DNA (84, 123). PCR assays targeting a diverse group of target genes, for e.g., *16S ribosomal RNA* (*16S* rRNA), *outer membrane multigenes 28 and 30* (*p28*; *p30*), *disulphide bond formation protein* (*dsb*) and *outer membrane protein 1* (*omp-1*), have been developed. The most performed amplify *16S* rRNA and *p30* (84, 124, 125). By combining IFAT tests with nested-PCR, a laboratory diagnosis could be made during the acute phase of infection, prior to detectable antibody levels in sera (126, 127). By combining PCR with DNA hybridisation, *E. canis* infection can be detected with greater sensitivity than conventional PCR (128, 129). A recent study has highlighted the challenge associated with diagnosing the disease in dogs in the subclinical and chronic phases of CME. In the former, there is a lack of clinical signs,

whilst in both disease states; low parasitaemia can be observed because bacteria reside in target organs. Consequently, these dogs are negative for *E. canis* in the blood when PCR is used to screen. A group of fifty-nine dogs that lacked clinical signs but had ticks were euthanised, after which; blood, bone marrow, liver, lymph node and spleen tissue samples were screened for *E. canis* by PCR. A negative blood PCR was confirmed in 52.5% of dogs, however, 61.3% were positive in tissue samples (130). In line with other studies these authors cited, there might be a case for combining detection in blood with splenic aspirates as an improved diagnostic approach and/or determining CME distribution.

Quantitative real-time PCR (qPCR) is more sensitive than conventional PCR, and it rapidly became the principal method of *E. canis* diagnosis. Some of the earliest examples of this assay being developed immediately underlined its usefulness. Based on amplification of *16S* rRNA, a qPCR TaqMan assay was created to discriminate single infections in canine blood with *Ehrlichia chaffeensis*, *E. canis*, *E. ewingii*, *A. phagocytophilum* and *Anaplasma platys*. It could also determine co-infection with *E. canis* and *A. platys* (131). This assay was later shown to be effective at detecting some *Ehrlichia* and *Anaplasma* in *Amblyomma americanum*, *Dermacentor* and *Ixodes* species, though not *E. canis* (132). The first tricolour TaqMan assay to detect and discriminate between different *Ehrlichia* species in a single reaction was based on amplification of *dsb*. This genus-specific target allowed singleplex quantification of *E. chaffeensis*, *E. ewingii* or *E. canis* from naturally or experimentally infected dogs without cross hybridisation of the probe (133). The primers also would not amplify *A. platys*, *A. phagocytophilum*, *R. conorii* or *Rickettsia typhi*, emphasising its specificity. An alternative variant to these assays has been subsequently developed to amplify the *16S* rRNA in *E. canis* and the heat shock protein (HSP) 70 (*hsp70*) in *B. canis vogeli* in a multiplex assay with dual labelled probes (134). Another multiplex qPCR assay using SYBR green is also available to amplify *B. gibsoni*, *B. vogeli*, *E. canis* and *H. canis*. The *virB9* is the target in *E. canis* (135).

Finally, a highly sensitive and reliable diagnostic method involves isolating *E. canis* by inoculating cell lines to demonstrate active infection and specific identification of the

pathogen (68, 109, 116, 136). Despite this, it is unrealistic since it requires 1 to 4 weeks to generate results (109, 128).

1.1.8. Treatment, control and prevention

The first line treatment for CME is doxycycline, a broad-spectrum tetracycline-class antibiotic, since it exhibits greater intracellular penetration and inhibits bacterial protein synthesis to prevent growth (136, 137). Tetracycline hydrochloride, oxytetracycline, minocycline and chloramphenicol have also been shown to target *E. canis* with some level of efficacy (113). As reviewed by Mylonakis et al. (2019), CME treatment with antimicrobials should be able to cause clinical remission and resolution of clinic and pathological alterations (138). Complete parasite elimination is not always possible or proved by diagnostic means (126).

A commercial vaccine for CME has yet to be developed; therefore, measures to control ticks remain the best preventative approach to restrict the transmission of *E. canis*. Strategies for tick control can be focussed on the on-host phase of the tick life cycle, achieved through targeting dogs as well as indoor spaces. The phase of the tick life cycle when it is off host can also be targeted, relying on knowledge of tick ecology. Often, a combination of both approaches is adopted. Naturally, controlling ticks outdoors is very challenging and since *R. sanguineus* ticks prefer indoor spaces, limiting infestations in these areas as well as on the host should be the primary focus of control measures. A combination of chemical and non-chemical approaches should be pursued (4). Chemical control on the host can be established using liquid formulations, sprays, repellents and impregnated collars, containing acaricides and/or insecticides such as fipronil, amitraz or permethrin. A comparison study using novel chewable compounds, afoxolaner (NexGard™) and fluralaner (Bravecto™) has found an impaired efficacy against *R. sanguineus* infestation with low efficacy times allowing *E. canis* transmission. Contrary, Advantix® (50 % permethrin:10 % imidacloprid) effectively blocked transmission of *E. canis* to dogs providing adequate protection for dogs against CME (139).

As a last resort, chemical control of indoor and outdoor spaces can be achieved using pesticides, for example carbamates or pyrethroids. Altering tick habitats' through sealing

cracks and crevices, and/or removing grass and weeds represent outdoor controls that do not require chemicals (4). It is essential that canine blood donors be screened to confirm seronegativity for antibodies to avoid *E. canis* transmission from a blood transfusion.

1.1.9. Vaccine development

Globally, ticks and TBDs affect approximately 80% of the cattle population, predominately in the tropics and subtropics (140). Their impact on the health of domestic animals, such dogs and cats, is also significant (141). As strict blood sucking parasites, ticks cause direct damage to the host skin through their mouth parts, with consequent local irritation and inflammation at the attachment site. In large infestations, blood spoliation results in anaemia. These effects lead to great economical losses in the animal production industry, with lower quality leather products, decreased milk production and body weight losses. In companion animals, the impact of these ectoparasites is also a reflection of their feeding habits (71). However, major losses caused by ticks are due to their ability to harbour and transmit protozoan, rickettsial, helminth and viral diseases, some of which are zoonotic, causing severe diseases in humans. An extensive review by Boulanger et al. (2019) summarises human infectious diseases transmitted by ticks, including tick-borne encephalitis, Crimean-Congo haemorrhagic fever, Q fever or Lyme borreliosis (142). For these reasons, tick control has been attempted for several decades with different approaches, of which the most used has been the employment of chemical acaricides.

Presently, with the increased concern about climate change and its impact on the ecosystem, the use of synthetic acaricides to control ectoparasites must be prudent. Their harmful residues reach grounds and waters causing severe damage in living organisms. Humans can also be affected through the consumption of meat and dairy products. The persistent use of chemical acaricides has also been linked to widespread cross-species resistance, which can be minimised by vaccination against ticks (12). The interest in controlling ticks through vaccination began several decades ago (143) and this concept is currently well established, with several promising single antigens identified (144). Hence, the development of vaccines is viewed as a vital cost-effective alternative, with a low environmental and health impact, to the use of acaricides to control tick infestations and

TBDs. Other advantages of using anti-tick vaccines is the possibility of combining multiple antigens or, at least, some that share conserved structural and sequence motifs, in a broad-spectrum vaccine acting against different tick species and tick-borne pathogens (TBPs) (145, 146). Ideally, a vaccine should also be able to act against all tick stages, increase tick mortality, reduce tick feeding time and engorgement, decrease egg mass weight and viability, and impede moulting. Other desirable characteristics would be long-lasting immunity and maintaining biological activity when in contact with the MG cells and in the passage to the haemolymph and other tick tissues, as reviewed (147). Ackerman et al. (1981) reported the passage of host antibodies through the midgut of *D. variabilis* and activity maintenance in the SGs and OV (148). Galay et al. (2018) has shown the passage of host antibodies to *Haemaphysalis longicornis* OV (149).

Several components of tick saliva have been investigated for the development of anti-tick vaccines, but the identification of suitable antigenic targets has been the main drawback. In the saliva, molecules with potential antigenic interest have been categorised as exposed antigen, normally produced in the SGs and secreted during the attachment and feeding on the host; as concealed antigen, mostly present on the tick MG wall and hidden from the host immune system, interacting only with specific immunoglobulins; or a mixture of exposed and concealed if both properties are present (147). Whilst exposed antigens elicit a host immune response during tick infestation, concealed antigens induce a specific immunoglobulin response, usually against a tick tissue. The main limitation associated with exposed antigens is related to the tick saliva immunomodulatory effect, by secretion of several molecules, to prevent host inflammatory and immune responses and to reduce haemostasis (150-152). The same mechanism that allows tick attachment and prolonged acquisition of blood meals might reduce or neutralise the effect of the host immune response to the exposed antigen, and consequently decrease vaccine protection. Concealed antigens can be isolated from different tick tissues, including the gut wall, vitellin (Vn) from eggs, female fat body or paramyosin from female gut extract (153, 154). The most well-known concealed antigen is *Rhipicephalus microplus* intestinal Bm86, a glycoprotein expressed in the luminal membrane of enterocytes (155) that interacts with specific immunoglobulins ingested in the blood meal from an immunised

animal. The binding of antibody to antigen leads to gut wall lysis, compromising digestive metabolism and later egg production, as reviewed (147).

The first two anti-tick vaccines were commercially available more than twenty years ago, the TickGARD®, in Australia, and Gavac®, in Latin America, developed against *R. microplus*. Immunisation with Gavac®, recombinant Bm86, has shown to be mainly effective against infestations caused by *Rhipicephalus annulatus*, *Rhipicephalus decoloratus* and *R. microplus*, and reduced the need of acaricide treatments (155). Since then, Bm86 is the principal constituent of the only commercialised anti-tick vaccine and several vaccination trials have been reported. In cattle, this recombinant protein had a negative impact on *R. microplus* feeding, number of oviposited eggs and *Babesia spp.* transmission (13, 145, 155). Likewise, cattle and camels vaccinated with Bm86 presented a lower number of *Hyalomma dromedarii* engorging nymphs and a decrease of adult body and egg weights, and less egg hatching (156). A cocktail vaccine with Bm86 and Bm91 only induced a moderate increase in cattle protection against *R. microplus* in comparison with Bm86 alone (157). Despite these encouraging results, protective immunity induced by Bm86-derived vaccines is short lived, requiring 6 monthly interval boosts (158), and vaccination with Bm86 has only been successful in a small number of tick species. For example, rabbit vaccination with two Bm86 orthologs from isolated from *Ixodes ricinus* did not affect tick feeding and oviposition (159).

Several other recombinant proteins have been identified and their efficacy determined experimentally, including subolesin (160), aquaporin (161), 64P cement protein (162), a cyclin-dependent kinase (163), amongst others. The progress towards effective anti-tick vaccines, with updates on emerging data, can be accessed in detailed reviews (10, 12, 13, 144-146, 164).

A different approach to prevent or reduce the incidence of TBDs is the formulation of transmission-blocking vaccines, which use tick antigens that directly affect the pathogen life cycle, reducing or blocking its invasion and multiplication in the tick tissues. This could also be achieved indirectly using a tick antigen that decreases tick survival and/or attachment and engorgement time limiting the possibility of pathogen acquisition during

the feeding process (13). Another aspect is that smaller body weights lead to decreased oviposition, preventing TBDs transmitted by the next tick generations. Transovarial and/or transstadial transmission has been described for some TBPs, including *Rickettsiae africae* in naturally infected *Amblyomma variegatum* (165) and *Amblyomma hebraeum* (166), Kyasanur forest disease virus in *Hyalomma spinigera* (167), *Rhipicephalus montana* and *Rhipicephalus rhipicephali* and *D. variabilis* (168). This indirect effect was observed in cattle vaccinated with this recombinant protein, causing a negative impact on *R. microplus* feeding process, number of oviposited eggs and *Babesia spp.* transmission (155). As reviewed by de la Fuente et al. (2007), other tick antigens such as 64P putative cement protein and subolesin, had the same indirect effect on the transmission of TBDs by reducing tick infestations (13).

The proof of concept of developing a transmission-blocking vaccine has been reported. Pal et al. (2004) identified the *Ixodes scapularis* tick receptor for outer surface protein A (TROSPA) that ligates to *Borrelia burgdorferi* outer surface protein A (OspA), allowing pathogen adherence to and colonisation of the tick gut. Gene silencing and blockage of TROSPA with antisera led to decreased levels of *B. burgdorferi* tick colonisation (169). A field vaccination trial carried out in wild white-footed mice, a reservoir for *B. burgdorferi,* using recombinant OspA resulted in a significant reduction of pathogen prevalence in *I. scapularis* nymphs (170). The same result was obtained in laboratory conditions using an OspA-based oral vaccine in mice. After immunization, mice developed a protective immune response with subsequent pathogen reduction in the vector *I. scapularis* (171). Thus, the survival of TBPs clearly depends on their capacity to use vector molecules to their advantage. Based on this premise, Nuttall & Labuda (2004) reviewed the concept of saliva-activated transmission (SAT). SAT is pathogen transmission using tick saliva components on the host or saliva-mediated host modulation (172). This review provides a detailed description of some TBPs that likely use direct SAT, although in 2004 SAT factors were not identified. Some of the proposed SAT factors present in tick saliva included histamine-binding proteins, complement and cytokine inhibitors, leukocyte and T cell modulators. Thus, in future investigating these SAT factors and their impact in TBPs transmission would contribute to the development of recombinant proteins to control ticks and TBDs.

The emergence of the coronavirus disease 2019 (COVID-19) in humans as a global pandemic, caused by the severe acute respiratory syndrome coronavirus 2 (SARS-CoV-2), led to an intensive search for targets to block the virus (173). As such, global vaccine development was rapidly accelerated to reduce morbidity and mortality associated with this syndrome. An area that greatly benefitted from the speed of this research was the development of mRNA vaccine technology, initially for use as COVID-19 prophylaxis, and later applied to other diseases including malaria, HIV, tuberculosis and cancer (174, 175). Two main types of mRNA vaccines are documented: the nonreplicating mRNA, that encode the antigen of interest untranslated region(s) (UTR), and the self-amplifying mRNA, that encodes the antigen and for the viral replication machinery for protein expression (176).

This vaccine technology also caught the interest of vector-borne diseases researchers. Recently, Sajid et al. (2021) carried out vaccination trials in guinea pigs using a nucleoside-modified mRNA-based vaccine to determine acquired tick resistance or tick immunity to *I. scapularis*. For this, they selected 19 highly immunogenic salivary proteins, previously described in other *I. scapularis* sialome studies, to produce the nucleoside-modified mRNAs. To facilitate *in vivo* delivery and avoid degradation, mRNAs were encapsulated in lipid nanoparticles (LNPs; I9ISP; nucleoside-modified mRNAs-LNP platform). I9ISP-immunised guinea pigs developed strong tick immunity, with early tick detachment and decreased tick feeding and engorgement weights. High levels of antibodies were found against the tick proteins Salp14, Salp15, Salp25D, Salp26A, TSLPI, IsPDIA3, TIX5, P32, SG10, and SG27. This study suggested that I9ISP-immunised guinea pigs can have some protection against *B. burgdorferi* infection, responsible for Lyme disease. The removal of ticks shortly after skin erythema development limits the attachment and, consequently, feeding time reducing the possibility of *B. burgdorferi* transmission to the host (177).

This study opens new horizons in tick vaccinology with the potential use of multivalent mRNA-based vaccines to control ticks and TBDs by inducing tick resistance in the host (178, 179).

1.1.10. RNAi

RNAi is a biological defence mechanism induced by small dsRNA molecules that inhibit the expression of a target gene in cells, by homology, through specific degradation (180). The RNAi mechanism is mainly present in eukaryotic cells, and some biological roles of RNA silencing pathways include maintenance of genome integrity by suppression of transposable elements and by regulation of endogenous gene expression, and antiviral innate immunity (181). Prokaryotes also seem to have an RNA-based translation repression mechanism with some similarities to RNAi (182).

The RNAi pathway starts with the cleavage of long dsRNA molecules into short double stranded molecules, the small interfering RNAs (siRNAs), by RNase III Dicer, a large endoribonuclease multidomain enzyme. Normally, Dicer cleavages the substrate dsRNA at the termini bound by the PAZ domain with affinity to 3′ expanded overhangs. Each specific Dicer defines the length of siRNAs, depending on the distance between the PAZ domain and the RNase III cleavage sites of dsRNA. Dicer has two RNase III domains with affinity for two cleavage sites, one for each dsRNA strand. This results in a siRNA duplex with two nucleotide 3′ overhangs and 5′ monophosphate and 3′ hydroxyl groups at the RNA termini. Small RNAs are then loaded onto an Argonaute (AGO) protein, with endonucleolytic activity, forming the RNAi effector complex or RNA-induced silencing complex (RISC). In vertebrates and arthropods this protein is AGO2. Here, siRNAs lose their double strand conformation, originating one guide strand and a passenger strand. The passenger strand is cleaved and degraded. This step is crucial for the selection of the target strain and to direct siRNAs to different RNA silencing pathways. The guide strand of siRNA is incorporated in the RISC complex, recognising the target mRNA by sequence complementary. The hybridization of both strands leads to mRNA degradation by the enzymatic activity of ARG, with subsequent gene silencing (181, 183).

Because RNAi provides selective gene species-specific gene targeting, the use of dsRNA has become an important method to analyse gene functions and block protein synthesis in several organisms including animals, plants and fungi (184, 185). RNAi has also been used for the study and therapeutics of disease-associated genes, including cancer, autoimmune diseases, dominant genetic disorders and viral infections (186).

RNAi has become the most used method for disruption of gene expression in tick-related research, allowing functional characterisation of genes and proteins or their effects on a metabolic pathway in different tick tissues (19, 187, 188). Besides gene characterisation, this tool has been extremely important to understand the tick-pathogen interface and for the investigation of potential tick protective antigens in ticks and tick cell lines (189-193). This technique could also be employed to reduce tick competence as vectors and to limit TBD transmission, as genes critical for pathogenesis could potentially be downregulated by RNAi (194). Despite its wide use, the RNAi mechanism in ticks is not fully understood, but some of the key RNAi-related proteins present in other vertebrates are also present in ticks (195). Kurscheid et al. (2009) proposed a putative RNAi pathway for ticks.

Several methods have been described to deliver dsRNA molecules in ticks, including injection, soaking, and electroporation through feeding. A comprehensive review of these has been made (196).

During our work, several published studies that describe the use of RNAi to investigate the effect of gene silencing in ticks and TBPs biology will be referenced accordingly.

1.2. Importance of ferritin 1 protein in ticks

Evolutionarily, ticks have evolved in a way that allows them to survive on a strictly haematophagous diet without suffering from the deleterious iron-mediated oxidative stress, using several strategies that maintain iron homeostasis during meals and digestion. One of them includes the involvement of iron-binding ferritin proteins to sequestrate, store and metabolise these ions.

Ferritins are highly conserved proteins ubiquitously present in different tissues and in different developmental stages of ticks (197). Additionally, ferritins are proteins present mostly in all organisms and their amino acid (a.a.) residues that interfere with iron-binding and ferroxidase activity, are highly conserved between different species (198).

Hard ticks have an intracellular ferritin (FER1) that stores or retains ferric iron (Fe^{3+}) obtained by oxidation of the toxic Fe^{2+} form within cells, and a secretory type ferritin (FER2) that concentrates and secretes or transports Fe^{3+} from the MG cells to the hemolymph and OV (197, 199, 200). Ferritin 1 is the primary ferritin in MG cells with a vital cytoprotective role in the antioxidant response (197, 201).

The first characterisation of FER1 was in the tick *I. ricinus*, whereby it was verified that the heavy chain sequence was identical to mammalian ferritin and that the ferroxidase centre had conserved motifs (202). Xu et al. (2004) have demonstrated that eight species of hard ticks presented a conserved iron-responsive element (IRE) (203), with no signal peptide, involved in post-transcriptional regulation (204). The expression of FER1 is regulated by the interaction among IRE and iron regulatory proteins (IRPs) at the mRNA level, according to iron cellular levels. For example, if iron levels are low, IRP binds to IRE at the UTR of *FER1* mRNA to block protein translation. Contrary, in the presence of high levels, the Fe-S forms an insert into the IRPs that further converts to aconitase and detaches from the mRNA iron loop. As a consequence, FER1 protein translation occurs to retain the iron and control its levels (198, 199).

In the hard tick *H. longicornis*, qPCR analysis of *Hl-fer1* has shown that it is expressed in the MG, SGs, hemocytes, fat body and OV during blood feeding. Using immunolocalisation, the native protein was found in the cytoplasm of MG digestive cells,

in the salivary acini and salivary duct of SGs and in the oviduct and oocytes in the OV (197). Western blot analysis confirmed that FER1 was present in all tick tissues except for hemolymph (197, 202). In the tick *Haemaphysalis flava Hf-fer1* and *Hf-fer2* were found expressed in all developmental stages, mainly in unfed larvae and fully engorged females. *Hf-fer1*was found in all tissues, predominantly in the SGs of fully engorged females, whereas *Hf-fer2* was mostly found in the MG and absent from the SGs for the same life cycle stage (205).

Tick *fer1* mRNA levels are constitutively expressed and not influenced by a blood meal (197, 199, 202, 206). These findings indicate that FER1 post-transcriptional regulation, by the IRP-IRE interaction, depends on the organ and that its constitutive expression in the MG relates with the fact that this is the main iron storage site. Contrary, *fer1* mRNA levels increase in the SGs during the blood meal due to the presence of iron in the diet (197). A different study carried out in ISE6 cells has shown this iron-depended expression by silencing *FER1* and subjecting the cells to different ferrous sulphate concentrations. Gene knockdown has led to an increase of ferrous iron concentration and to a decrease of ferric iron (207). *FER1* knockdown in ticks also resulted in a survival decrease and impaired reproduction in the presence of high levels of iron (197, 199).

Because of their high nucleotide and a.a. sequence conservation (197, 199), together with their role in iron homeostasis, blood feeding, reproduction and survival, these iron-binding proteins have been considered strong candidates for further investigation for developing anti-tick vaccines. Two studies have explored the ability of ferritins to elicit anti-tick immune responses. In rabbits immunised with two recombinant tick ferritins, one of these (rH1FER2) offered some protection (208). A similar study where cattle and rabbits were immunised with recombinant ferritins derived from different tick species, found that rFER2 conferred some protection in both mammals (209). Another important aspect to consider when developing anti-tick vaccines is that host antibodies should be passed on the oocytes, to disrupt tick reproduction capacity. Galay et al. (2018), investigated the presence of host antibodies against HIFER2 by IFAT in the OV and eggs of female *H. longicornis*. Positive fluorescence was detected in the ovaries, but not in cytoplasm of the *HIfer2*-silenced ticks' oocytes (149).

Chapter 2: Materials and Methods

2.1. Experimental animals

2.1.1. Ethics statement

German shepherd dogs (*Canis lupus familiaris*) used in the experiments were housed at Faculdade de Ciências Agrárias e Veterinárias – Campus de Jaboticabal, Universidade Estadual Paulista (FCAV-UNESP) facilities, in Brazil. This study was conducted according to the ethical and methodological norms of Lei Arouca 11.794/08 and Conselho Nacional de Controle da Experimentação Animal (CONCEA) and approved by the Comissão de Ética no Uso de Animais (CEUA) (FCAV-UNESP; Protocol nº 7.045/16).

New Zealand White rabbits (*Oryctolagus cuniculus*) were used as host to maintain all the developmental stages of the *R. sanguineus* tick colony at FCAV-UNESP facilities in Brazil. Rabbits were maintained according to the ethical and methodological norms of Lei Arouca 11.794/08 and CONCEA and approved by the CEUA (FCAV-UNESP; Protocol nº 7.045/16).

CD1 mice used in the experiments were reared and maintained at Biotério facilities of Instituto de Higiene e Medicina Tropical - Universidade Nova de Lisboa (IHMT-UNL) in Lisbon, Portugal. This study was carried out with the approval of the Divisão Geral de Alimentação e Veterinária (DGAV), Portugal, (Art◦ 49, Portaria n◦1005/92 of October 23rd, Authorisation Number 0421/2013) and the Council of Ethics of the IHMT-UNL. Animal experiments were conducted in accordance with the National and European Animal Welfare legislation (DL 113/2013 and Directive 2010/63/EU) and the *in vitro* models have been developed in order to meet the principle of the three Rs (Replacement, Reduction and Refinement).

2.1.2. German shepherd dogs

German shepherd dogs were selected for the experiments as they have been reported as being more susceptible to CME, when compared to other dog breeds (91, 210). To obtain

populations of *R. sanguineus* ticks uninfected and *E. canis*-infected, 2-month-old male German shepherd dogs were acquired from a certified breeder proved to be ehrlichiosis and ectoparasite-free. As an additional measure, 5 ml of blood were taken and tested for the presence of *Neospora caninum* (211), *Toxoplasma gondii* (212), *E. canis* (213) and *B. vogeli* (214) by IFAT, as previously described. Blood was also tested for the presence of *E. canis* (118) and *B. canis vogelli* (215) by PCR. For the template, genomic DNA (gDNA) was extracted from whole blood using the DNeasy Blood & Tissue Kit (Qiagen, Hilden, Germany), according to the manufacturer's instructions. All these tests were negative. The animals were also vaccinated twice with Vanguard Plus 5® (Zoetis, New Jersey, USA) and RecombiteK C6/CV® (Merial, Georgia, USA), with a 3-week interval, and dewormed. Dry food was provided twice a day and water *ad libitum*.

2.1.3. New Zealand white rabbits

The use of laboratory animals as hosts to provide blood meals for arthropods still is the most efficient method to maintain slowly feeding ixodid ticks, when compared with other methods including artificial feeding on animal skin or synthetic membranes. New Zealand white rabbits are easy to acquire and to handle in laboratory for the establishment and maintenance of a large variety of tick species colonies across the world. Furthermore, juvenile instars of several tick species are known to parasitise small mammals (216). For this study, New Zealand white rabbits, weighing approximately 1.000 kg and with undetermined sex, were used as host to provide the blood meals through artificial infestation to all the developmental stages of the *R. sanguineus* tick colony (larvae, nymphs and adults). Rabbits were certified to have no previous history of tick infestation and rabbit anti-tick immunity effects on blood feeding and survival was prevented by using each rabbit only once.

2.1.4. CD-1 mice

The CD-1 mouse is a versatile experimental model that can be used in several fields of biomedical research such as toxicology, aging and oncology. In this study, six 8-weeks-old CD-1 male mice were used to produce polyclonal antibodies.

2.2. Ticks and tick-borne pathogens

2.2.1. *Rhipicephalus sanguineus* colony

The laboratory pathogen-free colony of *R. sanguineus* s.l. ticks (tropical lineage) (GenBank accession no. KC018070 and JX997391) (217, 218) was maintained at the Department of Veterinary Pathology, FCAV-UNESP, Jaboticabal, Brazil. The tropical lineage of *R. sanguineus*, but not the temperate lineage, has been shown to be a competent vector of *E. canis* (58). Briefly, ticks (larvae, nymphs, and adults) were kept in a chamber regulated at 27±1ºC, 80% relative humidity and a photoperiod of 12:12 (light: dark) and maintained by feeding on the ears of New Zealand white rabbits (222). For the blood meals, ticks were placed in feeding bags on the rabbit ears and allowed to feed to repletion. Rabbits were kept in individual cages and the nails were covered with medical tape to prevent scratching and grooming. The engorgement status of ticks was observed every day whilst the infestations occurred, and twice a day while ticks were dropping-off. Fully engorged ticks were collected from the bags, transferred into polystyrene containers and kept under laboratorial conditions, as described above, for moulting and/or oviposition according to the developmental stage. The feeding method was repeated for hatched larvae, moulted nymphs, and adults.

2.2.2. *Ehrlichia canis* strain and cultivation

E. canis Jaboticabal strain (GenBank accession nr. DQ401044) was isolated from a Weimaraner dog blood sample during the acute phase of CME infection, in 1993 (Rosângela Z. Machado; unpublished data). Currently, the strain is maintained in DH82 cells (219) at the Immunoparasitology Laboratory, FCAV-UNESP, in Brazil, as described elsewhere (220). Briefly, DH82 cells were grown at 37ºC without additional CO_2 in Dulbecco's modified Eagle's medium (DMEM; ThermoFisher Scientific, Massachusetts, USA) supplemented with 2 mM L-glutamine (Sigma–Aldrich, Missouri, USA), antibiotics (100 U/ml penicillin, 100 µg/ml streptomycin; Lonza, Basel, Switzerland), 10% fetal bovine serum (FBS; Biosera, Manila, Philippines) and 1.5 M 4-(2-hydroxyethyl)-1-piperazineethanesulfonic acid (HEPES; ThermoFisher Scientific). The medium was replaced twice weekly. Cells were harvested by scraping (Greiner Bio-one, Kremsmünster, Austria) when the monolayer was 100% confluent, and subcultured at a

1:2 ratio for culture maintenance in 25 cm^2 or 75 cm^2 flasks (Nunc®, Roskilde, Denmark) with 5 ml or 15 ml of DMEM, respectively.

2.2.3. *Ehrlichia canis* experimental infection

For the experimental infection, dogs were inoculated intravenously with a dose of 4.5 - 5 ml of *E. canis* purified from highly infected DH82 cells, as described elsewhere (220). Following inoculation, the infection was monitored by qPCR targeting *dsb* (133) throughout the whole experimental period to confirm the presence of *E. canis*. For this, gDNA was extracted from 5 ml of whole blood using the DNeasy Blood & Tissue Kit (Qiagen). The qPCR was positive for *dsb* from day 3 *post*-inoculation. After the last engorged nymph or adult tick dropped-off the *E. canis*-infected dogs were treated with doxycycline 5 mg/kg every 12 hours for at least 4 weeks, according to the approved guidelines from the Lei Arouca 11.794/08, in Brazil, and as previously described (221). Dogs selected as unexposed controls were inoculated with 5 ml of sterile phosphate buffered saline (PBS; pH=7.2). The absence of infection was confirmed in these control dogs with no *dsb* amplification. When the experimental infection took place, dogs were between 5 and 9 months old.

After *E. canis*-inoculation, all dogs were monitored daily by a Veterinary Surgeon that conducted a physical examination, focusing on the rectal temperature, capillary repletion time (CRT) and palpation of abdominal organs and lymph nodes. To detect the presence of morulae, capillary blood was collected from the ear tip of each inoculated animal, up until the time when parasitaemia was confirmed on day 17 *post*-inoculation by light microscopy (Olympus CX31; Olympus, Tokyo, Japan) of Giemsa-stained smears, as described in section 2.3.2. Also, 2 ml of whole blood was collected from each dog for haematology and detection and quantification of *E. canis* by qPCR as described above.

2.2.4. *Rhipicephalus sanguineus* feeding

To obtain the population of *R. sanguineus* infected with *E. canis* and uninfected for the transcriptomic and proteomic studies, 17 days *post*-inoculation 4 tick feeding chambers were placed on each dog (inoculated and control) as described elsewhere (222) (Figure 3). The day after, approximately 1500 *R. sanguineus* nymphs were placed on each animal,

distributed by the 4 chambers, and allowed to feed until the drop-off. The engorged nymphs were collected up until the last nymph dropped-off and maintained under laboratory conditions afterwards, as described in section 2.2.1 to moult into adults for SGs excision.

For the *ferritin 1*-silencing study, the method was the same but using 2 tick feeding chambers fixed on an *E. canis*-infected dog to respectively feed two groups of 30 adult *R. sanguineus* females (*ferritin 1* dsRNA and elution buffer-inoculated control ticks), together with the same number of male ticks to stimulate co-feeding and copulation (217). Adult ticks were allowed to feed until detachment for SGs, OV and MG excision.

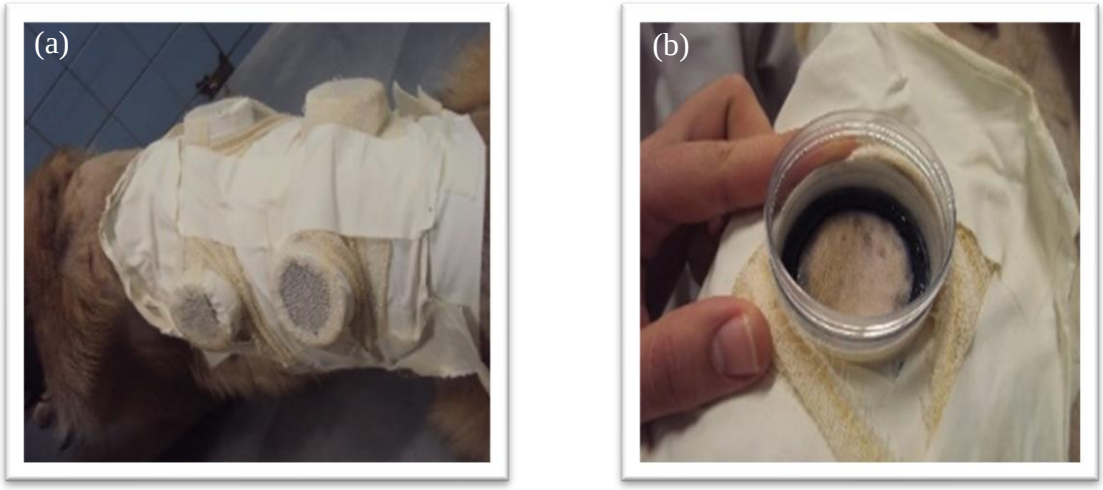

Figure 3. Tick feeding chambers placed on a German shepherd dog.
(a) Chamber distribution on the toracic and abdominal dorso-lateral region; **(b)** Open chamber exposing the dog skin where ticks will attach.

For the *putative serine carboxypeptidase* (*psc*; UniProtKB L7MH00), *putative prohibitin-like protein* (*prohib*; UniProtKB L7M5P4) and *putative heat shock-related protein* (*phsrp20*; UniProtKB L7M6Q5) silencing studies, 4 tick feeding chambers were attached an *E. canis*-infected dog 12 days *post*-inoculation. The day after, approximately 300 unfed *R. sanguineus* nymphs for each target gene (*psc, prohib* and *phsrp20* dsRNA) and the for the control group (*β*-2-microglobulin - *β2m* dsRNA), were transferred to each chamber and allowed to feed until detachment. Engorged nymphs were the collected and

maintained under laboratory conditions, as described in section 2.2.1 to moult into adults for SGs excision.

2.2.5. Tick dissection and tissue excision

Prior to tissue excision, ticks were rinsed twice in distilled water intercalated with a wash with 75% (v/v) ethanol. SGs (Figure 4), OV and MG were dissected with the aid of forceps and scalpels in ice-cold PBS, under a stereomicroscope at 4x magnification (Motic SMZ-171B; Motic, Hong Kong, China) or an Olympus SZX7 stereomicroscope (Olympus). Tissues were stored either in RNA*later* (Ambion, Texas, USA) at -20ºC, for RNA and DNA extraction, or the appropriate solutions for histological and histochemistry analysis.

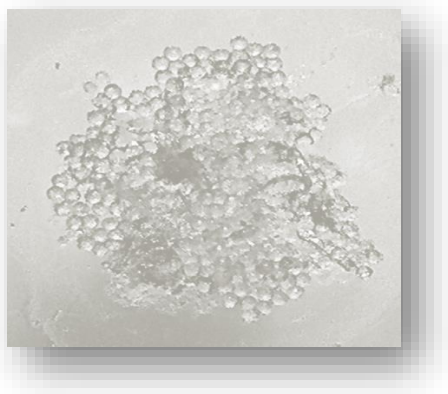

Figure 4. *Rhipicephalus sanguineus* salivary gland.
Image at 4x magnification (PBS; pH 7.4; Motic SMZ-171; Motic, Hong Kong, China).

2.3. Tick cell lines and tick-borne pathogens

2.3.1. *Ixodes scapularis* IDE8 cell line

The *I. scapularis* embryo-derived cell line IDE8 (223) was provided by Dr Lesley Bell-Sakyi from the Tick Cell Biobank – Institute of Infection and Global Health at The University of Liverpool, United Kingdom (UK), under a Material Transfer Agreement (MTA). IDE8 cells were grown at 32ºC in ambient air, in sealed flat-sided tubes (Nunc®) or 25 cm^2 flasks (Nunc®) with 2.2 ml or 5 ml of Leibovitz L-15B medium (224),

respectively. L-15B medium (Gibco®, ThermoFisher Scientific) was supplemented with 5% FBS (GE Healthcare Europe, Carnaxide, Portugal), 0.1% of bovine lipoprotein (MP Biomedicals, California USA), 10% tryptose phosphate broth (TPB; MP Biomedicals), 2 mM L-glutamine (Sigma–Aldrich) and antibiotics (100 U/ml penicillin, 100 µg/ml streptomycin; Lonza). Medium pH was adjusted to approximately 6.5. Medium was changed once weekly by removal and replacement of between 50% and 80% of the medium volume. Cells were subcultured when the monolayer was 100% confluent. Briefly, 1.5 ml of culture medium was removed, 3.7 ml of fresh medium was added, the cells resuspended, and 2.2 ml were transferred to a new tube (1:1 ratio parental: new culture). For the 25 cm^2 flasks, 3 ml of culture medium was removed, and 8 ml of fresh medium was added. Cells were resuspended, and 5 ml were transferred into a new flask.

The RSE8 cell line, derived from the *E. canis* natural vector *R. sanguineus*, has rarely been used in research for a couple of reasons. First, RSE8 cells present a heterogeneous morphology that varies from very small round and fusiform shaped cells with long filamentous protrusions to large vacuolated cells with granulated cytoplasm, and they normally grow as both individual cells and clumps (personal observation; unpublished data). This is a cell line difficult to growth in a consistent and robust way, which represents a problem in generating enough cell cultures to carry out reproducible studies. Secondly, the propagation of *E. canis* in this cell line it is possible but challenging as described in the literature (225, 226). Thus, since the main purpose of this study was to study gene expression and the effect of gene silencing on *E. canis* acquisition, invasion and multiplication, we have selected IDE8 cells once they are easier to maintain in cell culture, even when cultured in different culture media such as L-15B or *E. canis* medium (ECM) and different containers (flat-sided tubes, flasks or 24-well plates). IDE8 have a more consistent morphology, when compared with RSE8 and grow in monolayers as in Figure 5 – (a) and (b).

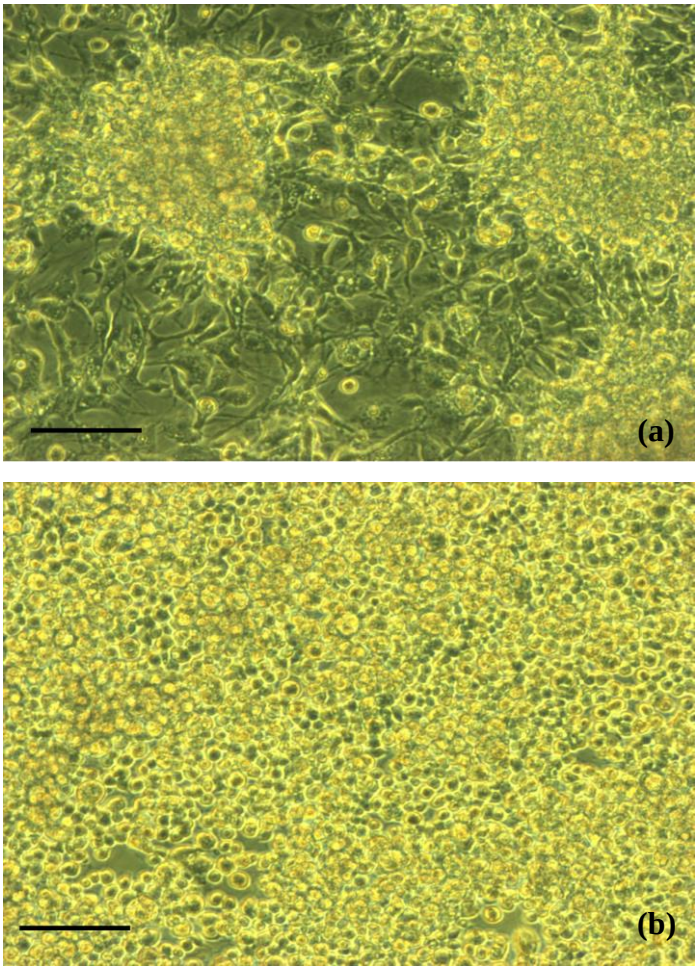

Figure 5. Live phase contrast images of tick cell lines.
(a) *Rhipicephalus sanguineus* cell line RSE8 (L-15/L-15B medium, passage 18); **(b)** *Ixodes scapularis* cell line IDE8 (L-15B medium, passage 83); Images were taken using a Zeiss AxioObserver D1 inverted microscope with Zeiss AxioCam ICc1 X and Zeiss Axiovision software; x10 objective (Zeiss, Jena, Germany); Scale bar represents 100 µm. Images obtained by Ferrolho (2013), at The Pirbright Institute, UK.

2.3.2. *Ehrlichia canis* strain and cultivation

The *E. canis* strain Spain 105 was provided by Dr Erich Zweygarth as growing cultures of infected IDE8 cells to Dr Lesley Bell-Sakyi (Tick Cell Biobank, The University of Liverpool, UK). This strain was isolated from a blood sample from an asymptomatic Spanish dog with a chronic infection, which had been imported from Spain to Germany (E. Zweygarth, personal communication). At the Tick Cell Biobank, *E. canis*-infected cell line IDE8 was grown at 32ºC in ambient air in L-15B (Gibco®) additionally supplemented with 1 M HEPES and 0.1% sodium bicarbonate ($NaHCO_3$), and without

antibiotics. *Ehrlichia canis* is sensitive streptomycin in culture media (E. Zweygarth, personal communication). This complete medium was designated ECM. The medium was changed twice weekly. When between 20 and 80% of the cells were infected, cells were harvested by scraping or by pipetting. A 0.5-2.0 ml aliquot of infected cell suspension was then transferred into uninfected cells. Immediately before the subculture, the uninfected culture medium was replaced by medium without antibiotics.

2.3.3. Bacterial semi-purification

When between 50 and 100% of the cells were infected, cells were harvested; the cell suspension was transferred to a 50 ml centrifuge tube (Corning disposable 50 ml centrifuge tubes; Sigma-Aldrich) and centrifuged at room temperature (RT) for 5 min at 200 x *g*. The supernatant was discarded, and the cell pellet was resuspended in 500 µl of trypsin (500 µg/ml in PBS) and incubated for 20 min at 37ºC. The original volume was restored by adding ECM; the cell suspension was gently mixed and transferred to a bijou (Sterilin™ 7 ml Polystyrene Bijou Containers; ThermoFisher Scientific). Cell suspension was aspirated up and down 10 times with a 5- or 10 ml syringe (B. Braun, Taunus, Germany) and a bent 26G needle (B. Braun) to mechanically rupture the cells and release the intracellular bacteria. The resultant suspension was transferred to a 50 ml centrifuge tube (Sigma-Aldrich) and centrifuged at RT for 5 min at 1500 x *g*. Supernatant containing cell-free bacteria was collected and aliquots were added to uninfected cell cultures. Presence of cell-free bacteria and subsequent *E. canis* growth were monitored by microscopic examination of Giemsa-stained cytocentrifuge smears (Section 2.9).

2.4. Nucleic acid and protein analysis

2.4.1. Sequence resources and alignments

Nucleotide, a.a. and protein sequences from ticks and TBPs were accessed from several internet-based genome browsers and sequence databases, including the UniProt Knowledgebase database (UniProtKB, http://www.UniProt.org/), the National Centre for Biotechnology Information (NCBI, https://www.ncbi.nlm.nih.gov) and Vector Base (https://vectorbase.org/vectorbase/app).

The TSA: *Rhipicephalus sanguineus* RS-75 mRNA sequence (GenBank accession nr. EZ406186.1) used for the *ferritin 1*-silencing study was obtained from a published *R. sanguineus* s.l. SG transcriptome database (227).

Alignments of multiple nucleotide sequences were carried to determine sequence similarity using the Basic Local Alignment Search Tool from NCBI (BLAST; http://blast.ncbi.nlm.nih.gov/Blast.cgi), with the integrated Needleman-Wunsch algorithm.

2.4.2. Primer design and optimisation

Primers used to amplify gDNA or complementary DNA (cDNA) templates by PCR or qPCR were designed using the Primer3 platform (v.0.4.0; https://bioinfo.ut.ee/primer3-0.4.0/).

The specificity of primer sequences was determined with the Primer-BLAST tool from NCBI (https://www.ncbi.nlm.nih.gov/tools/primer-blast/) or against the sequences deposited in the Vector Base database (https://www.vectorbase.org/blast).

All primers and probes were ordered from STAB VIDA (STAB VIDA, Lisbon, Portugal), reconstituted in RNase-free water (Sigma-Aldrich) to a 10 mM working stock and stored at -20ºC for further use.

Primer conditions were PCR-optimised using an increasing temperature gradient from 55 to 63ºC, and testing different primer final concentrations: 0.2 μM, 0.4 μM, 0.5 μM, 0.6 μM, 0.8 μM, 1 μM and 1.2 μM. Primer specificity was confirmed by the presence of a single band with the approximate amplicon size, on 1.2% agarose gel, by the absence primer dimers, and by a single peak in the Melting temperature (T_m) in qPCR.

The primers sequences used in this work and their PCR conditions are provided in Supplementary Table 1, except the ones retrieved from the literature in which the conditions were the ones published.

The primer pair *ferritin_T7_forward* and *ferritin_T7_reverse* for dsRNA synthesis was designed based on the TSA: *Rhipicephalus sanguineus* RS-75 mRNA sequence (GenBank accession nr. EZ406186.1) (227). For gene expression analysis by qPCR, the primer pair *ferritin_forward* and *ferritin_reverse* was designed based on the sequence *Rhipicephalus sanguineus* ferritin (Fer) mRNA, complete cds (GenBank accession nr. AY277907).

The primer pair *psc_IDE8_forward* and *psc_IDE8_reverse* was designed based on the sequence *Ixodes scapularis* conserved hypothetical protein, mRNA (GenBank accession nr. XM_002414145.1); *prohib_ IDE8_forward* and *prohib_IDE8 _reverse* primers were designed based on the sequence *Rhipicephalus pulchellus* RpIx75-674327 mRNA sequence (GenBank accession nr. GACK01005659.1); and *phsrp20_IDE8_forward* and *phsrp20_IDE8_reverse* primers were designed based on the sequence *Ixodes scapularis* small heat shock protein, putative, mRNA (GenBank accession nr. XM_002416230).

The sequence of *psc_RS_forward* and *psc_RS_reverse* primers was designed based on the TSA: *Rhipicephalus pulchellus* RpIx75-906737 mRNA sequence (ENA - GACK01002570); *imp_RS_forward* and *imp_RS_reverse* primers based on the *Rhipicephalus pulchellus* RpIx75-903092 mRNA sequence (ENA - GACK01006966.1); and the *phsrp20_RS_forward* and *phsrp20_RS_reverse* primers were designed based on the *Ixodes scapularis* small heat shock protein mRNA sequence (GenBank accession nr. XM_002416230). Sequences for *prohib_ RS_forward* and *prohib_RS _reverse* primers were the same as the one described for IDE8 cells, due to the successful amplification of the correct fragment in preliminary studies.

The primers used to synthesise dsRNA were designed based on the publicly available sequences for each gene, described above, aiming to PCR-amplify a fragment with approximately 400 base pairs (bp). The T7 promoter sequence was added to these primers in the 5′end (5'-TAATACGACTCACTATAGGGAGA-3'). The primer pairs *prohib_RS_T7_forward* and *reverse* and *phsrp20_RS_T7_forward* and *reverse* were the same as the ones to use in IDE8 cells, due to the successful amplification of the correct fragment in preliminary studies.

Other primer sequences used in the study were previously reported, including the ones for tick *β-actin*, *β-tubulin* and *elf* (228), *18S* rRNA (229) and *16S* rDNA (230), and for *E. canis dsb* (133) and *E. canis 16S* rRNA (118, 134).

2.4.3. RNA extraction

Total RNA was extracted from SGs and MG with TRI Reagent® Solution (Sigma-Aldrich), according to the manufacturer's described protocol for tissue samples with small modifications. Briefly, tissues were transferred from the RNA*later* solution (Ambion) to 150 µl of TRI Reagent® Solution (Sigma-Aldrich) and homogenised with a mortar and a pestle (VWR, Carnaxide, Portugal). After an incubation of 5 min at RT, 30 µl of chloroform was added to each sample, the suspension mixed thoroughly by shaking for at least 15 sec and incubated for 15 min at RT. Suspensions were centrifuged for 15 min at 12000 x *g* at 4ºC. The aqueous phase containing the RNA (colourless top layer) was transferred into a new microcentrifuge tube and 75 µl of isopropanol was added for RNA precipitation. Samples were vortexed at moderate speed for 10 sec, and then incubated for 10 min at RT, followed by a centrifugation at 12000 x *g* for 10 min at 4ºC. To wash the RNA pellets, the supernatant was carefully discarded, and the pellet resuspended with 150 µl of 75% ethanol. Samples were vortexed and centrifuged for 5 min at 7500 x *g* at 4ºC. The ethanol was removed, and the pellet air dried for at least 30 min. RNA was dissolved by resuspending the pellet in 30 µl of RNase-free water (Sigma-Aldrich), pipetting up and down, followed by an incubation in a heat block at 60ºC for 15 min. RNA was stored at -80ºC for further use.

Total RNA was extracted from IDE8 cells with TRIzol™ Reagent (ThermoFisher Scientific), according to the manufacturer's protocol for cells grown in suspension with minor modifications. Briefly, cells were harvested, centrifuged at 300 x *g* for 5 min and the supernatant discarded. To lyse the cells, the pellet was resuspended in 400 µl of TRIzol™ Reagent (ThermoFisher Scientific) and homogenised by pipetting up and down several times. The homogenate was incubated at RT for 5 min. One hundred µl of chloroform was added, the suspension mixed thoroughly by shaking and incubated for 2-3 min at RT. The suspension was centrifuged for 15 min at 12000 x *g* at 4ºC. The aqueous

phase containing the RNA was transferred into a new microcentrifuge tube and 200 µl of isopropanol was added for RNA precipitation. The sample was incubated for 10 min at 4ºC, followed by a centrifugation at 12000 x *g* at 4ºC for 10 min. To wash the RNA, the supernatant was discarded, and the pellet resuspended with 400 µl of 75% ethanol. The sample was vortexed briefly and then centrifuged for 5 min at 7500 x *g* at 4ºC. The supernatant was discarded, and the pellet air dried for at least 30 min. RNA was solubilised resuspending the pellet in 35 µl of RNase-free water (Sigma-Aldrich), pipetting up and down, followed by an incubation in a heat block at 60ºC for 15 min. RNA was stored at -80ºC for further use.

2.4.4. DNA extraction

gDNA was extracted from SG and MG with TRI Reagent® Solution (Sigma-Aldrich), according to the manufacturer's described protocol for tissue samples with small modifications. Briefly, DNA present in the interphase and organic phase (Section 2.4.3.) was precipitated by adding 120 µl of 100% ethanol. Samples were mixed by inversion, incubated at RT for 3 min and them centrifuged at 2000 x *g* for 5 min at 4ºC. The supernatant was removed, and the DNA pellet washed twice in with 400 µl of 0.1 M trisodium citrate - 10% ethanol solution. During each wash, the DNA pellet was allowed to stand on the mixer, with gentle shaking, for at least 30 min. Samples were centrifuged at 2000 x *g* for 5 min at 4ºC. The DNA pellet was resuspended in 600 µl of 75% ethanol and incubated for 20 min at RT. The DNA pellet was air dried and dissolved in 30 µl of 8 mM sodium hydroxide (NaOH) with repeated pipetting. DNA was stored at -20ºC for further use.

For the SGs used as samples for the proteomic analysis, gDNA was extracted using the All-in-One Purification Kit (Norgen Biotek Corporation, Ontario, Canada), according to the protocol for described by the manufacturer with some modifications. Prior to DNA extraction, RNA had to be eluted as follows: tissues were transferred from the RNA*later* solution (Ambion) to 350 µl of Buffer SK lysis solution with 10% β-mercaptoethanol (ThermoFisher Scientific) and homogenised with a mortar and a pestle (VWR). Three hundred and fifty µl of 100% ethanol (Sigma-Aldrich) was added to the lysate, the suspension transferred to a provided column and centrifuged at 4000 x *g* for 1 min at RT.

The flowthrough was collected to a microcentrifuge tube for subsequent protein purification and stored at -20ºC. The column was then washed with 400 µl of Wash Solution A, centrifuged at 14000 x *g* for 1 min at RT and the flowthrough discarded. A second wash was conducted, and the column centrifuged at 14000 x *g* for 2 min at RT to dry the membrane, discarding the flowthrough. RNA was eluted into a microcentrifuge tube by adding 20 µl of the Elution Solution A to the centre of the spin column membrane and centrifuging at 14000 x *g* for 2 min at RT. For gDNA extraction, the above column was transferred to new microcentrifuge tube, 500 µl of Wash Solution EL was added and the column centrifuged at 14000 x *g* for 2 min at RT. The flowthrough was discarded, and the column centrifuged repeating the conditions. DNA was eluted into a microcentrifuge tube by adding 20 µl of the Elution Solution F to the centre of the spin column membrane and centrifuging at 200 x *g* for 2 min. DNA was stored at -20ºC for downstream application.

2.4.5. Protein extraction

Protein extraction from the SGs was carried out using the All-in-One Purification Kit (Norgen Biotek Corporation), according to the manufacturer's instructions with some modifications. The flowthrough obtained after gDNA extraction, stored at -20ºC (Section 2.4.4), contained the proteins to be extracted. Six hundred µl of RNase-free water (Sigma-Aldrich) and 48 µl of Binding Buffer A were added to 600 µl of the flowthrough, and the suspension mixed thoroughly by vortexing. The suspension was then re-loaded onto the used column to bind the proteins, followed by centrifugation at 5000 x *g* for 2 min at RT. Five hundred µl of Wash Solution C was added and the column centrifuged at 5200 x *g* for 2 min at 4ºC. The flowthrough was discarded, and the column centrifuged using the same conditions to dry the membrane. Finally, the purified proteins were eluted into a microcentrifuge tube by adding 50 µl of Elution Buffer C to the column, followed by centrifugation at 5200 x *g* for 2 min at 4ºC and neutralisation with 4.65 µl of Protein Neutraliser. Proteins were precipitated with 200 µl of ice-cold acetone during a 15 min incubation period on ice, followed by a 10 min centrifugation at 14000 x *g* at 4ºC. The supernatant was removed, and the pellet was stored in 100 µl of acetone at -20ºC for further use.

For proteomic data validation, protein extraction from the SGs was carried out with TRI Reagent® Solution (Sigma-Aldrich), according to the manufacturer's instructions. Briefly, proteins of the supernatant resultant from gDNA extraction (2.4.4.) were precipitated with 200 µl of isopropanol during a 10 min incubation period at RT. Samples were centrifuged at 12000 x *g* for 10 min at 4ºC and the supernatant discarded. Pellets were washed three times with 300 µl of 0.3 M guanidine hydrochloride - 95% ethanol solution, being centrifuged at 7500 x *g* for 5 min at 8°C between each wash. During each wash, samples were left in the wash solution for 20 min at RT. After, 2 ml of 100% ethanol was added, the protein pellet vortexed and incubated for 20 min at RT. Finally, a last centrifugation was carried out at 7500 x *g* for 5 min at 8°C and the pellets air-dried. Pellets were dissolved in 20 µl sodium dodecyl sulphate (SDS) buffer.

2.4.6. Nucleic acid and protein yield and quality

Concentration and purity of total RNA extracted from SGs and MG was determined by spectrophotometry using a NanoDrop ND-1000 (ThermoFisher Scientific). After setting the equipment for RNA samples, 1 µl of a blank solution (RNase-free water; Sigma-Aldrich) was added to the equipment well for calibration. Measurements were carried out with 1 µl of each sample. For spectrophotometry the concentration is calculated as the absorbance of a 1 µl sample at 260 nm that equates to 1 optical density (OD) unit = 44 µg/ml RNA. RNA concentration is automatically calculated in ng/µl, based on the Beer-Lambert equation. RNA purity is also calculated as the ratio of absorbance at 260 nm and 280 nm (A_{260}/A_{280}). For pure RNA, this value should be in the range of 2.

Concentration of total RNA generated from IDE8 cells was determined by fluorescence using the Qubit 4.0 Fluorometer (ThermoFisher Scientific), according to the manufacturer's protocol with the commercial kit Qubit™ RNA HS Assay (ThermoFisher Scientific). This method detects fluorescent dyes that are specific to the target of interest (RNA, DNA or protein), even with very low concentrations. All reagents were set at RT. To calibrate the fluorometer, two standards were prepared by adding a working solution to Qubit™ standards, in 0.5 ml thin-wall clear tubes. The working solution was prepared by diluting the Qubit™ RNA HS reagent in Qubit RNA HS buffer using the ratio 1:200, respectively. Then, 190 µl of working solution was added to 10 µl of each Qubit™

standard tube, for a final volume of 200 µl. RNA samples were prepared by adding 5 µl of each sample to 195 µl of working solution, vortexing for 2-3 sec followed by an incubation of 2 min at RT. The samples were then read following the equipment instructions for "RNA" samples.

Concentration and purity of gDNA extracted from SGs and MG, of purified PCR-products and dsRNA was also accessed by spectrophotometry using a NanoDrop ND-1000 (ThermoFisher Scientific), following the same methodology described for total RNA selecting "DNA" samples. Here, the equipment calibration was made with NaOH or Elution Solution F (Norgen Biotek Corporation) for gDNA, Elution Buffer for purified PCR-products or reaction mix without template for dsRNA. For double-stranded DNA (dsDNA) templates 1 OD = 50 µg/ml DNA. DNA purity is also calculated using the $A_{260/280}$ and, if pure, should be 1.8.

Protein concentration of the samples used for proteomic data validation was measured by spectrophotometry using a NanoDrop ND-1000 (ThermoFisher Scientific), as described. After setting the equipment for "Protein" samples, the equipment calibration was made with 1 µl of SDS buffer followed by sample measurement.

Concentration of the peptide synthesised based on the small putative heat shock-related protein a.a. sequence (pPHSRP20; UniProtKB L7M6Q5) was determined by fluorescence using the Qubit 4.0 Fluorometer (ThermoFisher Scientific), according to the manufacturer's protocol. Briefly, a standard curve was prepared to calibrate the equipment using three standards from the Qubit™ Protein Assay kit, with concentrations ranging from 0 ng/µl to 400 ng/µl. The working solution was prepared by diluting the Qubit™ Protein Reagent in Qubit™ Protein Buffer using the ratio 1:200, respectively, in 0.5 ml thin-wall clear tubes. The working solution was then added to each assay tube to make up a final volume of 200 µl. An incubation period of 15 min at RT was carried out after adding the 10 µl and 20 µl of the pPHSRP20 sample to the assay tubes and vortexing for 3 sec. The samples were then read using the option "Proteins".

2.4.7. Complementary DNA synthesis

cDNA was synthesised from extracted total RNA samples using the iScript™ cDNA Synthesis Kit (Bio-Rad, California, USA), as follows. Before cDNA synthesis, RNA concentrations were normalised to a final concentration between 50 and 100 ng/µl. Twenty µl reaction mixes were prepared with 4 µl of 5x iScript Reaction Mix, 1 µl of iScript Reverse Transcriptase, between 100 µg and 1 µg of total RNA and RNase-free water (Sigma-Aldrich) up to the final volume. The mixture was heated at 25ºC for 5 min for priming, followed by a reverse transcription (RTr) at 46ºC for 20 min with a final RTr inactivation of 1 min at 95ºC in a T100 thermal cycler (Bio-Rad). cDNA was stored at -20ºC for further use.

2.4.8. Polymerase chain reaction

All PCR thermal cycling reactions were carried out in a T100 thermal cycler (T100 thermal cycler; Bio-Rad) and for each reaction negative controls were prepared with no template.

To detect false negative results due to PCR inhibition and to validate the efficiency of the gDNA extraction, *18S* rRNA amplicons were PCR-amplified with the primer pair *tick-sense* and *tick-antisense*. These primers amplify a 500 bp fragment and were designed based on ticks *18S* rRNA (*Rhipicephalus, Hyalomma, Haemophysalis, Dermacentor, Ixodes* and *Boophilus*), as described elsewhere (229). Briefly, 25 µl reactions were prepared with 12.5 µl Supreme NZYTaq II 2x Green Master Mix (NZYTech, Lisbon, Portugal), 1 µM of forward and reverse primers, 3 µl of gDNA and RNase-free water (Sigma-Aldrich) up to the final volume. PCR was carried out with a thermal cycling profile of 95ºC for 5 min, and 36 cycles of 94ºC for 45 sec, 58ºC for 45 sec and 72ºC for 45 sec, followed by 72ºC extension for 4 min and a 4ºC hold. Negative controls were prepared with no template.

PCR reactions were carried out to generate DNA templates for dsRNA synthesis. For each gene, 50 µl reactions were prepared with 25 µl of NZYProof 2x Green Master Mix Supreme (NZYTech), *x* µM of each primer with T7 promotor (Supplementary Table 1), 2 µl of cDNA and RNase-free water (Sigma-Aldrich) to the final volume. The thermal

cycling profile was 95ºC for 3 min, and 40 cycles of 95ºC for 30 sec, *x*ºC (Supplementary Table 1) for 30 sec and 72ºC for 60 sec, followed by a 72ºC final extension for 5 min and a 4ºC hold.

The presence of *E. canis* DNA in the SGs, used for transcriptomic data validation, was determined by nested-PCR to amplify the *16S rRNA* gene, as previously described (118). The primer pair ECC and ECB was used for the first reaction, to detect all *Ehrlichia* spp., and the primer pair ECAN5 and HE3 for the second reaction, for *E. canis* specific amplification. Briefly, 25 µl PCR reactions were prepared with 12.5 µl of Supreme NZYTaq II 2x Green Master Mix (NZYTech), 0.5 µM of each primer, 5 µl of SGs gDNA for the first reaction and 1 µl of PCR product of the first reaction for the second PCR, and RNase-free water (Sigma-Aldrich) to the final volume. The thermocycling conditions were set for both reactions as follows: initial denaturation for 5 min at 94ºC; 39 cycles of denaturation at 94ºC for 1 min, annealing at 60ºC for the first reaction and 55ºC for the second reaction for 1 min, followed by an extension at 72ºC for 1 min; and a final extension at 72ºC for 5 min. A positive control was prepared with *E. canis* Jaboticabal strain purified DNA.

2.4.9. Real time quantitative polymerase chain reaction

All qPCR thermal cycling reactions were carried out in a CFX96 Touch™ Real-Time PCR Detection System (Bio-Rad), using SYBR® Green or TaqMan™ probes. All reactions were loaded in triplicate into 96-well plates (Bioline), including triplicate negative controls with no template.

For qPCR to determine gene expression, 10 µl reactions were prepared with 5 µl of iTaq™ Universal SYBR® Green Supermix (Bio-Rad), *x* µM of each specific primer (Supplementary Table 1), 2 µl of gDNA or cDNA and RNase-free water (Sigma-Aldrich) to the final volume. qPCR was carried out with a thermal cycling profile of 95°C for 3 min, and 40 cycles of 95°C for 10 sec and *x*°C (Supplementary Table 1) for 45 sec. A Melting curve was produced (55ºC-95ºC; 0.5ºC/s melt rates) at the end of the amplification cycles, to ensure reaction specificity. Standard curves were prepared with

10-fold serial dilutions to determine reaction efficiency with gDNA or cDNA of samples generated from *R. sanguineus* SGs or MG, or IDE8 cells.

The Melting curve analysis allows the evaluation of the dissociation characteristics of a specific dsDNA during heating. The intercalating dyes used in qPCR, such as SYBR® Green, only emit fluorescence when they are bound to dsDNA. If the DNA is in the single-stranded (ssDNA) form or if the dye is free in the reaction solution, these dyes do not fluoresce. As the temperature of the sample is incrementally increased, the dsDNA denatures and converts in ssDNA with subsequent dye dissociation and fluorescence decrease. When the temperature at which 50% of the DNA is denatured, there is a change in slope of this curve plotted as a function of temperature to obtain the melt curve. The temperature at which this occurs is known as the T_m.

TaqMan™ qPCR was carried out to determine the presence of *E. canis* DNA targeting the *16S* rRNA (134) or the *dsb* gene (133). For *16S* rRNA amplification, 10 µl reactions were prepared with 5 µl of 2x PCR Mix SensiFAST™ Probe Low-ROX (Bioline), 0.2 µM of each primer, 0.2 µM of TaqMan Probe, 20 - 100 ng of gDNA and RNase-free water (Sigma-Aldrich) to make up to the final volume. The qPCR was carried out with a thermal cycling profile of 95ºC for 15 min, and 45 cycles of 93ºC for 10 sec and 61ºC for 30 sec. For *dsb* amplification, 10 µl reactions were prepared with 5 µl of Xpert Fast Probe 2x Mastermix PCR Mix (GRiSP Research Solutions, Porto, Portugal), 0.8 µM of each primer, 0.8 µM of TaqMan probe, 2 µl of cDNA and RNase-free water (Sigma-Aldrich) to make up to the final volume. The qPCR was carried out with a thermal cycling profile of 95ºC for 5 min, and 40 cycles of 95ºC for 10 sec and 60ºC for 30 sec. Positive controls were prepared with *E. canis* Jaboticabal strain purified DNA. Reaction efficiency was determined using 10-fold serial dilutions of the positive control.

Real-time PCR data was analysed based on the minimum information for publication of qPCR experiments - MIQE (231) and by the CFX Manager™ Software (Bio-Rad). Different reference tick genes were tested and used, including *β-actin, β-tubulin* and *elf* (228) and *16S* rDNA (230). For each biological system, the expression stability value (M-value; M< 1) of the reference genes was calculated through the *geNorm* algorithm (232)

incorporated in the CFX Manager™ Software (Bio-Rad). The suitability of reference genes can be classified in three categories, according to the algorithm: *(i)* ideal - this group of reference genes is stable and represents minimal variation across the samples tested. Any gene(s) from this group can be used as a reference gene(s) for the study; *(ii)* acceptable - this group of reference genes is not ideally stable and represents moderate variation across the samples tested. Where possible, it should be used at least three or more of these reference genes. If ideal reference genes are present within the study, these should be chosen over any acceptable gene in the analysis; *(iii)* unstable - this group of reference genes is unstable and represents excessive variation across the samples tested. It is recommended to exclude these genes from use as reference genes.

The threshold line values for each gene were manually set (Supplementary Table 2). Relative normalised gene expression was automatically determined by the CFX Manager™ Software (Bio-Rad) by the ΔΔCq (233) and the Pfaff (234) methods. From the normalised expression values, the outliers were singled out by the Tukey method (235).

2.4.10. Agarose gel electrophoresis

PCR and qPCR products, as well as synthesised dsRNA, were visualised on a 1.2% agarose gel using a UV transilluminator. Briefly, 1.2 g of agarose (NZYTech) was added to 100 ml of 0.5 x Tris-acetate-EDTA buffer (TAE; 20 mM Tris, 20 mM boric acid, 0.5 mM EDTA, pH 7.2) and heated in a microwave oven for 2 to 3 min, to dissolve the agarose powder. Melted gels were stained with SYBR® Safe DNA Gel Stain (ThermoFisher Scientific) with a dilution of 1:10.000 and allowed to solidify. Five to 15 µl of each sample was loaded directly into the wells and different molecular weight markers were used in the lane M, depending on the fragment size. Gels were run at 100 V for 30 to 45 min (Horizontal Electrophoresis System tray, Bio-Rad).

2.4.11. PCR product and dsRNA purification and sequencing

PCR and qPCR products that presented the expected molecular size were purified using the NZYGelpure Purification Kit (NZYTech), according to the manufacturer's instructions for DNA purification from an agarose gel or for PCR clean-up. Briefly, each

excised agarose gel slice was weighted and transferred into a 1.5 ml microcentrifuge tube. Three hundred µl of Binding Buffer was added for each 100 µl of gel weight and incubated at 60ºC in a heating block for 10 min, shaking occasionally to dissolve the gel slice. Then up to 700 µl of this solution was transferred to a NZYTech spin column placed into a Collection tube and centrifuged at 12 000 x *g* for 15 sec at RT. Flowthrough was discarded and this step was repeated when the sample volume was higher than 700 µl. Column membranes were washed by adding 500 µl of Wash Buffer and centrifuging at 12 000 x *g* for 1 min at RT. A second wash was performed by adding 600 µl of Wash Buffer and centrifuging using the same conditions. Flowthrough was discarded after each wash and the spin column was placed into a clean 1.5 ml microcentrifuge tube. The DNA was eluted by adding 30 µl of Elution Buffer to the centre of the column, followed by an incubation of 1 min at RT and final centrifugation at 12 000 x *g* for 1 min.

For PCR clean-up, the PCR-product was transferred to a 1.5 ml microcentrifuge tube, five volumes of Binding Buffer were added, and the mixture mixed by inverting a few times. After a centrifugation at 12 000 x *g* for 15 sec at RT, the mixture transferred to a NZYTech spin column placed into a Collection tube and centrifuged at 12 000 x *g* for 30 sec at RT. Membranes were washed by adding 600 µl of Wash Buffer and centrifuging at 12 000 x *g* for 1 min at RT. The flow-through was discarded followed by a second centrifugations to dry the membrane. The DNA was eluted by adding 30 to 50 µl of Elution Buffer to the centre of the column, followed by an incubation of 1 min at RT and final centrifugation at 12 000 x *g* for 1 min.

PCR and qPCR purified products were sent for sequencing to confirm the presence of the target sequence by the Sanger method at STAB VIDA (STAB VIDA). Samples were sent using the You Tube It service (STAB VIDA) with 10 µl of purified DNA (≥ 20 ng/µl) mixed with 3 µl of the forward or reverse PCR primer (10 ρmol/µl). Obtained sequences were trimmed and analysed as described in Section 2.4.1.

2.4.12. Protein extract preparation

For the proteomic study, protein extract preparation was carried out at the Proteomics Unit Centre for Neuroscience and Cell Biology, Universidade de Coimbra, Portugal.

Individual samples of SGs proteins, stored in acetone at -20ºC (Section 2.4.5), were centrifuged at 20 000 x *g* for 20 min at 4ºC, the supernatant was discarded and 20 µl of SDS buffer (1.7% SDS and 100 mM dithiothreitol (DTT) in 50 mM Tris buffer; pH 6.8) were added to each positive sample and 50 µl to each negative sample. Solubilisation of the pellet was performed by ultrasonication using a cuphorn device (VCX 750-Watt Ultrasonic Processor; Sonics Newton, USA) at 20% amplitude for 2 min. The protein content was assessed by Fourier-transform infrared spectroscopy using the Direct Detect® Infrared Spectrometer for Total Protein Quantitation (Merck, New Jersey, USA). Individual samples were then pooled in 3 pools of 15 SGs each, that constituted the group of *E. canis*-infected samples extracted from freshly moulted adult female *R. sanguineus* ticks fed on the experimentally infected dog; and 3 pools of 10 SGs each, that constituted the group of uninfected samples extracted from freshly moulted adult female *R. sanguineus* ticks fed on the naïve dog (Section 2.2.3). Each pool was precipitated with acetone, and independently processed and analysed by liquid chromatography - mass spectrometry (LC-MS). Briefly, six volumes of cold acetone were added to each pooled sample, then samples were kept at -80°C for at least 20 min and centrifuged at 20 000 x *g* for 20 min at 4°C. The resultant supernatant was discarded, and the pellet dissolved in 20 µl of SDS buffer to proceed to sodium dodecyl sulphate–polyacrylamide gel electrophoresis (SDS-PAGE) in the next Section.

2.4.13. SDS-PAGE and Western blot

SDS-PAGE was carried out with the protein extract that followed to proteomic data analysis. SDS-PAGE is a commonly used method to separate proteins by mass, usually performed to guarantee the integrity of the peptide after its solubilisation in water and to confirm its molecular weight. Following the precipitation and quantification of the samples, 2 µl of a 50% concentrated solution of glycerol (Sigma-Aldrich) with bromophenol blue (Sigma-Aldrich) were added to each sample. A volume of 1 µl of a recombinant protein (MBP-GFP fusion protein; Maltose-binding periplasmic protein combined with Green Fluorescent Protein) was added to each sample to act as an internal standard. Protein denaturation was achieved by boiling all the samples at 95°C for 5 min and 2 µl and 3 µl of acrylamide was added to the positive and negative samples, respectively, to induce protein alkylation. The total volume of each pool was then loaded

into a precast gel (4–20% Mini-Protean® TGX™ Gel, Bio-Rad), and the SDS-PAGE was partially run for 15 min at 110 V, as described elsewhere (236). When proteins were separated by the electric current, they were visualised within the gel by incubating the gel with Colloidal Coomassie Blue as previously described (237). The gel was allowed to stain for 1 h, and whenever necessary, more Coomassie powder was added. Once the desired staining was achieved, the gel was washed with distilled water.

For proteomic data validation, the representation of three proteins identified in the proteome as differentially represented by *E. canis* infection was investigated by SDS-PAGE followed by Western blot. The separation gel and the stacking gel were prepared by adding the reagents and respective amounts described in Supplementary Table 3. The separation gel was added to the cassette and once polymerized, Tetramethylethylenediamine (TEMED; BioChemica AppliChem, Darmstadt, Germany) and Adenosine 5'-Phosphosulfate kinase (APS; ThermoFisher Scientific) were added to the stacking gel, as these allow the gel to polymerize. The stacking gel was added on top of the polyacrylamide gel along with the comb. After gel polymerization, the cassette was transferred to an electrophoresis chamber (Bio-Rad) filled with running buffer consisting of 10x Tris-glycine-SDS Buffer diluted to 10:100 ratio in Milli-Q water. Five µl of the protein marker (NZYcolour protein marker II; NZYTech) was added on the first well and between 15 µl and 20 µl of total protein were loaded into each well of the 15% polyacrylamide gel with 5x SDS-PAGE sample loading buffer (NZYTech) in a 1:4 ratio with Laemmli 4x Loading Buffer (Sigma-Aldrich). After protein separation, a Western blot was carried out to transfer the proteins from the polyacrylamide gel onto a nitrocellulose membrane, to which they got ligated and immobilised. These membranes can be stained with different antibodies, allowing specific detection of proteins. Proteins transfer was carried out using the Mini Trans-Blot® Electrophoretic Transfer Cell (Bio-Rad). Transfer buffer was prepared with 3.03 g of Tris (Trizma base; Sigma-Aldrich), 14.4 g of glycine (PanReac AppliChem, Barcelona, Spain), 200 ml methanol (VWR) and distilled water to make up to 1 l. Before assembling the sandwich that goes in the transfer box (Bio-Rad), two fibber pads, four squares of filter paper and a 0.2 µm pure nitrocellulose membrane (Bio-Rad) were embedded in transfer buffer. Next, the polyacrylamide gel was placed against the membrane and then held between the filter

paper and the fibber pads. The cassette was closed and put in the buffer tank (Bio-Rad) with a magnet and an ice block. The tank was filled with transfer buffer and the proteins left to transfer at 30 V at 4ºC overnight with stirring. To guarantee the successful transfer, the nitrocellulose membrane was submerged in 0.2% Ponceau until the peptide was visible in different lanes. The membrane was then blocked for 1 h 30 min in 5% (w/v) non-fat dry milk (Bio-Rad), diluted in Tris-buffered saline complemented with 0.05% (v/v) Tween 20 (TBS-T; Sigma-Aldrich), with shaking in the dark. Three, 10 min washes in 0.05% TBS-T buffer were carried out with gentle mixing. The membrane was then incubated for 1 h 30 min with a specific dilution of the selected antibodies Prohibitin 2 (A-2) (sc-133094; Santa Cruz Biotechnology, Dallas, USA), MDH2 (1G12) (sc-293474; Santa Cruz Biotechnology) and PKAα/β/γ cat (B-4) (sc-36515; Santa Cruz Biotechnology) (Supplementary Table 4) in PBS containing 0.05% (v/v) Tween 20 (PBS-T; Sigma-Aldrich), with gentle agitation in the dark. Prohibitin 2 (A-2) is a mouse monoclonal IgG antibody raised against the a.a. 220-299 mapping at the C-terminus of Prohibitin 2 of human origin. MDH2 (1G12) is a mouse monoclonal antibody raised against a.a. 134-246 representing partial length MDH2 of human origin. PKAα/β/γ cat (B-4) is a mouse monoclonal antibody raised against a.a. 226-320 mapping near the C-terminus of PKAα cat of human origin. Five further 15 min washes in 0.05% PBS-T buffer were carried out to remove unbound antibody. The membrane was then incubated in a solution prepared with secondary antibody Anti-mouse polyvalent Ig (IgA, IgG and IgM - Alkaline Phosphatase conjugate (AP); Sigma-Aldrich), diluted 1:3000 in 0.05% PBS-T buffer. After incubating for 1 hour in the dark, the membrane was washed 5 times with 0.05% TBS-T buffer for 15 min for each wash with shaking at 1050 x *rpm*. Relative quantification of the protein bands from the Western blot nitrocellulose membranes was determined with ImageJ Software (Version 2.0.0). The quantification reflected the relative amounts, in pixel density, as a ratio of each target protein band in the *E. canis*-infected samples in comparison with uninfected samples.

SDS-PAGE was carried out with the synthesised pPHSRP20 as described above, to guarantee its integrity after solubilisation in water and to confirm its molecular weight, with a modification after the addition of the protein marker. After this step, between 7 µl and 15 µl of the peptide were added to the wells on a 1:1 ratio with Laemmli 4x Loading

Buffer (Sigma-Aldrich) and run for 2 h at 120 V. The gel was then put in 25 ml of BlueSafe (NZYTech) overnight to stain and then transferred to distilled water for 30 min to improve the contrast. A second SDS-PAGE was carried out with the pPHSRP20. followed by Western blot, with mouse sera obtained 9-weeks after the first immunisation (Section 2.8.3), following the above protocol with minor modifications. One μg of peptide was loaded in a 1:4 ratio with 5x SDS- PAGE sample loading buffer (NZYTech) for each well, and 1 ml of mouse blood serum was added to each membrane strip in a 1:15000 dilution in 0.05% PBS-T buffer as primary antibody.

2.4.14. Protein *in silico* analysis

Prediction of the topology of both α-helical and β-barrel transmembrane proteins and classification was carried out with TMHMM – 2.0 (CELLO v.2.5; http://cello.life.nctu.edu.tw/) (238, 239).

Signal peptide was analysed with the software SignalP-4.1 (SignalP-4.1; https://services.healthtech.dtu.dk/service.php?SignalP-4.1) (240).

Epitope position was predicted from the protein sequence using the Immune Epitope Database and Analysis Resource (IEDB; available at http://tools.iedb.org/bcell/), selecting the B cell epitope prediction (Bepipred Linear Epitope Prediction).

Protein solubility was predicted using the scaled solubility value (QuerySol) from the Protein-Sol (available at https://protein-sol.manchester.ac.uk/) (241).

Protein allergenicity was predicted with AllerTOP v.2.0 (available at https://www.ddg-pharmfac.net/AllerTOP/index.html).

Protein structure was predicted by homology modelling with the online tool SWISS-MODEL (https://swissmodel.expasy.org/) (242-246). Building a homology model includes four main steps: *(i)* identification of structural template, *(ii)* alignment of target sequence and template structure, *(iii)* model-building and *(iv)* model quality evaluation.

The network of predicted protein-protein interactions was investigated with STRING (v 11.5; https://string-db.org/), selecting a confidence interaction score of 0.900.

2.5. Transcriptome analysis

2.5.1. Complementary DNA libraries

Libraries preparation was performed at Unidad de Genómica – Fundación Parque Científico de Madrid, Spain. Total RNA from tick SGs (Section 2.4.3) was extracted from 18 samples, of which 2 pools of 4 SGs each constituted the group of uninfected SGs extracted from freshly moulted adult female *R. sanguineus* ticks fed on the naïve dog; and 2 pools of 5 SGs each composed the group of *E. canis*-infected SGs extracted from freshly moulted adult female *R. sanguineus* ticks fed on the experimentally infected dog (Section 2.2.3; Supplementary Table 5). Prior to cDNA library construction magnetic beads with oligo(dT) were used to enrich poly(A) mRNA from 1 µg of total RNA extracted from the SGs. Next, the purified mRNA was disrupted into short fragments, followed by purification and cDNA synthesis, using the Truseq Strand mRNA sample preparation kit (Illumina, California, USA), as instructed by the manufacturer. cDNA was subjected to end-repair and adenylation, then ligated with sequencing adapters. Suitable fragments of around 550 bp were purified by size selection protocol with AMPure XP Beads (Beckman Coulter, California, USA), and selected as templates for qPCR amplification with the Kappa Sybr Fast qPCR kit (ThermoFisher Scientific). The final library sizes and qualities were evaluated electrophoretically using an Agilent High Sensitivity DNA kit (Agilent Technologies, Santa Clara, USA), resulting in a fragment size ranging between 300 and 1300 bp.

2.5.2. RNA-sequencing

The cDNA library was sequenced using a HiSeq 2500 sequencer (Illumina) in rapid run mode. Cluster generation was performed, followed by 2 x 100 cycle sequencing reads separated by a paired-end turnaround. Image analysis was performed using the HiSeq control software version 1.8.4 (Illumina).

2.5.3. Bioinformatics analysis

Data was analysed at Era7 Bioinformatics- Parque Científico de Madrid, Spain. Quality analysis of the raw data was carried out with FASTQC tool (http://www.bioinformatics.babraham.ac.uk/projects/fastqc/). Illumina reads were pre-processed by right trimming where quality < Q30, left trimming of the first base and filtering out reads with Ns. For each of the four transcriptomes, three *de novo* assemblies were produced with hash length values (or *k*-mer) of 77, 79 and 81, using Oases assembler (0.2.01) (247). *De novo* assemblies were produced because a reference genome was not available in 2015. Transcript expression quantification was determined using the eXpress - Streaming quantification for high-throughput sequencing tool (https://pachterlab.github.io/eXpress/overview.html) (248). The annotation of each transcript was based on the BLAST results comparing the transcript to a database of reference proteins selected from the UniProtKB database (https://www.UniProt.org/UniProt/) from all the organisms belonging to the taxon "*Ixodidae*". A total of 80104 proteins were downloaded in August 2015 and used as reference proteins. A set of UniGenes was obtained for each sample. A UniGene is defined as a set of sequences that are probably transcribed from the same *locus*/gene; and the assignment of each transcript to a protein was based on the BLAST similarity. The functional annotation was conducted for each UniGene extracted from the UniProtKB proteins in which the read clustering process has been centred for this UniGene. To be able to compare the transcripts from the samples, these were clustered by protein in UniGenes and if two transcripts were annotated with the same protein, these were subsequently clustered in the same protein cluster (UniGene). This method allows the comparison of the protein cluster expression levels between two samples when the same protein cluster is present in both samples. This system also provides a set of sample-exclusive protein clusters specific for each sample. Further, the protein driven transcript clusters that resulted from the UniProtKB proteins were clustered by UniProtKB Reference Clusters (UniRef90) (249) with the UniProtKB retrieval tool (https://www.UniProtKB.org/uploadlists/)). The quantification for each UniRef90 cluster was calculated adding the quantification for each protein included in each UniRef90 cluster. Finally, Gene Ontology (GO) terms were assigned manually based on UniProtKB and associated databases. The raw data were deposited to the Sequence Read Archives

(SRA) of NCBI under the Bioproject accession nr. PRJNA362595, available since 19th of January 2017.

To compare the transcript expression data obtained in the RNA-seq study between uninfected and *E. canis*-infected SGs, Log2 fold-change was determined dividing each individual contig the number of reads of the infected samples by the number of reads of uninfected samples.

$$\textbf{Log2 fold-change } (\textbf{reads}_{\textbf{infected}}/\textbf{reads}_{\textbf{uninfected}})$$

2.6. Proteome analysis

2.6.1. In-gel digestion

In-gel digestion and liquid chromatography (LC) was carried out at the Proteomics Unit Centre for Neuroscience and Cell Biology, Universidade de Coimbra, Portugal. For the proteomic analysis, gel lanes with the protein extract were sliced into very small fractions with a scalpel, transferred into a 96-well plate (Bioline), and distained by adding a 50 mM ammonium bicarbonate solution (pH 7.5) with 30% acetonitrile (ACN), followed by an incubation period of 15 min shaking at 1050 x *rpm* (25°C) (Eppendorf ThermoMixer® C; Eppendorf, Hamburg, Germany). Three consecutive washes were carried out with 600 µl of distilled water, followed by a final incubation period of 15 min shaking at 1050 x *rpm* (25°C). Gel pieces were then dehydrated on Concentrator Plus/Vacufuge® Plus (Eppendorf) for 1 h at 60°C. To each dried gel band, 100 µl of trypsin (0.01 µg/µl solution in 10 mM ammonium bicarbonate; Thermo-Fisher Scientific) were added and left to incubate for 15 min at 4°C to rehydrate the gel pieces. One hundred µl of 10 mM ammonium bicarbonate were added to each well and in-gel digestion was carried out overnight at RT in the dark. After enzymatic digestion, the excess solution from gel pieces was collected to a low binding microcentrifuge tube (Eppendorf® LoBind, Eppendorf) and peptides were extracted from the gel pieces by sequential addition of three solutions with increasing percentage of acetonitrile (30%, 50%, and 98%) in 1% formic acid (FA). Immediately after the addition of 100 µl of each solution, the gel pieces were shaken at 1200 x *rpm* for 15 min (Eppendorf ThermoMixer® C; Eppendorf), and the solution

transferred to the tube containing the previous fraction. Peptide mixtures were dried by rotary evaporation under vacuum on a Concentrator Plus/Vacufuge® Plus (Eppendorf) for 2 hours at 60°C. After digestion, peptides were subjected to solid phase extraction with C18 sorbent (Bond Elut OMIX pipette tip; Agilent Technologies), according to the manufacturer's recommendations. Briefly, 100 µl a solution of 2% ACN 1% FA was added to each sample, followed by ultrasonication at 20% amplitude for 2 min (VCX 750-Watt Ultrasonic Processor; Sonics). Each column was firstly humidified with 200 µl of 50% ACN, and then equilibrated with 300 µl of 2% ACN 1% FA (mobile phase). Samples were loaded to each column and washed five times with 300 µl of the mobile phase. Four hundred µl of 70% ACN 0.1% FA was added to the flowthrough with the eluted peptides and the column discarded. Samples were dehydrated on a Concentrator Plus/Vacufuge® Plus (Eppendorf) for 2 hours at 60°C. Peptides where then solubilised in 30 µl of the mobile phase, aided by ultrasonication as described above. Samples were then centrifuged for 5 min at 14 100 x *g* and then ready for analysis by liquid chromatography with tandem mass spectrometry (LC-MS/MS).

2.6.2. LC-MS/MS

The Triple TOF™ 5600 System (ABSciex, Toronto, Canada) was operated in two phases: information-dependent acquisition (IDA) of each fraction, followed by sequential windowed data independent acquisition of the total high-resolution - mass spectra (SWATH™-MS) acquisition of each sample. After digestion, peptides were submitted to LC-MS/MS. Peptide separation was performed using LC (nanoUltra 2D; Eksigent, California, USA) on a ChromXP C18CL reverse phase column (300 µm x 15 cm, 3 µm, 120Å; Eksigent) at 5 µl/min with a 45 min linear gradient of 2% to 30% ACN in 0.1% FA, and the peptides were eluted into the mass spectrometer using an electrospray ionization source (DuoSpray™ Source; ABSciex). IDA experiments were performed by analysing 10 µl of each fraction. The mass spectrometer was set for IDA scanning full spectra (350-1250 m/z) for 250 ms, followed by up to 60 MS/MS scans (100–1500 m/z from a dynamic accumulation time – minimum 50 ms for precursor above the intensity threshold of 1000 counts for sec (cps) – in order to maintain a cycle time of 3.3 sec. Candidate ions with a charge state between +2 and +5 and counts above a minimum threshold of 10 cps were isolated for fragmentation and one MS/MS spectra was collected

before adding those ions to the exclusion list for 25 sec (mass spectrometer operated by Analyst® TF 1.6; ABSciex). Rolling collision energy was used with a collision energy spread of 5. The 3 fractions of each sample were combined into a single sample and adjusted to 30 µl, and a single injection of 10 µl of each sample was set for quantitative analysis by acquisition in SWATH™ mode. The SWATH™ setup was essentially as in Gillet et al. (2012), with the same chromatographic conditions used for SWATH™ and IDA acquisitions (250). For SWATH™-MS based experiments, the mass spectrometer operated in a looped product ion mode. The instrument was specifically tuned to allow a quadrupole resolution of 25 m/z mass selection. Using an isolation width of 26 m/z (containing 1 m/z for the window overlap), a set of 30 overlapping windows was constructed covering the precursor mass range of 350–1100 m/z. A 250 ms survey scan (350-1500 m/z) was acquired at the beginning of each cycle for instrument calibration and SWATH™ MS/MS spectra were collected from 100–1500 m/z for 100 ms resulting in a cycle time of 3.3 sec from the precursors ranging from 350 to 1100 m/z. The collision energy for each window was determined according to the calculation for a charge +2 ion centred upon the window with a collision energy spread of 15 (236).

2.6.3. Bioinformatics analysis

Specific libraries of precursor masses and fragment ions were created by combining all files from the IDA experiments and used for subsequent SWATH™ processing. The libraries were obtained using ProteinPilot™ software (v5.0, ABSciex), with the following search parameters: Canidae and *E. canis* SwissProt (release 2015_12) and unreviewed Ixodidae database (TrEMBL) from UniProtKB (release 2015_12) or Canidae and *E. canis* SwissProt (release 2015_12) and an in-house database from transcriptomics analysis as search databases; acrylamide alkylated cysteines as fixed modification; and the gel-based special focus option. An independent False Discovery Rate (FDR) analysis using the target-decoy approach provided with the ProteinPilot™ software was used to assess the quality of the identifications and positive identifications were considered when identified proteins and peptides reached a 1% local FDR (251, 252). Data processing was performed using SWATH™ processing plug-in for PeakView™ (v2.0.01; ABSciex). Briefly peptides were selected from the library using the following criteria: *(i)* unique peptides for a specific targeted protein were ranked by the intensity of the precursor ion from the

IDA analysis as estimated by the ProteinPilot™ software, and *(ii)* peptides that contained biological modifications and/or were shared between different protein entries/isoforms were excluded from selection. Up to 10 peptides were chosen for each protein, and SWATH™ quantitation was attempted for all proteins in library file that were identified below 1% local FDR from ProteinPilot™ searches. In SWATH™ Acquisition data, finding and scoring peak groups, which are a set of fragment ions for the peptide, confirm peptides. Up to 5-target fragment ions were selected and peak groups were scored. Peak group confidence threshold was determined based on an FDR analysis using the target-decoy approach and 1% extraction FDR threshold was used for all the analyses. Peptides that met the 1% FDR threshold in all three biological replicates were retained, and the peak areas of the target fragment ions of those peptides were extracted across the experiments using an extracted-ion chromatogram (XIC) window of 5 min and 0.01 Da XIC width. Protein levels were estimated by summing all the transitions from all the peptides for a given protein (253) and normalised to the total intensity at the protein level and to the internal standard. To ensure reliable quantitation, only proteins that had 3 or more peptides available for quantitation were selected for XIC peak area extraction and exported for analysis in the MarkerView™ 1.2.1 software (ABSciex). Global normalisation was performed according to the Total Area Sums of all detected proteins in the samples.

MS proteomics data was deposited in the ProteomeXchange Consortium via the PRIDE partner repository (254) with the dataset identifier PXD005468 (https://www.ebi.ac.uk/pride/archive/).

Quantification of the proteome was carried out by Era7 Bioinformatics- Parque Científico de Madrid, Spain, identifying 432 unique proteins. GO functional annotation using the 69 proteins that were significantly differentially represented in response to *E. canis* infection was then carried out.

A second BLAST was carried out using the OmicsBox Software (Version 2.1.14; BioBam Bioinformatics 2019, available at www.biobam.com/omicsbox) with the 69

differentially represented proteins to create a graphical representation of GO functional annotation.

Comparison of protein representation data in both conditions was determined by Log2 fold-change each individual protein the number of hits of the infected samples by the number of hits of uninfected samples.

Log2 fold-change (protein hits$_{infected}$/protein hits$_{uninfected}$)

2.7. Gene silencing

2.7.1. dsRNA synthesis

Functional analysis of *ferritin 1*, *psc*, *prohib* and *phsrp20* was carried out by RNAi in IDE8 cells and/or *R. sanguineus* ticks using dsRNA. Before dsRNA synthesis, the region of interest for each gene was PCR-amplified using specific primer pairs containing the T7 promoter (Section 2.4.8). To synthesise dsRNA, the DNA template must have the correct RNA polymerase promoter site T7 upstream of the sequence to be transcribed for the *in vitro* transcription (Figure 6).

Figure 6. Phage polymerase T7 promoter.
The +1 base in bold is the first base incorporated into RNA during transcription and the underlined sequence is the minimum promoter sequence required for efficient transcription (Source: https://www.thermofisher.com/, accessed in 11 of November 2020).

dsRNA synthesis was then carried out using the MEGAscript® T7 Kit (Ambion) according to manufacturer's instructions. Briefly, a 20 µl transcription reaction was assembled with 2 µl of ATP solution, 2 µl of CTP solution, 2 µl of GTP solution, 2 µl of UTP solution, 2 µl of 10x Reaction Buffer, 0.1-1 µg of template DNA containing the T7 promoter, 2 µl of Enzyme Mix and RNase-free water (Sigma-Aldrich) up to the final

volume. The mixture was mixed thoroughly and incubated at 37ºC in a heat block overnight.

β2m dsRNA was not synthesised during this study and was kindly provided by Joana Couto from IHTM-UNL, Lisbon, to use when indicated as an unrelated gene. β2m protein is originally from *Mus musculus* without similarities found in the BLAST search against tick genes (UniProtKB Q3U679).

2.7.2. RNAi

For *ferritin 1* gene silencing, 30 adult female ticks were injected with 0.2 µl of *ferritin 1* dsRNA, containing $9.74x10^{11}$ molecules, between the coxa and trochanter I, using a nanoinjector (Nanoject; Drummond Scientific, Broomall, USA) (Supplementary Table 6). The control group, also with 30 adult female ticks, was injected with the same volume of Elution Buffer from the NZYGelpure Purification Kit (NZYTech), as described in other studies (255, 256). Whilst the use of unrelated dsRNA is now a well-established control in species with full genome annotation, the *R. sanguineus* genome is poorly annotated, meaning inoculation with unconfirmed unrelated sequences can increase the off-target effects in silencing experiments with this species. Injected ticks were left overnight in a regulated chamber under controlled conditions (Section 2.2.1). The next day, each group was placed into a feeding chamber (section 2.2.4) to feed on *E. canis*-infected dogs. After the drop-off, fully engorged females were then collected, counted and weighed individually (mg). Immediately after, the SGs, OV and MG were dissected and stored as described in Section 2.2.5.

Silencing assay in IDE8 cells was performed at the Tick Cell Biobank – Institute of Infection and Global Health at The University of Liverpool, UK. For this study, three experimental groups were defined to investigate *(i)* the role of the selected gene on the *E. canis* cell invasion (Group B - IDE8 cells initially uninfected that were inoculated with *E. canis* 24 h after dsRNA inoculation) and *(ii)* their impact on *E. canis* multiplication (Group C - infected IDE8 cells), in comparison with the control group (Group A - uninfected IDE8 cells). Uninfected and *E. canis*-infected cells, previously maintained in 25 cm^3 flasks (Sections 2.3.1 and 2.3.2) were distributed in 24-well plates (Corning

Costar) to achieve a concentration of $4.16x10^5$ cells/ml/well. The following day, cells were inoculated with *x* molecules/µl (see Supplementary Table 7) of the dsRNA of each gene of interest (*psc, prohib* or *phsrp20*). One control group was included with cells inoculated with *β2m* dsRNA, as non-related dsRNA control. At 48 h after seeding, Group B was inoculated with 100 µl of *E. canis* suspension purified from an IDE8 culture with parasitaemia of 80%. For each condition and time point, four technical replicates were collected to evaluate gene knockdown efficiency and infection progression by qPCR. Three time points were evaluated after cell harvesting of different cultures: 48 h (T1), 120 h (T2) and 160 h (T3), being the initial time T0 = 0 h the time when the cells were seeded as shown in Figure 7. All samples were centrifuged at 200 x *g* for 5 min and the supernatant was discarded before freezing the cell pellet at -20ºC for subsequent shipment to IHMT-UNL, in Lisbon.

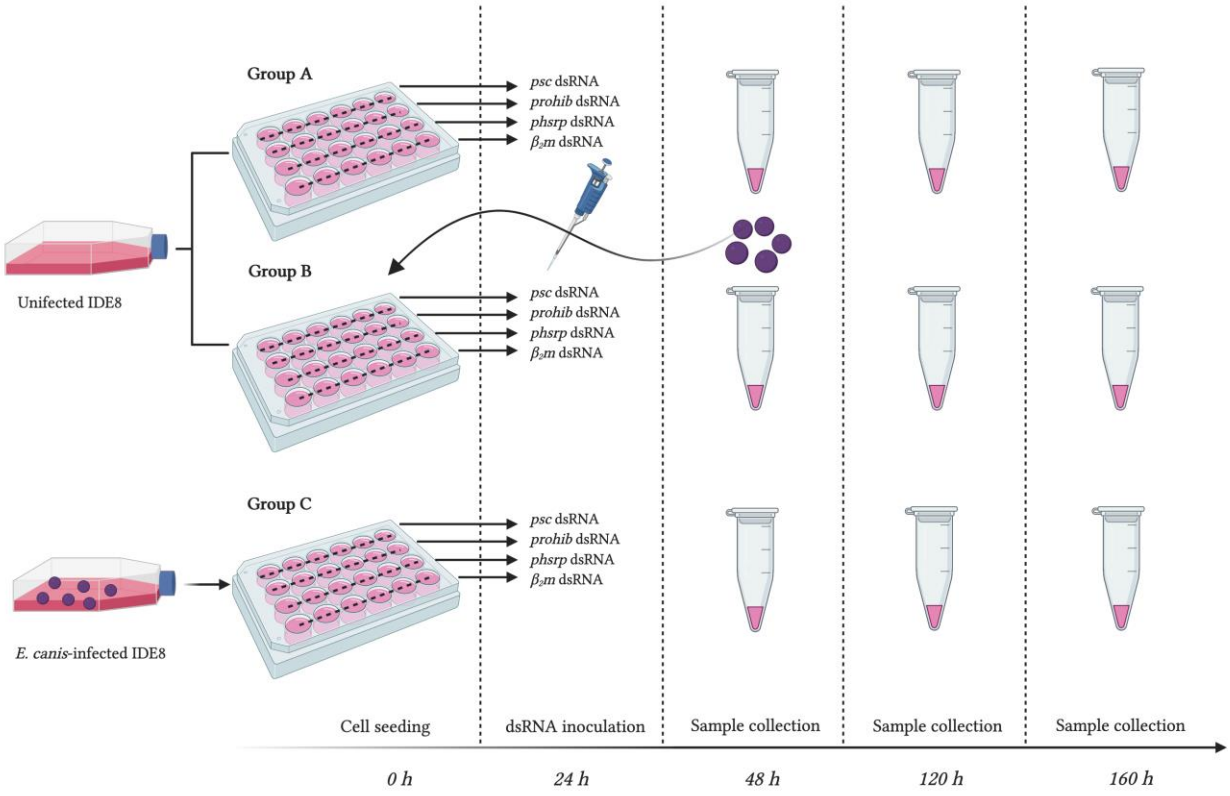

Figure 7. Experimental design for *in vitro* gene silencing in IDE8 cells.
Uninfected IDE8 cells and *E. canis*-infected cells were seeded in 24 well plates. After 24 hours, cells were inoculated with *psc, prohib, phsrp20* or *β2m* dsRNA as represented. At 48 hours **(T1)**, group B was inoculated with purified *E. canis*. At 48 **(T1)**, 120 **(T2)** and 160 hours **(T3)** cells were harvested for further RNA extraction, cDNA synthesis and gene expression analysis by qPCR (represented by a tube). **Group A –** Uninfected IDE8 cells; **Group B –** Uninfected IDE8 cells inoculated with *E. canis* at 48 hours after seeding; **Group C –** *E. canis*-infected IDE8 cells (Image created with BioRender.com).

For silencing assays *in vivo*, twelve days after *E. canis* inoculation four tick feeding chambers were placed on the dogs (see Section 2.2.4). The day after, approximately 300 unfed *R. sanguineus* nymphs for each gene were silenced using the soaking of the whole tick method (194, 257, 258). Briefly, each group was incubated for 3 h at RT with *x* µl and *x* number of molecules (see Supplementary Table 8) of the correspondent dsRNA in a total volume of 250 µl of PBS in 1.5 ml microcentrifuge tubes (Figure 8). The control group was incubated in the same total volume of PBS. Whilst the use of unrelated dsRNA is now a well-established control in species with full genome annotation, the *R.*

sanguineus genome was poorly annotated at the date of these experiments, meaning inoculation with unconfirmed unrelated sequences can increase the off-target effects in silencing experiments with this species. Thus, for the control group was only used PBS. After incubation, ticks were dried in filter paper for 3 h and then each group was placed into a feeding chamber and allowed to feed until detachment (Section 2.2.4). After drop-off, engorged nymphs were collected and let to moult into adults in regulated chambers as described in Section 2.2.1. Freshly moulted adult females were dissected under an Olympus SZX7 stereomicroscope (Olympus) as described in Section 2.2.5.

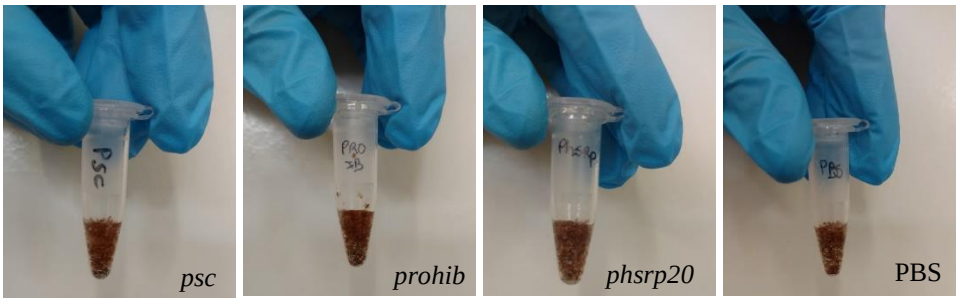

Figure 8. Gene silencing using the soaking method in *Rhipicephalus sanguineus* nymphs.
Approximately 300 unfed *R. sanguineus* nymphs were used for gene silencing. Each group was incubated for 3 h at room temperature with the correspondent dsRNA in a total volume of 250 µl of PBS. The control group was incubated in the same total volume of PBS. **Legend: *psc* -** putative serine carboxypeptidase; ***prohib*** **-** putative prohibitin-like protein; ***phsrp20*** **-** putative heat shock-related protein; **PBS -** control.

2.7.3. Gene-silencing efficiency

Gene silencing efficiency was determined by qPCR as described in Section 2.4.9. Efficiency was determined by comparison of gene expression levels between the samples subjected to dsRNA of the target gene and the control samples subjected to Elution Buffer (NZYTech), *β2m* dsRNA or PBS, depending on the study.

Silencing efficiency was calculated by subtracting the gene of interest normalised ΔΔCq expression value from the control normalised ΔΔCq expression value and multiplying by 100.

$$\mathbf{E_{silencing}\,(\%) = (\Delta\Delta Cq_{gene\ of\ interest} - \Delta\Delta Cq_{control}) \times 100.}$$

When the gene of interest ΔΔCq expression value was equal or higher than the control ΔΔCq expression value, the efficiency of silencing was considered 0%. If the ΔΔCq expression value of the interest gene was zero, silencing efficiency was considered 100%.

The comparison of gene regulation, down or up-regulation, between the gene of interest and the control group was determined by Log2 fold-change of the normalised ΔΔCq expression for the gene of interest divided by the normalised ΔΔCq value for the control.

$$\textbf{Log2 fold-change } (\Delta\Delta Cq_{\text{gene of interest}} / \Delta\Delta Cq_{\text{control}})$$

2.8. Polyclonal antibody production

2.8.1. Peptide selection

Peptide selection was based mainly on two criteria: *(i)* protein involvement with pathogen infection in the tick, and *(ii)* its potential protective capacity to be used as an antigen in a vaccine. From the proteomic data, the amino a.a. sequence of a small putative heat shock-related protein (PHSRP20; UniProtKB L7M6Q5) was selected and analysed *in silico* as described in Section 2.4.14.

2.8.2. Peptide synthesis

The peptide pPHSRP20 was synthesised by NZYTech (NZYTech) for polyclonal antibody production and immunoassays. The peptide sequence is the following:

H – RQASEGSVCPARQPGTSVACTPDKFAINVDTRHFAPEEITVKTQDNCVV IHGKHEEKSDDRGCYVKREFT - OH

Peptide length was 70 a.a., located between the 51 and 120 a.a. of PHSRP20, with a molecular weight of 7791.71 Da, purity of 91.17 %, and a total of 5.5 mg of white powder. A stock solution of pPHSRP20 was prepared by dissolving the powder with Milli-Q water to a final concentration of 1 mg/ml. This solution was stored at -20^{o}C for further use.

2.8.3. Mice immunisation

Three CD1 mice selected as the study group, R_1, R_2 and R_3, were primed with a solution prepared with 30 µl (1µg/µl) of pPHSRP20, 20 µl of PBS and 50 µl of Freud's complete adjuvant (Sigma-Aldrich). The control groups with 3 mice, CT_1, CT2 and CT_3, were inoculated with a solution prepared with 50 µl of PBS and 50 µl of Freud's complete adjuvant (Sigma-Aldrich). After the first immunisation, Freud's Complete adjuvant (Sigma-Aldrich) was replaced in the solution by Freud's Incomplete adjuvant (Sigma-Aldrich) for the following immunisations. Immunisations were carried out in 2 to 4 week-intervals. Blood samples were collected immediately before priming to obtain pre-immune serum, and just before each immunisation to monitor anti-pPHSRP20 antibody titters by indirect ELISA. Approximately 100 µl of blood was collected from the submandibular vein of each mouse, and the serum separated by centrifugation at 200 x *g* for 5 min. Serum was maintained at -20ºC for further use. After week 9, the mouse with higher antibody titre was selected and three days before euthanasia a final boost was given (Figure 9).

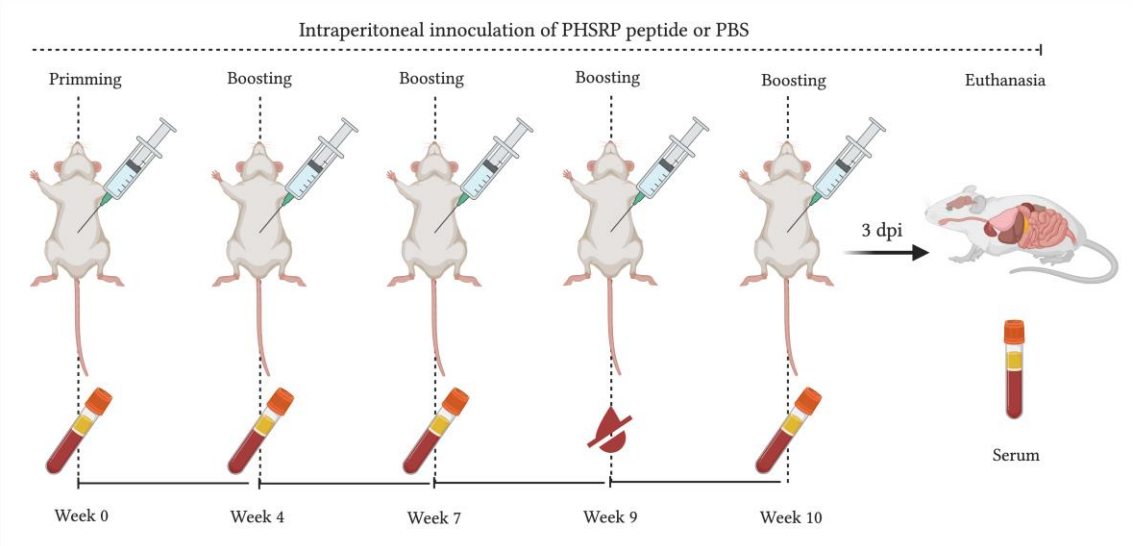

Figure 9. Experimental design for CD1 mice immunisation with pPHSRP20.
The time scale at the bottom represents the weeks after the first inoculation. At "Week 0" mice were immunised with pPHSRP20 or PBS, followed by boosts that varied between 2 to 4 week intervals. Blood samples were collected immediately before each immunisation to evaluate the presence of anti-pPHSRP20 antibodies by indirect ELISA. The mouse with the higher antibody titre was selected and 3 days *post* immunisation (dpi) a final immunisation boost was given (Image created with BioRender.com).

2.8.4. Indirect ELISA

Indirect ELISA was used to determine if antibodies against the pPHSRP20 were present in mice sera and to quantify the immune response. ELISA is a plate-based assay technique designed for detecting and quantifying soluble substances such as peptides, proteins, antibodies, and so on. In this molecular method, the antigen, which is the target macromolecule, is immobilised on a solid surface, normally a microplate, and then bounded to an antibody present in the test serum. This antigen-antibody complex is then incubated with a reporter enzyme-labelled antibody, which will allow the detection by measuring the activity after the incubation with the appropriate substrate. Briefly, high binding 96-well plates (Corning Costar, New York, USA) were coated with 100 µl of 0.5 µg of pPHSRP20 diluted in 1x PBS in each well and incubated overnight at 4ºC with parafilm to prevent evaporation. Negative control wells were coated with 100 µl of PBS alone. Plates were washed 3 times with 0.05% TBS-T buffer, and then incubated for 1 h

and 30 min at 37ºC with 250 µl of 5% (w/v) blotting grade blocker non-fat dry milk (Bio-Rad) diluted in TBS-T buffer. After washing with 0,05% TBS-T buffer, plates were incubated at 37ºC for 1 h with 100 µl of each mouse serum diluted to 1:200 and 1:500 in PBS. After incubation, plates were washed again as described before and incubated for 1 h with 100 µl of Anti-mouse polyvalent Ig (IgA, IgG and IgM; AP conjugate; Sigma-Aldrich) diluted in PBS-T to 1:30000, according to the manufacturer's instructions. After washing five times with 0,05% TBS-T buffer, plates were incubated for 30 min in the dark at RT with 100 µl of 4-nitrophenyl phosphate disodium salt hexahydrate (AP substrate; BioChemica AppliChem), previously diluted to 0.1 mg/ml in the substrate buffer. The absorbance at 405 nm was measured in an ELISA plate reader (Triad Multi Mode Microplate Reader; DYNEX Technologies, Virginia, USA).

2.8.5. Chessboard ELISA

Chessboard titrations were performed to determine mice antibody titters. An ELISA method was conducted as described in the previous Section, with some modifications and using serial dilutions. Briefly, a 96-well well plate (Corning Costar) was coated by adding 100 µl of 1x PBS to each well from row B to H and 200 µl of 0.5 µg of pPHSRP20 diluted in 1x PBS was added to row A. After mixing by pipetting up and down, a serial dilution of the peptide was carried out transferring 100 µl of the suspension from row A sequentially to row G. Negative controls were prepared by adding 100 µl of 1x PBS only. Plates were then incubated overnight at 4ºC covered with parafilm sealing film to prevent evaporation. After incubation, the peptide solution was removed, and the wells washed three times with 0,05% TBS-T. Two-hundred and fifty µl of 5% (w/v) blotting grade blocker non-fat dry milk (Bio-Rad) diluted in 0,05% TBS-T buffer were added to each well and the plates incubated at 37ºC for 1 h and 30 minutes, with parafilm. After removing the milk solution, wells were washed three times with 0,05%. TBS-T buffer. One hundred µl of 1x PBS was added to each well from columns 2 to 11. Mouse sera was diluted to 1:100 in 1x PBS and 200 µl was added to wells of column 1, including the control wells. As before, 100 µl of the solution from column 1 was transferred to column 2, and from column 2 to 3 and so on until column 11, always mixing between transfers by pipetting up and down. Column 12 was the positive control, with the mouse serum diluted to 1:100 in 1x PBS. Plates were incubated at 37ºC for 1 h. After removing the

serum, wells were washed three times with 0,05% TBS-T buffer. Anti-mouse polyvalent Ig (IgA, IgG and IgM; AP conjugate; Sigma-Aldrich) was diluted in PBS-T buffer to 1:30000, according to the manufacturer's instructions, and 100 µl was added to each well, including the negative controls. Plates were incubated at 37ºC for 1 h. Wells were washed five times with 0,05% TBS-T buffer after removing the anti-mouse Ig solution. One hundred µl of AP substrate (BioChemica AppliChem) was added to each well and the plates incubated at RT in the dark for 30 min. The absorbance at 405 nm was measured in an ELISA plate reader (Triad Multi Mode Microplate Reader; DYNEX Technologies).

2.9. Microscopy

E. canis growth was monitored by microscopic examination of Giemsa stained cytocentrifuge smears. Briefly, cells were resuspended and 50 µl aliquots of cell suspension were centrifuged for 5 min at 1000 x *g* (Shandon Cytospin 2; Marshall Scientific, Hampton, UK) and air-dried. The resultant smears were fixed in technical methanol (Honeywell Fluka™, New Jersey, USA) for 3 min and stained in 10% Giemsa for 20 min (259), rinsed twice with distilled water buffered to pH 7.2 (Gibco® Gurr Buffer Tablets pH 7.2; ThermoFisher Scientific) and air-dried. Giemsa-stained cytocentrifuged smears of uninfected and *E. canis*-infected tick cells were examined using a microscope (Leitz GmbH & Co. KG, Oberkochen, Germany) at 1000 x magnification with immersion oil to confirm the presence of infection and estimate the percentage of cells infected.

For characterisation, the OV dissected from 3 fully engorged females of the control and *ferritin 1*-silenced groups were fixed in Karnovsky solution for 24 h. The specimens were then dehydrated through an acetone series (50%, 75%, 90%, 95% and 100%) of 5 min each. The material was processed using the critical point drying technique, sputtered with gold, examined, and photographed using a HITASHI TM 3030 scanning electron microscope (Hitachi High-Technologies, Tokyo, Japan). For the histological and histochemistry analysis, the OV of 5 fully engorged females were collected from each group (control and *ferritin 1*-silenced) to perform an oogenesis and vitellogenesis comparison. The OV were dissected and fixed in 4% paraformaldehyde for 24 h, dehydrated for 30 min in an ethanol series (70%, 80%, 90% and 100%), embedded in Technovit 7100 solution A from the Technovit 7100 historesin kit (Heraeus Kulzer,

Hanau, Germany) for 24 h at 4°C, and transferred to plastic moulds previously filled with glycol methacrylate containing a catalyst, according to manufacturers' instructions. After resin polymerization, the material was fixed on wood blocks. Serial sections of 3 µm thickness were cut using a Sorvall JB4 microtome (Bio-Rad). Finally, the sections were stained with haematoxylin and eosin (H&E), following routine histological procedures; and histochemical tests were conducted to detect the presence of proteins with bromophenol blue, and lipids with Nile blue. The stained sections were observed and photographed under an Olympus CX31 light microscope (Olympus) coupled with a digital camera and Cell Sense Standard CS-ST 111 software (Olympus).

2.10. Statistical analysis

For the *ferritin 1*-silencing study, weights of engorged females were compared by student's *t*-test with unequal variance ($p = 0.05$) (Microsoft® Office Excel, v16.43). To analyse tick mortality, the Chi-square test (X^2; $p = 0.05$) was used with the null hypothesis that tick mortality and the capacity to complete feeding were not dependent on gene knockdown. A significant statistical difference was considered when *p*-value was inferior to 0.05 ($p < 0.05$). Graphs were designed with GraphPad Instat® (GraphPad Software Inc, version 3.06).

For the transcriptomic data, paired comparisons of the number of reads hitting each contig were calculated by X^2 to detect significant differences between samples. A significant statistical difference was considered when *p*-value was inferior to 0.05 ($p < 0.05$). Normalised fold-ratios of the sample reads were computed by adjusting the numerator by a factor based on the ratio of the total number of reads in each sample (Microsoft® Office Excel, v16.43).

For the proteome data, the student's *t* test was used to perform two-sample comparisons between the averaged area sums of all the transitions derived for each protein across the replicate runs, to identify proteins that were significantly differentially represented between uninfected and *E. canis*-infected SGs. A significant statistical difference was considered when *p*-value was inferior to 0.05 ($p < 0.05$) (Microsoft® Office Excel, v16.43).

For normalised gene expression, the Welch's unequal variances *t*-test (unpaired two-sample *t*-test) was used for two-sample comparisons between the conditions infected/uninfected and silenced/not silenced to identify statistically significant differences. A significant statistical difference was considered when *p*-value was inferior to 0.05 ($p < 0.05$). Analysis was carried out with GraphPad Prism software (GraphPad Software Inc, version 9 for macOS).

Chapter 3: Results

3.1. Animal experimental infection with *Ehrlichia canis*

3.1.1. Clinical evaluation, haematology and parasitaemia detection

For experimental infections, populations of adult female *E. canis*-infected ticks were required. For this purpose, German shepherd dogs were inoculated intravenously with *E. canis* purified from DH82 cells. When required, one dog was selected as an unexposed control and was inoculated with PBS only. All dogs were monitored daily after *E. canis* inoculation, with a physical examination focusing on the rectal temperature, CRT and palpation of abdominal organs and lymph nodes. During those examinations, blood was collected from each dog for haematology and detection of *E. canis* by qPCR targeting *dsb* (133), and Giemsa-stained smears.

The presence of *E. canis* in the blood was confirmed at least 3 days *post*-inoculation by qPCR in experimentally infected dogs. Intracytoplasmic morulae of *E. canis* in the monocytes of blood smears were detected between 14- and 17 days *post*-inoculation, in infected dogs. A schematic depicting *E. canis* in monocytes and macrophages is shown in Figure 10. No *E. canis* DNA or morulae were detected in the control dogs.

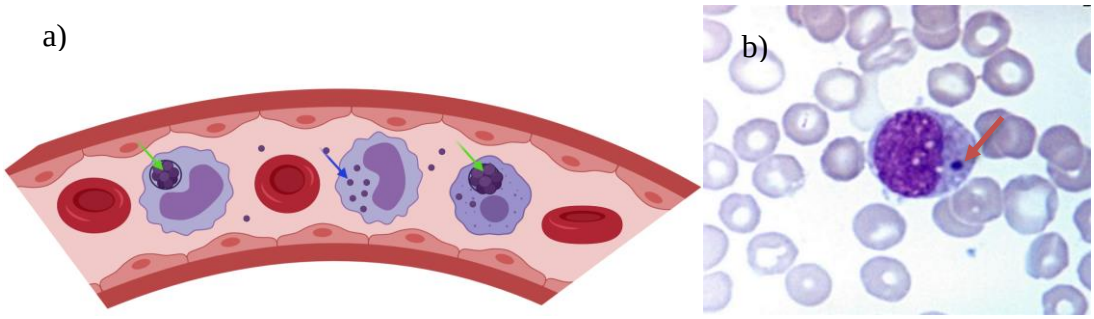

Figure 10. Schematic depicting *Ehrlichia canis* in monocytes and macrophages.
(a) Schematic view of a blood vessel with intracellular morulae (green arrow) in a monocyte and in a macrophage. Elementary bodies (blue arrow) in a monocyte (Created with BioRender.com); **(b)** Giemsa-stained canine blood smear containing an elementary body (red arrow) of *E. canis* within a circulating monocyte of a experimentally infected dog (Image kindly provided by Professor Rozângela Zacarias Machado; 1993).

Here we report the results of dogs A, B, and C, used to obtain the tick populations for the transcriptomic and proteomic studies. Dogs A and B were inoculated with *E. canis*, whereas dog C was the uninfected control. The infected dogs presented clinical signs of CME 16 days after the experimental infection, which included: hyperthermia, pale mucous membranes with CRT > 2 sec, lymphadenopathy, lethargy, and emaciation. After day 17 *post*-inoculation, dogs were monitored at day 17, 19, 21, 25 and 26. Haematological alterations were also found 18 days *post*-inoculation, such as leucocytosis (White Blood Cells - WBCs > $14.1x10^3$/µl), anaemia (RBCs < $4.95\ x10^6$/µl and Haematocrit - HCT < 35%) and thrombocytopenia (PLTs < $211\ x10^3$/µl). No clinical alterations were observed in the control animal (C), except a leucocytosis and hyperthermia at days 21 and 26 after the PBS inoculation, respectively, which could be explained by a dermatitis caused by the feeding chamber attachment and tick fixation on the skin. Hematologic results are shown in Table 1 and rectal temperatures are represented in Figure 11.

Table 1. Hematologic parameters evaluated in dogs experimentally infected with *Ehrlichia canis*. Values for the infected dogs **(A and B)** and the control dog **(C)** are presented at the different days *post*-inoculation (dpi). **WBCs** – White Blood Cells; **RBCs** – Red Blood Cells; **HTC** – Haematocrit; **PLT** – Platelets. In bold are the values outside the normal reference range.

Parameter	Dog	17 dpi	19 dpi	21 dpi	25 dpi	26 dpi	Reference Value*
WBCs (x10^3/µl)	**A**	9.7	10.5	**18.4**	**15.3**	**17.4**	5.0 – 14.1
	B	6.4	7.4	11.0	**16.8**	**25.8**	
	C	12.4	11.8	**16.1**	**22.0**	**19.4**	
RBCs (x10^6/µl)	**A**	**4.33**	**3.81**	**4.08**	**4.42**	**4.45**	4.95 – 7.87
	B	**4.47**	**4.2**	**4.07**	**4.24**	[(a)]	
	C	12.4	6.02	5.76	5.85	6.41	
HCT (%)	**A**	**28.2**	**25.3**	**27.1**	**29.2**	**29.3**	35 – 57
	B	**28.6**	**27.1**	**26.3**	**27.5**	**27.9**	
	C	39.1	38.9	37.1	37.4	40.4	
PLT (x10^3/µl)	**A**	**20**	**51**	**43**	**77**	**72**	211 – 621
	B	**16**	**8**	**23**	**20**	**71**	
	C	298	317	334	319	414	

* Source: https://www.msdvetmanual.com/special-subjects/reference-guides/hematologic-reference-ranges

[(a)] Blood was not collected.

At day 21 *post*-inoculation Dogs A and C, and Dog B at day 25 presented a leucocytosis that persisted until the last blood collection on day 26. The specific type of WBCs that were increased was not investigated. Dogs A and B showed a decrease in RBCs at all time points, except Dog B at day 26, when blood was not collected due to technical limitations. The RBC counts for Dog C were always within the reference range. The decrease in RBCs in both infected dogs directly translated in a decrease of the haematocrit to values below the physiological range. Finally, the haematological tests for Dogs A and B showed a large decrease in PLT levels, and thrombocytopenia far below the inferior physiological limit.

Regarding rectal temperature, in a healthy dog the reference values can vary between 37.9°C and 39.9°C, depending on several factors including age, environmental temperature or stress. In this study, all dogs presented temperatures above 39.4°C that reflected the high environmental temperature during the Brazilian summer when the study took place, and the stress of being manipulated for the experiments. Dog B presented values above the upper limit (T > 39.9 °C), except on day 25 *post*-inoculation, in which the value was within the normal range (T = 39.4°C). Dog C had a rectal temperature of

40.1°C on day 26 *post*-inoculation that could be associated with the same reasons that explain the leucocytosis. On all the other days, the temperatures measured were normal.

Other dogs used for experimental infections were monitored following the same protocol, but results regarding haematology and rectal temperatures are not shown. After the course of a 30-day treatment with doxycycline (138), all dogs recovered from clinical CME.

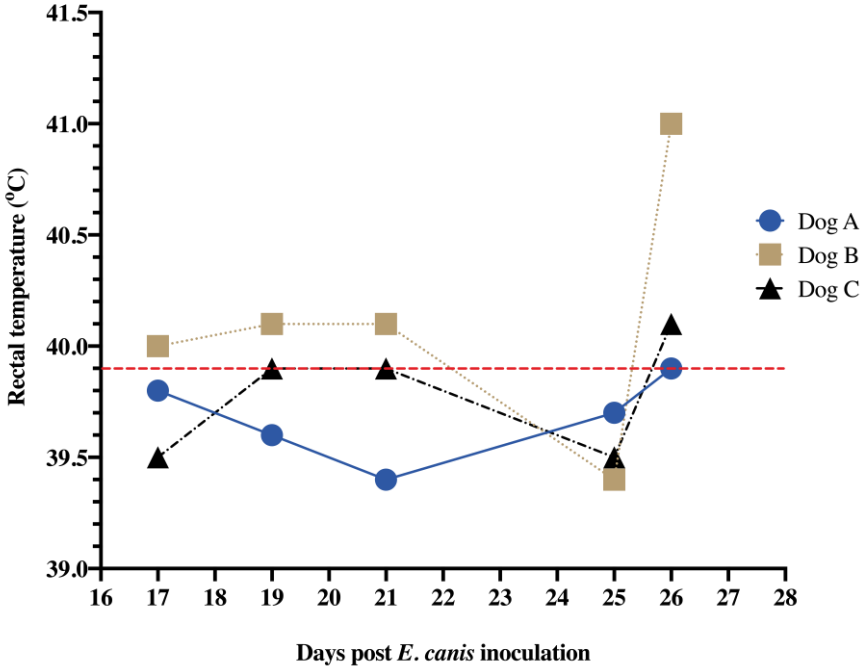

Figure 11. Rectal temperature (°C) determined in dogs experimentally infected with *Ehrlichia canis.* Values for the infected dogs **(A and B)** and the control dog **(C)** are presented at the different time points *post*-inoculation. Red-segmented line (---) represents the upper limit of the reference range (Reference values: 37.9 < TºC > 39.9 ºC; Source: https://www.msdvetmanual.com/special-subjects/reference-guides/normal-rectal-temperature-ranges) (Figure created with GraphPad Prism software; version 9 for macOS).

3.2. The effect of *ferritin 1*-silencing in *Rhipicephalus sanguineus* sensu lato (Acari: Ixodidae) during experimental infection with *Ehrlichia canis*

3.2.1. *Ferritin 1*-silencing efficiency in the salivary glands and midgut

The role of the ferritin protein in the SGs, OV and MG of adult *R. sanguineus* female ticks was investigated by functional analysis of *ferritin 1*-silencing by RNAi. To carry out RNAi, dsRNA was synthesised and used to inoculate the ticks. PCR was used to amplify a *ferritin 1* amplicon using the specific primer sets containing a T7 promoter. Figure 12 shows successful amplification of a 353 bp *ferritin 1* PCR product, separated on a 1.2% agarose gel.

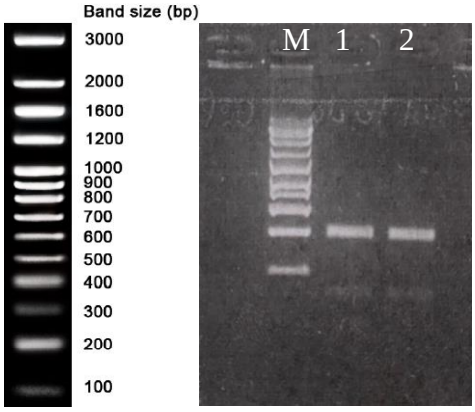

Figure 12. Agarose gel of *ferritin 1* PCR products following amplification from *Rhipicephalus sanguineus*. **Lane M:** Marker (NZYDNA Ladder VII, NZYTech); **Lane 1 and 2:** cDNA from *R. sanguineus* salivary glands showing an approximate 353 bp sized product on a 1.2% agarose gel amplified with the primers *ferritin_T7_forward and ferritin_T7_reverse*.

PCR products were purified from the gel and sent for Sanger sequencing following quality and concentration determination by spectrophotometry (amplicon in Lane 1 = 15.3 ng/µl and a A_{260}/A_{280} ratio = 1.86; amplicon in Lane 2 = 18.6 ng/µl and a A_{260}/A_{280} ratio of 1.80). A BLAST retrieved several sequences with homology to tick *ferritin* fragments, with the percentage of identity varying from 84.31 - 96.62%. From these, three sequences showed a percentage of identity above 96%: *Rhipicephalus sanguineus* isolate Thai ferritin (Fer) mRNA, partial cds (GenBank accession nr. KP688390.1), Predicted

Rhipicephalus sanguineus soma ferritin-like (LOC 119382540) mRNA (GenBank accession nr. XM_037650283.1), and *Rhipicephalus sanguineus* ferritin (Fer) mRNA, complete cds (GenBank accession nr. AY277907.1) (Supplementary Table 9).

For RNAi, dsRNA was synthesised with a final concentration of 926.60 ng/µl. Adult ticks were injected with $9.74x10^{11}$ molecules of *ferritin 1* dsRNA or elution buffer and allowed to feed on an *E. canis*-infected dog until drop-off. After drop-off, ticks were collected with survival and weight recorded up until 9 days *post*-infestation, at which point the remaining 2 attached ticks in the control group were manually removed. From the 30 ticks initially put into the feeding chambers for each group, a total of 15 ticks were collected from the control group, 2 of which removed manually from the host, and 20 were collected from the silenced group. The difference between the starting and the final number of collected ticks corresponds to ticks that did not attach to the host during the 9 days.

Total RNA and gDNA were extracted from the SGs of 19 *ferritin 1*-silenced ticks and 15 controls, and from the MG of 11 *ferritin 1*-silenced ticks and 13 controls. For the SGs, RNA concentrations measured by spectrophotometry in the *ferritin 1*-silenced ticks ranged from 21.95 ng/µl and 425.59 ng/µl; whereas for the controls, RNA concentration varied between 42.74 ng/µl and 342.40 ng/µl. RNA purity ($A_{260/280}$) for *ferritin 1*-silenced ticks varied between 1.68 and 2.14, and for the controls between 1.64 and 2.03 (Supplementary Table 10). For the MG, RNA concentrations in the *ferritin 1*-silenced ticks ranged from 214.77 ng/µl and 1481.15 ng/µl; whereas for the controls varied between 68.32 ng/µl and 435.62 ng/µl. RNA purity ($A_{260/280}$) for the *ferritin 1*-silenced ticks varied between 1.64 and 2.11, and for the controls between 1.70 and 2.20 (Supplementary Table 11).

DNA concentrations measured by spectrophotometry in the *ferritin 1*-silenced ticks ranged from 25.01 ng/µl and 211.34 ng/µl; whereas for the controls between 31.11 ng/µl and 86.22 ng/µl. The purity ($A_{260/280}$) for the silenced group varied between 1.53 and 1.89, and for the controls between 1.44 and 1.94 (Supplementary Table 12). DNA extracted from the MG presented concentrations between 7.93 ng/µl and 480.62 ng/µl in the silenced group, and between 14.37 ng/µl and 86.22 ng/µl for the controls. DNA purity

($A_{260/280}$) varied between 1.43 and 1.66 for the *ferritin 1*-silenced group, and for the controls between 1.37 and 2.00 (Supplementary Table 13).

To detect false negative results due to PCR inhibition and to validate the efficiency of DNA extraction, gDNA extracted from the SGs was analysed by PCR targeting the tick *18S* rRNA (229). Successful amplification was confirmed on a 1.2% agarose gel (Figure 13).

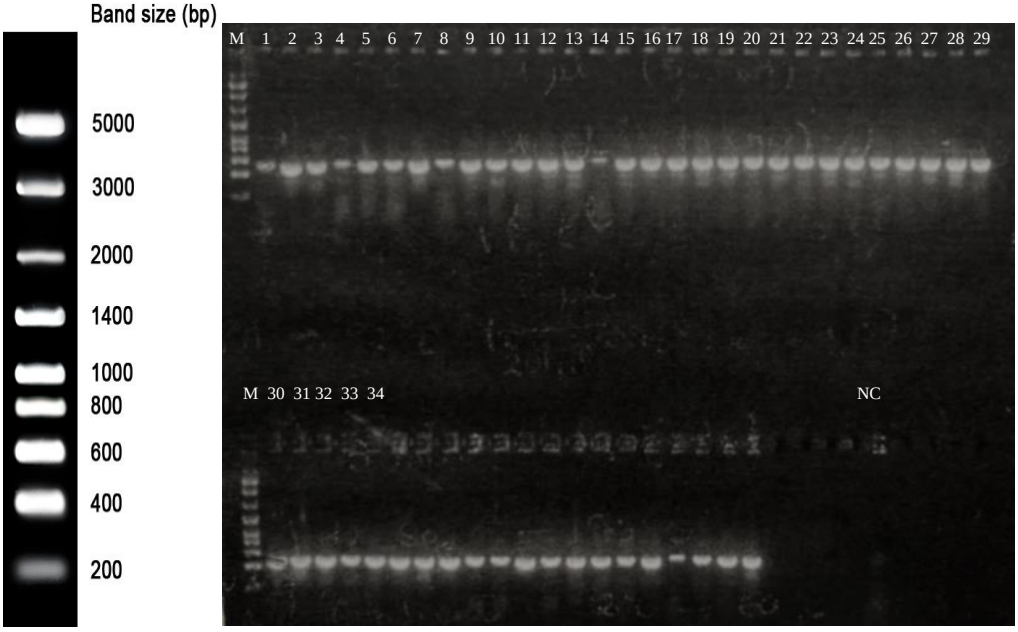

Figure 13. Agarose gel of *18s* rRNA PCR products following amplification from the salivary glands of *Rhipicephalus sanguineus* adult females.
Lane M: Marker (NZYDNA Ladder VIII, NZYTech); **Lanes 1 to 19:** DNA amplified from *ferritin 1*-silenced ticks; **Lanes 20 to 34:** DNA amplified from the control ticks. In both groups, a 500 bp product was amplified and visualised on a 1.2% agarose gel using the primers *tick-sense* and *tick-antisense* described by Shayan et al. (2007); **NC:** negative control.

DNA extracted from the MG was also analysed by PCR, targeting the tick *18S* rRNA, as described previously (229). Successful amplification was confirmed on a 1.2% agarose gel (Figure 14).

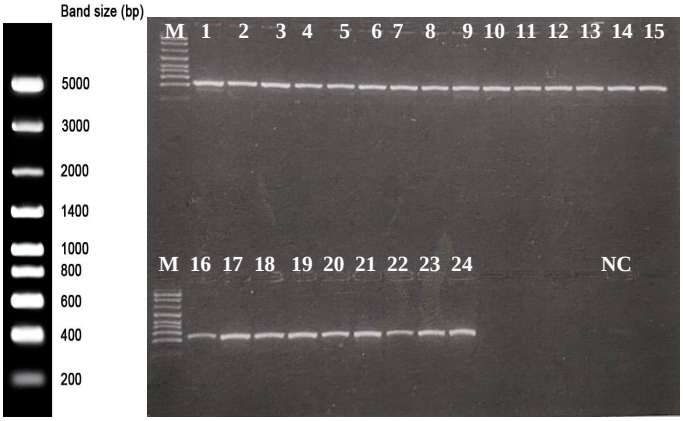

Figure 14. Agarose gel of *18s* rRNA PCR products following amplification from the midgut of *Rhipicephalus sanguineus* adult females.

Lane M: Marker (NZYDNA Ladder VIII, NZYTech); **Lanes 1 to 11:** DNA amplified from *ferritin 1*-silenced ticks; **Lanes 12 to 24:** DNA amplified from the control ticks. In both groups, a 500 bp product was amplified and visualised on a 1.2% agarose gel using the primers *tick-sense* and *tick-antisense* described by Shayan et al. (2007); **NC:** negative control.

The efficiency of *ferritin 1*-silencing in both organs was assessed by normalised relative gene expression in the SGs and MG using qPCR. First, primer conditions were optimised and their specificity to amplify the *ferritin 1* fragment was tested for both tick organs. A 10-fold dilution series of *R. sanguineus* cDNA from each organ (Figures 15-A and 16-A) was used to determine reaction efficiency. Reaction efficiencies were 101.9% for the SGs and 107.5% for the MG samples (Figures 15-B and 16-B). A single peak was observed in the Melting curve, with T_m = 84.0°C for the MG, and T_m = 84.5°C for the SGs; confirming the amplification of a single, specific DNA fragment (Figures 17-A and B).

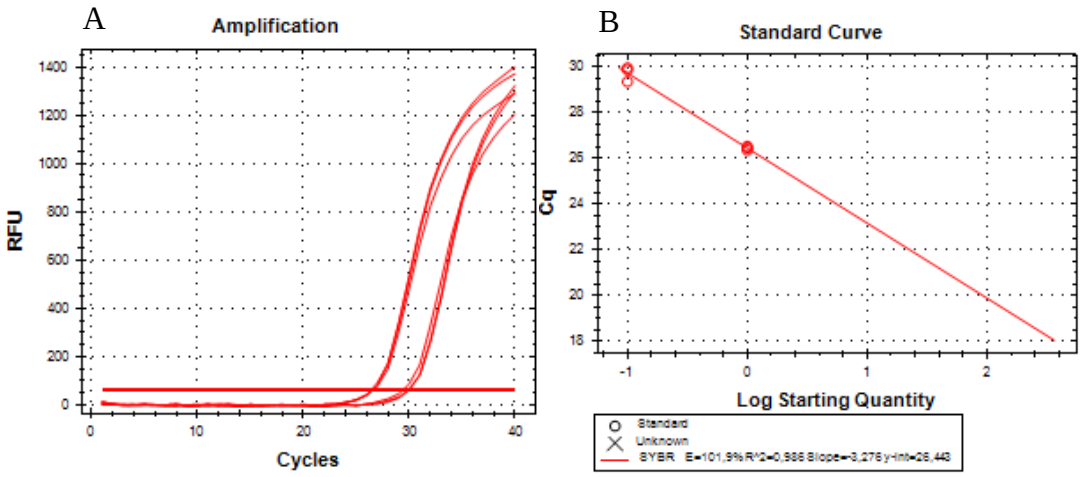

Figure 15. Real time PCR amplification curves and standard curve from *ferritin 1* primer optimisation in *Rhipicephalus sanguineus* salivary glands.

Data was obtained by qPCR using the *ferritin 1_forward* and *ferritin 1_reverse* primers and a 10-fold dilution series of salivary gland cDNA as the template. **A -** Amplification chart, and **B -** Standard Curve chart (Log_{10}). **Legend: RFU -** relative fluorescence units against the number of reaction cycles in the X-axis; **Cq –** quantification cycle. Reaction efficiency (%) and correlation coefficient (R^2) (E = 101.9%; R^2 = 0.986) were automatically determined by the CFX Manager™ Software (Bio-Rad).

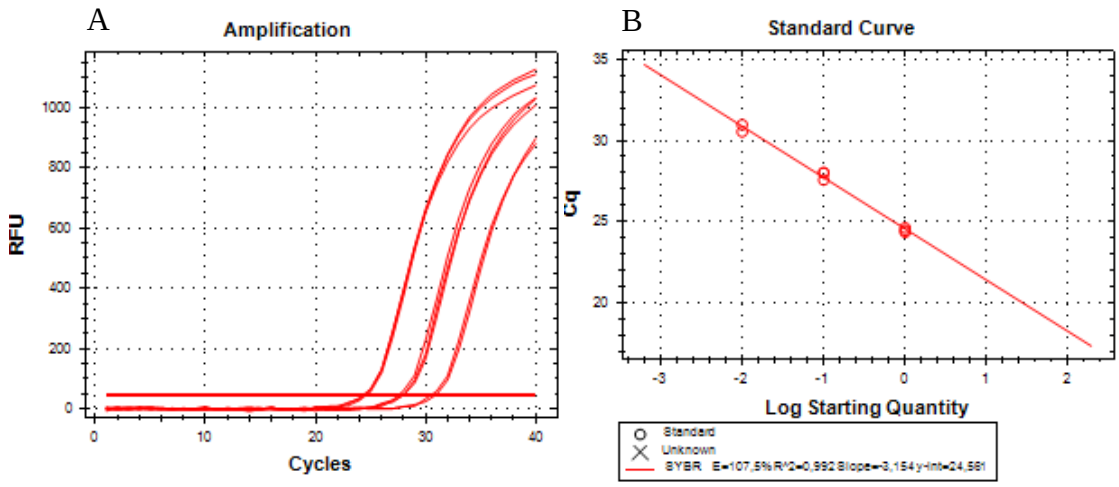

Figure 16. Real time PCR amplification curves and standard curve from *ferritin 1* primer optimisation in *Rhipicephalus sanguineus* midgut.

Data was obtained by qPCR using the *ferritin 1_forward* and *ferritin 1_reverse* primers and a 10-fold dilution series of midgut cDNA as the template. **A –** Amplification chart, and **B -** Standard Curve chart (Log_{10}). **Legend: RFU -** relative fluorescence units against the number of reaction cycles in the X-axis; **Cq –** quantification cycle. Reaction efficiency (%) and correlation coefficient (R^2) (E = 107.5%; R^2 = 0.992) were automatically determined by the CFX Manager™ Software (Bio-Rad).

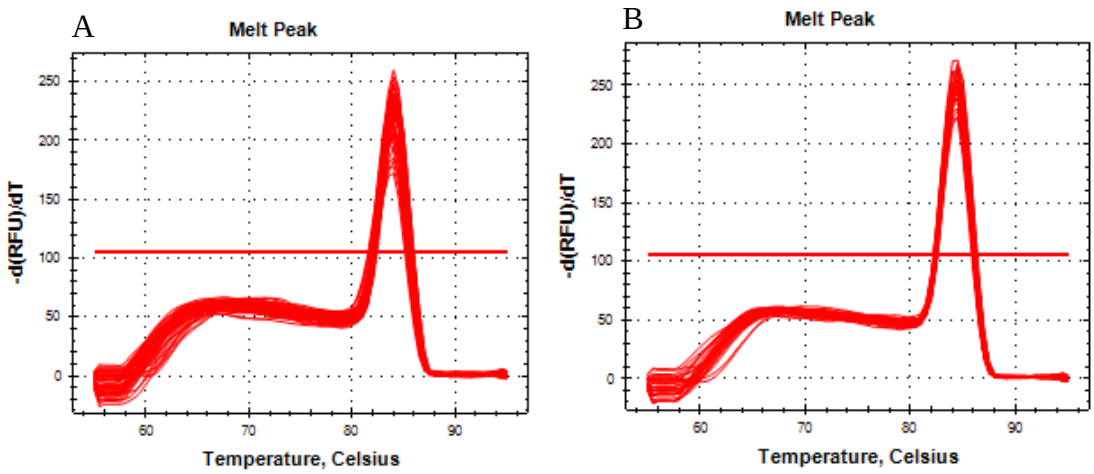

Figure 17. Real time PCR Melting curve of *ferritin 1* primer optimisation in *Rhipicephalus sanguineus*. Data was obtained by qPCR using the *ferritin 1_forward* and *ferritin 1_reverse* primers and a 10-fold dilution series of midgut or salivary gland cDNA as the template. **A –** Melting curve for the midgut samples (T_m = 84.0ºC), and **B -** Melting curve for the salivary gland samples (T_m = 84.5ºC). **Legend: Y axis -** normalised fluorescence units (-d(RFU)/dT) against **X axis** - temperature (ºC). Melting curve and dissociation temperature were automatically determined by the CFX Manager™ Software (Bio-Rad).

Some of the qPCR amplicons originated from the SGs and MG cDNA were run on a 1.2% agarose gel to confirm the presence of fragment spanning 150 bp (Figures 18 and 19, respectively).

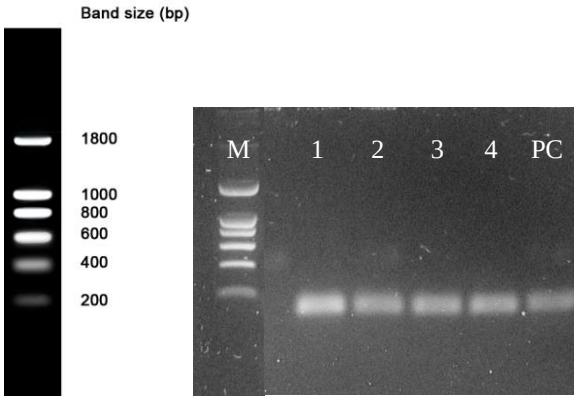

Figure 18. Agarose gel of *ferritin 1* PCR products following amplification from the salivary glands of *Rhipicephalus sanguineus* adult females.

Lane M: Marker (NZYDNA Ladder I, NZYTech); **Lanes 1 and 2:** DNA amplified from the control group injected with elution buffer; **Lanes 3 and 4:** DNA amplified from the *ferritin 1*-silenced group; **PC:** positive control with amplicon from the standard curve. Both groups show a PCR product of approximately 150 bp in length on a 1.2 agarose gel using the primers *ferritin 1_forward* and *ferritin 1_reverse.*

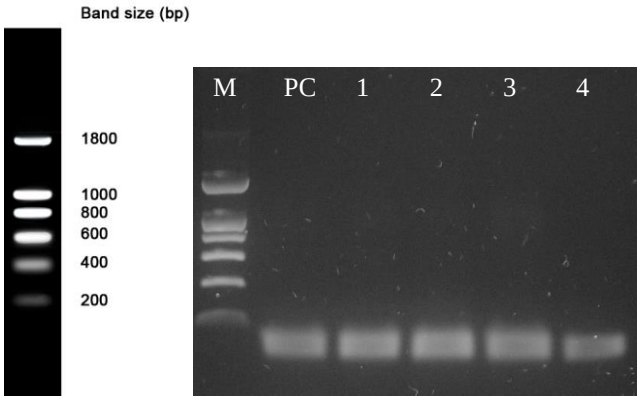

Figure 19. Agarose gel of *ferritin1* PCR products following amplification from the midgut of *Rhipicephalus sanguineus* adult females.

Lane M: Marker (NZYDNA Ladder I, NZYTech); **PC:** positive control with amplicon from the standard curve; **Lanes 1 and 2:** DNA amplified from the control group injected with elution buffer; **Lanes 3 and 4:** DNA amplified from the *ferritin 1*-silenced group. Both groups show a PCR product with approximately a 150 bp on a 1.2% agarose gel using the primers *ferritin 1_forward* and *ferritin 1_reverse*.

Real time PCR products amplified from both organs were purified from the gel and sent for Sanger sequencing, following quality and concentration determination by spectrophotometry (SGs amplicon = 11.8 ng/µl and a A_{260}/A_{280} ratio = 1.87; MG amplicon = 12.7 ng/µl and a A_{260}/A_{280} ratio = 1.68). A BLAST was conducted to confirm the identity of the amplified product, and small number of sequences were retrieved with high homology to tick *ferritin* (93.06 - 100.00% sequence identity). From these, three sequences had 100% identity: *Rhipicephalus sanguineus* isolate Thai ferritin (Fer) mRNA, partial cds (GenBank accession nr. KP688390.1); predicted *Rhipicephalus sanguineus* soma ferritin-like (LOC 119382540) mRNA (GenBank accession nr. XM_037650283.1); and *Rhipicephalus sanguineus ferritin* (Fer) mRNA, complete cds (GenBank accession nr. AY277907.1) (Supplementary Table 14).

Similarly, qPCR conditions for 4 reference genes were optimised and their specificity assessed to use in both organ samples of this tick species. Primer sequences were previously reported, including the ones for tick *β-actin*, *β-tubulin* and *elf* (228), and *16S* rDNA (230). Reaction efficiencies varied from 91.9 - 115.3% for the SGs and 90.0 -

98.9% for the MG samples. A single peak of T_m was observed in the Melting curve of each reference gene for the MG and for the SGs samples; thus, confirming the amplification of the specific DNA target (Table 2).

Table 2. Dissociation temperatures of reference gene PCR products to use in subsequent qPCR reactions with *Rhipicephalus sanguineus* salivary glands and midgut templates.
Temperatures of *β-actin*, *β-tubulin*, *elf* by Nijhof et al. (2009) and *16S* rDNA by Zivkovic et al. (2010), obtained for the control and *ferritin 1*-silenced groups DNA by qPCR. Results calculated automatically with CFX Manager™ Software (Bio-Rad).

	Dissociation temperature (T_m/ ºC)
***16S* rDNA**	73.5 – 74.0
β-actin	84.0 – 84.5
β-tubulin	83.0 – 83.5
elf	84.0 – 84.5

Some of the qPCR-amplified products derived from the MG template were separated on a 1.2% agarose gel to confirm the presence of bands with the correct size. Approximate sizes of bands on the gel: 212 bp for *16S* rDNA, 127 bp for *β-actin*, 140 bp for *β-tubulin* and 109 bp for *elf* (Figure 20).

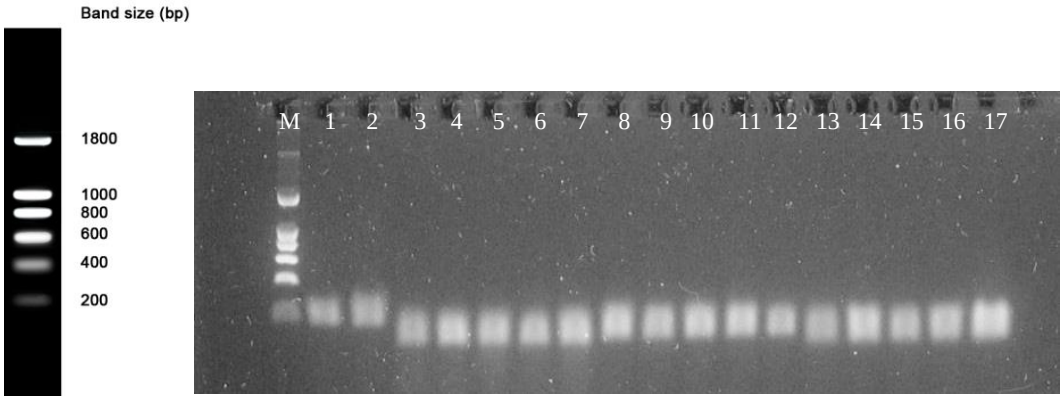

Figure 20. Agarose gel of *β-actin*, *β-tubulin*, *16S* rDNA and *elf* PCR products following amplification from the midgut of *Rhipicephalus sanguineus* adult females.

Lane M: Marker (NZYDNA Ladder I, NZYTech); **Lane 1:** *16S* rDNA amplified from the control group injected with elution buffer; **Lane 2:** *16S* rDNA positive control with amplicon from the standard curve; **Lanes 3 to 6:** *β-actin* DNA amplified from the *ferritin 1*-silenced **(3 and 4)** group, the control group **(5 and 6)**; **Lane 7:** *β-actin* DNA positive control with amplicon from the standard curve; **Lanes 8 to 11:** *β-tubulin* DNA amplified from the *ferritin 1*-silenced **(8 and 9)** group, the control group **(10 and 11)**; **Lane 12:** *β-tubulin* DNA positive control with amplicon from the standard curve; **Lanes 13 to 16:** *elf* DNA amplified from the *ferritin 1*-silenced **(13 and 14)** group, the control group **(15 and 16)**; **Lane 17:** *elf* DNA positive control with amplicon from the standard curve; PCR-product sizes were approximately 212, 127, 140 and 109 bp using the primers *16S_forward* and *16S_reverse* by Zivkovic et al. (2010), *β-actin_forward* and *β-actin_reverse*, *β-tubulin_forward* and *β-tubulin_reverse* and *elf_forward* and *elf_reverse* by Nijhof et al. (2009), respectively, visualised on a 1.2% agarose gel.

One PCR amplicon for each gene from both organs was purified from the gel and sent for Sanger sequencing, following quality and concentration determination by spectrophotometry (Table 3).

Table 3. Concentration and purity of *β-actin*, *β-tubulin*, *16S* rDNA and *elf* PCR-purified products from *Rhipicephalus sanguineus*.

DNA of *R. sanguineus* salivary glands and midgut was used as the template. Parameters measured by spectrophotometry using a NanoDrop ND-1000 (ThermoFisher Scientific).

	Salivary Glands		**Midgut**	
	DNA Concentration (ng/µl)	**A_{260}/A_{280} ratio**	**DNA Concentration (ng/µl)**	**A_{260}/A_{280} ratio**
***16S* rDNA**	12.3	1.87	22.3	1.89
β-actin	18.5	1.65	14.2	1.76
β-tubulin	9.8	1.90	8.3	1.82
elf	11.9	1.82	13.2	1.79

A BLAST with the amplicon sequences for *β-actin* has shown homology of 98.39% to the predicted *Rhipicephalus sanguineus* actin, clone 403 (LOC119400476), mRNA sequence (GenBank accession nr. XM_037667534.1); for *β-tubulin*, 100% homology with the predicted *Rhipicephalus sanguineus* tubulin beta chain (LOC119375769), transcript X2 mRNA sequence (GenBank accession nr. XM_037645905.1); and for *16S* rRNA, 100% homology with *Rhipicephalus sanguineus* isolate 3 *16S* ribosomal RNA gene, partial sequence (GenBank accession nr. MH765331.1) (Supplementary Table 15).

Normalised relative expression of *ferritin 1* was quantified by qPCR in the SGs and MG. The triplicate negative controls were clean (no amplification). For the SGs, plate efficiency varied between 91.9 - 115.3%, and for the MG between 90.0 - 107.5%. Data was normalised using the reference genes *β-actin*, *β-tubulin*, *elf* (228) and *16S* rDNA (230). All reference genes were considered acceptable for the gene study (M-value < 1; Table 4).

Table 4. Stability values (M-value) of the reference genes used in the control and *ferritin 1*-silenced groups in the salivary glands and midgut.

The genes *β-actin*, *β-tubulin* and *elf* by Nijhof et al. (2009), and *16S* rDNA by Zivkovic et al. (2010) were used as reference genes. Results were obtained by qPCR analysis and calculated automatically with CFX Manager™ Software (Bio-Rad).

	M-value	
	Salivary Glands	**Midgut**
***16S* rDNA**	0.6266	0.5028
β-actin	0.6436	0.5181
β-tubulin	0.3802	0.4431
elf	0.4127	0.4431

Gene knockdown was then confirmed in the SGs and MG, with 33.6% and 43.6% reductions in *ferritin 1* expression levels, respectively (Figure 21). Statistically significant differences were not found between the silenced and control groups ($p > 0.05$; $p = 0.875$ for the MG and $p = 0.058$ for the SGs).

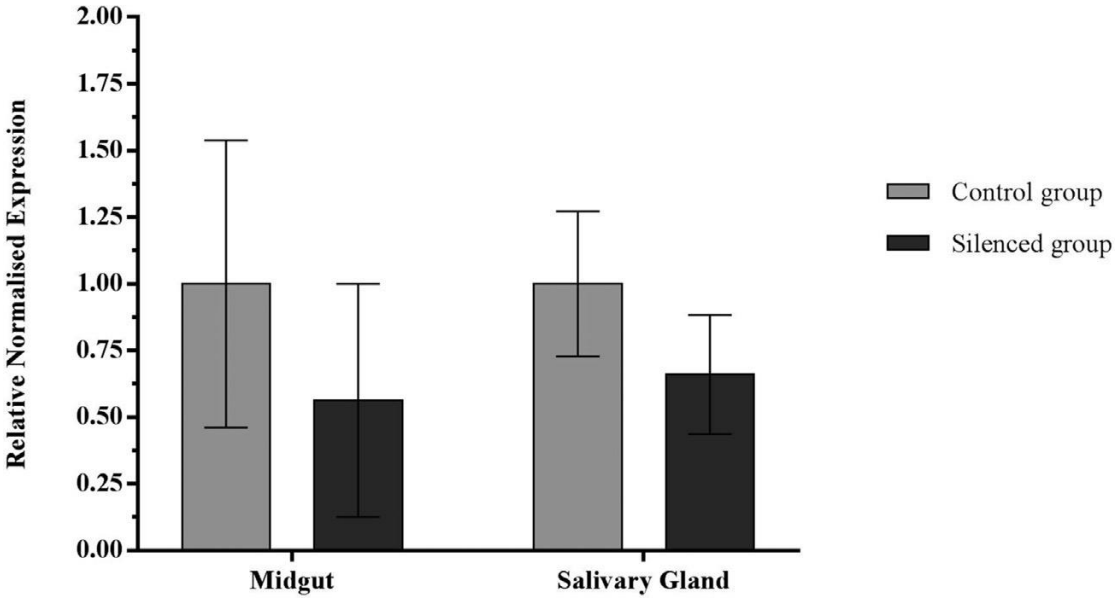

Figure 21. Relative normalised expression levels of *ferritin 1* in the midgut and salivary glands of *Rhipicephalus sanguineus* s.l. adult females during *Ehrlichia canis* experimental infection after RNAi. Data was normalised against the reference genes *β-actin*, *β-tubulin*, *elf* and *16S* rDNA. Columns represent the Mean of relative normalised expression of *ferritin 1* (*n* control = 13 and *n* silenced = 11 for MG) (*n* control = 15 and *n* silenced = 19 for SGs) and the error bars the ± Standard Error of the Mean (SEM). Results were calculated automatically with CFX Manager™ Software (Bio-Rad). Statistically significant differences were not found in the expression levels when compared with the control group using student's *t*-test with unequal variance ($p > 0.05$; $p = 0.058$ for the SGs and $p = 0.875$ for the MG) (Figure created with GraphPad Instat® version 3.06).

3.2.2. Evaluation of tick weight after RNAi

The importance of *ferritin 1* on tick engorgement and survival was evaluated after gene silencing until 9 days *post*-infestation. Table 5 shows the number of ticks that completed feeding, the average body weight and survival rate. Supplementary Table 16 shows individual tick weights. Results show that tick ability to complete feeding ($p > 0.05$; $p = 0.1205$), recognised in this study as natural drop-off, and tick mortality ($p > 0.05$; $p = 0.2974$) did not have a statistically significant difference between *ferritin 1* dsRNA injected ticks and the controls injected with elution buffer. Thus, the null hypothesis was accepted ($p > 0.05$), suggesting that, for the level of silencing achieved (33.6% in the SGs, 43.6% for the MG) *ferritin 1* downregulation does not affect tick survival. The average body weight was statistically significantly higher in the control group (124.4 mg ± 40.3) ($p < 0.05$; $p = 0.0013$) than the *ferritin 1*-silenced group (76.0 mg ± 35.8), demonstrating an impairment of the feeding process.

Table 5. *Rhipicephalus sanguineus* body weight after *ferritin 1*-silencing in ticks.
Adult female ticks were injected with *ferritin 1* dsRNA or with elution buffer as a control. Ticks were allowed to feed on a dog experimentally infected with *Ehrlichia canis*. Complete feeding was considered when ticks naturally detached from the host. After detachment, ticks were collected and weighed. Tick mortality was determined by the difference between the total number of female ticks put in the chamber (30) for each group and the ones considered dead.

Group	Number of ticks completing feeding (%)	Weight after detachment (mean ± s.d.; mg/tick)	Tick mortality (%)
Control	43.3 (13) *	124.4 ± 40.3	50.0 (15)
ferritin 1-silenced	63.3 (19)	76.0 ± 35.8 **	36.7 (11)

* At day 9 post-infestation, 2 ticks in the control group that did not detach were removed and their weight not considered.
** Significant differences between both groups were determined by the student's *t* test ($p < 0.05$; $p = 0.0013$).

3.2.3. Impact of *ferritin 1*-silencing on tick ovaries and oocyte development

To determine the effect of *ferritin 1*-silencing in tick ovary development, the ovaries were analysed by light microscopy. This part of the study was developed at the Department of Veterinary Pathology, FCAV-UNESP, Jaboticabal, Brazil, and is published in detail by Ferrolho et al. (2017) (260).

Our results show that ticks of the *ferritin 1*-silenced group presented larger amounts of immature oocytes, and that the mature oocytes were undergoing a degenerative and/or reabsorption process, in comparison with the controls. Furthermore, the cells of the pedicel showed morphological alterations, which included the loss of nuclei and of cell contact, decreased cell numbers forming the pedicel, and nucleated cells located in lateral areas. Oocytes in the stages I and II presented an irregular shape and vacuolated cytoplasm, with the vacuoles located near the marginal region. Oocytes III and IV presented loss of cellular contour with the presence of folds and deformations along the entire length of the chorion. The cytoplasm was heterogeneous, with a different distribution pattern of yolk granules and small areas of vacuolization. Oocytes IV also presented autophagic vesicles distributed through the cytoplasm. A schematic representation of the morpho-histological alterations observed in oocytes I to IV is presented in Figure 22.

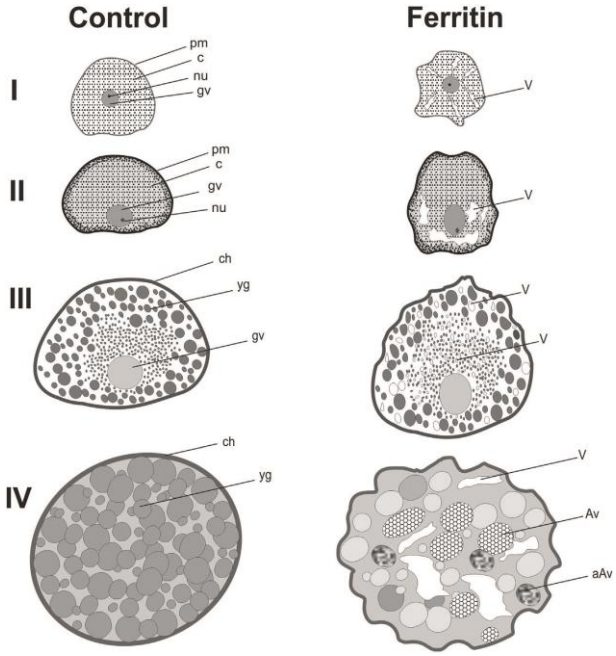

Figure 22. Schematic illustration of the morpho-histological alterations observed in oocytes (I–IV) of *Rhipicephalus sanguineus* s.l. females subjected to *ferritin 1*-silencing.

Legend: I = oocyte I; **II** = oocyte II; **III** = oocyte III; **IV** = oocyte IV; **pm** = plasmic membrane; **nu** = nucleolus; **gv** = germinal vesicle; **c** = cytoplasm; **ch** = chorion; **yg** = yolk granules; **v** = vacuolated area; **Av** = autophagic vesicle; **aAv** = autophagic vesicle in advanced digestion stage.

3.2.4. *Ehrlichia canis* quantification

The effect of *ferritin 1*-silencing in *E. canis* acquisition and multiplication by *R. sanguineus* was investigated by qPCR targeting *E. canis 16S* rRNA (134) in the SGs. Samples from the MG were not analysed because it was not possible to completely exclude the presence of host blood infected with this bacterium, despite all the washes during dissection with PBS.

No amplification was observed in the triplicate negative controls and reaction efficiency between plates, determined by 10-fold serial dilution standard curves of *E. canis* Jaboticabal strain purified DNA, was 97.5% in the *ferritin 1*-silenced, and 97.8% in the control group. Even though correct amplification was observed in the positive controls, when testing all the samples from both groups, no *E. canis* DNA was detected.

3.3. Transcriptome analysis

3.3.1. Gene expression profile of *Rhipicephalus sanguineus* salivary glands in response to *Ehrlichia canis* experimental infection

The sialome of fed uninfected and fed *E. canis*-infected *R. sanguineus* ticks was determined using high throughput RNA-seq.

Before cDNA library preparation, the presence of *E. canis* DNA was determined in all samples targeting the *16S* rRNA (134), after gDNA extraction. Samples included SGs from ticks fed on the naïve host (1 to 8) and from ticks fed on the *E. canis*-inoculated dog (9-18). The concentration and purity of each sample was assessed by spectrophotometry, with values ranging from 16.57 - 44.80 ng/µl and a $A_{260/280}$ between 1.38 - 1.81 (Supplementary Table 17).

The DNA extraction method and the absence of PCR inhibitors were validated by PCR targeting tick *18S* rRNA, as previously described (229). The amplification of a 500 bp PCR product visualised on a 1.2% agarose gel confirms the successful validation of the method (Figure 23).

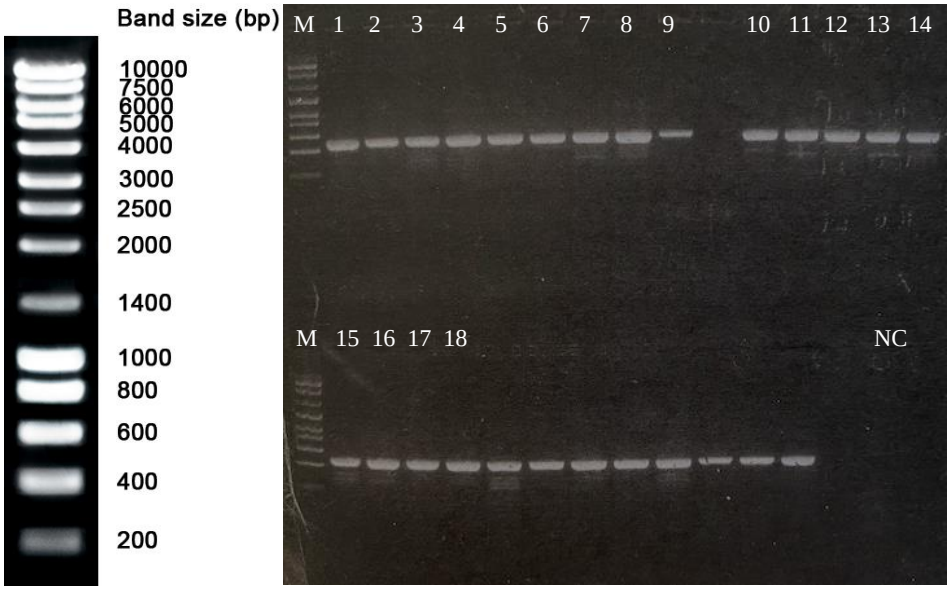

Figure 23. Agarose gel of *18s* rRNA PCR products following amplification from the salivary glands of *Rhipicephalus sanguineus* adult females.

Lane M: Marker (NZYDNA Ladder III, NZYTech); **Lane 1 to 8:** Samples of DNA from ticks fed on the naïve host, and **Lanes 9 and 18:** Samples of DNA from ticks fed on the inoculated host; Both groups show a 500 bp product visualised on a 1.2% agarose gel using the primers *tick-sense* and *tick-antisense* described by Shayan et al. (2007); **NC:** negative control.

qPCR was carried out using two tick reference genes, *ß-actin* and *ß-tubulin* (228) for data normalisation. Both reference genes were classified as acceptable (M-value <1; M-value$_{ß\text{-}actin}$ = 0.1171*;* M-value$_{ß\text{-}tubulin}$ 0.1171). Triplicate negative controls were clean (no amplification) and the reaction efficiency, determined by 10-fold serial dilution standard curves of *E. canis* Jaboticabal strain purified DNA, varied between 90% - 110%. Only samples 9 to 18 were confirmed to be positive for the presence of *E. canis*.

For RNA-seq data acquisition, total RNA was extracted from the same samples and their individual concentration and purity was assessed by spectrophotometry (Supplementary Table 5). The $A_{260/280}$ of the samples varied from 1.66 - 2.27, whilst concentrations ranged between 138.35 - 740.92 ng/µl.

Four pools of RNA samples were sequenced (RNA-seq) at Unidad de Genómica – Fundación Parque Científico de Madrid, Spain and the data was analysed at Era7 Bioinformatics - Parque Científico de Madrid, Spain. When these experiments were undertaken in 2015, the SGs of *R. sanguineus* lacked a pre-existing, publicly available, transcriptome. Therefore, *de novo* assemblies were produced for each of the four transcriptomes, which comprised of two biological replicates for the fed *E. canis*-infected SGs (SAP_1 and SAP_2) and two for the fed uninfected SGs (SAP_3 and SAP_4). After sequencing the RNA, primer sequences were removed from the reads and low-quality bases were trimmed. From this, three *de novo* assemblies, each with three different k values, were produced for each of the four transcriptomes. The GC-content was 52% and 53% for the two replicates of uninfected and *E. canis*-infected SGs, respectively. According to the standard quality metrics for the transcriptome assemblies (ExN50), 50% of the assembled bases were incorporated in transcripts of 1408 for SAP_1, 1227 for SAP_2, 1320 for SAP_3 and 996 for SAP_4, nt in length. The median coverage depth, total number of obtained and used reads during the assembly, and *loci* for each replicate, are described in Table 6.

Table 6. Assembly statistics for the *Rhipicephalus sanguineus* sialotranscriptome.
Technical replicates for fed and *Ehrlichia canis*-infected salivary glands were designated as SAP_1 and SAP_2 and for fed and uninfected salivary glands as SAP_3 and SAP_4.

	Median Coverage Depth	**Total Reads**	**Used Reads**	***Loci***
SAP_1	33.378906	100,689,126	41,044,265	12745
SAP_2	41.304878	111,682,940	48,036,412	8219
SAP_3	21.993080	95,653,364	55,747,531	16172
SAP_4	65.842593	91,488,664	33,505,285	4089

From a total of 399,514,094 high-quality reads, the assemblies resulted in 212,372,066 reads from the infected samples, from which 89,080,677 (41.94%) were used for the study. For the uninfected samples, a total of 187,142,028 reads were obtained, of which 89,252,816 (47.69%) were also used for the study.

3.3.2. Transcriptome annotation

A pan-proteomics approach was employed to annotate the four transcriptomes. Using a set of 80104 reference proteins belonging to the taxon "*Ixodidae*" derived from the UniProtKB database, translated *R. sanguineus* nucleotide sequences were queried using BLAST. A total of 23080 putative *R. sanguineus* sequences were submitted, returning a total of 22515 "hits" that were present in any of the four transcriptomes. This total was comprised of 7015, 2223, 12734 and 543 hits from the SAP1, 2, 3 and 4 libraries, respectively. After obtaining a set of UniGenes for each transcriptome and assigning each transcript to a known protein based on the BLAST similarity, expression levels of all the transcripts were quantified using eXpress (248). Clustering via UniRef90 identified a total of 15521 putative *R. sanguineus* proteins that were present in any of the four transcriptomes. From the 15521 transcripts identified, 11517 and 10304 transcripts were exclusive to the *E. canis*-infected and the uninfected samples, respectively. After the first step of annotation, a statistical analysis was conducted to detect significant differences ($p < 0.05$) using the X^2 to compare the gene expression data between uninfected and *E. canis*-infected SGs. A total of 10 differentially expressed transcripts were found, of which 6 were downregulated and 4 were upregulated. Only the transcripts with a significant difference between the two conditions that could be associated with pathogen infection, multiplication and transmission were classified according to their Molecular Function (MF), Biological Process (BP) and Cellular Component (CC) using UniProtKB tools (GO data available in Supplementary Table 18).

The downregulated transcripts encoded for a glutathione S-transferase (GST; UniProtKB Q6JVN0; Log_2 fold-change -1.888453347), a ubiquitin carboxyl-terminal hydrolase (UCH; UniProtKB L7M3C8; Log_2 fold-change -0.440572591), a putative trilaris (UniProtKB L7MCD9; Log_2 fold-change -0.23786383), two putative uncharacterized proteins (UniProtKB G3MH55; Log_2 fold-change -0.196743834 and B7QAF5; Log_2 fold-change -0.189166798) and a protein kish (UniProtKB G3MNA8; Log_2 fold-change -0.176994575).

Amongst those upregulated were transcripts encoding the following proteins: a putative mitochondrial import inner membrane translocase – subunit TIM21 (TIM - translocases

of the inner membrane; UniProtKB L7MF27; Log_2 fold-change 0.446198431), putative mitochondrial import inner membrane translocase – subunit TIM23 (UniProtKB B7PEW5; Log_2 fold-change 0.654326094), importin subunit α (IMP; UniProtKB L7M4M0; Log_2 fold-change 0.925483612) and putative serine carboxypeptidase (PSC; UniProtKB L7MH00; Log_2 fold-change 0.959774565).

The second BLAST carried out with the OmicsBox Software is represented in Figures 24 and 25 multi-level charts that summarise the functional annotation of the *R. sanguineus* female ticks transcriptome fed on uninfected and on an *E. canis* infected host for transcripts that were significantly differentially expressed ($p < 0.05$). From the 10 differentially expressed transcripts, 4 (40%) were GO annotated and 6 (60%) presented BLAST hits. The transcript corresponding to a putative uncharacterised protein (UniProtKB B7QAF5) did not retrieve any MF, BP and CC, being classified as unknown for these categories.

In Figure 24, GO annotation (level 2) highlights several BP according to the distribution level that includes cellular process (3), metabolic process (2) and localisation (1). Four transcripts had unknown BP. At the MF level, GO distribution was associated with catalytic activity (2) and transporter activity (1). Lastly, at CC level annotation included cellular anatomical entity (3) and protein-containing complex (2). Three transcripts had unknown MF and CC.

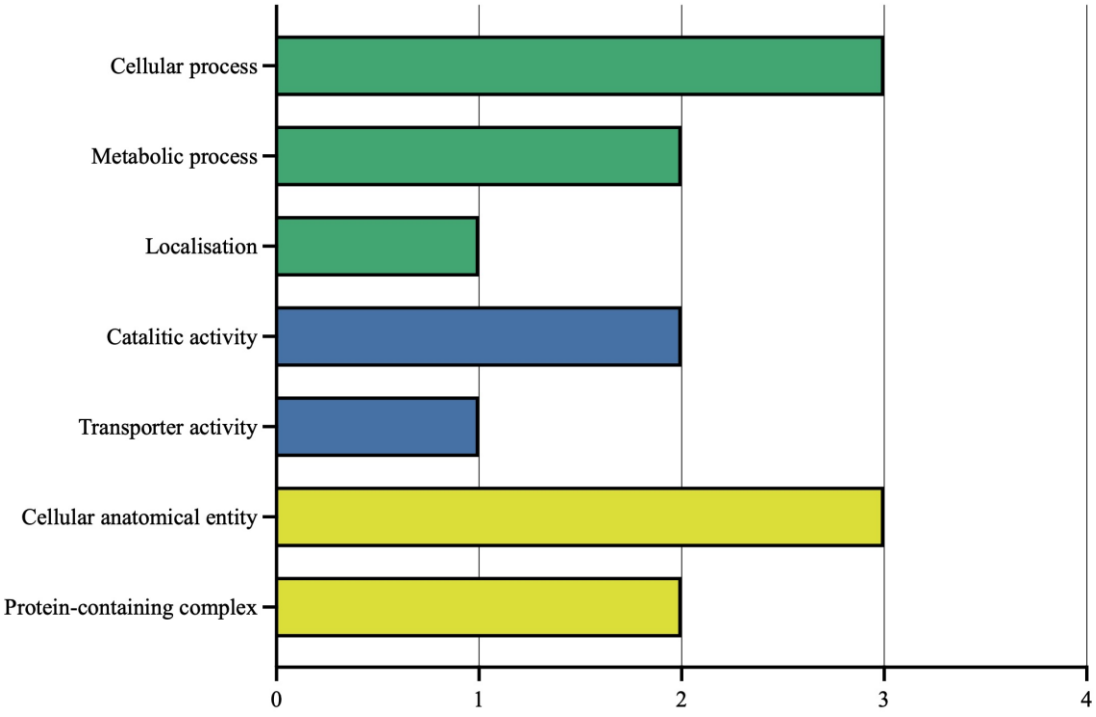

Figure 24. *Rhipicephalus sanguineus* transcriptome GO annotation (level 2) in response to *Ehrlichia canis* infection.

A total of 10 differentially expressed transcripts ($p < 0.05$) were annotated based on Biological Process **(BP)**, Molecular Function **(MF)** and Cellular Component **(CC)**. **X-axis –** Direct GO counts; **Green:** BP; **Blue:** MF; **Yellow:** CC. Data was analised using OmicsBox Software (Version 2.1.14; BioBam Bioinformatics 2019, available at www.biobam.com/omicsbox); (Figure created with GraphPad Prism software; version 9 for macOS).

At level 3, BP functions were related with the protein import into the mitochondrial complex (1), protein glycosylation (1) and glutathione metabolic process (1). MFs were related with transferase activity (1), protein transmembrane transporter activity and glutathione transferase activity (1). At CC level transcripts were located as integral component of membrane (2), at the Golgi membrane (1) and on an oligosaccharyl transferase complex (1). These results are shown in Figure 25.

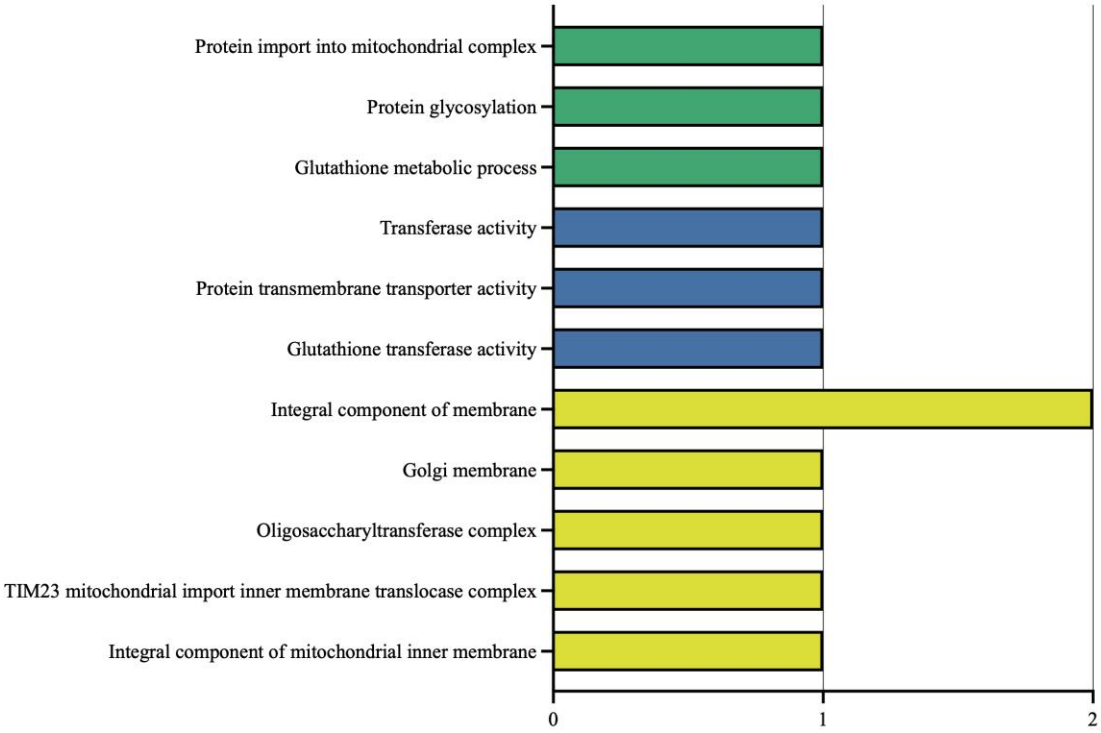

Figure 25. *Rhipicephalus sanguineus* transcriptome direct GO counts (level 3) in response to *Ehrlichia canis* infection.

A total of 10 differentially expressed transcripts ($p < 0.05$) were annotated based on Biological Process **(BP)**, Molecular Function **(MF)** and Cellular Component **(CC)**. **X-axis** – Direct GO counts; **Green:** BP; **Blue:** MF; **Yellow:** CC. Data was analised using OmicsBox Software (Version 2.1.14; BioBam Bioinformatics 2019, available at www.biobam.com/omicsbox); (Figure created with GraphPad Prism software; version 9 for macOS).

Regarding enzyme distribution, GO annotation resulted in two categories that included transferases (2) and translocases (1).

3.3.3. Validation of RNA-seq data

To validate the RNA-seq data, mRNA levels of two transcripts differentially expressed in the transcriptome data during *E. canis* infection were determined by qPCR. Selected genes corresponded to the proteins PSC (UniProtKB L7MH00) and IMP (UniProtKB L7M4M0).

Real-time PCR conditions for the primer pairs *psc_RS_forward* and *psc_RS_reverse* and *imp_RS_forward* and *imp_RS_reverse* were optimised and their specificity to amplify the *psc* and *imp* fragments was tested in *R. sanguineus* SGs. A 10-fold dilution series of *R. sanguineus* cDNA was used to determine the reaction efficiency and the T_m. Reaction efficiency for *psc* was 106.2% and a single peak was observed in the Melting curve with a T_m = 81.5˚C (Figure 26 – A). For *imp*, reaction efficiency was 101.2%, with a single peak in the Melting curve with a T_m = 83.0˚C (Figures 26 – B).

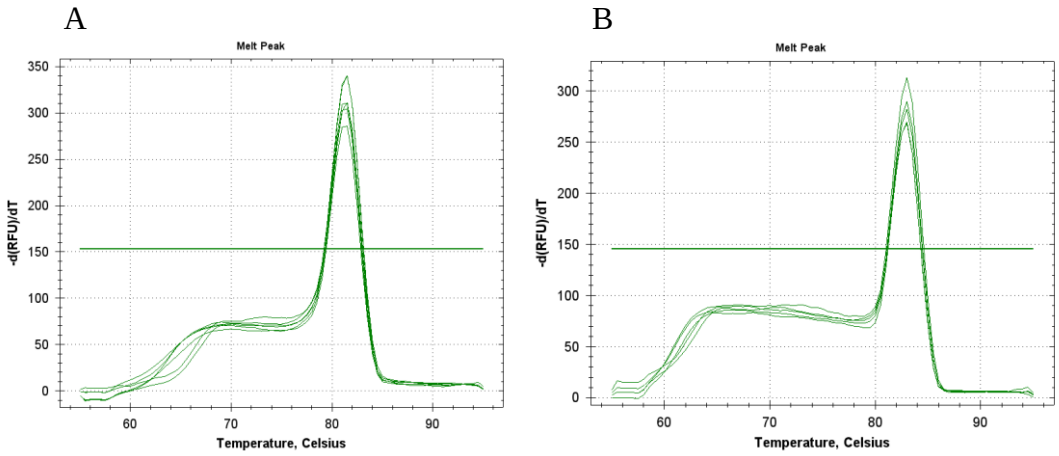

Figure 26. Real time PCR Melting curve of *psc* and *imp* primer optimisation in *Rhipicephalus sanguineus*. Charts were obtained with the *psc_RS_forward* and *psc_RS_reverse* and the *imp_forward* and *imp_reverse* using a 10-fold dilution series of cDNA. **A –** Melting curve for *psc* samples (T_m = 81.5ºC), and **B -** Melting curve for *imp* samples (T_m = 83.0ºC) **Legend: Y axis -** normalised fluorescence units (-d(RFU)/dT) against **X axis** - temperature (ºC). Melting curve and dissociation temperature were automatically determined by the CFX Manager™ Software (Bio-Rad).

Amplification of *psc* and *imp* DNA was confirmed by single bands of the expected sizes of approximately 129 bp and 103 bp, respectively, following 1.2% agarose gel (data not shown). For a final validation of primer specificity, qPCR products were sequenced, after quality and concentration determination by spectrophotometry. The concentration of *imp* purified amplicon = 9.8 ng/µl with a $A_{260/280}$ = 2.74; the purified *psc* amplicon = 4.4 ng/µl and a $A_{260/280}$ = 1.30. The BLAST showed a high identity between the *psc* amplicon and *Rhipicephalus sanguineus* serine carboxypeptidase (GenBank accession nr. XM_037642511.1 and XM_037673211.1) with 96.95% similarity, and between the *imp* amplicon and *Rhipicephalus sanguineus* importin subunit α-1-like (GenBank accession nr. XM_0376633282.1) with 99.02% similarity. Further details are shown in Supplementary Table 19.

Expression levels of *psc* and *imp* in the SGs were determined using cDNA synthesised from ticks fed on a naïve host and ticks fed on an *E. canis*-inoculated host. Samples were pooled in 3 groups of 10 SGs, for each group. Data was normalised using two reference genes, *ß-actin* and *ß-tubulin* (228). Both reference genes were classified as acceptable (M-value <1; M-value = 0.4213). Triplicate negative controls were clean (no amplification) and the reaction efficiency between plates, determined by 10-fold serial dilution standard curves of *R. sanguineus* SGs DNA, varied from 92.2 - 95.0% for *psc*, and 89.2 - 100.8% for *imp*.

Regarding the relative normalised expression, both genes were found downregulated, without statistical significance (p <0.05; *psc* p = 0.281661; *imp* p = 0.839141), when comparing the infected to the uninfected samples. A Log2 fold-change -1 and -0.23447 was verified for *psc* and *imp* expression levels, respectively (Figure 27). This result contrasts with what was found in the sialome where the transcription levels were upregulated, with Log_2 fold-change 0.278598328 for *imp* and 0.288920933 for *psc.*

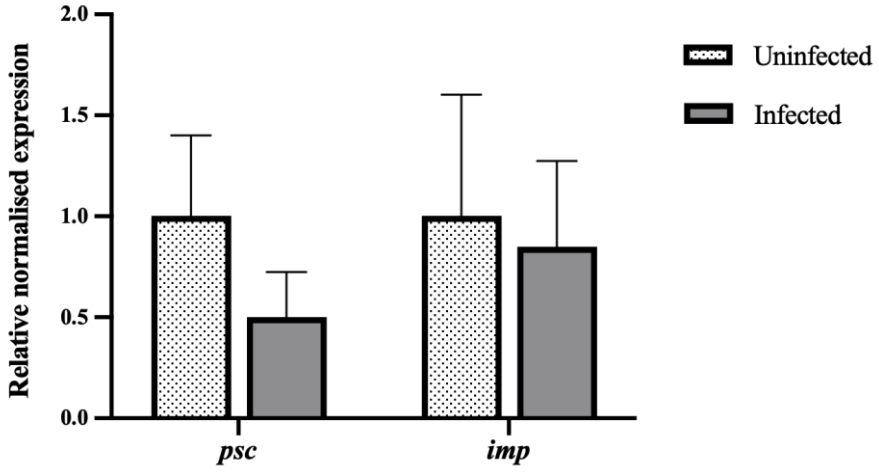

Figure 27. Relative normalised expression levels of *psc* and *imp* in the salivary glands of *Rhipicephalus sanguineus* s.l. adult females during *Ehrlichia canis* infection.
Relative normalised expression of both genes was evaluated in uninfected **(dotted)** and in *E. canis*-infected **(grey)** ticks. Data was normalised using the reference genes *β-actin* and *β-tubulin*. Results were calculated automatically with CFX Manager™ Software (Bio-Rad). Columns represent the Mean of relative normalised expression (*n* uninfected = 30 and *n* infected = 30) +SEM. Statistically significant differences were not found in the expression levels when comparing both groups of each gene using Welch's unequal variances *t*-test ($p < 0.05$; *psc* $p = 0.281661$; *imp* $p = 0.839141$); (Figure created with GraphPad Prism software; version 9 for macOS).

Several other genes differentially regulated ($p < 0.05$) in the transcriptomic data were tested for qPCR amplification but without success, including the ones encoding for the putative mitochondrial import inner membrane translocases – subunit TIM23 (UniProtKB B7PEW5), and – subunit TIM21 (UniProtKB L7MF27), the protein kish (UniProtKB G3MNA8), the putative trilaris (UniProtKB L7MCD9) and the GST (UniProtKB Q6JVN0).

To further investigate *psc* gene expression, a different model was tested using IDE8 cells even though this cell line is derived from embryonated eggs and may contain various cell populations with different morphology and behaviour, that could affect transcriptional response to infection (193).

Real time PCR primers were designed and optimised to use in IDE8 cells. Reaction efficiency was 90.5% and the Melting curve with T_m = 82.0 - 82.5ºC presented a single peak (Figure 28).

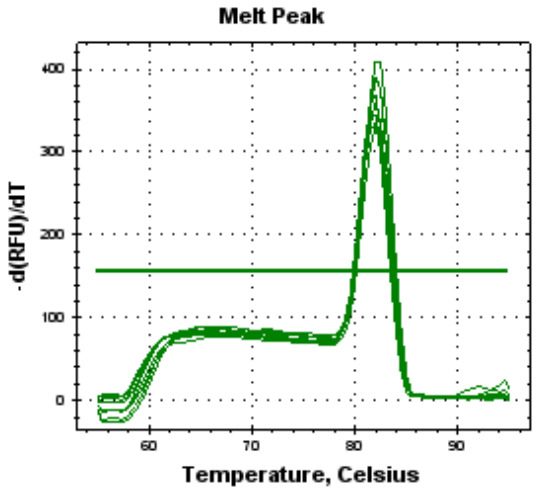

Figure 28. Real time PCR Melting curve of *psc* primer optimisation in IDE8 cells.
Chart was obtained with the *psc_IDE8*_forward and *psc_IDE8*_reverse primers using a 10-fold series of IDE8 cDNA dilutions. Melting curve with **T_m =** 82.0 - 82.5ºC. **Legend: Y axis -** normalised fluorescence units (-d(RFU)/dT) against **X axis** - temperature (ºC). Melting curve and dissociation temperature were automatically determined by the CFX Manager™ Software (Bio-Rad).

Amplification of *psc* DNA was confirmed by the presence of a single band of the expected size of approximately 146 bp following 1.2% agarose gel (data not shown). Further validation of primer specificity was carried with qPCR-product purification and sequencing after quality and concentration determination by spectrophotometry (*psc* amplicon = 10.7 ng/µl and a $A_{260/280}$ = 1.7). A BLAST was conducted, and the PCR product showed high identity with the retrieved sequence of *Ixodes scapularis* probable serine carboxypeptidase CPVL (LOC115310902), mRNA (GenBank accession nr. XM_029969380.4) with 98.29% similarity (E value 1e-^{47}; query cover 23%).

After primer optimisation, qPCR was used to analyse the differential expression of the *psc* gene in IDE8 cells. RNA used to synthesize cDNA was extracted from 4 biological replicates for each condition (uninfected and *E. canis*-infected cells), containing a concentration of 4.16x10^5 cells/ml *per* replicate (RNA concentration and purity not shown). *E. canis* infection was confirmed by microscopic examination of Giemsa-stained

cytocentrifuge smears. Two reference genes were selected to normalise the data: *β-tubulin* and *elf* and were classified as acceptable (M-value <1; M-value = 0.4528). Triplicate negative controls were clean (no amplification) and the reaction efficiency varied between 99.7 - 113.5%.

The relative normalised expression of *psc* in uninfected and *E. canis*-infected IDE8 cells is presented in Figure 30. Upregulated *psc* expression was found in the *E. canis*-infected cells (Log2 fold-change 0.31581), when compared to uninfected controls. Gene upregulation was not statistically significant ($p > 0.05$; $p = 0.091183$). This result is in accordance with what was found in the SGs, in which *psc* was upregulated in the infected samples (Figure 29).

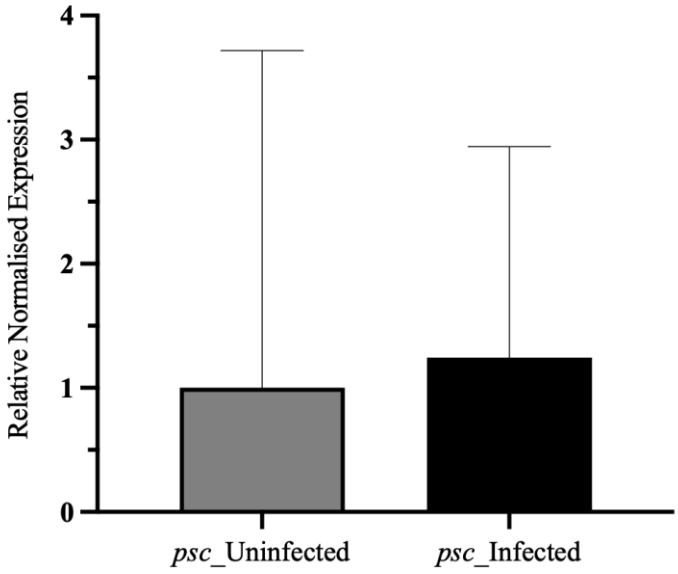

Figure 29. Relative normalised expression levels of *psc* in IDE8 cells during *Ehrlichia canis* infection. Relative normalised expression of *psc* was evaluated in uninfected **(grey)** and *E. canis*-infected **(black)** tick cells. Data was normalised using the reference genes *β-tubulin and elf*. Results were calculated automatically with CFX Manager™ Software (Bio-Rad). Columns represent the mean ($n = 4$) of relative normalised expression and the error bars the SEM. Statistically significant differences were not found in the expression levels when comparing both groups using Welch's unequal variances *t*-test ($p < 0.05$; $p = 0.091183$); (Figure created with GraphPad Prism software; version 9 for macOS).

3.3.4. *In vitro psc*-silencing and *Ehrlichia canis* quantification

In vitro gene knockdown was conducted in IDE8 cells to understand the role of *psc* in the vector-parasite interface using RNAi. DNA template for *psc* dsRNA synthesis was PCR-amplified with the primer pair *psc_IDE8_T7_forward* and *psc_IDE8_T7_reverse*, using IDE8 cDNA as template. Successful amplification was confirmed by the presence of a single band of approximately 412 bp following 1.2% agarose gel (Figure 30). The PCR product was purified and sequenced, following quality and concentration determination by spectrophotometry (*psc* amplicon = 15.1 ng/µl and $A_{260/280}$ = 1.82). A BLAST with the resulting sequence revealed 98.7% identity with the *Ixodes scapularis* probable serine carboxypeptidase CPVL (LOC115310902), mRNA (GenBank accession nr. XM_029969380.4) (E value 0.0; query cover 93%). The PCR amplicon was used as a template for dsRNA synthesis.

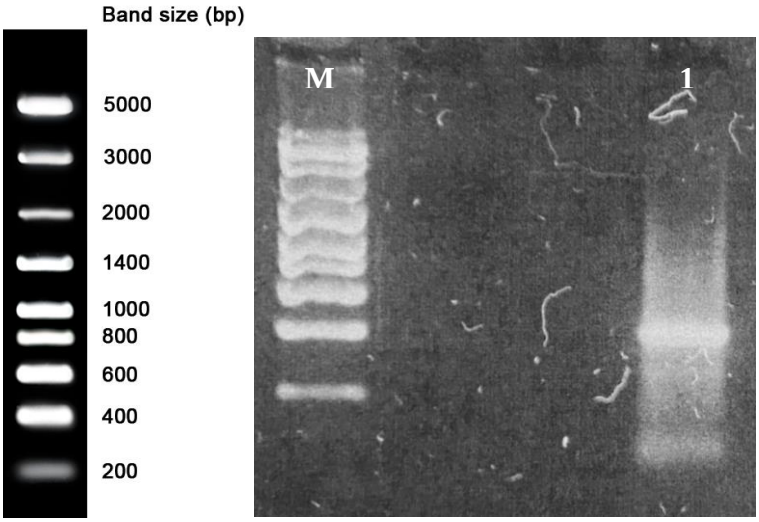

Figure 30. Agarose gel of purified *psc* PCR product following amplification from IDE8 cells.
Lane M: Marker (NZYDNA Ladder VIII, NZYTech); **Lane 1:** *psc* fragment of approximately 400 bp was amplified and visualised on a 1.2% agarose gel using *psc_IDE8_T7_forward* and *psc_IDE8_T7_reverse* primers.

For the *in vitro* knockdown assay, three experimental groups were defined: uninfected IDE8 cells (Group A; Figure 31 – (A)); uninfected cells inoculated with *E. canis* at 24 h *post*-seeding (Group B); and *E. canis*-infected cells (Group C; Figure 31 – (B)). Figure 32 confirms the presence of *E. canis* infection in IDE8 cells (Group C; Figure 32 – (B)) prior to cell seeding in Giemsa-stained cytocentrifuge smears, as well as its presence in the cell culture that originated the inoculum for Group B (Figure 31 – (C)).

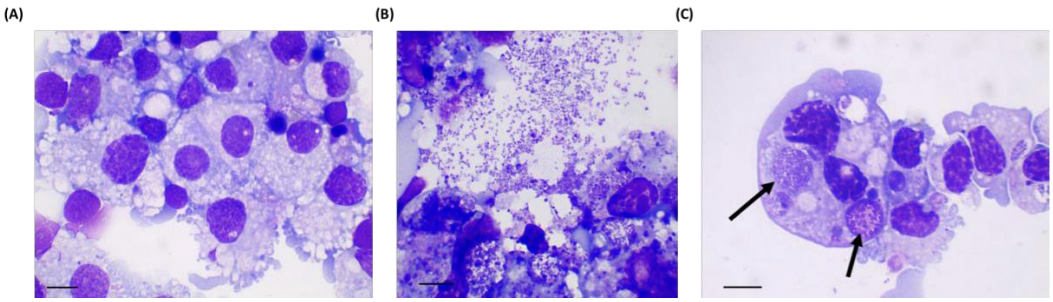

Figure 31. Light microscopy photographs of IDE8 cells infected with *Ehrlichia canis.*
(A) Uninfected IDE8 cells; **(B)** *E. canis*-infected IDE8 cells; and **(C)** *E. canis*-infected IDE8 cells before purification to generate the inoculum. Giemsa-stained cytocentrifuge smears were observed with a light microscope under 1000x magnification with immersion oil (Leitz GmbH & Co. KG, Oberkochen, Germany). Arrows indicate *E. canis* morulae. Scale bars = 20 µm.

IDE8 cells were inoculated either with $7.71x10^{12}$ molecules/µl of *psc* dsRNA or $1.79x10^{12}$ molecules/µl of *β2m* dsRNA as control (Supplementary Table 7). At each time point (T1, T2 and T3), cells were harvested for RNA extraction and cDNA synthesis. Supplementary Table 20 shows RNA concentration and purity for each sample assessed by spectrophotometry. In the group inoculated with *psc* dsRNA, the A_{260}/A_{280} ratio of the samples varied from 1.71 - 2.17 and concentrations ranged between 9.64 - 352.1 ng/µl. For the group inoculated with *β2m* dsRNA, the $A_{260/280}$ of the samples varied from 1.52 - 2.13, whilst concentrations ranged between 15.85 - 395.09 ng/µl. For cDNA synthesis, sample concentration was normalised to 50 ng/µl.

Relative normalised expression values were determined by qPCR for the unrelated control *β2m* and the gene of interest *psc*, as shown in Figure 32. Data was normalised against the reference genes *β-actin* and *β-tubulin* (228) and the obtained stability values were for $M\text{-value}_{T1}$ = 0.901, $M\text{-value}_{T2}$=0.557 and $M\text{-value}_{T3}$=0.223, therefore, they are

stable genes (M-value < 1). There was no amplification in the triplicate negative controls and reaction efficiency between plates, determined by a 10-fold serial dilution of IDE8 cDNA, varied between 90.2 - 115.2%. Gene silencing efficiency was calculated and the values at T1, T2 and T3 are presented in Table 7.

Table 7. Gene silencing efficiency for *psc* in IDE8 cells following RNAi.
Efficiency (%) was calculated from relative normalised expression of IDE8 cells inoculated with *psc* or *β2m* dsRNA. Expression values were obtained by qPCR analysis and calculated automatically with CFX Manager™ Software (Bio-Rad). Silencing efficiency was determined using the formula: $E_{silencing}$ (%) = ($\Delta\Delta Cq_{gene\ of\ interest}$ -$\Delta\Delta Cq_{control}$) x 100. **(T1) –** 48 hours; **(T2) –** 120 hours; **(T3) –** 160 hours.

	Silencing Efficiency (%)		
	T1	**T2**	**T3**
Uninfected	0%	13.02%	7.56%
Infected	0%	54.15%	0%
24h-*post* inoculation	0%	0%	68.30%

Gene silencing was not achieved (0%) in all the conditions in T1, in the samples inoculated with *E. canis* after seeding in T2, and in the *E. canis*-infected samples in T3. For T2, knockdown efficiency was 13.02% and 54.15%, for the uninfected and *E. canis*-infected samples, respectively. For T3, silencing efficiency was 7.56% and 68.30% for the uninfected and 24h *post*-inoculation samples, respectively.

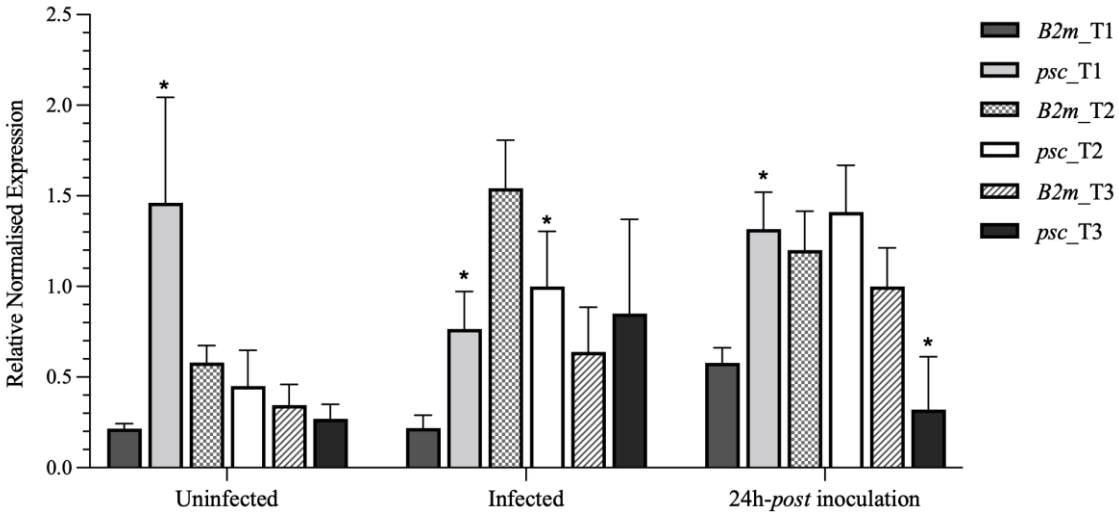

Figure 32. Relative normalised expression of *psc* in IDE8 cells following RNAi.

Relative *psc* expression was quantified in uninfected IDE8 cells, *E. canis*-infected cells and cells inoculated with *E. canis* 24 hours after the addition of dsRNA. Cells from the three groups were inoculated with *β2m* (control) or *psc* dsRNA. Samples were seeded at **(T0)**, inoculated 24 h later and harvested at three time points: 48 hours **(T1)**, 120 hours **(T2)** and 160 hours **(T3)**. Data was normalised using the reference genes *β-actin* and *β-tubulin*. Results were calculated automatically with CFX Manager™ Software (Bio-Rad). Columns represent the mean of relative normalised expression (n = 4) +SEM. *Statistically significant differences in gene expression levels when comparing both groups, at each time point, using Welch's unequal variances t-test ($p < 0.05$); (Figure created with GraphPad Prism software; version 9 for macOS).

For the uninfected samples at T1, *psc* expression levels were significantly upregulated in the *psc* dsRNA inoculated cells, when compared with the control group (Log2 fold-change 2.76; $p < 0.05$; $p = 0.008641$). This was contrary to what was observed for the same group at T2 and T3, where the expression levels of *psc* were lower in comparison with the control but lacked statistical significance (T2 Log2 fold-change -0.37; $p > 0.05$; $p = 0.234391$) (T3 Log2 fold-change -0.35; $p > 0.05$; $p = 0.70352$).

Regarding the *E. canis*-infected samples, *psc* expression levels at T1 and T3 were upregulated in the *psc* dsRNA-inoculated cells in comparison with *β2m*, with Log2 fold-change 1.81 and 0.41, respectively, showing a significant difference in gene regulation in T1 (T1 $p < 0.05$; $p = 0.002703$) (T3 $p > 0.05$; $p = p = 0.444691$). For T2, *psc* dsRNA inoculated cells presented significantly lower *psc* expression levels than the control group (Log2 fold-change – 0.62; $p < 0.05$; $p = 0.017426$).

Finally, the 24h *post*-inoculation samples cells subjected to *psc* dsRNA have shown a gene upregulation in the experimental time points T1 and T2, in comparison with *β2m* with Log2 fold-change 1.18 and 0.23, respectively. This upregulation was only significant in T1 (T1 $p < 0.05$; $p = 0.000534$) (T2 $p > 0.05$; $p = 0.201140$). At time point T3, *psc* expression levels were significantly lower in the *psc* dsRNA group when compared with the *β2m* dsRNA group (Log2 fold-change -1.64; $p < 0.05$; $p = 0.003649$).

Correlating gene regulation with silencing efficiency, results show that *psc* expression levels were consistently higher and statistically significant in T1 in the cells inoculated with *psc* dsRNA, a time point where gene silencing was not achieved (0%). A similar effect was observed in the infected and 24h *post*-inoculation samples in T3 and T2, respectively, with *psc* upregulation without gene silencing. In T2, silencing efficiency was 13.02% for the uninfected cells and with a non-significant downregulation in the *psc* dsRNA-inoculated cells. At this time point, gene knockdown of 54.15% resulted in a significant *psc* downregulation in the infected cells. In T3, *psc* dsRNA-inoculated cells in the uninfected *psc* group were non-significantly downregulated with a silencing efficiency of 7.56%, whereas in the 24h *post*-inoculation samples, *psc* was significantly downregulated with gene silencing efficiency of 68.30%. Thus, the results overall show a positive correlation between the effect of gene silencing on *psc* expression levels. Put simply, increased levels of gene silencing resulted in higher statistically significant downregulation (T2 - *E. canis*-infected cells $p = 0.017426$ and gene silencing efficiency of 54.15%; T3 - 24 h-*post* inoculation cells $p = 0.003649$ and gene silencing efficiency of 68.30%).

Quantification of *E. canis* was performed to evaluate the role of the *psc* gene in the invasion and multiplication of tick cells, after gene silencing. Relative normalised expression of *E. canis dsb* (133) was determined by qPCR. There was no amplification in the triplicate negative controls, and reaction efficiency, determined by a 10-fold serial dilution of *E. canis* Jaboticabal strain DNA, varied between 90.4 - 115%. All the uninfected cells (Group A) were negative for *dsb* amplification confirming the absence of infection. Data was normalised against two tick reference genes, *β-actin* and *β-tubulin*

(228), as before, to minimise sample variation due to differences in the amount of IDE8 genetic material. Stability values for the reference genes were for M-value$_{T1}$ = 0.518, M-value$_{T2}$ = 1.411 and M-value$_{T3}$ = 1.233. Only in T1 the M-value was within the range of acceptability (M-value < 1). For T2 and T3 M-value > 1, consequently these genes were considered unstable. Because these reference genes had too much variation across the samples, *dsb* differential gene expression was not considered valid in this study. Several other reference genes were tested but with no or inconsistent amplification of IDE8 cDNA, resulting in their exclusion.

Cell morphology was also assessed to determine the impact of *psc*-silencing on cell shape, size, and internal structure. In this assay, the observation of Giemsa-stained cytocentrifuge smears did not reveal relevant modifications in morphologic characteristics in the tick cells, and in the bacteria between groups and time-points. In future, this study would benefit from a cell count and viability assay to quantify the effect of *psc*-silencing in cells; however, the sensitivity of these cells to manipulation may affect these parameters.

3.3.5. *In vivo psc*-silencing and *Ehrlichia canis* quantification

In vivo gene knockdown was conducted in *R. sanguineus* nymphs by RNAi, using the soaking method, to determine if *psc* downregulation influences *E. canis* acquisition from the tick during the blood meal taken from an infected host and if, once in the SGs, it can become viable, multiply, and be transmitted transstadially from nymphs to the adult stage.

dsRNA was synthesised with a *psc* PCR-amplicon produced with the primer pair *psc_RS_T7_forward* and *psc_RS_T7_reverse*, using *R. sanguineus* SGs cDNA as template. Primer specificity was confirmed by the presence of a single band of approximately 400 bp in 1.2% agarose gel (Figure 33). PCR products were purified and sequenced following quality and concentration determination by spectrophotometry (*psc* amplicon = 4.4 ng/µl and $A_{260/280}$ = 1.3). A GenBank BLAST using the *psc* PCR product sequence showed 96.95% identity with *Rhipicephalus sanguineus* probable serine carboxypeptidase CPVL (LOC119372059), mRNA (accession nr. XM_037642511.1) (E value = 0; query cover 56%).

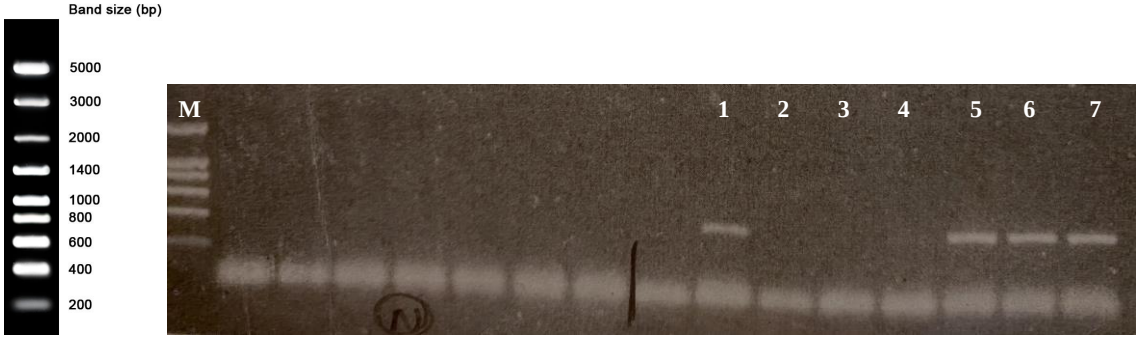

Figure 33. Agarose gel of purified *psc* PCR product following amplification from *Rhipicephalus sanguineus*.

Lane M: Marker (Ladder VIII, NZYTech); **Lanes 1, 5, 6 and 7:** PCR product obtained from *R. sanguineus* salivary glands cDNA; **Lanes 2, 3 and 4:** Negative control with no template. PCR-amplified products show a 400 bp product visualised on a 1.2% agarose gel with the primers *psc_RS_T7_forward* and *psc_RS_T7_reverse*.

After nymph moulting, a total of 12 adult female ticks were collected from the *psc* dsRNA group and from the PBS group. Total RNA was extracted from their SGs and the concentration of each sample was quantified by spectrophotometry. For the group soaked with *psc*-dsRNA, concentrations ranged between 0.41 - 15.58 ng/µl, while in the control group, concentrations ranged between 0.15 - 18.79 ng/µl (Supplementary Table 21). Complementary DNA was synthesised after sample concentrations were normalised to 100 ng/µl.

Relative normalised expression values of the control group and *psc* dsRNA group were determined by qPCR using the primer pair *psc_RS_forward* and *psc_RS_reverse*. No amplification was verified in the triplicate negative controls and reaction efficiency determined by 10-fold serial dilution of *R. sanguineus* cDNA ranged between 93.5 - 116.8%. Data was normalised against the reference genes *β-actin*, *β-tubulin* and *elf* (228), with the following stability values: M-value $_{\beta\text{-}actin,\ elf}$ = 1.870 and M-value $_{\beta\text{–}tubulin}$ = 3.170 (M-value > 1, unstable reference genes). This group of reference genes was classified as unstable and showed excessive variation across the samples tested, thus *psc* differential expression values were not considered, as well as *E. canis* quantification. Other reference genes were tested but without successful amplification.

3.4. Proteome analysis

3.4.1. Proteomic profile of *Rhipicephalus sanguineus* salivary glands in response to experimental *Ehrlichia canis* infection

The proteome of unfed uninfected and unfed *E. canis*-infected tick SGs was determined using LC-MS/MS.

The presence of *E. canis* DNA was determined in all samples by qPCR targeting the *16S* rRNA, as previously described (134), after gDNA extraction. Samples included 30 SGs from ticks fed on the naïve host and 45 SGs from ticks fed on the *E. canis*-inoculated dog (9-18). After DNA extraction, concentration and purity were assessed by spectrophotometry (data not shown). The DNA extraction method was validated by PCR targeting ticks *18S* rRNA (229) and successful amplification of a 500 bp product was observed following 1.2% agarose gel (data not shown). DNA amplification occurred in the positive controls with *E. canis* Jaboticabal strain purified DNA. No amplification was observed in the triplicate negative controls. All the SGs extracted from ticks fed on the naïve dog did not show amplification, whereas the SGs of ticks fed on the experimentally infected dog were positive for *E. canis 16S* rRNA (data not shown).

Total protein was then extracted from these samples and proteome quantification carried out at the Proteomics Unit Centre for Neuroscience and Cell Biology, Universidade de Coimbra, Portugal. Like the absence of an *R. sanguineus* genome sequence in 2015, the SGs of *R. sanguineus* lacked a publicly available proteome for mapping. Thus, protein-specific libraries of precursor masses and fragment ions from the three biological replicates in each condition were used to create a protein database. Using these, a BLAST against the Canidae and *E. canis* SwissProt databases (release 2015_12), the unreviewed Ixodidae database (TrEMBL) from UniProtKB (release 2015_12), and an in-house database from previous transcriptomic analysis (Proteomics Unit Centre for Neuroscience and Cell Biology, Universidade de Coimbra, Portugal) was carried out, which identified 432 tick proteins.

All the results refer to the identified proteins that reached a 1% local FDR threshold, after removing redundancies and contaminants. Protein levels were estimated by summing all the transitions from all the peptides for a given protein and normalised to the total intensity at the protein level and to the internal standard. Only proteins that had three or more peptides available for quantitation were selected for XIC peak area extraction and analysed with the MarkerView™ 1.2.1 software (ABSciex). Proteomic SWATH™ analysis from fed uninfected and fed *E. canis*-infected SGs resulted in a total of 452 proteins, though 20 of these belonged to the host *Canis lupus familiaris* and were removed from data analysis. Therefore, a total of 432 tick proteins that were present in both groups were analysed (Supplementary Table 22).

3.4.2. Proteome annotation

Statistical analysis was carried out with the 432 tick proteins using the student's *t* test to identify proteins that were significantly differentially represented ($p < 0.05$) (Supplementary Table 22). A total of 69 proteins were significantly differentially represented (15.97%), of which 5 (7.25%) were underrepresented and 64 (92.75%) were overrepresented. The most overrepresented proteins corresponded to a signal peptidase (UniProtKB C9W1S4; Log2 fold-change 3.403486154) and to an actin-depolymerizing factor 1 (UniProtKB A0A034WYZ2; Log2 fold-change 2.925568678). The most underrepresented protein was a ribosomal protein L19 (UniProtKB L7MEH0; Log2 fold-change -3.582496979).

These proteins were then functionally annotated according to their GO in different levels: MF, BP and CC using UniProtKB tools (GO data available in Supplementary Table 23) and later with the OmicsBox Software (Version 2.1.14; BioBam Bioinformatics 2019, available at www.biobam.com/omicsbox). Figures 35-36 show multi-level charts that summarise the functional annotation of proteins significantly differentially represented ($p < 0.05$) in the *R. sanguineus* SGs proteome during *E. canis* infection. From the 69 differentially represented proteins, 37 (53.63%) were GO annotated and 32 (46.38%) presented BLAST hits. Proteins with the UniProtKB I.D.s L7MD67, L7LQP4, L7M9B9 and L7M653 did not retrieve any MF, BP and CC, being classified as unknown for these categories.

In Figure 34, GO annotation level 2 underlines several BP according to the distribution level that include mostly cellular (35) and metabolic process (23), followed by biological regulation (7), regulation of biological processes (6), localisation (5), response to stimulus (4), signalling (3), negative (2) or positive (1) regulation of biological processes and detoxification (1). Six proteins had unknown BP.

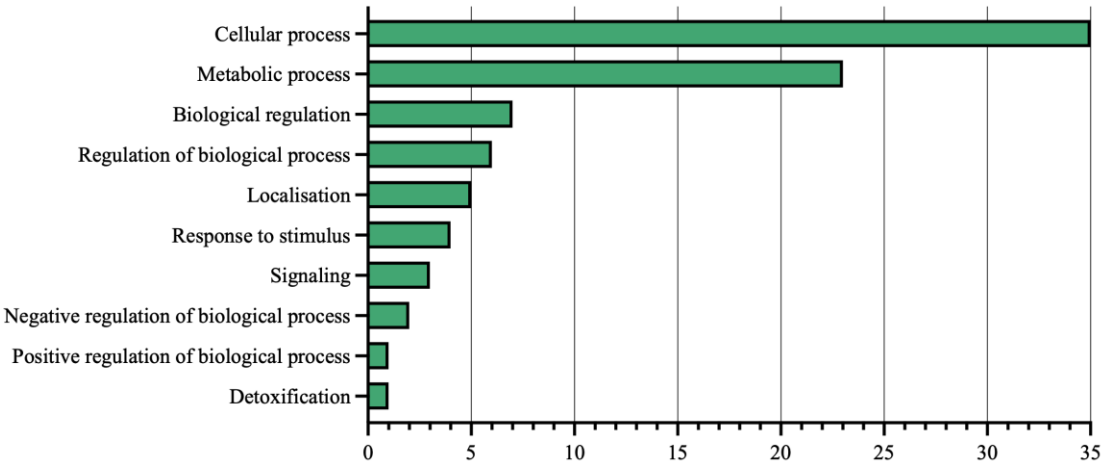

Figure 34. *Rhipicephalus sanguineus* salivary gland proteome GO annotation (level 2 – Biological Process) in response to *Ehrlichia canis* infection.

A total of 69 proteins differentially represented ($p < 0.05$) were annotated. **X-axis** – Direct GO counts. Data was analised using OmicsBox Software (Version 2.1.14; BioBam Bioinformatics 2019, available at www.biobam.com/omicsbox); (Figure created with GraphPad Prism software; version 9 for macOS).

At the MF level, GO distribution was most related with binding (23), structural molecule activity (19) and catalytic activity (10), followed by transporter activity (3), ATP-dependent activity (3), antioxidant activity (1) and protein tag (1) (Figure 35). Nine proteins had unknown MF.

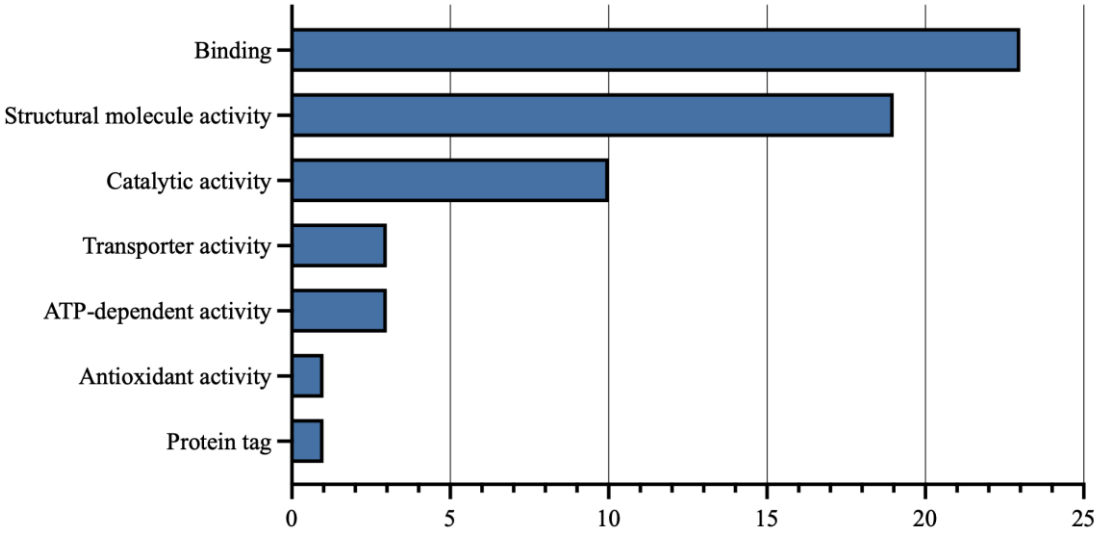

Figure 35. *Rhipicephalus sanguineus* salivary gland proteome GO annotation (level 2 – Molecular Function) in response to *Ehrlichia canis* infection.

A total of 69 proteins differentially represented ($p < 0.05$) were annotated. **X-axis** – Direct GO counts. Data was analised using OmicsBox Software (Version 2.1.14; BioBam Bioinformatics 2019, available at www.biobam.com/omicsbox); (Figure created with GraphPad Prism software; version 9 for macOS).

Finally, at CC level, proteins were annotated as in cellular anatomical entity (32) and in protein-containing complex (17) (Figure 36). Twenty proteins had unknown CC.

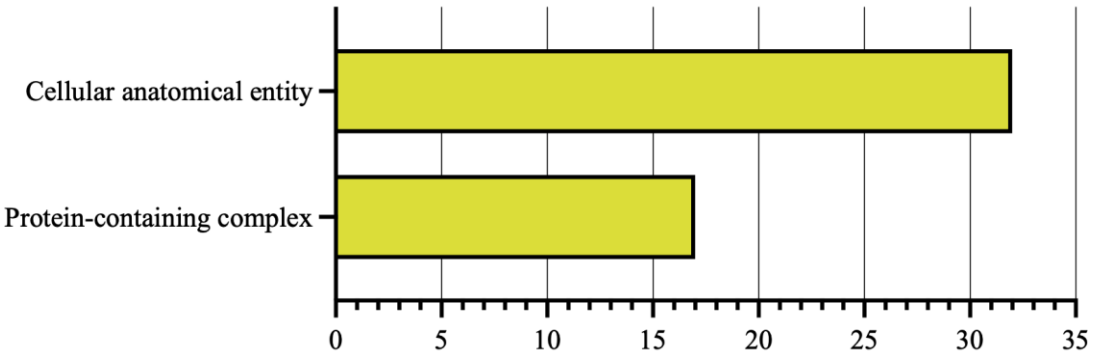

Figure 36. *Rhipicephalus sanguineus* salivary gland proteome GO annotation (level 2 – Cellular Component) in response to *Ehrlichia canis* infection.

A total of 69 proteins differentially represented ($p < 0.05$) were annotated. **X-axis –** Direct GO counts. Data was analised using OmicsBox Software (Version 2.1.14; BioBam Bioinformatics 2019, available at www.biobam.com/omicsbox); (Figure created with GraphPad Prism software; version 9 for macOS).

Regarding GO annotation - level 3 for BP, most of the processes were related with translation (16), followed by mitochondrial ATP and ADP transmembrane transport (2), protein folding (2) and ribosomal large subunit assembly (2) (Figure 37).

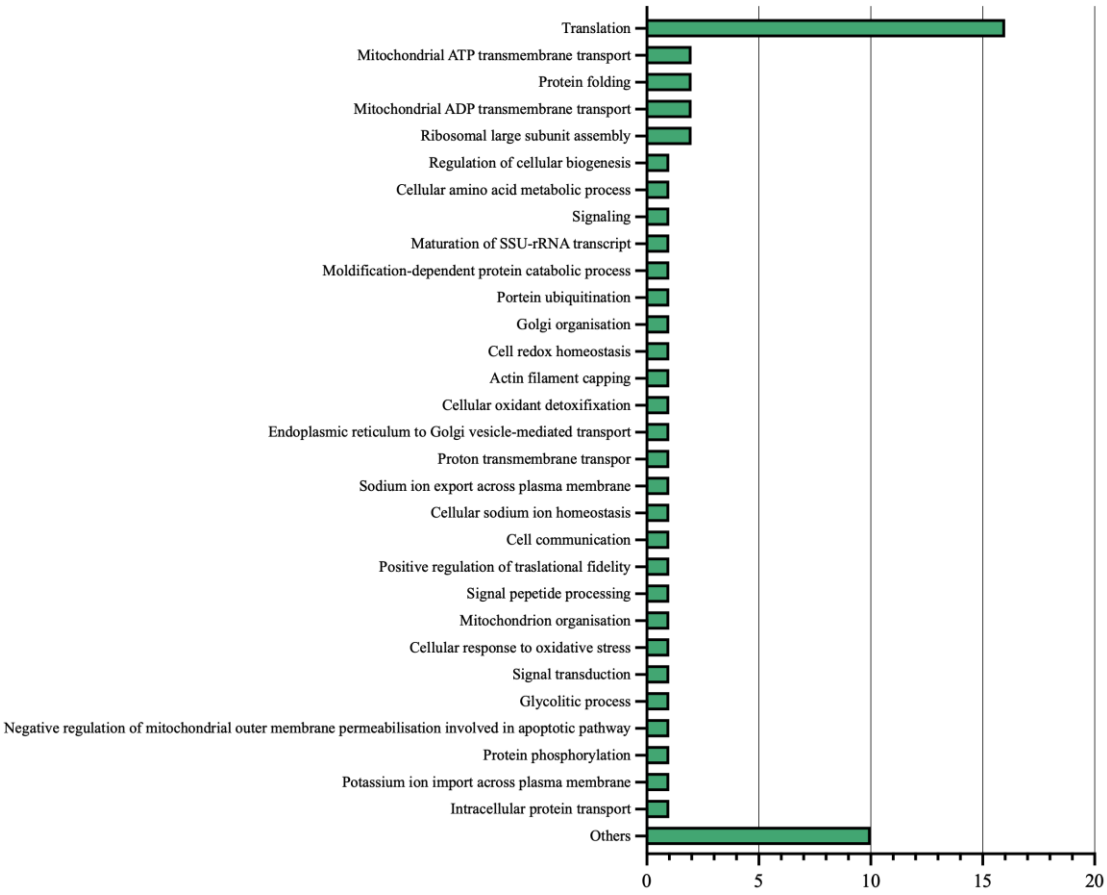

Figure 37. *Rhipicephalus sanguineus* salivary gland proteome GO annotation (level 3 - Biological Process) in response to *Ehrlichia canis* infection.

A total of 69 proteins differentially represented ($p < 0.05$) were annotated. **X-axis –** Direct GO counts. Data was analised using OmicsBox Software (Version 2.1.14; BioBam Bioinformatics 2019, available at www.biobam.com/omicsbox); (Figure created with GraphPad Prism software; version 9 for macOS).

GO annotation - level 3 for MF were predominately related with the structural constituent of the ribosome (18), RNA binding (12), ATP binding (6), metal ion binding (3) and ATP hydrolysis activity (3) (Figure 38).

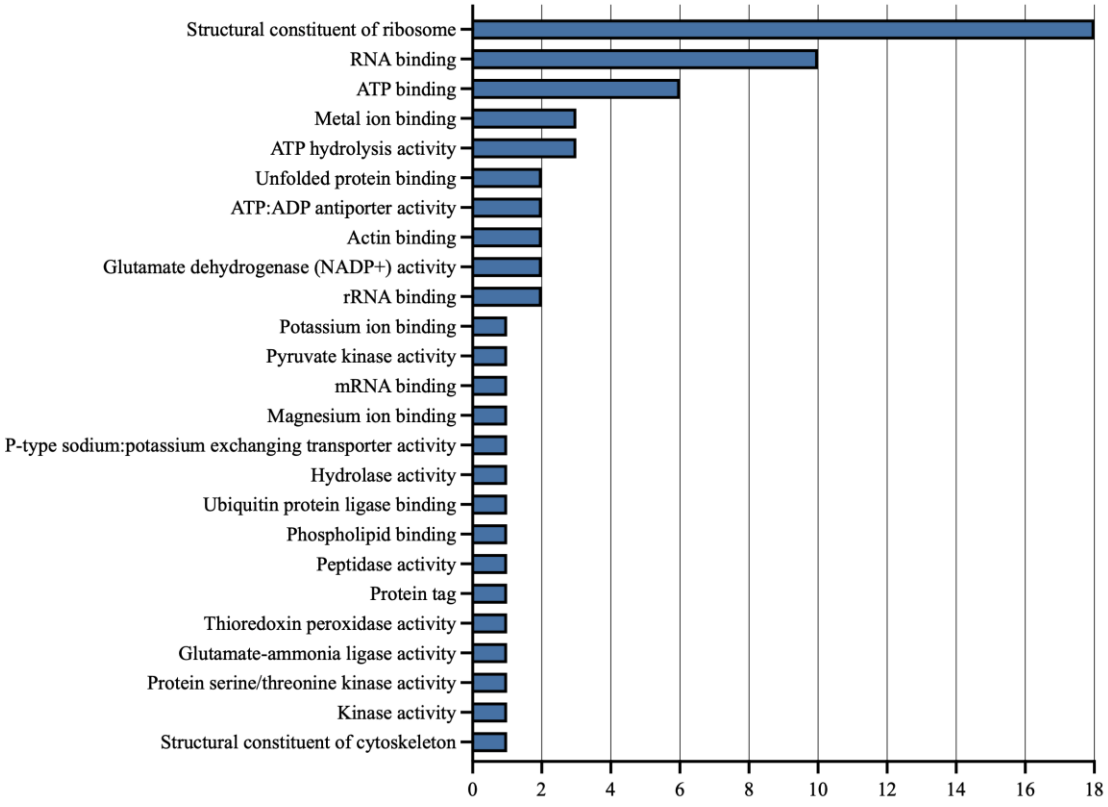

Figure 38. *Rhipicephalus sanguineus* salivary gland proteome GO annotation (level 3 - Molecular Function) in response to *Ehrlichia canis* infection.

A total of 69 proteins differentially represented ($p < 0.05$) were annotated. **X-axis –** Direct GO counts. Data was analised using OmicsBox Software (Version 2.1.14; BioBam Bioinformatics 2019, available at www.biobam.com/omicsbox); (Figure created with GraphPad Prism software; version 9 for macOS).

In GO annotation - level 3 for CC, proteins were mainly located in the cytosolic large ribosomal subunit (9), followed by integral component of membrane (5), cytoplasm (5), ribosome (5), cytosolic small ribosomal subunit (3), mitochondrial inner membrane (3), cytosol (2), nucleous (2) and small ribosomal subunit (2) (Figure 39).

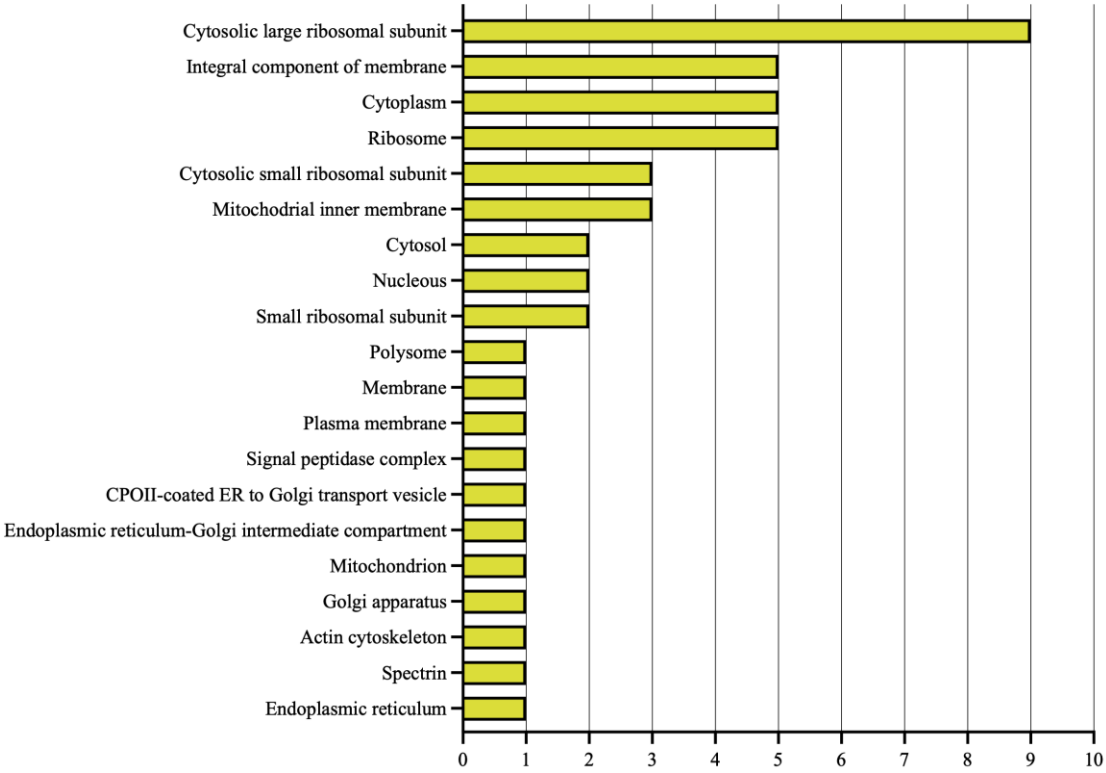

Figure 39. *Rhipicephalus sanguineus* salivary gland proteome GO annotation (level 3 - Cellular Component) in response to *Ehrlichia canis* infection.

A total of 69 proteins differentially represented ($p < 0.05$) were annotated. **X-axis –** Direct GO counts. Data was analised using OmicsBox Software (Version 2.1.14; BioBam Bioinformatics 2019, available at www.biobam.com/omicsbox); (Figure created with GraphPad Prism software; version 9 for macOS).

In terms of enzyme distribution (Figure 40), GO annotation resulted in five categories, such as hydrolases (5), translocases (3), transferases (2), oxireductases (2) and ligases (1).

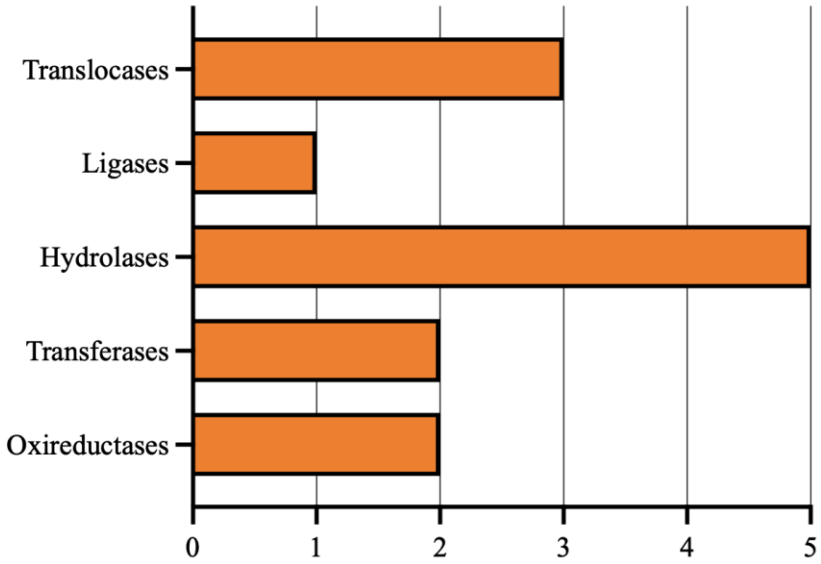

Figure 40. *Rhipicephalus sanguineus* salivary gland proteome enzyme distribution in response to *Ehrlichia canis* infection.

A total of 69 proteins differentially represented ($p < 0.05$) were annotated. **X-axis –** Direct GO counts. Data was analised using OmicsBox Software (Version 2.1.14; BioBam Bioinformatics 2019, available at www.biobam.com/omicsbox); (Figure created with GraphPad Prism software; version 9 for macOS).

3.4.3. Validation of proteomic data

To validate the proteomic data, three proteins identified in the proteome as differentially represented following *E. canis* infection were examined by SDS-PAGE, followed by Western blot. Several proteins were analysed by BLAST (data not shown), which identified three strong protein candidates requiring further validation. BLAST results are shown in Supplementary Table 24 for these three proteins. These proteins are cAMP-dependent protein kinase catalytic subunit isoform 2, *APK-C2* (APK-C2; UniProtKB O97115) from *Amblyomma americanum* (*Lone star tick*), malate dehydrogenase (MDH2; UniProtKB L7M8Y4), and PROHIB, these last two from *Rhipicephalus pulchellus (Yellow backed tick).*

SDS-PAGE and Western blot were carried out using uninfected and *E. canis*-infected SG samples to detect the proteins APK-C2, MDH2 and PROHIB, with the antibodies PKAα/β/γ, MDH2 and Prohibitin 2, respectively.

Prior to protein extraction, the presence of *E. canis* in the SGs was determined by nested-PCR targeting the *16S rRNA*, as described elsewhere (118). gDNA was extracted from 3 pools of 10 SGs of ticks fed on a naïve dog (NI_1, NI_2 and NI_3) and 3 pools of 10 SGs of ticks fed on an *E. canis*-infected dog (I_1, I_2 and I_3). Individual sample concentration and purity was assessed by spectrophotometry. The $A_{260/280}$ varied from 1.87 - 2.02, whilst concentrations ranged between 73.04 - 350.44 ng/µl. Results are shown in Supplementary Table 25. Amplification of the correct amplicon in the second reaction was confirmed by the presence of a single band, of approximately 220 bp, by 1.2% agarose gel in the pools I_2 and I_3, and in the positive control using *E. canis* Jaboticabal strain DNA. The samples I_1, NI_1, NI_2 and NI_3, were negative for amplification, as well as the negative control (data not shown).

For SDS-PAGE and Western blot, the protein concentration of these samples, except I_1, was determined by spectrophotometry and values varied between 3.22 - 8.58 ng/µl. Results are shown in Table 15. Relative quantification was determined in the Western blot plots by the pixel density ratio between *E. canis*-infected and uninfected sample bands using ImageJ software (Version 2.0.0.). Western blot results are shown in Figure 42. For the protein APK-C2, a band between 35 and 48 kDa was detected (Figure 41 (a), expected size = 48 kDa) with pixel intensity of 19710.070 for the uninfected (NI) and 28792.996 for the *E. canis*-infected (I) SGs, respectively. The comparison between the two conditions has shown that this protein was overrepresented in the infected samples (Log2 fold-change 0.5468). For PROHIB, a band between 35 and 48 kDa was detected (Figure 41 (b), expected size = 33 kDa), with pixel intensity of 43146.881 for the uninfected (NI) and 48904.898 for the infected (I) samples, respectively, showing overrepresentation in the presence of *E. canis* (Log2 fold-change 0.1807). For MDH2, a band with a molecular weight between 35 and 48 kDa was detected (Figure 41 (c), expected size = 36 kDa), with a pixel intensity of 60077.291 for the uninfected (NI) and 65557.219 for *E. canis*-infected (I) SGs, respectively. This protein was also

overrepresented in the infected samples when compared with uninfected controls (Log2 fold-change = 0.1259). These results contrasted with the proteomic data, where these three proteins were underrepresented (APK-C2 Log2 fold-change -1.44018961; MDH2 Log2 fold-change -2.418110495; PROHIB Log2 fold-change -1.84993621).

Several other proteins that were differentially represented ($p < 0.05$) in the proteome analysis were tested for data validation but without successful antibody recognition, including the putative mitochondrial import inner membrane translocases – subunit TIM23 (UniProtKB B7PEW5), and – subunit TIM21 (UniProtKB L7MF27), the protein kish (UniProtKB G3MNA8), the putative trilaris (UniProtKB L7MCD9) and the GST (UniProtKB Q6JVN0).

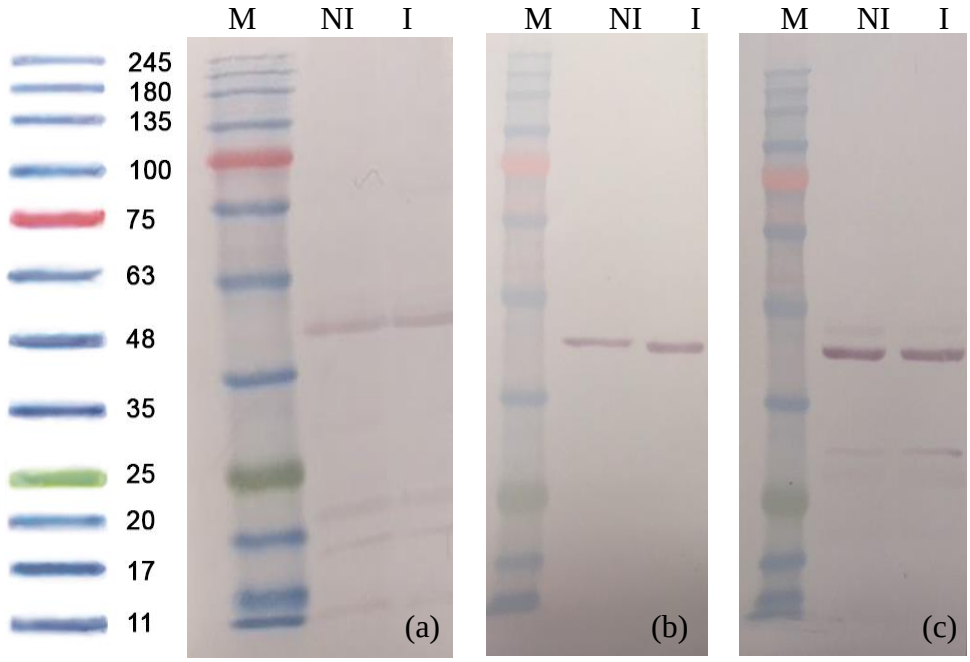

Figure 41. SDS-PAGE and Western blot analysis of *Rhipicephalus sanguineus* salivary gland proteins during *Ehrlichia canis* infection.

Proteins were detected with the monoclonal antibodies PKAα/β/γ cat (B-4) (sc-36515) for APK-2, Prohibitin 2 (A-2) (sc-133094) for PROHIB, and MDH2 (1G12) (sc-293474) for MDH2 (all from Santa Cruz Biotechnology, Dallas, USA). All samples have shown a size between 35 and 48 kDa. **(a)** APK-C2; **(b)** PROHIB; **(c)** MDH2. **Lane M:** NZYColour Protein Marker II (NZYTech); **Lane NI:** fed uninfected salivary glands; **Lane I:** fed and *E. canis*-infected salivary glands.

3.4.4. Differential *prohib and phsrp20* gene expression in IDE8 cells during infection

The proteomic data also identified other candidates that were differentially represented in response to *E. canis* infection. SDS-PAGE and Western blot analysis of one of these, PHSRP20 (UniProtKB L7M6Q5), did not detect any protein species. We therefore sought to determine an effect at the transcriptional level by qPCR. The differential representation results for PROHIB in the proteome contrasted with the Western blot analysis data. Due to this discrepancy or lack of detection, we chose to also quantify *prohib* and *phsrp20* mRNA expression by qPCR in the two experimental conditions in IDE8 cells.

qPCR primers for *prohib* and *phsrp20* were designed and optimised to use in IDE8 cells. Primer optimisation of *prohib_IDE8_forward* and *prohib_IDE8_reverse* and *phsrp20_IDE8_forward* and *phsrp20_IDE8_reverse* primers was carried using IDE8 gDNA as template. A 10-fold dilution series of IDE8 gDNA was used to determine reaction efficiency and T_m. For *prohib*, reaction efficiency was 90% and a single peak was observed in the Melting curve with T_m = 85.5 – 86.0°C (Figure 42 – A). For *phsrp20*, reaction efficiency was 92.8% and a single peak was observed in the Melting curve with T_m = 86.0 - 86.5°C (Figure 42 – B).

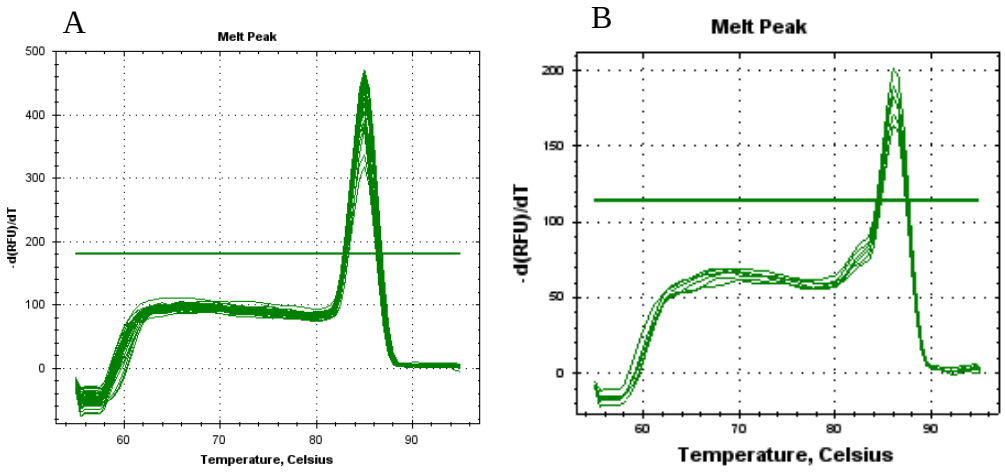

Figure 42. Real time PCR Melting curve for *prohib* and *phsrp20* primer optimisation in IDE8 cells. Data was obtained using **(A)** *prohib_IDE8_forward* and *prohib_IDE8_reverse* primers with T_m = 85.5 – 86°C; **(B)** *phsrp20_IDE8_forward* and *phsrp20_IDE8_reverse* primers with T_m = 86.0 – 86.5°C, using a 10-fold series of IDE8 gDNA dilutions. **Legend: Y axis -** normalised fluorescence units (-d(RFU)/dT) against X - axis temperature (°C). Melting curve and dissociation temperature were automatically determined by the CFX Manager™ Software (Bio-Rad).

Amplification of *prohib* and *phsrp20* was confirmed by the presence of single bands spanning 168 and 147 bp, respectively, following 1.2% agarose gel (data not shown). Sanger sequencing was used to confirm amplicon specificity, following spectrophotometry to determine quality and concentration (*prohib* amplicon = 20.96 ng/µl, $A_{260/280}$ = 1.75; *phsrp20* amplicon = 27.9 ng/µl, $A_{260/280}$ = 1.95). The BLAST conducted with this *prohib* sequence had 96.09% identity with the *Ixodes scapularis* prohibitin-2 (LOC8036376), mRNA (GenBank accession nr. XM_002411792.5) (E value = 2e-^{49}; query cover = 96%), and 80.15% identity with *Rhipicephalus sanguineus* prohibitin-2-like (LOC119405271), mRNA (GenBank accession nr. XM_037672083.1) (E value = 4e-^{16}; query cover = 99%). BLAST analysis with the *phsrp20* PCR product sequence revealed 93.97% homology with *Ixodes scapularis* small heat shock protein, putative, mRNA (GenBank accession n. XM_002416230.1) (E value = 2e-^{49}; query cover = 99%).

Relative normalised expression of *prohib* and *phsrp20* in IDE8 cells during experimental infection was determined by qPCR, as described in Section 3.3.3 for *psc*. Data was

normalised using the reference genes *β-tubulin* and *elf* (228), and these were classified as ideal (M-value <1; M-value = 0.304). There was no amplification in the triplicate negative controls and the reaction efficiency, determined by 10-fold serial dilution standard curves using IDE8 gDNA, varied between 99.7 - 113.5%. Gene expression data (Figure 43), shows a statistically significant downregulation of *prohib* in the infected samples ($p < 0.05$; $p = 0.000001$; Log2 fold-change -6.26424), compared to uninfected cells. Likewise, downregulation of *phsrp20* was also observed, but without a statistical significance ($p < 0.05$; $p = 0.06331$; Log2 fold-change -3.37079).

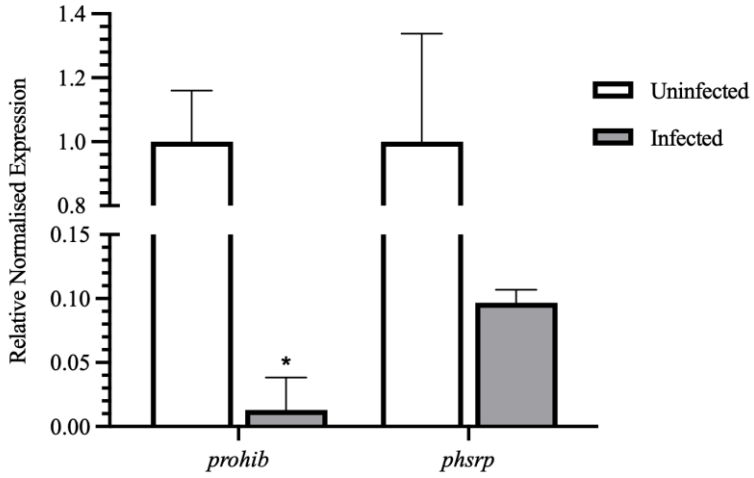

Figure 43. Relative normalised expression levels of *prohib* and *phsrp20* in IDE8 cells during *Ehrlichia canis* infection.

Relative normalised expression of was evaluated in uninfected **(white)** and in *E. canis*-infected **(grey)** tick cells. Data was normalised against the reference genes *β-tubulin and elf*. Results were calculated automatically with CFX Manager™ Software (Bio-Rad). Columns represent the mean ($n = 4$) of relative normalised expression +SEM. *Statistically significant differences were found in the expression levels of *prohib* infected cells when compared with the control using Welch's unequal variances *t*-test ($p < 0.05$; $p = 0.000001$). No statistically significant differences were found in the expression levels of *phsrp20* infected cells when compared with the control ($p < 0.05$; $p = 0.06331$); (Figure created with GraphPad Prism software; version 9 for macOS).

3.4.5. Differential *prohib and phsrp20* gene expression in *Rhipicephalus sanguineus* during infection

In addition to IDE8 cells, we also quantified *prohib* and *phsrp20* in the SGs of *R. sanguineus* adult females. qPCR primer sequences and conditions for *prohib* amplification were the same as for IDE8 cells (*prohib_RS_forward* and *prohib_RS_reverse* in Supplementary Table 1), with T_m = 84.5 – 85.0°C. Amplification specificity was confirmed by sequencing the purified qPCR amplicon, after concentration and purity evaluation (*prohib* amplicon = 6.9 ng/µl and $A_{260/280}$ = 2.71). BLAST analysis showed 95.47% identity with *Rhipicephalus sanguineus* prohibitin-2-like (LOC119405271), mRNA (GenBank accession nr. XM_037672083.1) (E value = 0; query cover = 91%).

For *phsrp20,* primer sequences were designed to use in *R. sanguineus* SGs. Optimisation of *phsrp20_RS_forward* and *phsrp20_RS_reverse* was carried out using SG gDNA as template. A 10-fold series of dilutions of SGs gDNA determined a reaction efficiency of 100.6% and a single peak in the Melting curve with T_m = 86.0 – 86.5°C (Figure 44).

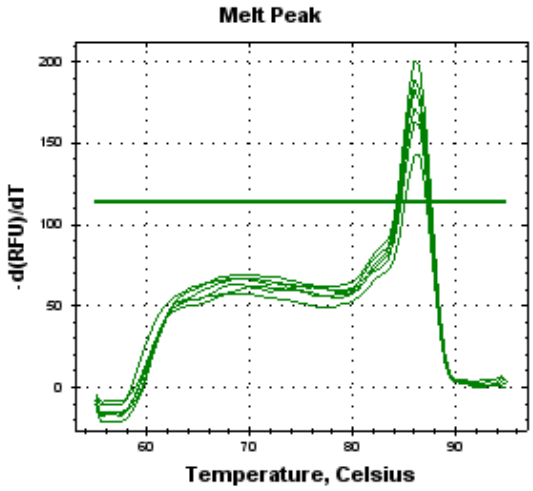

Figure 44. Real time PCR Melting curve for *phsrp20* primer optimisation in *Rhipicephalus sanguineus*. Chart was obtained with the *phsrp20_IDE8_*forward and *phsrp20_IDE8_*reverse primers using a 10-fold series of SGs gDNA dilutions. Melting curve with $\mathbf{T_m}$ **=** 86.0 - 86.5°C. Legend: **Y axis -** normalised fluorescence units (-d(RFU)/dT) against **X axis -** temperature (°C). Melting curve and dissociation temperature were automatically determined by the CFX Manager™ Software (Bio-Rad).

Amplification of *phsrp20* fragment produced a single band of the expected size of approximately 133 bp following 1.2% agarose gel (data not shown). The amplicon was then gel purified and sequenced, after quality and concentration determination by spectrophotometry (*phsrp20* amplicon = 19.6 ng/µl and $A_{260/280}$ = 1.95). A BLAST search was conducted, and the PCR product showed high homology with the retrieved sequence of predicted *Rhipicephalus sanguineus* heat shock protein Hsp-12.2-like (LOC119404707), mRNA (GenBank accession nr. XM_037671353.1) with 84.11% similarity (E value = $6e^{-72}$; query cover = 38%).

Expression levels of *prohib* and *phsrp20* in the SGs were determined using cDNA synthesised from RNA isolated from ticks fed on a naïve host and ticks fed on an *E. canis*-infected host. Samples were pooled in 3 groups of 10 SGs, for each group. *E. canis* infection in the SGs was confirmed by qPCR targeting *dsb* (133). Data was normalised using two reference genes, *ß-actin* and *ß-tubulin* (228), and these were classified as ideal (M-value <1; M-value = 0.1171). There was no amplification in the triplicate negative controls and the reaction efficiency between plates, determined by 10-fold serial dilution

standard curves of *R. sanguineus* SGs gDNA, varied between 92.2 - 95% for *prohib*, and 89.2 - 100.8% for *phsrp20*.

Gene expression analysis of the *E. canis*-infected SGs showed that *prohib* was statistically significantly upregulated ($p < 0.05$; $p = 0.030$; Log2 fold-change 0.9855), compared with uninfected SGs. By contrast, *phsrp20* was downregulated in the infected samples (Log2 fold-change -0.044), when compared with uninfected controls, but was not statistically significant ($p > 0.05$; $p = 0.3145$) (Figure 45). When compared with the proteomic data, the PROHIB (UniProtKB L7M5P4) had lower representation, with Log2 fold-change -1.18499362, whereas in this gene expression analysis, it was upregulated. Furthermore, in contrast to the *phsrp20* mRNA expression data, proteomic data showed an overrepresentation of the PHSRP20 (UniProtKB L7M6Q5) with Log2 fold-change 0.476880497.

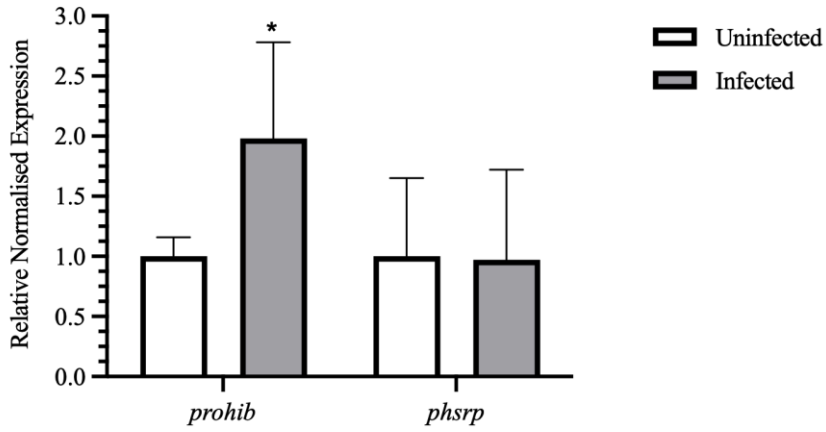

Figure 45. Relative normalised expression levels of *prohib* and *phsrp20* in *Rhipicephalus sanguineus* salivary glands during *Ehrlichia canis* infection.

Relative normalised expression of was evaluated in uninfected **(white)** and in *E. canis*-infected **(grey)** tick SGs. Data was normalised against the reference genes *β-tubulin and β-actin*. Results were calculated automatically with CFX Manager™ Software (Bio-Rad). Columns represent the Mean of relative normalised expression (*n* uninfected = 30 and *n* infected = 30) +SEM. *Statistically significant differences were found in the expression levels of *prohib* infected SGs when compared with the control using Welch's unequal variances *t*-test ($p < 0.05$; $p = 0.030$). No statistically significant differences were found in the expression levels of *phsrp20* when comparing both groups ($p < 0.05$; $p = 0.3145$); (Figure created with GraphPad Prism software; version 9 for macOS).

3.4.6. *In vitro prohib*- and *phsrp20*-silencing and *Ehrlichia canis* quantification

In vitro gene silencing was carried out with IDE8 cells to deepen the knowledge about how *E. canis* infects and multiplies within the cells. Similar to what was carried out for *psc* in Section 3.3.4, here the selected genes subjected to RNAi were *prohib* and *phsrp20*.

The primer pairs *prohib_IDE8_T7_forward* and *prohib_IDE8_T7_reverse* and *phsrp20_IDE8_T7_forward* and *phsrp20_IDE8_T7_reverse*, with the T7 promoter, were designed and optimised to use in IDE8 cells (Supplementary Table 1). Primer specificity was confirmed by the presence of a single band with approximately 442 and 379 bp, for *prohib* and *phsrp20* respectively, following 1.2% agarose gel. Figure 46 shows the PCR product obtained for *prohib* (for *phsrp20,* data is not shown).

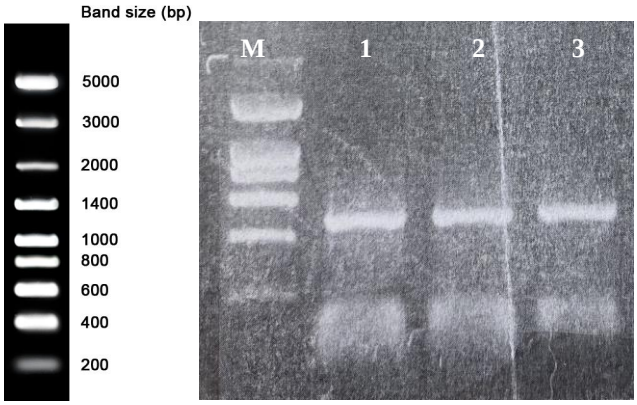

Figure 46. Agarose gel electrophoresis of PCR amplification of a *prohib* fragment of IDE8 cells.
Lane M: Marker (Ladder VIII; NZYTech); **Lane 1 to 3:** Samples of gDNA from IDE8 cells. PCR products show a 442 bp product visualised on a 1.2% agarose gel amplified with the primers *prohib_IDE8_T7_forward* and *prohib_IDE8_T7_reverse*.

In the BLAST search, *prohib* amplicons showed high homology with *Ixodes scapularis* prohibitin-2 (LOC80336376), mRNA (GenBank accession nr. XM_002411792.5) with 99.50% similarity (E value 0.0; query cover 92%). A BLAST carried out with the *phsrp20*-amplified PCR product sequence showed 99.57% identity with *Ixodes scapularis* small heat shock protein, putative, mRNA (GenBank accession nr. XM_002416230.1) (E value = $8e^{-124}$; query cover = 84%).

The PCR amplicons were gel purified and used as a template for dsRNA synthesis. The RNAi assay followed the same methodology described in Figure 7 (Section 2.7.2). Here, IDE8 cells were inoculated either with $4.86x10^{12}$ or $84x10^{12}$ molecules/µl of *prohib* dsRNA or *phsrp20* dsRNA, respectively, or $1.79x10^{12}$ molecules/µl of *β2m* dsRNA as control (Supplementary Table 7). RNA was extracted, and its concentration and purity determined. For the group inoculated with *prohib* dsRNA, the $A_{260/280}$ varied from 1.72 - 2.39, whilst concentrations were between 6.96 - 386.21 ng/µl. In the group inoculated with *phsrp20* dsRNA, $A_{260/280}$ varied from 1.78 - 2.12, whilst concentrations = 37.7 - 411.46 ng/µl. Results are shown in Supplementary Table 26.

Relative normalised expression of both genes was evaluated by qPCR and the results are shown in Figure 48. In both gene studies, no template negative controls were clean and reaction efficiency between plates was determined by 10-fold serial dilution standard curves of IDE8 cDNA. When testing *prohib*, plate efficiency varied between 87.9 - 113.9%. For *phsrp20*, plate efficiency varied from 85.6 - 113.9%. Data was normalised against the reference genes *β-actin* and *β-tubulin* (228). Stability values for the *prohib* analysis were M-value$_{T1}$ = 0.081, M-value$_{T2}$ = 0.300 and M-value$_{T3}$ = 0.074, therefore stable enough to proceed in the study (M-value < 1). For the *phsrp20* analysis, stability values were M-value$_{T1}$ = 1.425, M-value$_{T2}$ = 0.426 and M-value$_{T3}$ = 1.180. At time points T1 and T3 the M-value > 1, thus the reference genes were too unstable to proceed with the differential gene expression study for this gene. Several other reference genes were tested but without successful amplification in IDE8 cells. Due to this limitation, *phsrp20* gene silencing efficiency, differential gene expression and *E. canis* quantification were not carried out.

Complete *prohib* silencing (100%) was achieved for the uninfected cells at T1, for the *E. canis*-infected cells at T2 and T3, and for the *E. canis*-inoculated cells at T2. Gene silencing was not achieved (0%) for uninfected cells at T2 and T3, and for the *E. canis*-inoculated cells at T3. For T1, a knockdown of 9.48% and 91.75% was observed in the infected and the *E. canis*-inoculated cells, respectively (Figure 47).

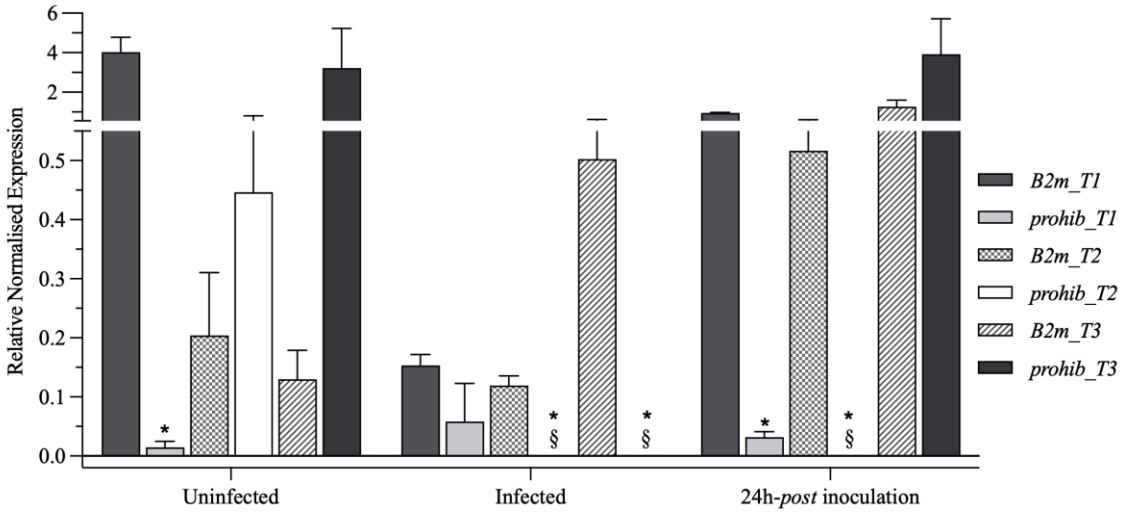

Figure 47. Relative normalised expression of *prohib* in IDE8 cells following RNAi.

Relative normalised expression of the *prohib* gene was determined in uninfected IDE8 cells, *E. canis*-infected cells and cells inoculated with *E. canis* 24 hours after the addition of dsRNA. Cells from the three groups were inoculated with *β2m* (control) or *prohib* dsRNA. Samples were seeded at **(T0)**, inoculated 24 h later and harvested at three time points: 48 hours **(T1)**, 120 hours **(T2)** and 160 hours **(T3)**. Data was normalised against the reference genes *β-actin* and *β-tubulin*. Results were calculated automatically with CFX Manager™ Software (Bio-Rad). Columns represent the mean of relative normalised expression (n = 4) +SEM. *Statistically significant differences in gene expression levels when comparing the silenced with the control group, at each time point, using Welch's unequal variances t-test ($p < 0.05$); (Figure created with GraphPad Prism software; version 9 for macOS).

For the uninfected samples at T1, gene expression levels in the *prohib* dsRNA inoculated group were significantly lower than in the control group (Log2 fold-change -8.09; $p < 0.05$; $p = 0.005884$); the opposite results were observed in T2 and T3 with increased expression levels in the *prohib* dsRNA inoculated group in comparison with the control but without statistical significance (T2 Log2 fold-change 1.13; $p > 0.05$; $p = 0.5522050$) (T3 Log2 fold-change 4.63; $p > 0.05$; $p = 0.126182$)).

Regarding the *E. canis*-infected samples, throughout the experimental times *prohib* expression levels were always downregulated in the *prohib*-silenced cells when compared with the controls (T1 Log2 fold-change -1.39; $p > 0.05$; $p = 0.219050$). In these cells, no *prohib* gene expression was verified in T2 and T3. Complete knockdown of this gene was significant compared with expression levels in *β2m* dsRNA-inoculated cells (T2 $p < 0.05$; $p = 0.001720$) (T3 $p < 0.05$; $p = 0.016269$).

Ultimately, for the 24h *post*-inoculation samples in T1, *prohib* expression levels were significantly downregulated in the *prohib* dsRNA-inoculated cells when compared with the controls (Log2 fold-change -4.90; $p < 0.05$; $p = 0.000002$). No *prohib* gene expression was verified in T2 in the *prohib* dsRNA-inoculated cells ($p < 0.05$; $p = 0.004311$). At time point T3, *prohib* expression levels were upregulated in the *prohib* dsRNA-inoculated cells, without statistical significance, when compared with *β2m* dsRNA-inoculated cells (Log2 fold-change 1.63; $p > 0.05$; $p = 0.211633$).

Comparing gene regulation with silencing efficiency, results show that *prohib* expression levels were directly correlated with the level of knockdown. Complete *prohib* silencing (100%) in the uninfected cells at T1, *E. canis*-infected cells at T2 and T3, and *E. canis*-inoculated cells at T2, resulted in statistically significant gene downregulation. In contrast, when gene silencing was not successful (0%) for the uninfected cells (T2 and T3), and for the *E. canis*-inoculated cells at T3 an overall upregulation was observed in the *prohib* dsRNA cells. Gene silencing (91.75%) was highly efficient in *E. canis*-inoculated cells in T1, with a statistically significant gene downregulation. In cells with a low silencing efficiency (9.48%), we still observed a downregulation of *prohib* expression, however, it was not significant.

Quantification of *E. canis* was also carried out to evaluate the role of this gene in cell invasion and multiplication after RNAi. Relative normalised expression of *E. canis dsb* (133) was determined by qPCR. Both *dsb* and *psc* (quantified in Section 3.3.4) were measured in the same plates. Reaction efficiencies were adequate; however, reference gene stability values were not acceptable, invalidating subsequent attempts to quantify *E. canis* DNA levels.

3.4.7. *In vivo prohib-* and *phsrp20-silencing* and *Ehrlichia canis* quantification

In vivo gene silencing was conducted in *R. sanguineus* nymphs to understand the role of *prohib* and *phsrp20* in the main arthropod vector when *E. canis* infection is present.

The primer pairs *prohib_RS_T7_forward* and *prohib_RS_T7_reverse* and *phsrp20_RS_T7_forward* and *phsrp20_RS_T7_reverse*, with the T7 promoter had the same oligonucleotide sequence as the ones used in IDE8 cells (Supplementary Table 1).

PCR amplification of *prohib* and *phsrp20* using tick SGs gDNA as the template, produced single bands of 442 bp and 379 bp, respectively, following 1.2% agarose gel (Figure 48).

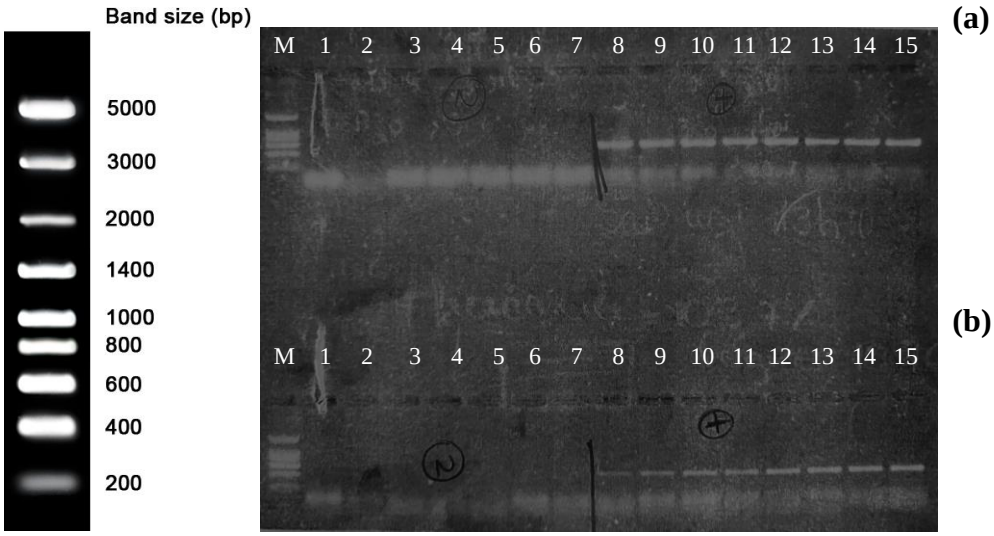

Figure 48. Agarose gel of a PCR amplification of a *prohib* and *phsrp20* fragment of *Rhipicephalus sanguineus*.

Lanes M: Marker (Ladder VIII, NZYTech); **(a)** PCR products with a 442 bp frangment of *R. sanguineus prohib* amplified with the primers *prohib_RS_T7_forward* and *prohib_RS_T7_reverse*. **Lanes 1 - 7:** Negative control with no template; **Lanes 8 – 15:** Samples of gDNA from *R. sanguineus* salivary glands; **(b)** PCR products with a 379 bp fragment of *R. sanguineus phsrp20* with the primers *phsrp20_RS_T7_forward* and *phsrp20_RS_T7_reverse*. **Lanes 1 - 7:** Negative control with no template; **Lanes 8 – 15:** Samples of gDNA from *R. sanguineus* salivary glands. PCR products were run on a 1.2% agarose gel.

PCR products were gel purified and sequenced, after quality and concentration determination by spectrophotometry (*prohib* amplicon = 6.9 ng/µl and $A_{260/280}$ = 2.71; *phsrp20* amplicon = 19.6 ng/µl and $A_{260/280}$ = 1.35).

Primer specificity was confirmed using BLAST. The *prohib* PCR product sequence showed 95.47% homology with *Rhipicephalus sanguineus* prohibitin-like (LOC119405271), mRNA (GenBank accession nr. XM_0376772083.1) (E value = 0; query cover = 91%). The *phsrp20* PCR product sequence had high homology with *Rhipicephalus sanguineus* heat shock protein Hsp-12.2-like (LOC119404707), mRNA (GenBank accession nr. XM_037671353.1) with 84% similarity (E value = $6e^{-72}$; query cover = 38%).

PCR amplicons were used as the template for dsRNA synthesis. RNAi was carried out in *R. sanguineus* nymphs with the same experimental conditions described in Section 2.7.2.

Prior to qPCR, RNA was extracted from the SGs of freshly moulted adult females and quantified by spectrophotometry. For the group soaked with *prohib* dsRNA, RNA concentration = 1.09 - 11.2 ng/µl; for the group soaked with *phsrp20* dsRNA concentration = 1.74 - 12.65 ng/µl; and for the control group = 0.93 - 4.80 ng/µl. Results are shown in Supplementary Table 27. Complementary DNA was synthesised after sample concentration normalisation to 100 ng/µl.

Relative normalised expression levels in the control group (PBS) and *prohib* or *phsrp20* dsRNA groups were determined by qPCR, using *prohib_RS_forward* and *prohib_RS_reverse* or *phsrp20_RS_forward* and *phsrp20_RS_reverse* primers. Triplicate no template controls were negative and reaction efficiency was determined by 10-fold serial dilution of *R. sanguineus* cDNA. For *prohib*, plate efficiency varied between 97.6 - 104.2%.; and for *phsrp20* varied between 85 - 105.5%. Data was normalised against the reference genes *β-actin* and *elf* for *prohib*; and *β-actin*, *β-tubulin* and *elf* for *phsrp20* (228). Stability values for *phsrp20* were M-value = 0.084 and 0.737, and for *prohib* M-value = 0.133. Reference genes were considered stable (M-value < 1) to proceed with gene expression data analysis.

Relative normalised expression was determined for both genes in comparison with the control group (Figure 49). Results showed both *prohib* and *phsrp20* were significantly downregulated ($p < 0.05$) in comparison with the control group (PBS) (*prohib* Log2 fold-change -1.43; $p = 0.000027$; *phsrp20* Log2 fold-change -3.32; $p = 0.003397$). Gene silencing was successfully achieved for both genes, with expression downregulated by 62.80% and 74.10%, for *prohib* and *phsrp20*, respectively.

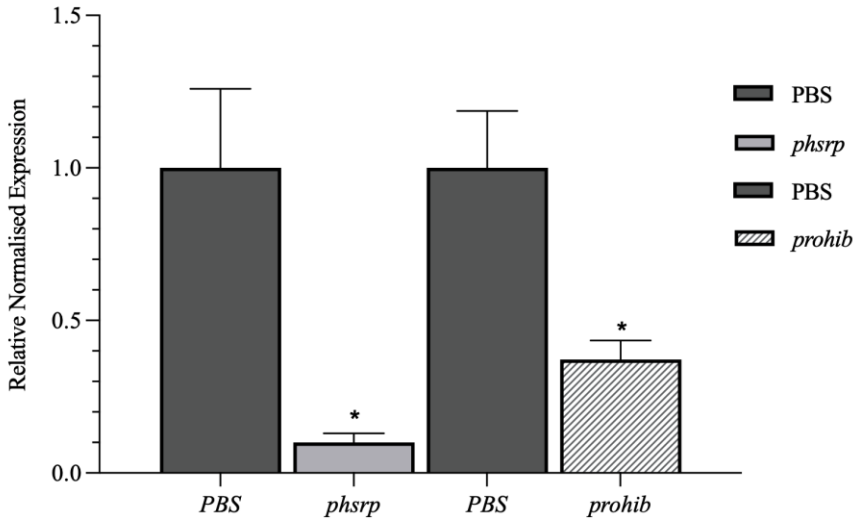

Figure 49. Relative normalised expression levels of *phsrp20 and prohib* in salivary glands of *Rhipicephalus sanguineus* unfed freshly moulted females.

Relative normalised expression was determined in *E. canis*-infected salivary glands. Nymphs were soaked 3 hours in *phsrp20* or *prohib* dsRNA or PBS for the control group, and allowed to fed on a infected host. After moulting, salivary glands were excised from unfed adult females. Data was normalised against the reference genes *β-actin*, *β-tubulin* and *elf* for *phsrp20,* and *β-actin* and *elf* for *prohib*. Results were calculated automatically with CFX Manager™ Software (Bio-Rad). Columns represent the Mean of relative normalised expression (*n* control = 12 and *n phsrp20* = 12; *n* control = 12 and *n prohib* = 12) +SEM. *Statistically significant differences in gene expression levels, when comparing the silenced with the control group using Welch's unequal variances *t*-test ($p < 0.05$; *phsrp20* $p = 0.003397$; *prohib* $p = 0.000027$); (Figure created with GraphPad Prism software; version 9 for macOS).

Quantification of *E. canis* was also carried out by qPCR targeting *E. canis dsb* (133) to determine whether downregulating *prohib* and *phsrp20* would affect bacteria multiplication. No amplification was verified in the triplicate negative controls and reaction efficiency between plates was determined by 10-fold serial dilution standard curves of *E. canis* Jaboticabal strain DNA. Plate efficiency was 64.5 and 114.1% for the *prohib* and for *phsrp20* studies, respectively. Even though correct amplification was observed in the positive controls, reference gene stability values were not acceptable, invalidating subsequent attempts to quantify *E. canis* DNA levels.

3.5. *In silico* analysis of *Ehrlichia canis* infection-related genes and putative proteins

From the *R. sanguineus* SGs sialome and proteome, this study identified genes and proteins that were significantly differentially expressed and represented ($p < 0.05$), respectively. One putative gene and two putative proteins were selected for further investigation due to their possible function in *E. canis* infection, multiplication, and transmission in ticks.

In silico analysis was carried out to predict protein secondary structure and protein-protein interactions of PROHIB (UniProtKB L7M5P4), from the proteome, and the PSC (UniProtKB L7MH00), from the sialome. *In silico* analysis of PHSRP20 (UniProtKB L7M6Q5), from the proteome, is described in more detail in section 3.6.1. Protein structure was predicted by homology modelling using the online tool SWISS-MODEL (https://swissmodel.expasy.org/) (242-246). Figure 50 shows the prediction for the PROHIB putative protein and Figure 51 for the PSC putative protein.

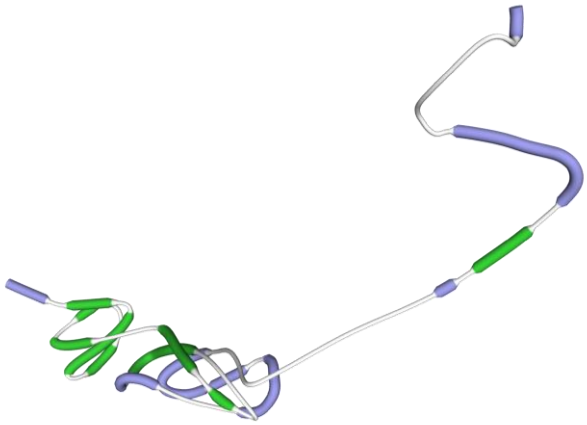

Figure 50. Predicted secondary structure for the putative prohibitin-like protein (PROHIB; UniProtKB L7M5P4).

Protein structure was predicted by homology modelling with the online tool SWISS-MODEL (https://swissmodel.expasy.org/). In **green** are the areas with a.a. homology (21.82%) between the PHSRP20 sequence and the sofware template used to best predict the structure (Modulator of FtsH protease HflC - 7vhq.1). In **purple** the areas without homology.

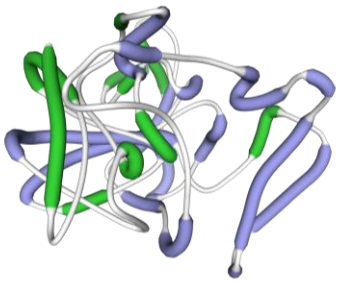

Figure 51. Predicted secondary structure for the putative serine carboxypeptidase protein (PSC; UniProtKB L7MH00).

Protein structure was predicted by homology modelling with the online tool SWISS-MODEL (https://swissmodel.expasy.org/). In **green** are the areas with a.a. homology (20.00%) between the PSC20 sequence and the sofware template used to best predict the structure (Crystal structure of kex1deltap, a prohormone-processing carboxypeptidase from *Saccharomyces cerevisiae* – 1ac5.1). In **purple** the areas without homology.

The network of predicted protein-protein interactions was investigated for PROHIB and PSC using STRING (v 11.5; https://string-db.org/), selecting a confidence interaction score = 0.900. Figure 52 shows PROHIB (8036376) associations with a putative ubiquinol cytochrome C reductase subunit RIP1 (8042691), other prohibitin (8025164), a putative processing peptidase β-subunit (8024783), a putative mitochondrial processing peptidase α subunit (8033890) and a putative processing peptidase β subunit (8024783). The protein-protein interaction was determined for the protein PSC, but no interactions have been found in the analysis.

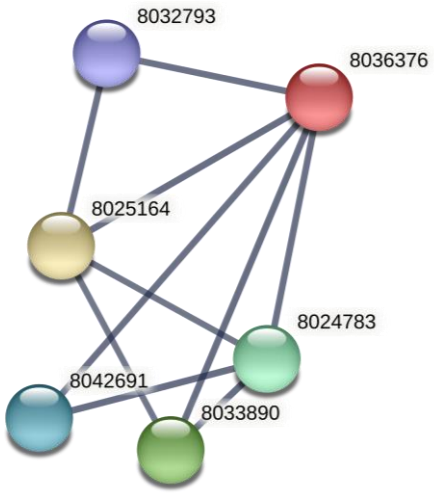

Figure 52. STRING analysis of putative prohibitin-like protein (PROHIB; UniProtKB L7M5P4). Network of predicted associations for PROHIB (8036376) with putative ubiquinol cytochrome C reductase, subunit RIP1 (8042691), prohibitin (8025164), putative processing peptidase β-subunit (8024783), putative mitochondrial processing peptidase α subunit (8033890) and putative processing peptidase β subunit (8024783). The lines predict protein-protein interactions. Confidence interaction score of 0.900. Protein-protein interaction was predicted with STRING (v 11.5; https://string-db.org/).

3.6. Polyclonal antibody production

3.6.1. Peptide *in silico* analysis

Peptide selection was based mainly on two criteria: *(i)* protein involvement with pathogen infection in the tick, and *(ii)* its potential protective capacity to be used as an antigen in a vaccine. Based on the pre-established criteria, the a.a. of PHSRP20 (UniProtKB L7M6Q5) was selected and analysed *in silico* using the FASTA sequence retrieved from the UniProtKB database:

MALFPLLNNRGSWGPSDLVRRFLDDDFGGSFLDGELFDPPFYHQRFYIQPRQAS
EGSVCPARQPGTSVACTPDKFAINVDTRHFAPEEITVKTQDNCVVIHGKHEEKS
DDRGCYVKREFTRRYVLPEDVDPESVKCHLKPNGLLALEAPRKNAPKEQPKAI
PIEVKHEGASGsDVAKK

Transmembrane proteins are important for vaccine development since they have exposed targets for antibodies. Thus, the topology of both α and β-barrel transmembrane helices of this protein was predicted and classified using TMHMM – 2.0 (CELLO v.2.5; http://cello.life.nctu.edu.tw/) (238, 239). The prediction gives the most probable location and orientation of transmembrane helices in the sequence with the N-best algorithm (or 1-best in this case) that sums over all paths through the model with the same location and direction of the helices. According to the sequence analysis, the most probable location and orientation was labelled as non-cytoplasmic (Figure 53).

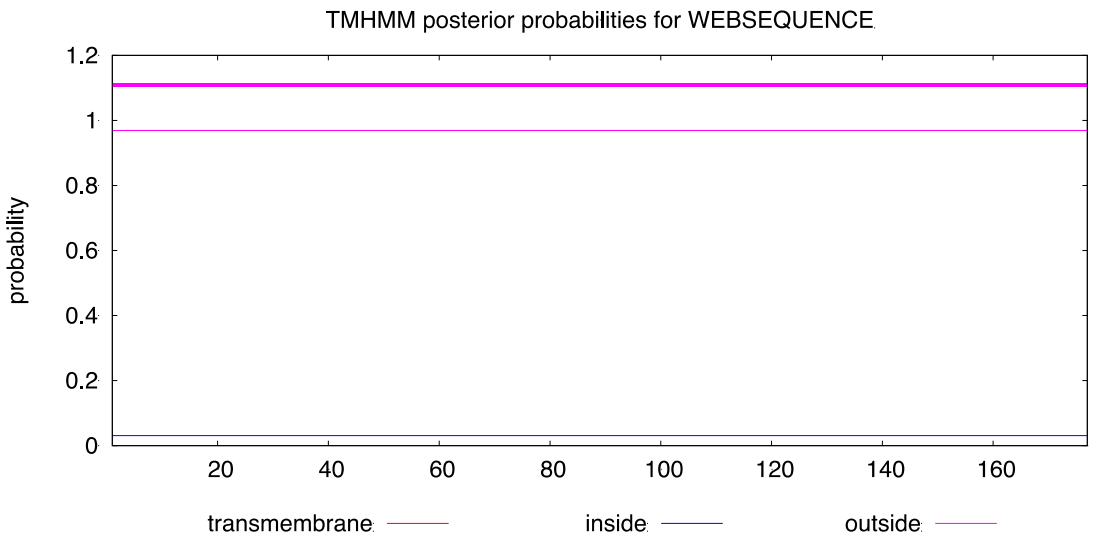

Figure 53. Plot of topology prediction and classification of the putative heat shock-related protein a.a. sequence (UniProtKB L7M6Q5).

Plot shows the topology probabilities of inside/outside/transmembrane of both α and β-barrel transmembrane helices. At the top of the plot (between 1 and 1.2) the N-best prediction is non-cytoplasmic. Analysis was carried out with TMHMM – 2.0 (CELLO v.2.5; http://cello.life.nctu.edu.tw/).

The signal peptide is a region of a protein sequence, generally located in the N-terminal, that directs the protein across the endoplasmic reticulum (ER) membrane in eukaryotic cells. Signal peptides can also be in the C-terminal or internally, for example in the nucleus. Even though proteins that have signal peptides are targeted to the secretory pathway, they are not always secreted (240). They are also known as *ER signal peptides* or *secretory signal peptides*. The sequence was analysed for the presence of a signal peptide using the online prediction tool SignalP-4.1 (SignalP-4.1; https://services.healthtech.dtu.dk/service.php?SignalP-4.1) (240). This server predicts the presence and location of signal peptide cleavage sites in a.a. sequences from different organisms. The graphical output (Figure 54) shows three different scores, *C*, *S* and *Y*, for each position in the sequence. In the summary below the plot, the maximal values of the three scores are reported. According to the D-score, used to discriminate signal peptides from non-signal peptides, this protein lacks a signal peptide (D-score = 0.135 with cut-off of 0.450). Finally, for non-secretory proteins, all the scores represented in the SignalP output should ideally be very low (close to the negative target value of 0.1). Thus, this

protein is predicted to be intracellular and would not be actively secreted (C-score = 0.108; Y-score = 0.119; mean S-score = 0.149).

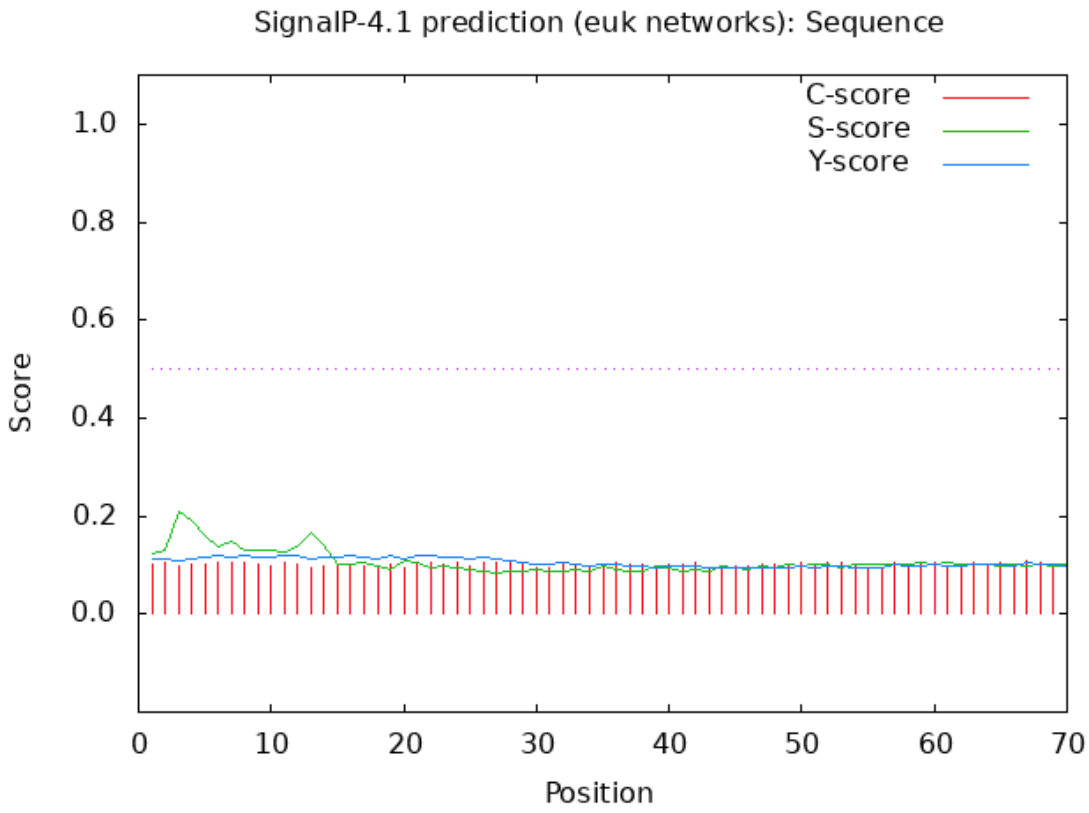

# Measure	Position	Value	Cutoff	signal peptide?
max. C	67	0.108		
max. Y	11	0.119		
max. S	3	0.211		
mean S	1-10	0.149		
D	1-10	0.135	0.450	NO

Figure 54. Plot of signal peptide prediction of the putative heat shock-related protein a.a. sequence (UniProtKB L7M6Q5).

The plot predicts the presence and location of the signal peptide cleavage sites in the a.a. sequence. **C-score:** raw cleavage site score; **S-score:** signal peptide score; **Y-score:** combined cleavage site score; **Mean S:** average S-score of the possible signal peptide; **D-score:** discriminate signal peptides from non-signal peptides. This protein can be classified as non-secretory and without signal peptide. Analysis was carried out with SignalP-4.1 (SignalP-4.1; https://services.healthtech.dtu.dk/service.php?SignalP-4.1).

Epitope position was predicted from the a.a. sequence using the IEDB (available at http://tools.iedb.org/bcell/), selecting the B cell epitope prediction (Bepipred Linear Epitope Prediction). Here each residue has a calculated score and the scores above the threshold (0.350) could be interpreted as the residue having a higher probability of being part of an epitope (Figure 55). A total of ten predicted peptides were found that might be part of the epitope, which is important for the development of an immune response (Figure 56).

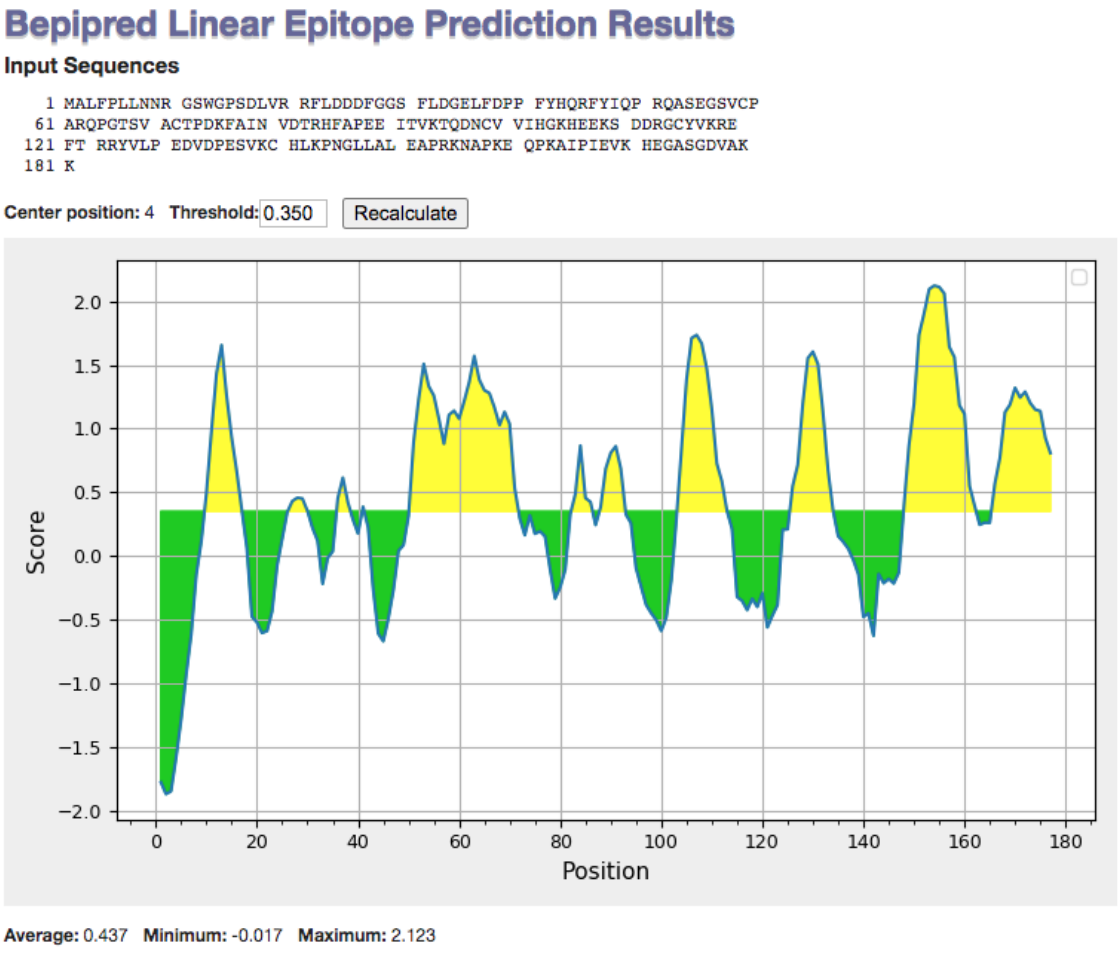

Figure 55. B-cell epitope prediction for the putative heat shock-related protein a.a. sequence (UniProtKB L7M6Q5).

Y-axis: score for each residue; **X-axis:** residue positions in the sequence; **Yellow:** scores above the threshold of 0.350 might be interpreted as that the residue might have a higher probability to be part of epitope. Analysis was carried out with Immune Epitope Database and Analysis Resource (IEDB) (available at http://tools.iedb.org/bcell/).

Predicted peptides:

No.	Start	End	Peptide	Length
1	10	17	RGSWGPSD	8
2	27	30	FGGS	4
3	36	38	LFD	3
4	41	41	F	1
5	51	71	RQASEGSVCPARQPGTSVACT	21
6	83	86	HFAP	4
7	88	92	EITVK	5
8	104	113	HEEKSDDRGC	10
9	126	134	PEDVDPESV	9
10	148	162	APRKNAPKEQPKAIP	15

Figure 56. B-cell epitope predicted peptide sequences of the putative heat shock-related protein a.a. sequence (UniProtKB L7M6Q5).
Columns Start and End: Peptide position in the protein sequence; **Column Peptide:** a.a. sequence; **Column Length:** Peptide size. Analysis was carried out with Immune Epitope Database and Analysis Resource (IEDB) (available at http://tools.iedb.org/bcell/).

Protein solubility was predicted using the scaled solubility value (QuerySol) from the online tool Protein-Sol (available at https://protein-sol.manchester.ac.uk/) (241). The population solubility average for the control dataset is 0.45, so any scaled solubility value superior to 0.45 is predicted to have a higher solubility than the average soluble *E. coli* protein. Contrary, any protein with a lower scaled solubility value is predicted to be less soluble. The predicted scaled solubility value for PHSRP20 is 0.578; thus, is considered soluble in comparison with the control.

Protein allergenicity was predicted using the bioinformatics tool AllerTOP v.2.0 (available at https://www.ddg-pharmfac.net/AllerTOP/index.html). The result determined that the protein sequence is a probable non-allergen.

Protein structure was predicted by homology modelling with the online tool SWISS-MODEL (available at https://swissmodel.expasy.org/) (242-246). The predicted secondary structure is shown in Figure 57.

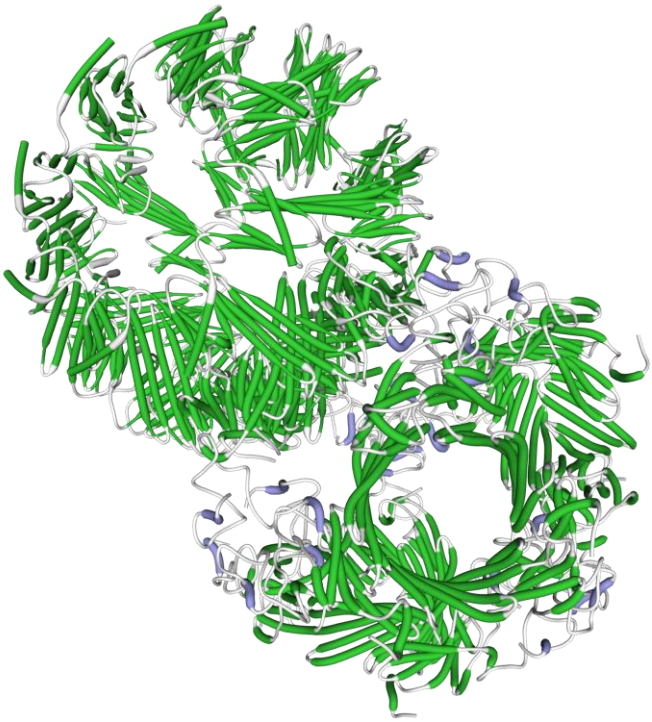

Figure 57. Predicted secondary structure for the putative heat shock-related protein (PHSRP20; UniProtKB L7M6Q5).

Protein structure was predicted by homology modelling with the online tool SWISS-MODEL (https://swissmodel.expasy.org/). In **green** are the areas with a.a. homology (31.88%) between the PHSRP20 sequence and the sofware template used to best predict the structure (Stress induced protein from *Caenorhabditis elegans* – 4ydz.1.A). In **purple** the areas without homology.

The network of predicted protein-protein interactions was investigated using STRING (v 11.5; https://string-db.org/), selecting a confidence interaction score of 0.900. Figure 58 shows one association of PHSRP20 (8027107) with a putative small heat shock protein (8043348).

Figure 58. STRING analysis of putative heat shock-related protein (UniProtKB L7M6Q5).
Network of predicted associations for PHSRP20 (8027107) with a putative small heat shock protein (8043348). The line predicts protein-protein interaction. Confidence interaction score of 0.900. Protein-protein interaction was predicted with STRING (v 11.5; https://string-db.org/)

3.6.2. Immune response evaluation

For polyclonal antibody production, pPHSRP20 was solubilised in Milli-Q water, according to the manufacturer instructions, and the concentration determined by fluorescence using the Qubit 4.0 Fluorometer (ThermoFisher). Samples had a concentration = 0.16 µg/µl, both for the final volume of 10 µl and 20 µl.

SDS-PAGE was carried out to determine peptide integrity after its solubilisation. Figure 59 shows the presence of a single band in both lanes 1 and 2, which differ in intensity because different volumes (i.e., amounts) of peptide were loaded (14 µl for lane 1 and 30 µl for lane 2). The presence of a unique band reflects the absence of peptide degradation. The synthesised peptide has a molecular weight = 7 kDa so, as expected, both bands had a molecular weight below 11 kDa.

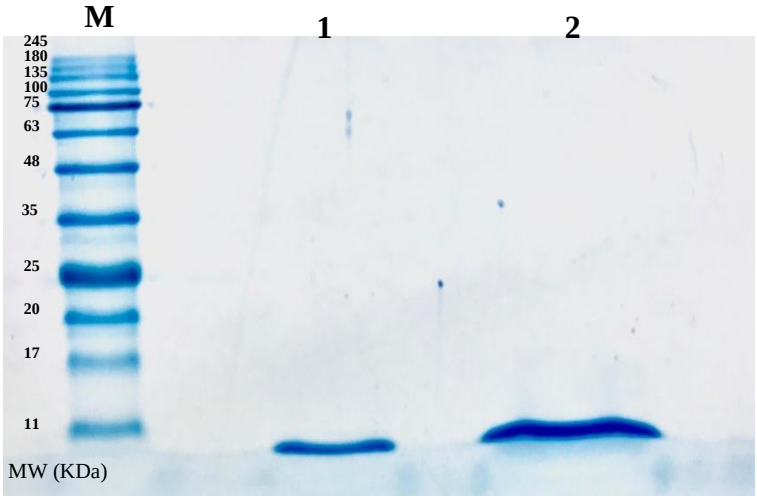

Figure 59. SDS-PAGE gel of the synthesised pPHSRP20.
Lane M: NZYColour Protein Marker II (NZYTech); **Lane 1:** 14 µl of loaded sample; **Lane 2:** 30 µl of loaded sample. Expected size of 7 kD.

Indirect and chessboard ELISA were carried out with sera from CD1 mice to detect the presence of specific antibodies that recognise the peptide, and to quantify the immune response in each animal. CD1 mice were separated in two groups, in which R_1, R_2, and R_3 were the animals immunised with pPHSRP20; and NC_1, NC_2, and NC_3 were the control animals inoculated with PBS. The experimental design is outlined in Figure 9. Overall results show that negative controls, CT_1, CT_2, and CT_3, did not present an immune response, as expected, maintaining the absorbance values very low (data not shown). Pre-immune values were 0.0340, 0.0323 and 0.0306 for R_1, R_2, and R_3, respectively. The existence of an immune response was defined as an absorbance value triple that of the pre-immunisation absorbance value (at 0 weeks).

From the pPHSRP20-immunised group, R_1 presented an immune response in the serum obtained at weeks 7, 9, and 10, with titres of 1:102400, 1:204800, and 1:80000, respectively. At week 4, the immune response was below the threshold value to be considered positive. Figure 60 shows the antibody titres for R_1.

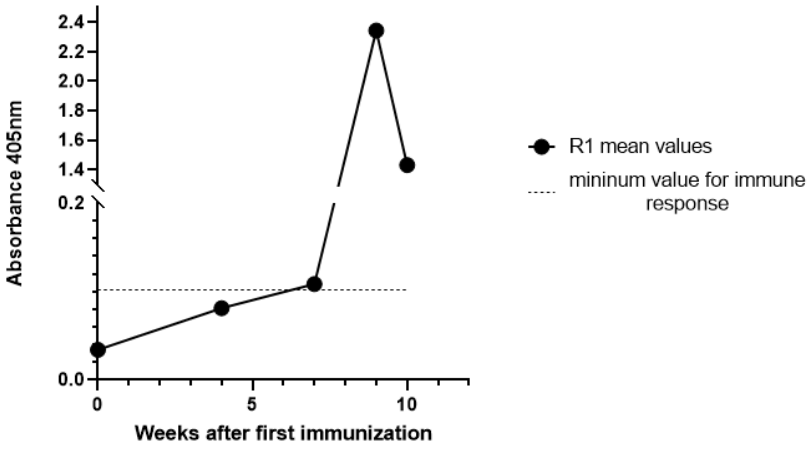

Figure 60. Polyclonal antibody production in R_1 CD1 mouse in response to pPHSRP20 immunisation. Serum was obtained at weeks 4, 7, 9, and 10, after immunisation. Time point 0, represents the pre-immune antibody titer. ELISA was carried out with 1:500 serum dilution. **(---)** represents the threshold value above which is considered a positive immune response (Figure created with GraphPad Prism software; version 9 for macOS).

Mouse R_2 showed a mild increase in specific antibodies at week 10, with a titre of 1:800. For mouse R_3, absorbance values were very low throughout all the time points and below the threshold. In weeks 0, 4 and 7, the values were 0.0306, 0.0318 and 0.0330, respectively. In comparison with R_1 and R_2, mouse R_3 did not have a positive immune response to pPHSRP20. Due to their weak immune responses, ELISA results were not graphically represented for R_2 and R_3.

SDS-PAGE followed by Western blot was carried out with the pPHSRP20 using sera from all animals obtained 9 weeks after the first immunisation, which was when a higher antibody titre was verified by ELISA. Figure 61 shows that the control mice (NC_1, NC_2 and NC_3) did not present a band, confirming the absence of antibody detection for the pPHSRP20. In the pPHSRP20-immunised group (R_1, R_2 and R_3), a band was detected in mice R_1 and R_3. Both bands presented a size below 11 kDa, which corresponds to the peptide molecular weight of 7 kDa. Also, a strong band visualised in R_1 confirms that the absorbance reading at 9 weeks after the first immunisation corresponds to a specific antigen-antibody interaction, ruling out ELISA false positives. Mouse R_2 did not show detectable bands.

Overall results confirm that the pPHSRP20, based on the proteomic data analysis, is recognised by the immune system of CD1 mice.

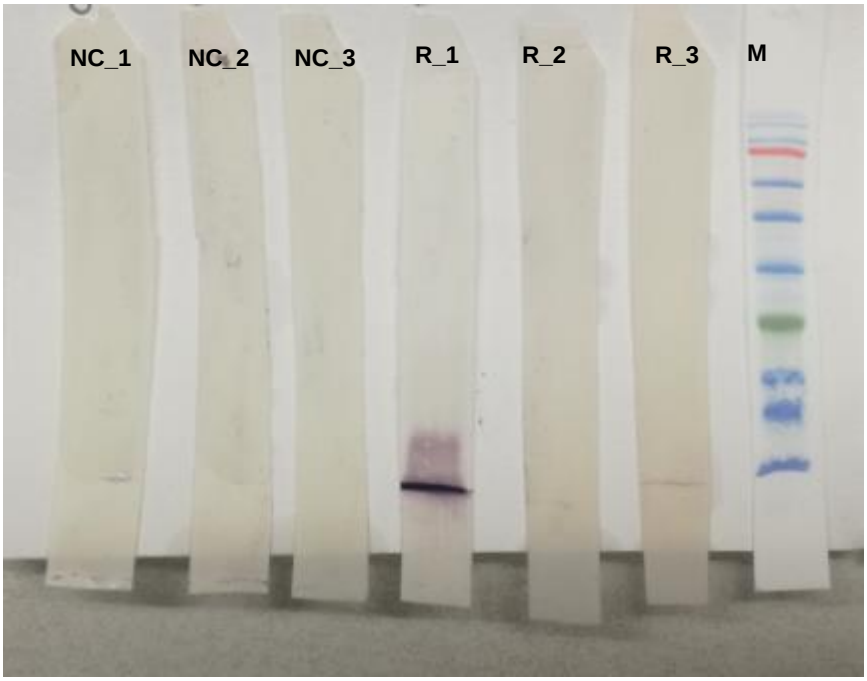

Figure 61. SDS-PAGE and Western blot of pPHSRP20 in CD mice.

Protein was detected with mice polyclonal antibodies from sera collected 9 weeks after peptide first immunisation. **Lanes NC_1, NC_2 and NC_3:** control mice immunised with PBS; **Lanes R_1, R_2 and R_3:** mice immunised with the peptide (7 kDa); **Lane M:** NZYColour Protein Marker II (NZYTech). Mouse R_1 and R_3 show a band size below 11 kDa.

Chapter 4. Discussion and Conclusions

4.1. Vertebrate host clinical *status* and parasitemia detection

CME is a potentially fatal tick-borne infectious, non-contagious disease of canids transmitted by the obligate intracellular rickettsia *E. canis*. This bacterium invades and develops in canine monocytes and macrophages, leading to fever, depression, leukopenia, thrombocytopaenia and, in more severe cases death. *E. canis* is a cosmopolitan parasite mainly transmitted by the brown dog tick *R. sanguineus*. The pathogenesis of CME is characterised by an incubation period that varies between 8- and 20-days after infection that is followed by three possible different clinical stages, the acute, the subclinical and the chronic (37).

For our studies we carried out a series of experimental infections in German shepherd dogs, a highly susceptible breed, to obtain uninfected and *E. canis*-infected tick populations for transcriptomic, proteomic and RNAi data. Inoculated dogs were confirmed positive for infection and soon after manifested clinical signs of acute disease, such as fever, prostration and hyporexia. Haematologically, dogs presented leucocytosis because of the immune response, and anaemia and thrombocytopenia. These last two are frequently associated with an excessive immunological reaction of the dog to the rickettsial agent, resulting in immune-mediated haemolytic anaemia and thrombocytopenia by haemocyte and PLT destruction (261, 262). All dogs successfully recovered from the disease after treatment. The control dogs did not manifest any symptoms of disease, as expected.

4.2. *Ferritin 1*-silencing effect in *Rhipicephalus sanguineus* sensu lato

Ticks are obligatory blood-sucking arthropods totally dependent on their vertebrate hosts to acquire nutrients thorough blood meals to survive and to reproduce (197, 263). Tick digestion metabolism differs from other species in that it occurs intracellularly in digestive cells of the MG, which incorporate the blood components by absorptive receptor-mediated endocytosis in organelles (264, 265). Blood digestion takes place in three different stages, a first stage of continuous digestion immediately after the beginning of the feeding process, when engorgement is slow, followed by a second stage of reduced digestion, initiated by mating during the rapid engorgement, and a final stage of continuous digestion initiated by detachment and that lasts until oviposition (265). During each blood meal, ticks are exposed to non-heme and to heme iron resulting from erythrocyte lysis within the lysosomal vesicles of the digestive cells. Both types of iron can have a beneficial or a detrimental effect on tick physiology. Iron is required as a biological cofactor for metabolic and transport functions, amongst others, and heme is vital for tick reproduction during vitellogenesis once it is incorporated into the major yolk protein, Vn, and into the Vn precursor, vitellogenin (Vg). Vn and Vg, along with other heme-binding storage and antioxidant proteins, protect ticks from heme toxicity (266, 267). Simultaneously, if in excess, iron can act as a highly toxic precursor of reactive species of oxygen (ROS), causing serious damage to the cells, culminating in apoptosis. The non-heme transferrin with Fe^{3+} converts into Fe^{2+} and when it is released, contributes to ROS formation by reacting with hydrogen peroxide (H_2O_2) through the Fenton reaction (200, 263, 268). It also seems that ticks lack an efficient system to excrete iron through the faeces (70). Thus, iron molecules must be very well balanced in the cells.

Based on this information and on the fact that *R. sanguineus* s.l. is a tick of great medical and veterinarian importance, the present study investigated the effects of silencing *ferritin 1* in ticks on the ability to feed, OV and oocyte development and pathogen acquisition.

The present study demonstrated that *ferritin 1* knockdown resulted in a significant decrease in tick weight after detachment in comparison to the negative control, suggesting that their capability to feed or to attain full engorgement was altered. In this experiment, Elution buffer was used as the genome of *R. sanguineus* s.l. was not available when these experiments were carried out so we could not be sure whether potential control dsRNA

sequences would bind to tick mRNAs. Furthermore, there is no evidence that non-specific effects caused by dsRNA could lead to effects on tick phenotype.

Although in our study only *ferritin 1* was silenced, the overall results are similar to others previously reported for *I. ricinus* female ticks, in which silencing the genes encoding FER1, FER2 and the IRP-1 had an adverse impact on feeding with a consequent decrease in weight after a blood meal (199). The same was observed in *I. persulcatus* whereby a vaccination trial was carried out using FER2, had a significant reduction in the engorgement weight of adult ticks observed (269). Results suggest that the reduction in tick feeding capacity, and thus to fully engorge, may be related to an imbalance in iron homeostasis and consequent iron accumulation, leading to toxicity. Moreover, Galay et al. (2013) observed that after *Hl-fer* silencing, fewer digestive cells with hematin, one of the products of blood digestion, were present in the MG. This probably jeopardised the normal engorgement capacity of a tick by decreasing MG digestive activity (197).

Under the conditions undertaken in this study, no significant effect on survival rate was observed in the silenced *R. sanguineus* s.l. ticks. Despite this, another study conducted in *H. longicornis* demonstrated an antioxidant protective role of ferritin promoted tick survival (201).

For the perpetuation of any species, the role of the female reproductive system is crucial. In our study, adult females of *R. sanguineus* s.l. in which *ferritin 1* was silenced presented morphologic changes in the oocytes and alterations in the dye affinity for lipids and proteins, not seen in the controls. Morphologically, the oocytes were less developed, and those in a more advanced stage of maturation presented typical characteristics of degeneration and reabsorption, such as an irregular shape with folds and deformations, heterogeneous vacuolated cytoplasm, and autophagic vesicles. Some authors have related the presence of autophagic vacuoles in cells with active processes of degradation and recycling in certain areas of the cytoplasm or organelles (270, 271).

According to the histochemical results for lipid and protein detection, in the control group it was observed that the yolk granulation was in the central region as expected (272);

while in the *ferritin-1* silenced group, the granulation was extended from the central to the marginal region. The increase of vacuolation and different pattern and distribution of yolk granules in the oocytes might be related to the degradation of cell organelles with formation of autophagic vacuoles as a defence mechanism; but it might also reflect the fact that yolk production is happening at a slower rate or being impaired. Normally, during endogenous yolk production, smaller granules located mainly in the central region of oocytes III gradually fuse together, becoming larger and moving towards the oocyte periphery (272).

The alterations detected in the present study and others suggest that a reduction in the normal gene expression levels of the iron-binding protein *ferritin 1* might cause structural changes in *R. sanguineus* s.l. germ cells. In the tick *H. longicornis* it was shown that when *FER1* and *FER2* were silenced, both tick feeding and reproductive capacity were greatly impaired (197). The same result of reduced weight and reduction in the number of eggs and hatched eggs was verified but was less profound when adult ticks ingested anti-HlFER 1 and 2 antibodies during a blood meal (208); and when *fer1* was silenced, with a reduction in oviposition and prevention of egg hatching (199). *Fer2* knockdown in *Ornithodoros moubata* also reduced egg hatchability rate and the number of hatching nymphs, suggesting its role in embryogenesis. The same was not verified for *Ornithodoros erraticus* (273). More recently, Zhao et al. (2022) also demonstrated that *Hf-fer1* and *Hf-fer2* affect tick fertility in *H. flava.* After gene silencing, ticks that were able to do oviposition presented lower egg weight to body weight ratios, with abnormal morphologies (205).

Thus, these studies suggest that iron storage is crucial for proper embryo development, without which the hatching of larvae does not occur. Lastly, the reduction in feeding among the silenced group might also have led to the difficulty in achieving the female critical weight (CW) and consequently the difficulty in OV maturation, with overall reduction of the size of the OV. In *A. hebraeum* it is only when the CW is achieved that 20-hydroxyecdysone is synthesised for further Vg production, required for OV maturation (274). Taken together, these results become interesting and promising under the perspective of controlling tick populations through reproductive blockage.

The role of ferritin proteins during pathogen infection has been a subject of interest. Ferritins are iron-binding proteins that, for some types of infection, could directly compete with the pathogen for available iron and limit its multiplication. It is now known that some bacteria need iron to successfully multiply, such as with *E. coli*. Galay et al. (2016) investigated the role of ferritins in the innate immunity of *H. longicornis*, and their results have shown that gene silencing, mainly of *Hl-fer2*, significantly decreased the survival of ticks when exposed to *E. coli* (275). Also, high numbers of *E. coli* were found in *Hl-fer1* and *Hl-fer2* silenced groups suggesting that when this bacterium has more Fe^{2+} available in the haemolymph and haemocytes, bacterial multiplication is favoured (275). Interestingly, based on transcriptional analysis of *D. variabilis* it was found that *ferritin* was upregulated during *Rickettsia montanensis* infection (276). The same gene upregulation was later observed after *E. coli* injection in the tick haemocoel (206).

To evaluate whether the *ferritin 1* silencing interferes with pathogen acquisition and multiplication, *E. canis* was quantified in the SGs. Unfortunately, no *E. canis* DNA was detected, despite the fact the ticks were feeding on an infected dog. One possibility is that the number of bacteria in the SGs was too low to be detected by molecular methods.

This study aimed to characterise the effects of *ferritin 1*-silencing using RNAi in tick feeding, OV and oocyte development, and pathogen acquisition in *R. sanguineus* s.l. Our study reinforced the importance of intracellular ferritin 1 on the capacity of ticks to engorge and to achieve reproductive maturity, which are closely related functions. This is the first study conducted in the hard tick *R. sanguineus* s.l. reporting a reduction in tick weight after detachment and abnormalities in the OV and oocyte morphology after *ferritin 1* knockdown.

Identification and functional characterisation of genes and proteins that are involved in iron metabolism is of great importance because ticks rely on their blood meals to survive and reproduce. Accordingly, using these proteins as anti-tick vaccine targets will theoretically increase biological toxicity by raising iron levels, reducing tick survival. Moreover, the development and use of a vaccine that reduces tick feeding capacity,

survival and fecundity would uncover new targets to disrupt the tick life cycle and disease transmission. The long-term aim being improvement of current control measures to reduce environmental tick populations, host tick infestations and TBDs.

4.3. Gene expression profile of *Rhipicephalus sanguineus* salivary glands in response to *Ehrlichia canis* experimental infection

Ticks are obligatory hematophagous parasites that depend exclusively on their vertebrate host to obtain the vital nutrients for development, reproduction, and ultimately, survival. During the feeding process, ticks can become competent vectors of several pathogen species, acquired from the blood of an infected host, and transmitted through the saliva during the next meal. Thus, tick saliva plays a crucial role during feeding through the action of several secreted molecules. These facilitate tick attachment and prolonged feeding necessary for engorgement, modulating host inflammatory responses and interfering with haemostasis cascades. Salivary secretions include cement, anticoagulants, different enzymes, cytolysins, pharmacological agents and toxic substances. Saliva mediators can also facilitate pathogen transmission (277, 278). The secretion of these components is mostly found in slow-feeding ticks, apart from some *Ixodes* species that can attach the mouthparts deeply into the host dermis (279). Recently, studies carried out by Chávez et al. (2021) elucidated the role of tick extracellular vesicles (EVs), showing that EVs have different regulatory roles in pathogen infection in mice during feeding. EVs derived from *I. scapularis* SGs favoured the establishment of *A. phagocytophilum*, whereas EVs from *D. andersoni* reduced the spreading of *Francisella tularencis* (280)

Studying the *R. sanguineus* sialome may lead to the discovery of vaccine targets that ideally would block or disrupt tick attachment time to the host, feeding process, reproductive viability, and pathogen transmission. During the last decade, several studies have been published reporting transcriptomic analyses in this tick species in larvae (17), synganglia (20), sialotranscriptome of unfed (227) and blood feed ticks (281), amongst other species. In 2020, the genome of *R. sanguineus* larvae was *de novo* sequenced (Genome Warehouse available at https://ngdc.cncb.ac.cn/gwh/ with accession No. GWHAMMM00000000; Bioproject PRJCA002240; Biosample SAMC136623) (282), allowing transcript sequence reads to be mapped with a high level of confidence.

Here our objective was to characterise the *R. sanguineus* sialome during *E. canis* infection to explore potential targets involved in pathogen transmission. During co-evolution, ticks

and microorganisms have developed symbiotic strategies that involve molecules present in saliva, facilitating pathogen acquisition and transmission by ticks with subsequent systemic dissemination within the vertebrate host. Thus, our hypothesis is that upon infection, the SGs transcripts that encode these proteins will be differentially expressed and be good candidates for further research in transmission-blocking vaccines.

In this study, we investigated the sialotranscriptome of fed uninfected and fed *E. canis*-infected tick SGs using high throughput RNA-seq. Clustering via UniRef90 identified a total of 15521 putative *R. sanguineus* proteins that were present in any of the four transcriptomes. A higher number of the transcripts were exclusive in the *E. canis*-infected samples, which might reflect the fact that the proteins they encode have a role in the infection process. After the first step of annotation, ten differentially expressed transcripts were found, of which four were upregulated and six were downregulated. The upregulated transcripts included the ones encoding the following proteins: putative mitochondrial import inner membrane translocases, an importin subunit α, and a putative serine carboxypeptidase. The downregulated transcripts included a glutathione S-transferase, a ubiquitin carboxyl-terminal hydrolase, a putative trilaris, and finally a protein kish. The functional categories of these transcripts were mostly related with protein cellular processes, protein catalytic activity and, in terms of cellular component, integral constituents of membranes. To validate our RNA-seq data, the expression of *psc* and *imp*, identified in the transcriptome as differentially expressed during *E. canis* infection, was investigated by qPCR. Contrary to the transcriptomic data, in the validation experiments both genes were found downregulated, without statistical significance. The samples used for RNA-seq and the ones for data validation were obtained in two independent studies, although the experiments were replicated exactly under the same protocols and conditions. Precise spatial and temporal gene expression and modification in living experimental models is difficult to control, and in our case was not achieved, which might explain the contradictory results. When investigated in IDE8 cells, *psc* gene expression levels were found upregulated in the *E. canis*-infected samples, which agreed with the sialome data, even though *I. scapularis* cells are an embryo-derived cell line (223) that might not reflect directly what happens in *in vivo* models.

The most relevant proteins encoded by the differentially expressed transcripts during infection will be discussed in the following sub-chapters.

4.3.1. Mitochondrial import inner membrane translocases

Our transcriptomic data has revealed the upregulation of the two transcripts that encode the putative mitochondrial import inner membrane translocases (TIM) – subunit 21 (UniProtKB L7MF27) and – subunit 23 (UniProtKB B7PEW5). Like other hematophagous arthropods, ticks have developed mechanisms to obtain blood meals and stay attached for days while they escape host immune defence mechanisms (283), and haemostatic and inflammatory triggered responses (284, 285). Indeed, ticks have in their SGs molecules that reduce and modulate these effects (278, 286).

Currently, mitochondrial protein import machinery is well studied in different organisms, from humans to plants and fungi. Most nuclear-encoded proteins that go to the mitochondria are synthesised in the cortisol and must cross two membranes to reach the matrix. Mitochondrial preproteins have very specific targeting signals, which proteins such as translocases can recognise *via* their receptors. These first translocases are in the mitochondrial outer membrane and are part of the pathway machinery that allows the import of mitochondrial precursor proteins to their correct destination through one or both organelle membranes (287). Once these proteins cross the outer membrane, they are transported to the mitochondrial matrix, inner membrane, or the intermembrane space by TIMs such as TIM23 and TIM22. The putative mitochondrial import TIM – subunit 21 found in this study is an essential channel-forming subunit component of the TIM23 complex. In the absence of a preprotein, the TIM23 complex is normally inactive, and the channel is maintained closed under influence of the TIM50 (288). When a preprotein is translocated though the channel, other inner membrane proteins act in the import reaction cycle to release the protein in the mitochondrial matrix (287). Thus, in eukaryotic cells, TIM21 component is required to keep the translocase of the outer membrane and the TIM23 complexes in close contact for protein transport into the mitochondrial matrix and for the respiratory chain. The upregulation of the two transcripts that encode TIM21 (UniProtKB L7MF27) and TIM23 (UniProtKB B7PEW5) verified in our sialotranscriptome data might be involved in critical mitochondrial functions in cellular processes, such as energy metabolism, apoptosis, signalling and metabolic pathways. To date, their exact involvement during pathogen infection is still unclear and not reported in tick species.

4.3.2. Importin subunit α

Another upregulated transcript in our study was *importin subunit α* (*imp*; UniProtKB L7M4M0). The traffic of molecules between the nucleus and the cytoplasm is vital for the survival and development of eukaryotic cells. The active import of proteins in this direction across the nuclear pore complexes is generally dependent on carrier molecules that recognise a transport signal in the molecule to be transported, the nuclear localisation signal (NLS) (289). This type of transport is mediated by members of the importin superfamily, which have nuclear import signal receptor activity. Depending on their functional and structural characteristics, importins are classified as either importin α, which are adaptor molecules between cytoplasmic NLS-bearing cargo protein; and importin β, the carrier molecule in the cytoplasm. Importin α includes three conserved structural features, being a N-terminal importin β-binding domain, a series of armadillo repeats that directly interact with NLS-proteins, and a C-terminal region, a binding region for the nuclear export of importin α. This protein can also participate in other functions depending on cellular states, including nuclear envelope formation, gene expression or protein degradation. Importantly, in response to cellular stress caused by heat shock, oxidative stress or ultraviolet irradiation, importin α rapidly accumulates in the nucleus blocking the nuclear import (289-292)

In our sialome study, upregulated *importin α* could be associated with the stress response at the cellular level in the SGs, due to the presence of *E. canis* infection. Although, when mRNA expression levels were quantified by qPCR in this tick tissue, they were downregulated in the infected samples. We also quantified this transcript in IDE8 cells, and this data correlated with the sialome, showing elevated *imp* expression in response to infection. Despite this, IDE8 cells are a cell line derived from embryonated eggs, which may contain cell populations with different morphology and behaviour. Which could affect the transcriptional response to infection (193). A combination of using mixed cell populations (*in vitro* and *in vivo*) coupled with a low number of RNA-seq biological replicates indicates further sampling is required to consistently find the actual trend in expression for this gene in response to infection.

Data is scarce regarding the role of importin α in ticks. Recently, the interaction between importin α and subolesin, the latter containing two distinct NLS domains for importin-α-mediated transport into the nucleus, was investigated in unfed and fed *I. ricinus* female ticks. Gene expression levels of *importin α* did not vary between unfed and fed ticks but tended to be higher in the OV, suggesting a role in gametogenesis, when compared to those in the MG, fat body, SGs and Malpighian tubules. RNAi of *importin α* has shown no effect in tick feeding or oviposition suggesting that subolesin can enter the nucleus in the absence of importin α (293).

In the tick-borne bacterium *A. phagocytophilum*, responsible for human granulocytic anaplasmosis, successful propagation requires a β-importin-dependent pathway (294). So, in the context of this result, the hypothesis is that *E. canis* could modulate cellular transcription factors for the upregulation of *importin* to favour its growth in the SGs.

4.3.3. Serine carboxypeptidases

In our study, a *putative serine carboxypeptidase* (*psc*; UniProtKB L7MH00) was upregulated in the *R. sanguineus* sialome during infection. PSCs are exopeptidase proteolytic enzymes, that cleave peptide bonds at the end of a peptide or protein, releasing a.a., di- or tripeptides from the C-terminus (295). As they are generally secreted into the extracellular environment, these proteins become exposed to host antibodies, making them an attractive candidate for anti-tick-vaccines. The presence of these proteins or their gene has been described in the MG of several tick species, such as *D. variabilis* (296), *H. longicornis* (297), *Ornithodoros mimon* (298) and *I. ricinus* (299). In the SGs of *I. ricinus* (300), *R. microplus* (21, 301), *H. dromedarii* (18), *Ixodes holocyclus* (302), *Rhipicephalus pulchellus* (303) and *R. sanguineus* (281). It has also been described in the OV of partially engorged *H. longicornis* ticks (304).

The role of PSCs in the digestion of a host blood meal has been shown in different studies. Proteins, excluding water, represent approximately 95% of the host blood constituents which means that ticks need protease enzymes in the MG to digest each meal (305). In *I. ricinus*, PSCs have been reported to act as C-terminal monopeptidases, liberating dipeptides and releasing a.a. from fragments resulting from haemoglobinolytic activity

upon blood feeding (306). Furthermore, in *H. longicornis*, *psc* mRNA is strongly upregulated by blood digestion, and its protein can hydrolyse bovine haemoglobin (295, 297). Similarly, in a MG transcriptome comparison between blood and serum-fed *I. ricinus*, it was found that the genes encoding serine proteases were upregulated in the final stage of feeding (299). Additionally, knockdown of serine proteases in *H. longicornis* and *I. scapularis* resulted in lower levels of active trypsin, reduced haemoglobin degradation activity, a reduction in the volume of blood ingested with subsequent reduced fertility, and lower body weights (305, 307).

In *R. microplus*, the SG membrane-bound carboxydipeptidase Bm91 has been characterised in both sequence and biochemical specificity in comparison with the mammalian angiotensin converting enzymes (308). PSCs in the saliva has been demonstrated in fed *D. andersoni* ticks, being overrepresented on day 2 in fed saliva (309), and in the saliva of *A. americanum* fed males (310). In *R. bursa*, carboxypeptidase inhibitors have been isolated and their function associated with the inhibition of thrombin-activatable fibrinolysis, resulting in an accelerated or prolonged clot lysis time (311). The action is a result of the removal of the fibrine lysine-residue (312). In *Ixodes dammini*, the presence of a salivary carboxypeptidase has been associated with the inactivation of serum inflammatory anaphylatoxins at the attachment site (313).

Besides blood digestion, PSCs in the saliva have been associated with the regulation of tick-host interactions, but their exact role in parasite infection and development is still unclear in ticks. In the mosquito *Anopheles stephensi*, there was no difference in the MG enzyme activity when comparing uninfected and *Plasmodium* yoelii *nigeriensis*-infected mosquitoes (314). Conversely, in our study, the transcript that encodes this protein was upregulated in the *R. sanguineus* sialome during infection. In principle, the effect of feeding was excluded from our study once both groups, uninfected and infected, were equally fed on a host. So, the upregulation observed in the *E. canis*-infected group can be associated with the presence of infection. In *Heterorhabditis bacteriophora*, a nematode that parasites insects, PSC *Hb-sc-1* was found upregulated, supressing phagocytic activity, limiting antimicrobial peptide activity upregulation, and phenoloxidase activity in *Drosophila melanogaster* (315). Phenoloxidase activity is a defence mechanism

present in invertebrates that involve pathogen and damaged tissue melanisation. Similarly, in the nematode *Steinernema carpocapsae*, this protein was also associated with the induction of apoptosis and the invasion of host tissues (316-318). In *Brugia malayi*, microfilariae secreted protein suppresses granulocyte chemotaxis in human blood (319).

The precise mechanism of action that leads to the upregulation of *psc* in the sialome of infected *R. sanguineus* cannot be directly inferred from our data. Interestingly, this result corroborates with what was found in IDE8 cells when *psc* expression levels were determined. Cells infected with *E. canis* presented higher expression levels when compared with the uninfected control. This upregulation could be related to the activation of tick or IDE8 cell defence mechanisms, and/or the inactivation of serum inflammatory anaphylatoxins, or the pathogen that positively modulates gene transcription at the SG level. Whether this will benefit the general immunosuppressive capacity of the protein to better invade the host tissues and thrive is still to be determined.

To better understand the effect of *psc* in bacterial invasion and multiplication, we subjected IDE8 cells and *R. sanguineus* nymphs to RNAi. Even though gene silencing was successfully achieved at two time points in IDE8 cells, *E. canis* quantification was not possible due to the instability of the reference genes. The same limitation was observed for the SGs of freshly moulted females when quantifying differential expression in the gene and subsequent *E. canis* quantification.

4.3.4. Glutathione S-transferases

In our study, *glutathione S-transferase* (*gst*; UniProtKB Q6JVN0) transcription was downregulated during experimental infection with *E. canis.* GSTs are dimeric multifunctional antioxidant enzymes that regulate stress-induced signalling, cell survival or death and metabolic detoxifying pathways for endo- and exobiotics, which are all essential for cellular homeostasis (320, 321). They are also implicated in the catalysis of fatty acid reduction and phospholipid metabolism (322). Their biology is complex and their location can vary from the cytoplasm, mitochondria or attached to membranes (321).

GSTs are ubiquitous in tick tissues, being found in the MG, SGs, OV, fat body and haemocytes of *H. longicornis* and *D. marginatus* and present in different developmental stages during blood-feeding (323, 324). GSTs have also been reported in other tick species, for example *R. microplus* (325, 326) and *R. sanguineus* (255).

In ticks, GSTs play a role in acaricide metabolism, particularly on pyrethroids. In *H. longicornis*, GST recombinant proteins were inhibited by flumethrin, cypermethrin, chlorpyrifos and cypermethrin. When exposed to sublethal doses of acaricide, *GST* was found upregulated, and its knockdown led to an increase in larvae and adult males' susceptibility to high doses (327). Similarly, *gst* gene silencing in *R. sanguineus* females followed by exposure to sublethal doses of permethrin, resulted in higher acaricide susceptibility and death (255). In *R. bursa*, GST activities were found significantly elevated in field populations when compared with a susceptible strain (328). In India, GST activity was found increased in field isolates of *Hyalomma anatolicum* and positively correlated with deltamethrin resistance (329).

Like the function of ferritin proteins, another important function of GSTs is to reduce cytotoxic effects of intracellular haemoglobin hydrolysis. During a blood meal, *gst* transcription increases (323), suggesting a positive correlation with the level of oxidative stress caused by RBC haemoglobin, and not iron, in the diet (330). This result was similar in *D. marginatus* (324).

Due to their involvement in detoxification, these proteins have been targeted as potential candidates for anti-tick vaccines. Studies have shown partial cross-protective immunity against *R. microplus* in cattle (331) and *R. appendiculatus* in rabbits with *H. longicornis* recombinant GST-Hl (rGST-Hl) (332). *R. appendiculatus* engorged adult ticks presented lower infestation numbers, a decrease in weight and fertility, and morphologic alterations on the SGs and OV, after vaccination. Similar results were obtained in *D. marginatus* in rabbits challenged with recombinant DmGST (324). Rabbit vaccination with rGST-Hl did not elicit any effect in *R. sanguineus* ticks (332). A study using a rGST-cocktail based on *R. decoloratus* and *A. variegatum* GSTs was able to induce immune protection against tick infestation (333). Lastly, limited protection was achieved in cattle against *R.*

microplus using a vaccine cocktail of three recombinant proteins: *H. longicornis* rGST-Hl and Vn-degrading cysteine endopeptidase, and boophilus yolk pro-cathepsin from *R. microplus* (334).

Some studies have reported that infection affects GSTs translation, reinforcing the involvement of these proteins in arthropod innate immune responses, protecting cells from oxidative stress caused by pathogens. Mulenga et al. (2003) found an upregulation of *GST* mRNA in *D. variabilis* OV in response to *R. montanensis* infection (276). Likewise, *GST* was induced in *I. ricinus* after a *B. burgdorferi*-blood meal (335) and in *Anopheles gambiae* and *Glossina morsitans* insects upon microbial infection (336, 337). In *I. scapularis* nymphs and ISE6 cells infected with *A. marginale GST* mRNA levels were also upregulated (338).

In our study, *gst* transcription in the SGs was downregulated during experimental infection with *E. canis.* While this contrasts with the studies described above, a similar result was found in *D. variabilis* when fed adult ticks were challenged with *E. coli* injection. Here, DvGST1 and DvGST2 were found partially suppressed upon infection (339). Furthermore, in *I. scapularis* nymphs and ISE6 cells infected with two different *A. phagocytophilum* strains, *GST* mRNA levels were significantly downregulated (338). Another study found that proteins homologous to GST were underrepresented in *A. marginale*-infected IDE8 cells when compared with uninfected controls. RNAi of *gst* inhibited *A. marginale* infection in *D. variabilis* MG and SGs and impaired tick attachment capacity (340). In human endothelial cells infected with *R. rickettsii*, the activity of these enzymes was significantly decreased (341). Downregulated *gst* mRNA expression or reduced enzyme activity may be a consequence of cell damage caused by microbial infection.

4.3.5. Ubiquitin carboxyl-terminal hydrolases

In our *R. sanguineus* transcriptome, a *ubiquitin carboxyl-terminal hydrolase* (*uch*; UniProtKB L7M3C8) transcript was downregulated. UCHs, a subfamily of deubiquitinating enzymes, are key components of protein degradation pathways. They

hydrolyse thiol esters formed between the ubiquitin terminus and small thiols, such as glutathione (342). Several other functions have been reported in vertebrates, including DNA repair, cell signalling and trafficking, endocytosis, and degradation. UCH function in ticks is unclear and information is limited. Rodrigues et al. (2017) reported the discovery of several UCHs suggesting a functional ubiquitination complex in *A. variegatum* saliva may exist (343). In *A. marginale*-infected IDE8 cells, ubiquitin gene was upregulated and its silencing increased *D. variabilis* mortality, reduced tick attachment and inhibited pathogen MG infection (340).

In the last decade, the role of ubiquitination in the immune response has been further elucidated. Immune response modulation by ubiquitin has been shown in Regulatory T (Treg) cells. Enhanced chemotactic migration, the inhibition of Treg proliferation, and decreased apoptosis was observed after supplementing cells growing in culture with extracellular ubiquitin (344). Furthermore, ubiquitination reduces tumour necrosis factor-α (TNF-α) production, inhibiting inflammation (345, 346). In cattle, lymphocyte proliferation was inhibited, and TNF-α production was decreased by tick saliva (343). Thus, ticks might use the ubiquitination complex to mitigate the effects of the host immune system during the feeding process.

The protein encoded by the *uch* transcript downregulated in our transcriptome contains a UCH-1 domain in position 11-212. The protein UCH-L1 is abundant and highly specific to neurons and the peripheral nervous system, and a reduction in its expression leads to a general decrease in protein degradation, with subsequent accumulation of ubiquitinated protein. *Drosophila uch* knockdown led to defective tissue development and function, with a subsequent compromise in insect locomotion (347). The interaction of UCHs between hosts and parasites are still unclear, but our data leads to the hypothesis that in the presence of *E. canis* in the SGs, *uch-L1* mRNA downregulation will decrease protein translation and consequently its enzymatic activity. Hard tick type I and II SGs are vastly innervated by axonal projections that enter and innervate each individual acinus, and by surrounding the glandular lumen they regulate myoepithelial cells (348). Thus, lower levels of UCH might reduce or block nervous system conductivity at the cell-axon level in the SGs which might favour bacterial invasion and passage through the tissues.

The role of the ubiquitin cycle, and particularly UCH-L1, in bacterial entry to cells has been investigated. UCH-L1 was found to facilitate cell invasion by *Listeria monocytogenes* and *Salmonella enterica*, as *UCH-L1* knockdown resulted in decreased bacterial cell entry (349). This is because when *L. monocytogenes* enters the cell by binding the receptor tyrosine kinase Met, it becomes phosphorylated, activating the ubiquitination cascade, which is initially controlled by UCH-L1. In our study, *uch-L1* downregulation might be also caused by specific bacterial deubiquitylating proteases that suppress or inhibit the inflammatory response, probably by disrupting cellular signalling, from the host. This effect has been described for bacteria such as *Salmonella*, *E. coli* and *Yersinia*, which has been reviewed (350).

4.3.6. Putative trilaris

In our transcriptome, a putative *trilaris* (UniProtKB L7MCD9) transcript, encoding a serine protease inhibitor (SPI), was downregulated during *E. canis* infection. SPIs are a superfamily of conserved proteins that inhibit serine protease activity, acting in defence mechanisms such as complement activation and inflammation, and in blood coagulation and fibrinolysis. Most proteins containing a Kunitz domain are included in this superfamily (351). In ticks, inhibitors with a Kunitz domain are abundantly secreted in the saliva as anti-haemostatic proteins, allowing hematophagy, and are some of the most abundant protein families in the SGs (352-355). Kunitz domains can be found in tandem and depending on the number of repeats can be classified as mono, bi, tri and tetralaris. Monolaris have been functionally characterised in hard and soft ticks, functioning mainly as anticlotting agents or antiplatelet inhibitors (356, 357). Trilaris transcripts have been found upregulated in the sialome of adult *R. pulchellus* (303). In *I. ricinus*, protease inhibitors were one of the most abundant secreted protein families found in the *de novo* sialome assembly during tick feeding, of which trilaris was included (16).

SPIs identified in ticks have shown antimicrobial action. For example, ixodidin of *R. microplus* demonstrated an efficient inhibitory activity against *Micrococcus luteus*, possibly by interfering with bacterial membranes (358). Later, Du et al. (2020) showed antibacterial activity of two SPIs in the tick *Haemaphysalis doenitzi*. The recombinant

enzymes rHDS1 and rHDS2 exerted strong bactericidal effect against *Candida albicans* and *Bacillus subtilis*; and against *Cryptococcus neoformans* and *Enterococcus faecalis*, respectively (359).

In our data, a putative *trilaris* transcript was downregulated during infection, suggesting that *E. canis* may be suppressing host immune responses, reducing the antibacterial effect, to counteract the protection conferred by the tick salivary protein as a primary line of defence.

4.4. Proteomic profile of *Rhipicephalus sanguineus* salivary glands in response to *Ehrlichia canis* experimental infection

In recent years, studies have quantified the *R. sanguineus* proteome in tick saliva (360) and in SGs and MG (281, 361). The published data we discussed in previous chapters underlines the importance of salivary components for blood feeding and pathogen transmission. We therefore studied in greater depth the differences in protein representation in the SGs of fed uninfected and fed *E. canis*-infected *R. sanguineus* by LC-MS/MS. Our hypothesis states that in the presence of infection, the differentially represented proteins in the SGs may be promising candidates for further research into transmission-blocking vaccines. SGs were targeted because this organ plays a role in *E. canis* release to the saliva. As part of this, we considered the possibility of identifying tissue-specific gene expression and protein translation in response to this infection.

We identified a total of 432 tick proteins that were present in fed uninfected and fed *E. canis*-infected SGs. From these, 69 proteins were significantly differentially represented, of which 5 were underrepresented and 64 were overrepresented. The two most overrepresented proteins were a signal peptidase (UniProtKB C9W1S4), which cleaves signal peptides; and an actin-depolymerizing factor 1 (UniProtKB A0A034WYZ2), involved in actin filament depolymerisation and actin binding. The most underrepresented protein was a ribosomal protein L19 (UniProtKB L7MEH0), involved in translation and a structural constituent of the ribosome. Overall, most proteins were involved in cellular and metabolic processes, particularly translation by ribosomes. We attempted to validate the proteomic data using Western blotting; however, the results did not correlate for APK-C2, MDH2 and PROHIB. All three proteins were overrepresented in our blots in the infected samples but underrepresented for the same condition in the proteome. Like what happened with our RNA-seq data validation, the samples used for the proteomic data were obtained from a different experimental infection than the samples we examined with Western blots. Sample collection on different occasions may explain the discrepancies in the protein data. Furthermore, the molecular weights of bands on our Western blots did not correspond exactly with their predicted values. This may be due to

protein cleavage, the existence of splice variants, or post-translational modifications such as glycosylation.

Additionally, none of the differentially expressed transcripts found in the sialome matched any of the differentially represented proteins in the proteomic data.

The most relevant proteins differentially represented during infection will be discussed in more detail in the following sub-chapters. All these proteins were found underrepresented in the proteome, except the putative heat shock-related protein (PHSRP20; UniProtKB L7M6Q5) that was overrepresented.

4.4.1. Prohibitins

We identified a prohibitin-like protein (PROHIB; UniProtKB L7M5P4) in the SGs proteome, which was underrepresented upon *E. canis* infection. Prohibitins are highly conserved, ubiquitously expressed proteins in eukaryotic cells. They have been identified in the inner membrane of mitochondria, acting as chaperones, and in the plasma membrane of B lymphocytes, associated with the IgM receptor (362). They are involved in regulatory functions in cell proliferation, apoptosis, and replicative senescence, with antiproliferative activity. In the nucleus they modulate transcription (362, 363). Their role in cellular defence against oxidative stress and inflammation has been studied in humans and other vertebrates (364).

Prohibitins may play a role in viral internalisation in host cells. In *Aedes aegypti* and *Aedes albopictus* insect cell lines, gene knockdown led to reduced dengue serotype 2 infection levels and viral production. Here, prohibitin was identified as receptor for viral envelope protein necessary for host cell binding and fusion during infection (365). Likewise, in Chikungunya virus this protein was identified as a mediator for virus internalisation in microglial cells (366).

In our study, the PROHIB was underrepresented in the SGs during *E. canis* infection, with a putative location in the mitochondrion inner membrane. Our results agree with the study carried out by Rachinsky et al. (2008). Here, prohibitin was underrepresented in the

MG proteomic profile of *R. microplus* in the presence of *B. bovis* infection (367). Under physiological conditions, this protein should have been found overrepresented in the proteomic data in response to oxidative stress caused by bacterial infection.

When *prohib* mRNA expression levels were determined in *E. canis*-infected IDE8 cells, they were significantly downregulated compared with uninfected samples. By contrast, in infected *R. sanguineus* SGs, *prohib* mRNA levels were significantly upregulated compared with uninfected controls. It is worth mentioning that differences observed at the transcription level do not always correlate directly with trends in protein expression.

To better understand the effect of *prohib* in *E. canis* invasion and multiplication, we subjected IDE8 cells and *R. sanguineus* nymphs to RNAi. Our silencing studies carried out in these two models demonstrated considerable gene knockdown efficiency, that resulted in differentially downregulated mRNA levels in freshly moulted adult female SGs and IDE8 cells. The significant gene downregulation verified in the adult females showed that the effect of silencing persisted in the SGs through the nymph feeding and moulting process. Aljamali et al. (2003) suggested that the effect of RNAi using dsRNA molecules could be reduced by prolonged feeding due to saliva discharge. Furthermore, during active feeding, SG mass increases which may also dilute the dsRNA concentration (257).

Even though gene silencing was accomplished, with subsequent significant gene downregulation in these ticks and tick cells, *E. canis* quantification was not possible due to the instability of the reference genes. Future studies will be required to use other reference genes that are stable to guarantee consistent, reproducible data.

4.4.2. Heat shock or stress response proteins

In our study, two HSPs were found in the *R. sanguineus* proteomic data during *E. canis* infection. One HSP, an underrepresented putative heat shock protein (UniProtKB L7MEG0) had sequence similarity with the HSP90 family. The other HSP, an overrepresented putative heat shock protein (PHSRP20; UniProtKB L7M6Q5) resembles the HSP20 in molecular weight and structure, containing a α-crystallin domain. HSPs, or

stress proteins, are amongst the most highly conserved proteins, present in all organisms and in all cells. HSPs are a typically large family, named according to their molecular weight, e.g., *hsp10*, *hsp60*, *hsp70*; and can be located intra- or extracellularly. These proteins have several cellular functions including protein folding, transport of other proteins, signalling, chaperones in antigen presentation and protection against stress and apoptosis (368). The heat shock or stress response, or HSPs synthesis, allows cells to adapt to their environment and survive during mild perturbations; but in severe cases of heat or stress, an extremely rapid and intense mechanism is activated to protect cells from sublethal and lethal conditions, avoiding apoptosis (369). Once the cells are subjected to a stress stimulus, HSPs increase their levels and diffuse to other cell compartments or appear on the cell surface to prevent and limit this effect through the removal of denatured proteins, known as a house keeping function of HSPs, or by correcting protein folding/refolding (370, 371). HSPs have been reported as immunoregulatory agents able to stimulate cytokine production by other cells and deliver maturation signals and peptides to antigen presenting cells (372). HSPs are also induced during the normal development of an organism, usually located intracellularly, but in lower levels.

Their antagonistic action during cell infection is counterintuitive, as they contain epitopes for cell protection close to epitopes relevant for pathogenesis. During microbial infection, Igs and cytotoxic T cells developed against pathogen antigens simultaneously recognise and react against HSPs. In the case of intracellular pathogens, host Igs and T cells recognise HSP epitopes presented on the surface of infected cells with subsequent cell destruction to control the infection. Opposite to this effect, host cells counteract microbial invasion by increasing the translation of these proteins during the beginning of invasion (371).

HSPs have been found and extensively studied in ticks and tick cell lines exposed to stress conditions such as heat, blood feeding, infection, and questing behaviour (340, 367, 373, 374).

A study in *I. scapularis* ticks and ISE6 cells verified in both models that *hsp20* and *hsp70* mRNA levels were increased at high temperatures and during blood feeding, confirmed by *hsp70* silencing, that resulted in tick weight reduction (374). The same results of Busby

et al. (2012) were found in *I. scapularis* ISE6 cells in response to heat shock with upregulation of both *HSP20* and *HSP70* at 37°C (375) and *H. longicornis* (HLHsp70) at the same temperature and as a result of blood-feeding (376). In contrast, in *H. flava, Hf-Hsc70* expression was not significantly induced under heat stress (377). Analysis of *hsp20* and *hsp70* in *R. sanguineus* nymphs and eggs revealed increased expression at a higher temperature and lower relative humidity levels implying a lower tolerance to environmental conditions of thermal stress (378). On the contrary, under cold stress of -20°C, *D. silvarum Dshsp70* silencing resulted in significantly increased mortality, suggesting a potential role in low temperature adaptation, especially for overwintering ticks (379). *Rhipicephalus haemaphysaloides RH-Hsp70* silencing inhibited tick blood feeding, decreased tick engorgement and increased tick mortality (380).

In *I. scapularis*, *hsp70* mRNA levels were higher than *hsp20* at all tick developmental stages, except in eggs. Interestingly, *hsp20* and *hsp70* mRNA levels did not change significantly during *A. phagocytophilum* infection in ISE6 tick cells compared with the controls, but *hsp20* knockdown resulted in increased infection levels. In the SGs and MG of female ticks fed on an *A. phagocytophilum*-infected host, *hsp20* and *hsp70* mRNA levels were found significantly higher and lower, respectively. Expression of *hsp20* and *hsp70* were higher in the MG, and the SGs, respectively. Silencing of both genes in the MG had no effect on *A. phagocytophilum* infection levels; but *hsp70* silencing resulted in increased bacteria levels in the SGs and lower questing speed at 22°C (374). Different results were found in *A. marginale*-infected IDE8 cells where *hsp70* was differentially upregulated (340). HSP70 are involved in binding to antigens and presenting them to the immune system (371). Transcriptomic data has shown *HSP90* and *HSP70* upregulation in feeding *R. microplus* females (381) and *A. marginale*-infected IDE8 cells (375). The same results were observed for *HSP20* mRNA in *A. marginale*-infected ISE6 cells, implying the activation of stress response mechanisms in infected tick cells when exposed to infection (375).

In our proteomic data, HSP90 and PHSRP20 were under- and overrepresented, respectively, in the *R. sanguineus* SGs during *E. canis* infection. Regarding HSP90, our results agree with those of Rachinsky et al. (2008) that reported a downregulation of HSPs

in the *R. microplus* MG proteome during *B. bovis* infection (367). For HSP20, our results are contrary to what was found in the proteomic analysis of ISE6 cells in response to *A. phagocytophilum* infection, in which this protein was underrepresented in the infected samples (375).

We further quantified *phsrp20* mRNA expression levels in *E. canis*-infected IDE8 cells and *E. canis*-infected tick SGs. Our results have shown a *phsrp20* downregulation in both models, being significant in the SGs. Contrary results were found in the SGs and MG of female ticks fed on an *A. phagocytophilum*-infected host, in which *hsp20* mRNA levels were found significantly higher in comparison with the uninfected controls (374). Differential upregulation of *HSP20* was also observed in *A. marginale*-infected IDE8 and ISE6 cells (340, 374, 375).

To better understand the effect of *phsrp20* in *E. canis* invasion and multiplication, we subjected IDE8 cells and *R. sanguineus* nymphs to RNAi. Our results showed that nymphs soaked in *phsrp20* dsRNA demonstrated considerable gene knockdown efficiency, with statistically significant downregulation of mRNA levels in the SGs of freshly moulted adult females. For this gene, the effect of silencing also persisted in the SGs through the nymph feeding and moulting process. Even though gene silencing was accomplished in these ticks, *E. canis* quantification was not possible due to the instability of the reference genes. In IDE8 cells, the reference genes were too unstable to proceed with *phsrp20* differential gene expression analysis and *E. canis* quantification. In future, other reference genes that are stable will be required to guarantee consistent, reproducible data.

Disparities in PHSRP20 expression between mRNA and protein levels reported in the literature and in our study, might be associated with posttranscriptional mechanisms induced by pathogens to control tick responses to infection. HSP synthesis is expected to increase during parasite invasion (370), but this was only found for PHSRP20 in our study. Overall, results suggest that during microbial infection, specific tick cellular mechanisms involving protein modification and processing, and immune response might be supressed and/or triggered at different levels. Future studies will be necessary to

confirm if mRNA levels of the putative HSP90 and HSP20 found in our proteome are indeed downregulated in response to *E. canis* infection in tick SGs.

4.4.3. Lipocalins

Our proteomic data revealed an underrepresentation of a putative salivary lipocalin (UniProtKB L7LQP4) during *E. canis* infection. As part of the innate and acquired immune response, mast cells and basophils secrete histamine in connective tissue. To overcome the host immune response at the attachment site, ticks secrete bioactive molecules in their saliva such as antihistamines that compete for histamine receptors, suppressing inflammation. Tick histamine-binding lipocalins are one of the most abundant extracellular protein families in tick saliva; and as well as their role in modulating immune responses, they regulate cell homeostasis, eliminate endo- and exogenous substances, and in soft ticks, have toxic properties (382, 383). Even though tick lipocalins are evolutionary related with the kernel lipocalin family, they lack three conserved structural regions, so are classified as outliers (384). Their structure has been characterised, revealing two internal binding sites, an H site that binds histamine molecules with high affinity, and an L site with weaker affinity (385, 386). In the tick *R. appendiculatus*, high affinity histamine-binding proteins have been described and one of them (RaHBP2) presented a lipocalin fold (387). Other tick lipocalins have been found and characterised in soft ticks *A. monolakensis*, *Argas reflexus* and *Ornithodoros savignyi*, and in the hard ticks *I. scapularis*, *I. ricinus* and *R. sanguineus* (281, 388-390). The presence of these proteins has also been reported in fed female *R. sanguineus* saliva (360). Thus, lipocalin secretion by ticks may represent a form of parasitic adaptation to cope with the host defence mechanisms. A negative impact of histamine activity was observed in *R. microplus* larvae attachment (391), and in *D. andersoni in vitro* feeding (392).

Our proteomic data has shown an underrepresentation of the putative salivary lipocalin, with a calycin-like and signal domain, during *E. canis* infection. Calicyns are a large family of proteins that share identical β-barrel structures. The same result was found in the *R. sanguineus* tropical lineage proteome during *E. canis* infection (361) and in *I. ricinus* in response to *Borrelia afzelii* infection (390). Thus, decreased lipocalin activity

may favour pathogen transmission via a reduction in the vertebrate host inflammatory response.

4.4.4. Spectrins

In our proteomic data, underrepresentation of a putative spectrin β-chain protein (UniProtKB V5GYK8) was observed. To establish an infection in a host cell, obligate cellular organisms, such as *Rickettsii, Listeria and Shigella*, induce rearrangement of the cytoskeleton by actin polymerisation, recruiting the host filaments of (F)-actin (393). This filament forms an actin-tail in the pathogen that works as a propeller to circulate in the host cell cytoplasm (394). The cytoskeleton rearrangement is achieved by the activity of proteins such as spectrin and fodrin α-chains, involved in cell growth and maintenance. This beneficial parasitic mechanism has been studied at the tick-pathogen interface. A previous study conducted by Sultana et al. (2010) has shown evidence *in vivo* and *in vitro* that *A. phagocytophilum* induces actin phosphorylation, modifying the ratio of monomeric/filamentous (G/F) actin to enable infection through selective gene transcription regulation with RNA polymerase II and a TATA-binding protein (395).

Our proteomic data revealed an underrepresentation of the putative spectrin β-chain protein, one subunit of spectrin protein, with a calponin domain. Calponin domains are present in actin-binding signalling proteins involved in the organisation of the cytoskeleton (396). In ISE6 tick cells, gene expression and proteins involved in cell growth and transport have been studied during *A. phagocytophilum* infection. In cell culture, *spectrin α-chain* or *α-fodrin (CG8)*, encoding a protein that connects the plasma membrane to the actin cytoskeleton, determining cell shape and organisation of transmembrane proteins and organelles, were downregulated; but in *I. scapularis* MG cells, these were upregulated. Interestingly, *CG8* silencing reduced the level of *A. phagocytophilum* infection in ISE6 tick cells and in *I. scapularis* MG and SGs which may be a consequence of the deficient actin filament rearrangement which necessary for pathogen infection (397). Similarly, spectrin α-chain and spectrin β-chain were found underrepresented in *I. ricinus* adult ticks SGs proteins infected with *B. burgdorferi* (398). The role of spectrins in pathogen infection has also been demonstrated in macrophages infected with *E. coli*. Cell infection led to major rearrangements of the actin filaments by

fodrin-like proteins (399). In *E. canis*-infected DH82 cells, reduced infection was observed in cytochalasin D-treated cells, identifying the actin cytoskeleton as crucial. This compound inhibits actin polymerisation, which is important for pathogen spreading (101).

The underrepresentation of putative spectrin β-chain protein was apparent in our study, as well as in infected tick cells and *I. scapularis* SGs (397), and in *I. ricinus* adult ticks SGs infected with *B. burgdorferi* (398). This might be a consequence of pathogen manipulation of host cellular machinery to block cell apoptosis and reduce the immune response.

4.5. Antibody production in mice in response to pPHSRP20

In this part of the study, our objective was to investigate the immunogenicity of a tick peptide in a vertebrate host. This would serve as a proof of concept that could then be applied in dogs, immunising uninfected and *E. canis*-infected animals with antigens of interest. It could then be possible to determine the impact of these canine antibodies on ticks and/or *E. canis* infection.

Poly- and monoclonal antibodies are fundamental tools for biomedical research and of great medical and commercial interest. Their use extends from therapeutic agents, for example in cancer, infections and autoimmune diseases, to diagnosis (400). Antibodies are host glycoproteins, present mainly in serum, that are secreted by specialised B lymphocytes. Also known as Igs, they are part of the adaptive immune system and act to neutralise and eliminate foreign molecules or microorganisms. Activated B-cells that have encountered antigen engulf and digest it, followed by its presentation on the cell surface by class II MHC molecules. These MHC-antigen complexes are recognised by helper T cells that release cytokines that stimulate the maturation of these B cells into plasma cells. These plasma cells then secrete antibodies specific for the encountered antigen. B cells then divide and produce memory B cells. Generally, antigens are very complex and have several epitopes recognised by B cells, which results in a naturally polyclonal response *in vivo* (401). Laboratory-based polyclonal antibody production is based on the immunisation of animal models using an antigen of interest. Antibody production *in vivo* can be quantified by analysing the serum using an ELISA.

In our proteomic data, an overrepresented small putative heat shock-related protein (PHSRP20; UniProtKB L7M6Q5) with sequence similarity to the mammalian HSP20 family was identified as a strong candidate to produce polyclonal antibodies. *In silico* analysis of the a.a. sequence determined that the peptide, named pPHSRP20, is an outer membrane protein, without a signal peptide, non-secretory, non-allergenic and soluble. B cell epitope prediction analysis returned ten a.a. sequences that may act as epitopes to elicit an immune response in our animal model. Each of our analyses indicated pPHSRP20 would be a good candidate to induce an immune response, therefore it was synthesised and used to immunise CD1 mice. Evidence of an immune response to

pPHSRP20 antigen in mice R_1 and R_2 was confirmed by analysis of their sera using an ELISA. The specificity of the antibody-antigen interaction was further confirmed by Western blot. Other studies have reported immunisation of rabbits with recombinant proteins synthesised based on tick HSPs, including rHLHSP70 of *H. longicornis.* Although, an immune response was confirmed there was not a significant effect in the reduction of tick engorgement and oviposition (376).

Further studies, including vaccination trials, are necessary to determine the immunogenicity of pPHSRP20 antigen in other vertebrate hosts and the effect of anti-PHSRP20 antibodies on tick physiology, and pathogen acquisition and transmission.

Informative molecular tools now exist to deeply explore cellular aspects of the interactions between ticks and the pathogens they are vectors of. As strict hematophagous arthropods, ticks rely on their saliva and mouthparts to successfully attach to a host and prolong blood meals. In this interplay, several salivary molecules secreted during the feeding process modulate host immunity and modulate haemostasis cascades and ultimately interfere with pathogen acquisition, multiplication, and transmission. Therefore, studying the SG-specific transcriptome and proteome is of extreme importance to decipher molecular events underlying the symbiotic cooperation between vector and pathogen. Our data shows the existence of *E. canis* infection-induced alterations in gene and protein expression in the *R. sanguineus* SGs. In this system, most transcriptional and translational responses to infection affected protein cellular and metabolic processes and catalytic activities. Amongst these, the regulation of molecules involved in stress responses and inflammation suggest that *E. canis* co-evolved with the vector in a way that enables the subversion, manipulation and/or control of host-encoded proteins. These mechanisms allow the bacteria to establish, survive and be transmitted by the tick. Ideally, targeting these would be a good option for transmission-blocking vaccines and, by association with other potential functions of these molecules in tick feeding, survival, and reproduction. Effective control measures against ticks are still lacking in human and veterinary medicine, with the increase of acaricide resistance and lack of effective targets for vaccines. Finally, studies in this field should focus more on the immature stages of larvae and nymphs. During the life cycle, studies indicate that larvae act as receptors of infection, nymphs are the key transmitters of TBPs and adult females lay eggs to

perpetuate the cycle (172). Further investigations will be required to elucidate the functions and precise involvement in infection of differentially expressed genes and proteins obtained in this study.

Chapter 5. References

1. Bremer WG, Schaefer JJ, Wagner ER, Ewing SA, Rikihisa Y, Needham GR, et al. Transstadial and intrastadial experimental transmission of *Ehrlichia canis* by male *Rhipicephalus sanguineus.* Vet Parasitol. 2005;131(1-2):95-105.

2. Wen B, Cao W, Pan H. Ehrlichiae and ehrlichial diseases in china. Ann N Y Acad Sci. 2003;990:45-53.

3. Dantas-Torres F. Biology and ecology of the brown dog tick, *Rhipicephalus sanguineus.* Parasites & vectors. 2010;3:26.

4. Dantas-Torres F. The brown dog tick, *Rhipicephalus sanguineus* (Latreille, 1806) (Acari: Ixodidae): from taxonomy to control. Vet Parasitol. 2008;152(3-4):173-85.

5. Maeda K, Markowitz N, Hawley RC, Ristic M, Cox D, McDade JE. Human infection with *Ehrlichia canis,* a leukocytic rickettsia. N Engl J Med. 1987;316(14):853-6.

6. Dawson JE, Anderson BE, Fishbein DB, Sanchez JL, Goldsmith CS, Wilson KH, et al. Isolation and characterization of an *Ehrlichia* sp. from a patient diagnosed with human ehrlichiosis. J Clin Microbiol. 1991;29(12):2741-5.

7. Brouqui P, Le Cam C, Kelly PJ, Laurens R, Tounkara A, Sawadogo S, et al. Serologic evidence for human ehrlichiosis in Africa. Eur J Epidemiol. 1994;10(6):695-8.

8. Perez M, Rikihisa Y, Wen B. *Ehrlichia canis*-like agent isolated from a man in Venezuela: antigenic and genetic characterization. J Clin Microbiol. 1996;34(9):2133-9.

9. Perez M, Bodor M, Zhang C, Xiong Q, Rikihisa Y. Human infection with *Ehrlichia canis* accompanied by clinical signs in Venezuela. Ann N Y Acad Sci. 2006;1078:110-7.

10. Ghosh S, Azhahianambi P, Yadav MP. Upcoming and future strategies of tick control: a review. J Vector Borne Dis. 2007;44(2):79-89.

11. Rodriguez-Vivas RI, Trees AJ, Rosado-Aguilar JA, Villegas-Perez SL, Hodgkinson JE. Evolution of acaricide resistance: phenotypic and genotypic changes in field populations of *Rhipicephalus (Boophilus) microplus* in response to pyrethroid selection pressure. Int J Parasitol. 2011;41(8):895-903.

12. Willadsen P. Anti-tick vaccines. Parasitology. 2004;129 Suppl:S367-87.

13. de la Fuente J, Kocan KM, Blouin EF. Tick vaccines and the transmission of tick-borne pathogens. Vet Res Commun. 2007;31 Suppl 1:85-90.

14. Marcelino I, de Almeida AM, Ventosa M, Pruneau L, Meyer DF, Martinez D, et al. Tick-borne diseases in cattle: applications of proteomics to develop new generation vaccines. J Proteomics. 2012;75(14):4232-50.

15. Villar M, Popara M, Bonzon-Kulichenko E, Ayllon N, Vazquez J, de la Fuente J. Characterization of the tick-pathogen interface by quantitative proteomics. Ticks Tick Borne Dis. 2012;3(3):154-8.

16. Schwarz A, von Reumont BM, Erhart J, Chagas AC, Ribeiro JM, Kotsyfakis M. *De novo Ixodes ricinus* salivary gland transcriptome analysis using two next-generation sequencing methodologies. FASEB J. 2013;27(12):4745-56.

17. De Marco L, Epis S, Comandatore F, Porretta D, Cafarchia C, Mastrantonio V, et al. Transcriptome of larvae representing the *Rhipicephalus sanguineus* complex. Mol Cell Probes. 2017;31:85-90.

18. Bensaoud C, Nishiyama MY, Jr., Ben Hamda C, Lichtenstein F, Castro de Oliveira U, Faria F, et al. *De novo assembly* and annotation of *Hyalomma dromedarii* tick (Acari: Ixodidae) sialotranscriptome with regard to gender differences in gene expression. Parasit Vectors. 2018;11(1):314.

19. de la Fuente J, Almazan C, Blouin EF, Naranjo V, Kocan KM. RNA interference screening in ticks for identification of protective antigens. Parasitol Res. 2005;96(3):137-41.

20. Lees K, Woods DJ, Bowman AS. Transcriptome analysis of the synganglion from the brown dog tick, *Rhipicephalus sanguineus*. Insect Mol Biol. 2010;19(3):273-82.

21. Maruyama SR, Garcia GR, Teixeira FR, Brandao LG, Anderson JM, Ribeiro JMC, et al. Mining a differential sialotranscriptome of *Rhipicephalus microplus* guides antigen discovery to formulate a vaccine that reduces tick infestations. Parasit Vectors. 2017;10(1):206.

22. Villar M, Torina A, Nunez Y, Zivkovic Z, Marina A, Alongi A, et al. Application of highly sensitive saturation labeling to the analysis of differential protein expression in infected ticks from limited samples. Proteome Sci. 2010;8:43.

23. Ewing SA. Canine ehrlichiosis. Adv Vet Sci Comp Med. 1969;13:331-53.

24. Dumler JS, Barbet AF, Bekker CP, Dasch GA, Palmer GH, Ray SC, et al. Reorganization of genera in the families Rickettsiaceae and Anaplasmataceae in the order Rickettsiales: unification of some species of *Ehrlichia* with *Anaplasma*, *Cowdria* with *Ehrlichia* and *Ehrlichia* with *Neorickettsia*, descriptions of six new species combinations and designation of *Ehrlichia equi* and 'HGE agent' as subjective synonyms of *Ehrlichia phagocytophila.* Int J Syst Evol Microbiol. 2001;51(Pt 6):2145-65.

25. Donatien A, Lestoquard F. Existence in Algerie d'une Rickettsia du chien. Bull Soc Pathol Exot. 1935;28:418-9.

26. Groves MG, Dennis GL, Amyx HL, Huxsoll DL. Transmission of *Ehrlichia canis* to dogs by ticks (*Rhipicephalus sanguineus*). Am J Vet Res. 1975;36(7):937-40.

27. Walker JS, Rundquist JD, Taylor R, Wilson BL, Andrews MR, Barck J, et al. Clinical and clinicopathologic findings in tropical canine pancytopenia. J Am Vet Med Assoc. 1970;157(1):43-55.

28. Harvey JW, Simpson CF, Gaskin JM, Sameck JH. Ehrlichiosis in wolves, dogs, and wolf-dog crosses. J Am Vet Med Assoc. 1979;175(9):901-5.

29. Ewing SA, Buckner RG, Stringer BG. The Coyote, a Potential Host for *Babesia Canis* and *Ehrlichia* Sp. J Parasitol. 1964;50:704.

30. Amyx HL, Huxsoll DL. Red and gray foxes--potential reservoir hosts for *Ehrlichia canis*. J Wildl Dis. 1973;9(1):47-50.

31. Cardoso L, Gilad M, Cortes HC, Nachum-Biala Y, Lopes AP, Vila-Vicosa MJ, et al. First report of *Anaplasma platys* infection in red foxes (*Vulpes vulpes*) and molecular detection of *Ehrlichia canis* and *Leishmania infantum* in foxes from Portugal. Parasit Vectors. 2015;8:144.

32. Bouloy RP, Lappin MR, Holland CH, Thrall MA, Baker D, O'Neil S. Clinical ehrlichiosis in a cat. J Am Vet Med Assoc. 1994;204(9):1475-8.

33. Breitschwerdt EB, Abrams-Ogg AC, Lappin MR, Bienzle D, Hancock SI, Cowan SM, et al. Molecular evidence supporting *Ehrlichia canis*-like infection in cats. J Vet Intern Med. 2002;16(6):642-9.

34. Stich RW, Schaefer JJ, Bremer WG, Needham GR, Jittapalapong S. Host surveys, ixodid tick biology and transmission scenarios as related to the tick-borne pathogen, *Ehrlichia canis*. Vet Parasitol. 2008;158(4):256-73.

35. Yabsley MJ, Murphy SM, Luttrell MP, Little SE, Massung RF, Stallknecht DE, et al. Experimental and field studies on the suitability of raccoons (*Procyon lotor*) as hosts for tick-borne pathogens. Vector Borne Zoonotic Dis. 2008;8(4):491-503.

36. Rikihisa Y. The tribe Ehrlichieae and ehrlichial diseases. Clin Microbiol Rev. 1991;4(3):286-308.

37. Woldehiwet Z, Ristic M. Rickettsial and chlamydial diseases of domestic animals. 1st ed. Oxford, England ; New York: Pergamon Press; 1993. xiii, 427 p. p.

38. Ristic M, Holland CJ. Canine ehrlichiosis. Pergamon Press - Oxford. 1993.

39. Popov VL, Han VC, Chen SM, Dumler JS, Feng HM, Andreadis TG, et al. Ultrastructural differentiation of the genogroups in the genus *Ehrlichia*. J Med Microbiol. 1998;47(3):235-51.

40. McQuiston JH, McCall CL, Nicholson WL. Ehrlichiosis and related infections. J Am Vet Med Assoc. 2003;223(12):1750-6.

41. Bell-Sakyi L, Zweygarth E, Blouin EF, Gould EA, Jongejan F. Tick cell lines: tools for tick and tick-borne disease research. Trends Parasitol. 2007;23(9):450-7.

42. Otranto D, Dantas-Torres F, Brianti E, Traversa D, Petric D, Genchi C, et al. Vector-borne helminths of dogs and humans in Europe. Parasit Vectors. 2013;6:16.

43. Ewing SA, Harkess JR, Kocan KM, Barker RW, Fox JC, Tyler RD, et al. Failure to transmit *Ehrlichia canis* (Rickettsiales: Ehrlichieae) with *Otobius megnini* (Acari: Argasidae). J Med Entomol. 1990;27(5):803-6.

44. Johnson EM, Ewing SA, Barker RW, Fox JC, Crow DW, Kocan KM. Experimental transmission of *Ehrlichia canis* (Rickettsiales: Ehrlichieae) by *Dermacentor variabilis* (Acari: Ixodidae). Vet Parasitol. 1998;74(2-4):277-88.

45. Nava S, Estrada-Pena A, Petney T, Beati L, Labruna MB, Szabo MP, et al. The taxonomic status of *Rhipicephalus sanguineus* (Latreille, 1806). Vet Parasitol. 2015;208(1-2):2-8.

46. Szabo MP, Mangold AJ, Joao CF, Bechara GH, Guglielmone AA. Biological and DNA evidence of two dissimilar populations of the *Rhipicephalus sanguineus* tick group (Acari: Ixodidae) in South America. Vet Parasitol. 2005;130(1-2):131-40.

47. Burlini L, Teixeira KR, Szabo MP, Famadas KM. Molecular dissimilarities of *Rhipicephalus sanguineus* (Acari: Ixodidae) in Brazil and its relation with samples throughout the world: is there a geographical pattern? Exp Appl Acarol. 2010;50(4):361-74.

48. Moraes-Filho J, Marcili A, Nieri-Bastos FA, Richtzenhain LJ, Labruna MB. Genetic analysis of ticks belonging to the *Rhipicephalus sanguineus* group in Latin America. Acta Trop. 2011;117(1):51-5.

49. Levin ML, Studer E, Killmaster L, Zemtsova G, Mumcuoglu KY. Crossbreeding between different geographical populations of the brown dog tick, *Rhipicephalus sanguineus* (Acari: Ixodidae). Exp Appl Acarol. 2012;58(1):51-68.

50. Nava S, Mastropaolo M, Venzal JM, Mangold AJ, Guglielmone AA. Mitochondrial DNA analysis of *Rhipicephalus sanguineus sensu lato* (Acari: Ixodidae) in the Southern Cone of South America. Vet Parasitol. 2012;190(3-4):547-55.

51. Dantas-Torres F, Latrofa MS, Annoscia G, Giannelli A, Parisi A, Otranto D. Morphological and genetic diversity of *Rhipicephalus sanguineus sensu lato* from the New and Old Worlds. Parasit Vectors. 2013;6:213.

52. Liu GH, Chen F, Chen YZ, Song HQ, Lin RQ, Zhou DH, et al. Complete mitochondrial genome sequence data provides genetic evidence that the brown dog tick *Rhipicephalus sanguineus* (Acari: Ixodidae) represents a species complex. Int J Biol Sci. 2013;9(4):361-9.

53. Sanches GS, Evora PM, Mangold AJ, Jittapalapong S, Rodriguez-Mallon A, Guzman PE, et al. Molecular, biological, and morphometric comparisons between different geographical populations of *Rhipicephalus sanguineus sensu lato* (Acari: Ixodidae). Vet Parasitol. 2016;215:78-87.

54. Jones EO, Gruntmeir JM, Hamer SA, Little SE. Temperate and tropical lineages of brown dog ticks in North America. Vet Parasitol Reg Stud Reports. 2017;7:58-61.

55. Dantas-Torres F, Latrofa MS, Ramos RAN, Lia RP, Capelli G, Parisi A, et al. Biological compatibility between two temperate lineages of brown dog ticks, *Rhipicephalus sanguineus* (sensu lato). Parasit Vectors. 2018;11(1):398.

56. de Oliveira PR, Bechara GH, Denardi SE, Saito KC, Nunes ET, Szabo MP, et al. Comparison of the external morphology of *Rhipicephalus sanguineus* (Latreille, 1806) (Acari: Ixodidae) ticks from Brazil and Argentina. Vet Parasitol. 2005;129(1-2):139-47.

57. Labruna MB, Gerardi M, Krawczak FS, Moraes-Filho J. Comparative biology of the tropical and temperate species of *Rhipicephalus sanguineus sensu lato* (Acari: Ixodidae) under different laboratory conditions. Ticks Tick Borne Dis. 2017;8(1):146-56.

58. Moraes-Filho J, Krawczak FS, Costa FB, Soares JF, Labruna MB. Comparative Evaluation of the Vector Competence of Four South American Populations of the *Rhipicephalus sanguineus* Group for the Bacterium *Ehrlichia canis*, the Agent of Canine Monocytic Ehrlichiosis. PLoS One. 2015;10(9):e0139386.

59. Cicuttin GL, Tarragona EL, De Salvo MN, Mangold AJ, Nava S. Infection with *Ehrlichia canis* and *Anaplasma platys* (Rickettsiales: Anaplasmataceae) in two lineages of *Rhipicephalus sanguineus sensu lato* (Acari: Ixodidae) from Argentina. Ticks Tick Borne Dis. 2015;6(6):724-9.

60. Aguiar DM, Cavalcante GT, Pinter A, Gennari SM, Camargo LM, Labruna MB. Prevalence of *Ehrlichia canis* (Rickettsiales: Anaplasmataceae) in dogs and *Rhipicephalus sanguineus* (Acari: Ixodidae) ticks from Brazil. J Med Entomol. 2007;44(1):126-32.

61. Souza BM, Leal DC, Barboza DC, Uzeda RS, De Alcantara AC, Ferreira F, et al. Prevalence of ehrlichial infection among dogs and ticks in Northeastern Brazil. Rev Bras Parasitol Vet. 2010;19(2):89-93.

62. Venzal JM, Estrada-Peña A, Castro O, De Souza CG, Portillo A, J.A. O. Study on seasonal activity in dogs and ehrlichial infection in *Rhipicephalus sanguineus* (Latreille, 1806) (Acari: Ixodidae) from southern Uruguay. Parasitol Latinoam. 2007;62:23-6.

63. Luzzi MC, Carvalho LAL, Pinheiro DG, Lima-Duarte L, Camargo JV, Kishi LT, et al. Analysis on the prokaryotic microbiome in females and embryonic cell cultures of *Rhipicephalus sanguineus* tropical and temperate lineages from two specific localities in Brazil. Rev Bras Parasitol Vet. 2021;30(3):e005721.

64. Neer TM, Breitschwerdt EB, Greene RT, Lappin MR. Consensus statement on ehrlichial disease of small animals from the infectious disease study group of the ACVIM. American College of Veterinary Internal Medicine. J Vet Intern Med. 2002;16(3):309-15.

65. Keefe TJ, Holland CJ, Salyer PE, Ristic M. Distribution of *Ehrlichia canis* among military working dogs in the world and selected civilian dogs in the United States. J Am Vet Med Assoc. 1982;181(3):236-8.

66. Estrada-Pena A, Jongejan F. Ticks feeding on humans: a review of records on human-biting Ixodoidea with special reference to pathogen transmission. Exp Appl Acarol. 1999;23(9):685-715.

67. Hua P, Yuhai M, Shide T, Yang S, Bohai W, Xiangrui C. Canine ehrlichiosis caused simultaneously by *Ehrlichia canis* and *Ehrlichia platys*. Microbiol Immunol. 2000;44(9):737-9.

68. Aguirre E, Sainz A, Dunner S, Amusategui I, Lopez L, Rodriguez-Franco F, et al. First isolation and molecular characterization of *Ehrlichia canis* in Spain. Vet Parasitol. 2004;125(3-4):365-72.

69. Maxwell OICOCGO. Environmental and multi-host infestation of the brown dog tick, *Rhipicephalus sanguineus* in Owerri, South-east Nigeria- a case report. Veterinarski arhiv. 2006;76(1).

70. Sonenshine DE. Biology of ticks. New York: Oxford University Press; 1991.

71. Jongejan F, Uilenberg G. The global importance of ticks. Parasitology. 2004;129 Suppl:S3-14.

72. Dantas-Torres F, Otranto D. *Rhipicephalus sanguineus* on dogs: relationships between attachment sites and tick developmental stages. Exp Appl Acarol. 2011;53(4):389-97.

73. Koch HG. Oviposition of the Brown Dog Tick (Acari, Ixodidae) in the Laboratory. Annals of the Entomological Society of America. 1982;75(5):583-6.

74. Regendanz P, Muniz J. O *Rhipicephalus sanguineus* como transmissor da piroplasmose canina no Brasil. Mem Inst Oswaldo Cruz. 1936;31:81-4.

75. Sen SK. The vector of canine piroplasmosis due to *Piroplasma gibsoni.* Ind J Vet Sci Anim Husband. 1933;3:356-63.

76. Mantovani A, Benazzi P. The isolation of *Coxiella burnetii* from *Rhipicephalus sanguineus* on naturally infected dogs. J Am Vet Med Assoc. 1953;122(911):117-8.

77. Nordgren RM, Craig TM. Experimental transmission of the Texas strain of *Hepatozoon canis.* Vet Parasitol. 1984;16(3-4):207-14.

78. Brumpt E. Longevite du virus de la fievre boutonneuse chez la tique, *Rhipicephalus sanguineus.* Compt Rend Soc Biol. 1932;8:1199-202.

79. Parker RR, Philip CB, Jellison WL. Rocky Mountain spotted fever: potentialities of tick transmission in relation to geographical occurence in the United States. Am J Trop Med Hyg. 1933;13:341-79.

80. Coutinho MT, Bueno LL, Sterzik A, Fujiwara RT, Botelho JR, De Maria M, et al. Participation of *Rhipicephalus sanguineus* (Acari: Ixodidae) in the epidemiology of canine visceral leishmaniasis. Vet Parasitol. 2005;128(1-2):149-55.

81. Smith RD, Sells DM, Stephenson EH, Ristic MR, Huxsoll DL. Development of *Ehrlichia canis*, causative agent of canine ehrlichiosis, in the tick *Rhipicephalus sanguineus* and its differentiation from a symbiotic *Rickettsia.* Am J Vet Res. 1976;37(2):119-26.

82. Huxsoll DL, Hildebrandt PK, Nims RM, Amyx HL, Ferguson JA. Epizootiology of tropical canine pancytopenia. J Wildl Dis. 1970;6(4):220-5.

83. Harrus S, Kass PH, Klement E, Waner T. Canine monocytic ehrlichiosis: a retrospective study of 100 cases, and an epidemiological investigation of prognostic indicators for the disease. Vet Rec. 1997;141(14):360-3.

84. Harrus S, Waner T. Diagnosis of canine monocytotropic ehrlichiosis (Ehrlichia canis): an overview. Vet J. 2011;187(3):292-6.

85. Leiva M, Naranjo C, Pena MT. Ocular signs of canine monocytic ehrlichiosis: a retrospective study in dogs from Barcelona, Spain. Vet Ophthalmol. 2005;8(6):387-93.

86. Harrus S, Waner T, Aizenberg I, Foley JE, Poland AM, Bark H. Amplification of ehrlichial DNA from dogs 34 months after infection with *Ehrlichia canis.* J Clin Microbiol. 1998;36(1):73-6.

87. Buhles WC, Jr., Huxsoll DL, Ristic M. Tropical canine pancytopenia: Clinical, hematologic, and serologic response of dogs to *Ehrlichia canis* infection, tetracycline therapy, and challenge inoculation. J Infect Dis. 1974;130(4):357-67.

88. Greene CE. Clinical microbiology and infectious diseases of the dog and cat. Philadelphia: Saunders; 1984. xviii, 967 p. p.

89. Gal A, Harrus S, Arcoh I, Lavy E, Aizenberg I, Mekuzas-Yisaschar Y, et al. Coinfection with multiple tick-borne and intestinal parasites in a 6-week-old dog. Can Vet J. 2007;48(6):619-22.

90. Hildebrandt PK, Huxsoll DL, Walker JS, Nims RM, Taylor R, Andrews M. Pathology of canine ehrlichiosis (tropical canine pancytopenia). Am J Vet Res. 1973;34(10):1309-20.

91. Nyindo M, Huxsoll DL, Ristic M, Kakoma I, Brown JL, Carson CA, et al. Cell-mediated and humoral immune responses of German Shepherd Dogs and Beagles to experimental infection with *Ehrlichia canis.* Am J Vet Res. 1980;41(2):250-4.

92. Harrus S, Waner T, Bark H, Jongejan F, Cornelissen AW. Recent advances in determining the pathogenesis of canine monocytic ehrlichiosis. J Clin Microbiol. 1999;37(9):2745-9.

93. Waner T, Harrus S, Bark H, Bogin E, Avidar Y, Keysary A. Characterization of the subclinical phase of canine ehrlichiosis in experimentally infected beagle dogs. Vet Parasitol. 1997;69(3-4):307-17.

94. Swirski FK, Nahrendorf M, Etzrodt M, Wildgruber M, Cortez-Retamozo V, Panizzi P, et al. Identification of splenic reservoir monocytes and their deployment to inflammatory sites. Science. 2009;325(5940):612-6.

95. Villaescusa A, Tesouro MA, Garcia-Sancho M, Ayllon T, Rodriguez-Franco F, Sainz A. Evaluation of lymphocyte populations in dogs naturally infected by *Ehrlichia canis* with and without clinical signs. Ticks Tick Borne Dis. 2012;3(5-6):279-82.

96. Gianopoulos A, Mylonakis ME, Theodorou K, Christopher MM. Quantitative and qualitative leukocyte abnormalities in dogs with experimental and naturally occurring acute canine monocytic ehrlichiosis. Vet Clin Pathol. 2016;45(2):281-90.

97. Silvestre-Roig C, Fridlender ZG, Glogauer M, Scapini P. Neutrophil Diversity in Health and Disease. Trends Immunol. 2019;40(7):565-83.

98. Netea MG, Quintin J, van der Meer JW. Trained immunity: a memory for innate host defense. Cell Host Microbe. 2011;9(5):355-61.

99. Moorlag S, Rodriguez-Rosales YA, Gillard J, Fanucchi S, Theunissen K, Novakovic B, et al. BCG Vaccination Induces Long-Term Functional Reprogramming of Human Neutrophils. Cell Rep. 2020;33(7):108387.

100. Mylonakis ME, Ceron JJ, Leontides L, Siarkou VI, Martinez S, Tvarijonaviciute A, et al. Serum acute phase proteins as clinical phase indicators and outcome predictors in naturally occurring canine monocytic ehrlichiosis. J Vet Intern Med. 2011;25(4):811-7.

101. Alves RN, Levenhagen MA, Levenhagen MM, Rieck SE, Labruna MB, Beletti ME. The spreading process of *Ehrlichia canis* in macrophages is dependent on actin cytoskeleton, calcium and iron influx and lysosomal evasion. Vet Microbiol. 2014;168(2-4):442-6.

102. Mavromatis K, Doyle CK, Lykidis A, Ivanova N, Francino MP, Chain P, et al. The genome of the obligately intracellular bacterium *Ehrlichia canis* reveals themes of complex membrane structure and immune evasion strategies. J Bacteriol. 2006;188(11):4015-23.

103. Felek S, Huang H, Rikihisa Y. Sequence and expression analysis of *virB9* of the type IV secretion system of E*hrlichia canis* strains in ticks, dogs, and cultured cells. Infect Immun. 2003;71(10):6063-7.

104. Harrus S, Waner T, Friedmann-Morvinski D, Fishman Z, Bark H, Harmelin A. Down-regulation of MHC class II receptors of DH82 cells, following infection with *Ehrlichia canis.* Vet Immunol Immunopathol. 2003;96(3-4):239-43.

105. Boschiroli ML, Ouahrani-Bettache S, Foulongne V, Michaux-Charachon S, Bourg G, Allardet-Servent A, et al. Type IV secretion and *Brucella* virulence. Vet Microbiol. 2002;90(1-4):341-8.

106. Ohashi N, Zhi N, Lin Q, Rikihisa Y. Characterization and transcriptional analysis of gene clusters for a type IV secretion machinery in human granulocytic and monocytic ehrlichiosis agents. Infect Immun. 2002;70(4):2128-38.

107. Luo T, Patel JG, Zhang X, Walker DH, McBride JW. Immunoreactive Protein Repertoires of *Ehrlichia chaffeensis* and *E. canis* Reveal the Dominance of Hypothetical Proteins and Conformation-Dependent Antibody Epitopes. Infect Immun. 2021;89(11):e0022421.

108. Luo T, Patel JG, Zhang X, Walker DH, McBride JW. *Ehrlichia chaffeensis* and *E. canis* hypothetical protein immunoanalysis reveals small secreted immunodominant proteins and conformation-dependent antibody epitopes. NPJ Vaccines. 2020;5:85.

109. Iqbal Z, Chaichanasiriwithaya W, Rikihisa Y. Comparison of PCR with other tests for early diagnosis of canine ehrlichiosis. J Clin Microbiol. 1994;32(7):1658-62.

110. Kakoma I, Hansen RD, Anderson BE, Hanley TA, Sims KG, Liu L, et al. Cultural, molecular, and immunological characterization of the etiologic agent for atypical canine ehrlichiosis. J Clin Microbiol. 1994;32(1):170-5.

111. Kelly PJ, Matthewman LA, Mahan SM, Semu S, Peter T, Mason PR, et al. Serological evidence for antigenic relationships between *Ehrlichia canis* and *Cowdria ruminantium.* Res Vet Sci. 1994;56(2):170-4.

112. Breitschwerdt EB, Hegarty BC, Hancock SI. Sequential evaluation of dogs naturally infected with *Ehrlichia canis, Ehrlichia chaffeensis, Ehrlichia equi, Ehrlichia ewingii,* or *Bartonella vinsonii.* J Clin Microbiol. 1998;36(9):2645-51.

113. Woody BJ, Hoskins JD. Ehrlichial diseases of dogs. Vet Clin North Am Small Anim Pract. 1991;21(1):75-98.

114. Cadman HF, Kelly PJ, Matthewman LA, Zhou R, Mason PR. Comparison of the dot-blot enzyme linked immunoassay with immunofluorescence for detecting antibodies to *Ehrlichia canis.* Vet Rec. 1994;135(15):362.

115. Waner T, Strenger C, Keysary A, Harrus S. Kinetics of serologic cross-reactions between *Ehrlichia canis* and the *Ehrlichia phagocytophila* genogroups in experimental *E. canis* infection in dogs. Vet Immunol Immunopathol. 1998;66(3-4):237-43.

116. Rikihisa Y, Ewing SA, Fox JC, Siregar AG, Pasaribu FH, Malole MB. Analyses of *Ehrlichia canis* and a canine granulocytic *Ehrlichia* infection. J Clin Microbiol. 1992;30(1):143-8.

117. Harrus S, Alleman AR, Bark H, Mahan SM, Waner T. Comparison of three enzyme-linked immunosorbant assays with the indirect immunofluorescent antibody test for the diagnosis of canine infection with *Ehrlichia canis.* Vet Microbiol. 2002;86(4):361-8.

118. Murphy GL, Ewing SA, Whitworth LC, Fox JC, Kocan AA. A molecular and serologic survey of *Ehrlichia canis, E. chaffeensis,* and *E. ewingii* in dogs and ticks from Oklahoma. Vet Parasitol. 1998;79(4):325-39.

119. Doyle CK, Nethery KA, Popov VL, McBride JW. Differentially expressed and secreted major immunoreactive protein orthologs of *Ehrlichia canis* and *E. chaffeensis* elicit early antibody responses to epitopes on glycosylated tandem repeats. Infect Immun. 2006;74(1):711-20.

120. McBride JW, Doyle CK, Zhang X, Cardenas AM, Popov VL, Nethery KA, et al. Identification of a glycosylated *Ehrlichia canis* 19-kilodalton major immunoreactive

protein with a species-specific serine-rich glycopeptide epitope. Infect Immun. 2007;75(1):74-82.

121. Cardenas AM, Doyle CK, Zhang X, Nethery K, Corstvet RE, Walker DH, et al. Enzyme-linked immunosorbent assay with conserved immunoreactive glycoproteins gp36 and gp19 has enhanced sensitivity and provides species-specific immunodiagnosis of *Ehrlichia canis* infection. Clin Vaccine Immunol. 2007;14(2):123-8.

122. Aguiar DM, Zhang X, Braga IA, Taques I, McBride JW. Detection of genotype-specific *Ehrlichia canis* exposure in Brazilian dogs by TRP36 peptide ELISA. Ticks Tick Borne Dis. 2016;7(1):142-5.

123. Nazari M, Lim SY, Watanabe M, Sharma RS, Cheng NA, Watanabe M. Molecular detection of *Ehrlichia canis* in dogs in Malaysia. PLoS Negl Trop Dis. 2013;7(1):e1982.

124. Stich RW, Rikihisa Y, Ewing SA, Needham GR, Grover DL, Jittapalapong S. Detection of *Ehrlichia canis* in canine carrier blood and in individual experimentally infected ticks with a p30-based PCR assay. J Clin Microbiol. 2002;40(2):540-6.

125. McClure JC, Crothers ML, Schaefer JJ, Stanley PD, Needham GR, Ewing SA, et al. Efficacy of a doxycycline treatment regimen initiated during three different phases of experimental ehrlichiosis. Antimicrob Agents Chemother. 2010;54(12):5012-20.

126. Wen B, Rikihisa Y, Mott JM, Greene R, Kim HY, Zhi N, et al. Comparison of nested PCR with immunofluorescent-antibody assay for detection of *Ehrlichia canis* infection in dogs treated with doxycycline. J Clin Microbiol. 1997;35(7):1852-5.

127. Alexandre N, Santos AS, Nuncio MS, Sousa R, Boinas F, Bacellar F. Detection of *Ehrlichia canis* by polymerase chain reaction in dogs from Portugal. Vet J. 2009;181(3):343-4.

128. McBride JW, Corstvet RE, Gaunt SD, Chinsangaram J, Akita GY, Osburn BI. PCR detection of acute *Ehrlichia canis* infection in dogs. J Vet Diagn Invest. 1996;8(4):441-7.

129. Homer MJ, Aguilar-Delfin I, Telford SR, 3rd, Krause PJ, Persing DH. Babesiosis. Clin Microbiol Rev. 2000;13(3):451-69.

130. Rodriguez-Alarcon CA, Beristain-Ruiz DM, Olivares-Munoz A, Quezada-Casasola A, Perez-Casio F, Alvarez-Martinez JA, et al. Demonstrating the presence of *Ehrlichia canis* DNA from different tissues of dogs with suspected subclinical ehrlichiosis. Parasit Vectors. 2020;13(1):518.

131. Sirigireddy KR, Ganta RR. Multiplex detection of *Ehrlichia* and *Anaplasma* species pathogens in peripheral blood by real-time reverse transcriptase-polymerase chain reaction. J Mol Diagn. 2005;7(2):308-16.

132. Sirigireddy KR, Mock DC, Ganta RR. Multiplex detection of *Ehrlichia* and *Anaplasma* pathogens in vertebrate and tick hosts by real-time RT-PCR. Ann N Y Acad Sci. 2006;1078:552-6.

133. Doyle CK, Labruna MB, Breitschwerdt EB, Tang YW, Corstvet RE, Hegarty BC, et al. Detection of medically important *Ehrlichia* by quantitative multicolor TaqMan real-time polymerase chain reaction of the *dsb* gene. J Mol Diagn. 2005;7(4):504-10.

134. Peleg O, Baneth G, Eyal O, Inbar J, Harrus S. Multiplex real-time qPCR for the detection of *Ehrlichia canis* and *Babesia canis vogeli.* Vet Parasitol. 2010;173(3-4):292-9.

135. Padmaja M, Singh H, Panwar H, Jyoti, Singh NK, Singh NK. Development and validation of multiplex SYBR Green real-time PCR assays for detection and molecular surveillance of four tick-borne canine haemoparasites. Ticks Tick Borne Dis. 2022;13(3):101937.

136. Iqbal Z, Rikihisa Y. Reisolation of *Ehrlichia canis* from blood and tissues of dogs after doxycycline treatment. J Clin Microbiol. 1994;32(7):1644-9.

137. Breitschwerdt EB, Hegarty BC, Hancock SI. Doxycycline hyclate treatment of experimental canine ehrlichiosis followed by challenge inoculation with two *Ehrlichia canis* strains. Antimicrob Agents Chemother. 1998;42(2):362-8.

138. Mylonakis ME, Harrus S, Breitschwerdt EB. An update on the treatment of canine monocytic ehrlichiosis (Ehrlichia canis). Vet J. 2019;246:45-53.

139. Jongejan F, Crafford D, Erasmus H, Fourie JJ, Schunack B. Comparative efficacy of oral administrated afoxolaner (NexGard) and fluralaner (Bravecto) with topically applied permethrin/imidacloprid (Advantix) against transmission of *Ehrlichia canis* by infected *Rhipicephalus sanguineus* ticks to dogs. Parasit Vectors. 2016;9(1):348.

140. Walker AR. Ticks and associated diseases: a retrospective review. Med Vet Entomol. 2014;28 Suppl 1:1-5.

141. Uilenberg G. Veterinary significance of ticks and tick-borne diseases. Fivaz B, Petney T, Horak I, editors Tick Vector Biology Medical and Veterinary Aspects. 1992:23-33.

142. Boulanger N, Boyer P, Talagrand-Reboul E, Hansmann Y. Ticks and tick-borne diseases. Med Mal Infect. 2019;49(2):87-97.

143. Trager W. Acquired immunity to ticks. J Parasitol. 1939;25:57-81.

144. Valle MR, Guerrero FD. Anti-tick vaccines in the omics era. Front Biosci (Elite Ed). 2018;10(1):122-36.

145. de la Fuente J, Almazan C, Canales M, Perez de la Lastra JM, Kocan KM, Willadsen P. A ten-year review of commercial vaccine performance for control of tick infestations on cattle. Anim Health Res Rev. 2007;8(1):23-8.

146. de la Fuente J, Contreras M. Tick vaccines: current status and future directions. Expert Rev Vaccines. 2015;14(10):1367-76.

147. Nuttall PA, Trimnell AR, Kazimirova M, Labuda M. Exposed and concealed antigens as vaccine targets for controlling ticks and tick-borne diseases. Parasite Immunol. 2006;28(4):155-63.

148. Ackerman S, Clare FB, McGill TW, Sonenshine DE. Passage of host serum components, including antibody, across the digestive tract of *Dermacentor variabilis* (Say). J Parasitol. 1981;67(5):737-40.

149. Galay RL, Matsuo T, Hernandez EP, Talactac MR, Kusakisako K, Umemiya-Shirafuji R, et al. Immunofluorescent detection in the ovary of host antibodies against a secretory ferritin injected into female *Haemaphysalis longicornis* ticks. Parasitol Int. 2018;67(2):119-22.

150. Ribeiro JM. Role of saliva in tick/host interactions. Exp Appl Acarol. 1989;7(1):15-20.

151. Brossard M, Wikel SK. Tick immunobiology. Parasitology. 2004;129 Suppl:S161-76.

152. Francischetti IM, Sa-Nunes A, Mans BJ, Santos IM, Ribeiro JM. The role of saliva in tick feeding. Front Biosci (Landmark Ed). 2009;14(6):2051-88.

153. Tellam RL, Kemp D, Riding G, Briscoe S, Smith D, Sharp P, et al. Reduced oviposition of *Boophilus microplus* feeding on sheep vaccinated with vitellin. Vet Parasitol. 2002;103(1-2):141-56.

154. Ferreira CA, Barbosa MC, Silveira TC, Valenzuela JG, Vaz Ida S, Jr., Masuda A. cDNA cloning, expression and characterization of a *Boophilus microplus* paramyosin. Parasitology. 2002;125(Pt 3):265-74.

155. de la Fuente J, Rodriguez M, Montero C, Redondo M, Garcia-Garcia JC, Mendez L, et al. Vaccination against ticks (*Boophilus* spp.): the experience with the Bm86-based vaccine Gavac. Genet Anal. 1999;15(3-5):143-8.

156. Rodriguez-Valle M, Taoufik A, Valdes M, Montero C, Ibrahin H, Hassan SM, et al. Efficacy of *Rhipicephalus (Boophilus) microplus* Bm86 against *Hyalomma dromedarii* and *Amblyomma cajennense* tick infestations in camels and cattle. Vaccine. 2012;30(23):3453-8.

157. Willadsen P, Smith D, Cobon G, McKenna RV. Comparative vaccination of cattle against *Boophilus microplus* with recombinant antigen Bm86 alone or in combination with recombinant Bm91. Parasite Immunol. 1996;18(5):241-6.

158. de la Fuente J, Rodriguez M, Redondo M, Montero C, Garcia-Garcia JC, Mendez L, et al. Field studies and cost-effectiveness analysis of vaccination with Gavac against the cattle tick *Boophilus microplus*. Vaccine. 1998;16(4):366-73.

159. Coumou J, Wagemakers A, Trentelman JJ, Nijhof AM, Hovius JW. Vaccination against Bm86 Homologues in Rabbits Does Not Impair *Ixodes ricinus* Feeding or Oviposition. PLoS One. 2014;10(4):e0123495.

160. Almazan C, Blas-Machado U, Kocan KM, Yoshioka JH, Blouin EF, Mangold AJ, et al. Characterization of three *Ixodes scapularis* cDNAs protective against tick infestations. Vaccine. 2005;23(35):4403-16.

161. Contreras M, de la Fuente J. Control of infestations by *Ixodes ricinus* tick larvae in rabbits vaccinated with aquaporin recombinant antigens. Vaccine. 2017;35(9):1323-8.

162. Trimnell AR, Davies GM, Lissina O, Hails RS, Nuttall PA. A cross-reactive tick cement antigen is a candidate broad-spectrum tick vaccine. Vaccine. 2005;23(34):4329-41.

163. Gomes H, Moraes J, Githaka N, Martins R, Isezaki M, Vaz Ida S, Jr., et al. Vaccination with cyclin-dependent kinase tick antigen confers protection against *Ixodes* infestation. Vet Parasitol. 2015;211(3-4):266-73.

164. Parizi LF, Githaka NW, Logullo C, Konnai S, Masuda A, Ohashi K, et al. The quest for a universal vaccine against ticks: cross-immunity insights. Vet J. 2012;194(2):158-65.

165. Socolovschi C, Huynh TP, Davoust B, Gomez J, Raoult D, Parola P. Transovarial and trans-stadial transmission of *Rickettsiae africae* in *Amblyomma variegatum* ticks. Clin Microbiol Infect. 2009;15 Suppl 2:317-8.

166. Kelly PJ, Mason PR. Transmission of a spotted fever group rickettsia by *Amblyomma hebraeum* (Acari: Ixodidae). J Med Entomol. 1991;28(5):598-600.

167. Singh KR, Pavri K, Anderson CR. Experimental Transovarial Transmission of Kyasanur Forest Disease Virus in *Haemaphysalis spinigera*. Nature. 1963;199:513.

168. Macaluso KR, Sonenshine DE, Ceraul SM, Azad AF. Infection and transovarial transmission of rickettsiae in *Dermacentor variabilis* ticks acquired by artificial feeding. Vector Borne Zoonotic Dis. 2001;1(1):45-53.

169. Pal U, Li X, Wang T, Montgomery RR, Ramamoorthi N, Desilva AM, et al. TROSPA, an *Ixodes scapularis* receptor for *Borrelia burgdorferi.* Cell. 2004;119(4):457-68.

170. Tsao JI, Wootton JT, Bunikis J, Luna MG, Fish D, Barbour AG. An ecological approach to preventing human infection: vaccinating wild mouse reservoirs intervenes in the Lyme disease cycle. Proc Natl Acad Sci U S A. 2004;101(52):18159-64.

171. Gomes-Solecki MJ, Brisson DR, Dattwyler RJ. Oral vaccine that breaks the transmission cycle of the Lyme disease spirochete can be delivered via bait. Vaccine. 2006;24(20):4440-9.

172. Nuttall PA, Labuda M. Tick-host interactions: saliva-activated transmission. Parasitology. 2004;129 Suppl:S177-89.

173. Muralidar S, Ambi SV, Sekaran S, Krishnan UM. The emergence of COVID-19 as a global pandemic: Understanding the epidemiology, immune response and potential therapeutic targets of SARS-CoV-2. Biochimie. 2020;179:85-100.

174. Pardi N, Hogan MJ, Porter FW, Weissman D. mRNA vaccines - a new era in vaccinology. Nat Rev Drug Discov. 2018;17(4):261-79.

175. May M. After COVID-19 successes, researchers push to develop mRNA vaccines for other diseases. Nat Med. 2021;27(6):930-2.

176. Liu T, Liang Y, Huang L. Development and Delivery Systems of mRNA Vaccines. Front Bioeng Biotechnol. 2021;9:718753.

177. Sajid A, Matias J, Arora G, Kurokawa C, DePonte K, Tang X, et al. mRNA vaccination induces tick resistance and prevents transmission of the Lyme disease agent. Sci Transl Med. 2021;13(620):eabj9827.

178. O'Leary K. An mRNA vaccine against tick bites. Nat Med. 2021.

179. Flemming A. Tick-targeted mRNA vaccine to tackle disease transmission? Nat Rev Immunol. 2022;22(1):4-5.

180. Fjose A, Ellingsen S, Wargelius A, Seo HC. RNA interference: mechanisms and applications. Biotechnol Annu Rev. 2001;7:31-57.

181. Svoboda P. Key Mechanistic Principles and Considerations Concerning RNA Interference. Front Plant Sci. 2020;11:1237.

182. van der Oost J, Brouns SJ. RNAi: prokaryotes get in on the act. Cell. 2009;139(5):863-5.

183. Mello CC, Conte D, Jr. Revealing the world of RNA interference. Nature. 2004;431(7006):338-42.

184. Xu J, Wang XF, Chen P, Liu FT, Zheng SC, Ye H, et al. RNA Interference in Moths: Mechanisms, Applications, and Progress. Genes (Basel). 2016;7(10).

185. Rosa C, Kuo YW, Wuriyanghan H, Falk BW. RNA Interference Mechanisms and Applications in Plant Pathology. Annu Rev Phytopathol. 2018;56:581-610.

186. Kim D, Rossi J. RNAi mechanisms and applications. Biotechniques. 2008;44(5):613-6.

187. Ramakrishnan VG, Aljamali MN, Sauer JR, Essenberg RC. Application of RNA interference in tick salivary gland research. J Biomol Tech. 2005;16(4):297-305.

188. de la Fuente J, Kocan KM, Almazan C, Blouin EF. RNA interference for the study and genetic manipulation of ticks. Trends Parasitol. 2007;23(9):427-33.

189. de la Fuente J, Kocan KM, Almazan C, Blouin EF. Targeting the tick-pathogen interface for novel control strategies. Front Biosci. 2008;13:6947-56.

190. Kocan KM, Blouin E, de la Fuente J. RNA interference in ticks. J Vis Exp. 2011(47).

191. Barry G, Alberdi P, Schnettler E, Weisheit S, Kohl A, Fazakerley JK, et al. Gene silencing in tick cell lines using small interfering or long double-stranded RNA. Exp Appl Acarol. 2013;59(3):319-38.

192. Weisheit S, Villar M, Tykalova H, Popara M, Loecherbach J, Watson M, et al. *Ixodes scapularis* and *Ixodes ricinus* tick cell lines respond to infection with tick-borne encephalitis virus: transcriptomic and proteomic analysis. Parasit Vectors. 2015;8:599.

193. Alberdi P, Mansfield KL, Manzano-Roman R, Cook C, Ayllon N, Villar M, et al. Tissue-Specific Signatures in the Transcriptional Response to *Anaplasma phagocytophilum* Infection of *Ixodes scapularis* and *Ixodes ricinus* Tick Cell Lines. Front Cell Infect Microbiol. 2016;6:20.

194. Kang S, Hong YS. RNA interference in infectious tropical diseases. Korean J Parasitol. 2008;46(1):1-15.

195. Kurscheid S, Lew-Tabor AE, Rodriguez Valle M, Bruyeres AG, Doogan VJ, Munderloh UG, et al. Evidence of a tick RNAi pathway by comparative genomics and reverse genetics screen of targets with known loss-of-function phenotypes in *Drosophila*. BMC Mol Biol. 2009;10:26.

196. Galay RL, Umemiya-Shirafuji R, Masami Mochizuki M, Fujisaki K, Tanaka T. RNA Interference – A Powerful Functional Analysis Tool for Studying Tick Biology and its Control. RNA Interference. 2016.

197. Galay RL, Aung KM, Umemiya-Shirafuji R, Maeda H, Matsuo T, Kawaguchi H, et al. Multiple ferritins are vital to successful blood feeding and reproduction of the hard tick *Haemaphysalis longicornis*. J Exp Biol. 2013;216(Pt 10):1905-15.

198. Harrison PM, Arosio P. The ferritins: molecular properties, iron storage function and cellular regulation. Biochim Biophys Acta. 1996;1275(3):161-203.

199. Hajdusek O, Sojka D, Kopacek P, Buresova V, Franta Z, Sauman I, et al. Knockdown of proteins involved in iron metabolism limits tick reproduction and development. Proc Natl Acad Sci U S A. 2009;106(4):1033-8.

200. Hernandez EP, Shimazaki K, Niihara H, Umemiya-Shirafuji R, Fujisaki K, Tanaka T. Expression analysis of glutathione S-transferases and ferritins during the embryogenesis of the tick *Haemaphysalis longicornis.* Heliyon. 2020;6(3):e03644.

201. Galay RL, Umemiya-Shirafuji R, Bacolod ET, Maeda H, Kusakisako K, Koyama J, et al. Two kinds of ferritin protect ixodid ticks from iron overload and consequent oxidative stress. PLoS One. 2014;9(3):e90661.

202. Kopacek P, Zdychova J, Yoshiga T, Weise C, Rudenko N, Law JH. Molecular cloning, expression and isolation of ferritins from two tick species - *Ornithodoros moubata* and *Ixodes ricinus.* Insect Biochem Mol Biol. 2003;33(1):103-13.

203. Xu G, Fang QQ, Keirans JE, Durden LA. Ferritin gene coding sequences are conserved among eight hard tick species (Ixodida: Ixodidae) Ann Entomol Soc Am. 2004:567–73.

204. Aziz N, Munro HN. Iron regulates *ferritin* mRNA translation through a segment of its 5' untranslated region. Proc Natl Acad Sci U S A. 1987;84(23):8478-82.

205. Zhao Y, Liu L, Liu JB, Wu CY, Duan DY, Cheng TY. Cloning, expression, and function of ferritins in the tick *Haemaphysalis flava.* Ticks Tick Borne Dis. 2022;13(2):101892.

206. Mulenga A, Simser JA, Macaluso KR, Azad AF. Stress and transcriptional regulation of tick ferritin HC. Insect Mol Biol. 2004;13(4):423-33.

207. Hernandez EP, Kusakisako K, Talactac MR, Galay RL, Yoshii K, Tanaka T. Induction of intracellular ferritin expression in embryo-derived *Ixodes scapularis* cell line (ISE6). Sci Rep. 2018;8(1):16566.

208. Galay RL, Miyata T, Umemiya-Shirafuji R, Maeda H, Kusakisako K, Tsuji N, et al. Evaluation and comparison of the potential of two ferritins as anti-tick vaccines against *Haemaphysalis longicornis.* Parasit Vectors. 2014;7:482.

209. Hajdusek O, Almazan C, Loosova G, Villar M, Canales M, Grubhoffer L, et al. Characterization of ferritin 2 for the control of tick infestations. Vaccine. 2010;28(17):2993-8.

210. Harrus S, Aroch I, Lavy E, Bark H. Clinical manifestations of infectious canine cyclic thrombocytopenia. Vet Rec. 1997;141(10):247-50.

211. Mineo TW, Carrasco AO, Marciano JA, Werther K, Pinto AA, Machado RZ. Pigeons (*Columba livia*) are a suitable experimental model for *Neospora caninum* infection in birds. Vet Parasitol. 2009;159(2):149-53.

212. Domingues LM, Machado RZ, Tinucci CM, Carvalho CS, Costa AJ, Malheiro EB. Canine toxoplasmosis: a comparative evaluation of the detection of anti-*Toxoplasma gondii* antibodies by the indi rect immunoenzymatic assay (ELISA) and the indirect immunofluorescence reaction (IIF). Revista Brasileira de Parasitologia Veterinária1998. p. 79-85.

213. André MR, Adania CH, Machado RZ, Allegretti SM, Felippe PA, Silva KF, et al. Molecular and serologic detection of *Ehrlichia* spp. in endangered Brazilian wild captive felids. J Wildl Dis. 2010;46(3):1017-23.

214. Furuta PI, Oliveira TM, Theixeira MC, Rocha AG, Machado RZ, Tinucci-Costa MG. Comparison between a soluble antigen-based ELISA and IFAT in detecting antibodies against *Babesia canis* in dogs. Rev Bras Parasitol Vet. 2009;18(3):41-5.

215. Jefferies R, Ryan UM, Irwin PJ. PCR-RFLP for the detection and differentiation of the canine piroplasm species and its use with filter paper-based technologies. Vet Parasitol. 2007;144(1-2):20-7.

216. Tatchell RJ. Interactions between ticks and their hosts. Int J Parasitol. 1987;17(2):597-606.

217. Sanches GS, de Oliveira PR, André MR, Machado RZ, Bechara GH, Camargo-Mathias MI. Copulation is necessary for the completion of a gonotrophic cycle in the tick *Rhipicephalus sanguineus* (Latreille, 1806) (Acari: Ixodidae). J Insect Physiol. 2012;58(7):1020-7.

218. Sanches G. Comparação biológica, morfológica e molecular entre carrapatos do Complexo *Rhipicephalus sanguineus* (Acari: Ixodidae). *PhD Thesis, Universidade Estadual Paulista* .2013.

219. Wellman ML, Krakowka S, Jacobs RM, Kociba GJ. A macrophage-monocyte cell line from a dog with malignant histiocytosis. In Vitro Cell Dev Biol. 1988;24(3):223-9.

220. Aguiar DM, Saito TB, Hagiwara MK, Machado RZ, Labruna MB. Serological diagnosis of canine monocytic ehrlichiosis with Brazilian antigen of *Ehrlichia canis*. Cienc. Rural; 2007. p. 796-802.

221. Harrus S, Kenny M, Miara L, Aizenberg I, Waner T, Shaw S. Comparison of simultaneous splenic sample PCR with blood sample PCR for diagnosis and treatment of experimental *Ehrlichia canis* infection. Antimicrob Agents Chemother. 2004;48(11):4488-90.

222. Bechara GH, Szabo MP, Ferreira BR, Garcia MV. *Rhipicephalus sanguineus* tick in Brazil: Feeding and reproductive aspects under laboratorial conditions. Rev Bras Parasitol Vet. 1995;4(2):61-6.

223. Munderloh UG, Liu Y, Wang M, Chen C, Kurtti TJ. Establishment, maintenance and description of cell lines from the tick *Ixodes scapularis*. J Parasitol. 1994;80(4):533-43.

224. Munderloh UG, Kurtti TJ. Formulation of medium for tick cell culture. Exp Appl Acarol. 1989;7(3):219-29.

225. Ferrolho J, Simpson J, Hawes P, Zweygarth E, Bell-Sakyi L. Growth of *Ehrlichia canis*, the causative agent of canine monocytic ehrlichiosis, in vector and non-vector ixodid tick cell lines. Ticks Tick Borne Dis. 2016;7(4):631-7.

226. Barros-Battesti DM, Machado RZ, Andre MR, de Sousa KCM, Franze DA, Lima-Duarte L, et al. Successful Infection of Tick Cell Cultures of *Rhipicephalus sanguineus* (Tropical Lineage) with *Ehrlichia canis*. Vector Borne Zoonotic Dis. 2018.

227. Anatriello E, Ribeiro JM, de Miranda-Santos IK, Brandao LG, Anderson JM, Valenzuela JG, et al. An insight into the sialotranscriptome of the brown dog tick, *Rhipicephalus sanguineus.* BMC Genomics. 2010;11:450.

228. Nijhof AM, Balk JA, Postigo M, Jongejan F. Selection of reference genes for quantitative RT-PCR studies in *Rhipicephalus (Boophilus) microplus* and *Rhipicephalus appendiculatus* ticks and determination of the expression profile of Bm86. BMC Mol Biol. 2009;10:112.

229. Shayan P, Hooshmand E, Rahbari S, Nabian S. Determination of *Rhipicephalus* spp. as vectors for *Babesia ovis* in Iran. Parasitol Res. 2007;101(4):1029-33.

230. Zivkovic Z, Torina A, Mitra R, Alongi A, Scimeca S, Kocan KM, et al. Subolesin expression in response to pathogen infection in ticks. BMC Immunol. 2010;11:7.

231. Bustin SA, Beaulieu JF, Huggett J, Jaggi R, Kibenge FS, Olsvik PA, et al. MIQE precis: Practical implementation of minimum standard guidelines for fluorescence-based quantitative real-time PCR experiments. BMC Mol Biol. 2010;11:74.

232. Vandesompele J, De Preter K, Pattyn F, Poppe B, Van Roy N, De Paepe A, et al. Accurate normalization of real-time quantitative RT-PCR data by geometric averaging of multiple internal control genes. Genome Biol. 2002;3(7):RESEARCH0034.

233. Livak KJ, Schmittgen TD. Analysis of relative gene expression data using real-time quantitative PCR and the 2(-Delta Delta C(T)) Method. Methods. 2001;25(4):402-8.

234. Pfaffl MW. A new mathematical model for relative quantification in real-time RT-PCR. Nucleic Acids Res. 2001;29(9):e45.

235. Tukey JW. Some thoughts on clinical trials, especially problems of multiplicity. Science. 1977;198(4318):679-84.

236. Anjo SI, Santa C, Manadas B. Short GeLC-SWATH: a fast and reliable quantitative approach for proteomic screenings. Proteomics. 2015;15(4):757-62.

237. Manadas B, Santos AR, Szabadfi K, Gomes JR, Garbis SD, Fountoulakis M, et al. BDNF-induced changes in the expression of the translation machinery in hippocampal neurons: protein levels and dendritic mRNA. Journal of proteome research. 2009;8(10):4536-52.

238. Sonnhammer EL, von Heijne G, Krogh A. A hidden Markov model for predicting transmembrane helices in protein sequences. Proc Int Conf Intell Syst Mol Biol. 1998;6:175-82.

239. Krogh A, Larsson B, von Heijne G, Sonnhammer EL. Predicting transmembrane protein topology with a hidden Markov model: application to complete genomes. J Mol Biol. 2001;305(3):567-80.

240. Nielsen H. Predicting Secretory Proteins with SignalP. Methods Mol Biol. 2017;1611:59-73.

241. Hebditch M, Carballo-Amador MA, Charonis S, Curtis R, Warwicker J. Protein-Sol: a web tool for predicting protein solubility from sequence. Bioinformatics. 2017;33(19):3098-100.

242. Guex N, Peitsch MC. SWISS-MODEL and the Swiss-PdbViewer: an environment for comparative protein modeling. Electrophoresis. 1997;18(15):2714-23.

243. Bienert S, Waterhouse A, de Beer TA, Tauriello G, Studer G, Bordoli L, et al. The SWISS-MODEL Repository-new features and functionality. Nucleic Acids Res. 2017;45(D1):D313-D9.

244. Bertoni M, Kiefer F, Biasini M, Bordoli L, Schwede T. Modeling protein quaternary structure of homo- and hetero-oligomers beyond binary interactions by homology. Sci Rep. 2017;7(1):10480.

245. Waterhouse A, Bertoni M, Bienert S, Studer G, Tauriello G, Gumienny R, et al. SWISS-MODEL: homology modelling of protein structures and complexes. Nucleic Acids Res. 2018;46(W1):W296-W303.

246. Studer G, Rempfer C, Waterhouse AM, Gumienny R, Haas J, Schwede T. QMEANDisCo-distance constraints applied on model quality estimation. Bioinformatics. 2020;36(6):1765-71.

247. Schulz MH, Zerbino DR, Vingron M, Birney E. Oases: robust *de novo* RNA-seq assembly across the dynamic range of expression levels. Bioinformatics. 2012;28(8):1086-92.

248. Roberts A, Pachter L. Streaming fragment assignment for real-time analysis of sequencing experiments. Nat Methods. 2013;10(1):71-3.

249. Suzek BE, Wang Y, Huang H, McGarvey PB, Wu CH, Consortium U. UniRef clusters: a comprehensive and scalable alternative for improving sequence similarity searches. Bioinformatics. 2015;31(6):926-32.

250. Gillet LC, Navarro P, Tate S, Rost H, Selevsek N, Reiter L, et al. Targeted data extraction of the MS/MS spectra generated by data-independent acquisition: a new concept for consistent and accurate proteome analysis. Molecular & cellular proteomics. 2012;11(6):O111 016717.

251. Tang WH, Shilov IV, Seymour SL. Nonlinear fitting method for determining local false discovery rates from decoy database searches. Journal of proteome research. 2008;7(9):3661-7.

252. Sennels L, Bukowski-Wills JC, Rappsilber J. Improved results in proteomics by use of local and peptide-class specific false discovery rates. BMC bioinformatics 2009;10: 179.

253. Collins BC, Gillet LC, Rosenberger G, Rost HL, Vichalkovski A, Gstaiger M, et al. Quantifying protein interaction dynamics by SWATH mass spectrometry: application to the 14-3-3 system. Nature methods 2013;10(12):1246-53.

254. Vizcaíno JA, Csordas A, Del-Toro N, Dianes JA, Griss J, Lavidas I, et al. 2016 update of the PRIDE database and its related tools. Nucleic Acids Res. 2016;44(22):11033.

255. Duscher GG, Galindo RC, Tichy A, Hummel K, Kocan KM, de la Fuente J. Glutathione S-transferase affects permethrin detoxification in the brown dog tick, *Rhipicephalus sanguineus.* Ticks and tick-borne diseases. 2014;5(3):225-33.

256. Hussein HE, Scoles GA, Ueti MW, Suarez CE, Adham FK, Guerrero FD, et al. Targeted silencing of the Aquaporin 2 gene of *Rhipicephalus (Boophilus) microplus* reduces tick fitness. Parasit Vectors. 2015;8:618.

257. Aljamali MN, Bior AD, Sauer JR, Essenberg RC. RNA interference in ticks: a study using histamine binding protein dsRNA in the female tick *Amblyomma americanum.* Insect Mol Biol. 2003;12(3):299-305.

258. Galay RL, Hernandez EP, Talactac MR, Maeda H, Kusakisako K, Umemiya-Shirafuji R, et al. Induction of gene silencing in *Haemaphysalis longicornis* ticks through immersion in double-stranded RNA. Ticks Tick Borne Dis. 2016;7(5):813-6.

259. Shute PG. The staining of malaria parasites. Trans R Soc Trop Med Hyg. 1966;60(3):412-6.

260. Ferrolho J, Antunes S, Sanches GS, Couto J, Evora PM, Rosa C, et al. *Ferritin 1* silencing effect in *Rhipicephalus sanguineus sensu lato* (Acari: Ixodidae) during experimental infection with *Ehrlichia canis.* Ticks Tick Borne Dis. 2017;8(1):174-84.

261. Waner T, Harrus S, Weiss DJ, Bark H, Keysary A. Demonstration of serum antiplatelet antibodies in experimental acute canine ehrlichiosis. Vet Immunol Immunopathol. 1995;48(1-2):177-82.

262. Harrus S, Waner T, Weiss DJ, Keysary A, Bark H. Kinetics of serum antiplatelet antibodies in experimental acute canine ehrlichiosis. Vet Immunol Immunopathol. 1996;51(1-2):13-20.

263. Galay RL, Umemiya-Shirafuji R, Mochizuki M, Fujisaki K, Tanaka T. Iron metabolism in hard ticks (Acari: Ixodidae): the antidote to their toxic diet. Parasitol Int. 2015;64(2):182-9.

264. Balashov IUS. A translation of Bloodsucking ticks (Ixodoidea) - vectors of diseases of man and animals. College Park, Md.,: Entomological Society of America; 1972. 161-376 p. p.

265. Tarnowski BI, Coons LB. Ultrastructure of the midgut and blood meal digestion in the adult tick *Dermacentor variabilis.* Exp Appl Acarol. 1989;6(4):263-89.

266. Donohue KV, Khalil SM, Sonenshine DE, Roe RM. Heme-binding storage proteins in the Chelicerata. J Insect Physiol. 2009;55(4):287-96.

267. Boldbaatar D, Umemiya-Shirafuji R, Liao M, Tanaka T, Xuan X, Fujisaki K. Multiple vitellogenins from the *Haemaphysalis longicornis* tick are crucial for ovarian development. J Insect Physiol. 2010;56(11):1587-98.

268. Wang J, Pantopoulos K. Regulation of cellular iron metabolism. Biochem J. 2011;434(3):365-81.

269. Githaka NW, Konnai S, Isezaki M, Goto S, Xavier MA, Fujisawa S, et al. Identification and functional analysis of ferritin 2 from the Taiga tick *Ixodes persulcatus* Schulze. Ticks Tick Borne Dis. 2020;11(6):101547.

270. Carvalho HF, Recco-Pimentel SM. A Célula. Editora Manole, São Paulo 2012;3 Ed.

271. Junqueira LC, Carneiro J. Histologia Básica. Guanabara Koogan, Rio de Janeiro. 2013.

272. de Oliveira PR, Bechara GH, Denardi SE, Nunes ET, Camargo Mathias MI. Morphological characterization of the ovary and oocytes vitellogenesis of the tick *Rhipicephalus sanguineus* (Latreille, 1806) (Acari: Ixodidae). Exp Parasitol. 2005;110(2):146-56.

273. Oleaga A, Gonzalez-Perez S, Perez-Sanchez R. First molecular and functional characterisation of ferritin 2 proteins from *Ornithodoros* argasid ticks. Vet Parasitol. 2022;304:109684.

274. Weiss BL, Reuben Kaufman W. The relationship between 'critical weight' and 20-hydroxyecdysone in the female ixodid tick, *Amblyomma hebraeum*. J Insect Physiol. 2001;47(11):1261-7.

275. Galay RL, Takechi R, Umemiya-Shirafuji R, Talactac MR, Maeda H, Kusakisako K, et al. Impaired cellular immune response to injected bacteria after knockdown of ferritin genes in the hard tick *Haemaphysalis longicornis.* Parasitol Int. 2016;65(3):251-7.

276. Mulenga A, Macaluso KR, Simser JA, Azad AF. Dynamics of *Rickettsia*-tick interactions: identification and characterization of differentially expressed mRNAs in uninfected and infected *Dermacentor variabilis.* Insect Mol Biol. 2003;12(2):185-93.

277. Wikel S. Ticks and tick-borne pathogens at the cutaneous interface: host defenses, tick countermeasures, and a suitable environment for pathogen establishment. Front Microbiol. 2013;4:337.

278. Simo L, Kazimirova M, Richardson J, Bonnet SI. The Essential Role of Tick Salivary Glands and Saliva in Tick Feeding and Pathogen Transmission. Front Cell Infect Microbiol. 2017;7:281.

279. Sauer JR. Acarine salivary glands - physiological relationships. J Med Entomol. 1977;14(1):1-9.

280. Oliva Chavez AS, Wang X, Marnin L, Archer NK, Hammond HL, Carroll EEM, et al. Tick extracellular vesicles enable arthropod feeding and promote distinct outcomes of bacterial infection. Nat Commun. 2021;12(1):3696.

281. Tirloni L, Lu S, Calvo E, Sabadin G, Di Maggio LS, Suzuki M, et al. Integrated analysis of sialotranscriptome and sialoproteome of the brown dog tick *Rhipicephalus sanguineus (s.l.):* Insights into gene expression during blood feeding. J Proteomics. 2020;229:103899.

282. Jia N, Wang J, Shi W, Du L, Sun Y, Zhan W, et al. Large-Scale Comparative Analyses of Tick Genomes Elucidate Their Genetic Diversity and Vector Capacities. Cell. 2020;182(5):1328-40 e13.

283. Kazimirova M, Stibraniova I. Tick salivary compounds: their role in modulation of host defences and pathogen transmission. Front Cell Infect Microbiol. 2013;3:43.

284. Fontaine A, Diouf I, Bakkali N, Misse D, Pages F, Fusai T, et al. Implication of haematophagous arthropod salivary proteins in host-vector interactions. Parasit Vectors. 2011;4:187.

285. Chmelar J, Calvo E, Pedra JH, Francischetti IM, Kotsyfakis M. Tick salivary secretion as a source of antihemostatics. J Proteomics. 2012;75(13):3842-54.

286. Kotal J, Langhansova H, Lieskovska J, Andersen JF, Francischetti IM, Chavakis T, et al. Modulation of host immunity by tick saliva. J Proteomics. 2015;128:58-68.

287. Chacinska A, Koehler CM, Milenkovic D, Lithgow T, Pfanner N. Importing mitochondrial proteins: machineries and mechanisms. Cell. 2009;138(4):628-44.

288. Meinecke M, Wagner R, Kovermann P, Guiard B, Mick DU, Hutu DP, et al. Tim50 maintains the permeability barrier of the mitochondrial inner membrane. Science. 2006;312(5779):1523-6.

289. Miyamoto Y, Yamada K, Yoneda Y. Importin alpha: a key molecule in nuclear transport and non-transport functions. J Biochem. 2016;160(2):69-75.

290. Kodiha M, Chu A, Matusiewicz N, Stochaj U. Multiple mechanisms promote the inhibition of classical nuclear import upon exposure to severe oxidative stress. Cell Death Differ. 2004;11(8):862-74.

291. Furuta M, Kose S, Koike M, Shimi T, Hiraoka Y, Yoneda Y, et al. Heat-shock induced nuclear retention and recycling inhibition of importin alpha. Genes Cells. 2004;9(5):429-41.

292. Miyamoto Y, Saiwaki T, Yamashita J, Yasuda Y, Kotera I, Shibata S, et al. Cellular stresses induce the nuclear accumulation of importin alpha and cause a conventional nuclear import block. J Cell Biol. 2004;165(5):617-23.

293. Artigas-Jeronimo S, Villar M, Cabezas-Cruz A, Caignard G, Vitour D, Richardson J, et al. Tick Importin-alpha Is Implicated in the Interactome and Regulome of the Cofactor Subolesin. Pathogens. 2021;10(4).

294. Kim Y, Wang J, Clemens EG, Grab DJ, Dumler JS. *Anaplasma phagocytophilum* Ankyrin A Protein (AnkA) Enters the Nucleus Using an Importin-beta-, RanGTP-Dependent Mechanism. Front Cell Infect Microbiol. 2022;12:828605.

295. Sojka D, Franta Z, Horn M, Caffrey CR, Mares M, Kopacek P. New insights into the machinery of blood digestion by ticks. Trends Parasitol. 2013;29(6):276-85.

296. Anderson JM, Sonenshine DE, Valenzuela JG. Exploring the mialome of ticks: an annotated catalogue of midgut transcripts from the hard tick, *Dermacentor variabilis* (Acari: Ixodidae). BMC Genomics. 2008;9:552.

297. Motobu M, Tsuji N, Miyoshi T, Huang X, Islam MK, Alim MA, et al. Molecular characterization of a blood-induced serine carboxypeptidase from the ixodid tick *Haemaphysalis longicornis*. FEBS J. 2007;274(13):3299-312.

298. Landulfo GA, Patane JSL, Silva D, Junqueira-de-Azevedo ILM, Mendonca RZ, Simons SM, et al. Gut transcriptome analysis on females of *Ornithodoros mimon* (Acari: Argasidae) and phylogenetic inference of ticks. Rev Bras Parasitol Vet. 2017;26(2):185-204.

299. Perner J, Provaznik J, Schrenkova J, Urbanova V, Ribeiro JM, Kopacek P. RNA-seq analyses of the midgut from blood- and serum-fed *Ixodes ricinus* ticks. Sci Rep. 2016;6:36695.

300. Valenzuela JG, Francischetti IM, Pham VM, Garfield MK, Mather TN, Ribeiro JM. Exploring the sialome of the tick *Ixodes scapularis.* J Exp Biol. 2002;205(Pt 18):2843-64.

301. Giachetto PF, Cunha RC, Nhani A, Jr., Garcia MV, Ferro JA, Andreotti R. Gene Expression in the Salivary Gland of *Rhipicephalus (Boophilus) microplus* Fed on Tick-Susceptible and Tick-Resistant Hosts. Front Cell Infect Microbiol. 2019;9:477.

302. Rodriguez-Valle M, Moolhuijzen P, Barrero RA, Ong CT, Busch G, Karbanowicz T, et al. Transcriptome and toxin family analysis of the paralysis tick, *Ixodes holocyclus*. Int J Parasitol. 2018;48(1):71-82.

303. Tan AW, Francischetti IM, Slovak M, Kini RM, Ribeiro JM. Sexual differences in the sialomes of the zebra tick, *Rhipicephalus pulchellus.* J Proteomics. 2015;117:120-44.

304. Gong H, Zhou J, Liao M, Hatta T, Harnnoi T, Umemiya R, et al. Characterization of a carboxypeptidase inhibitor from the tick *Haemaphysalis longicornis.* J Insect Physiol. 2007;53(10):1079-87.

305. Reyes J, Ayala-Chavez C, Sharma A, Pham M, Nuss AB, Gulia-Nuss M. Blood Digestion by Trypsin-Like Serine Proteases in the Replete Lyme Disease Vector Tick, *Ixodes scapularis.* Insects. 2020;11(3).

306. Horn M, Nussbaumerova M, Sanda M, Kovarova Z, Srba J, Franta Z, et al. Hemoglobin digestion in blood-feeding ticks: mapping a multipeptidase pathway by functional proteomics. Chem Biol. 2009;16(10):1053-63.

307. Miyoshi T, Tsuji N, Islam MK, Alim MA, Hatta T, Huang X, et al. A set of serine proteinase paralogs are required for blood-digestion in the ixodid tick *Haemaphysalis longicornis.* Parasitol Int. 2008;57(4):499-505.

308. Jarmey JM, Riding GA, Pearson RD, McKenna RV, Willadsen P. Carboxydipeptidase from *Boophilus microplus:* a "concealed" antigen with similarity to angiotensin-converting enzyme. Insect Biochem Mol Biol. 1995;25(9):969-74.

309. Mudenda L, Pierle SA, Turse JE, Scoles GA, Purvine SO, Nicora CD, et al. Proteomics informed by transcriptomics identifies novel secreted proteins in *Dermacentor andersoni* saliva. Int J Parasitol. 2014;44(13):1029-37.

310. Radulovic ZM, Kim TK, Porter LM, Sze SH, Lewis L, Mulenga A. A 24-48 h fed *Amblyomma americanum* tick saliva immuno-proteome. BMC Genomics. 2014;15:518.

311. Arolas JL, Lorenzo J, Rovira A, Castella J, Aviles FX, Sommerhoff CP. A carboxypeptidase inhibitor from the tick *Rhipicephalus bursa:* isolation, cDNA cloning, recombinant expression, and characterization. J Biol Chem. 2005;280(5):3441-8.

312. Bouma BN, Meijers JC. Thrombin-activatable fibrinolysis inhibitor (TAFI, plasma procarboxypeptidase B, procarboxypeptidase R, procarboxypeptidase U). J Thromb Haemost. 2003;1(7):1566-74.

313. Ribeiro JM, Spielman A. *Ixodes dammini:* salivary anaphylatoxin inactivating activity. Exp Parasitol. 1986;62(2):292-7.

314. Jahan N, Docherty PT, Billingsley PF, Hurd H. Blood digestion in the mosquito, *Anopheles stephensi:* the effects of *Plasmodium yoelii* nigeriensis on midgut enzyme activities. Parasitology. 1999;119 (Pt 6):535-41.

315. Kenney E, Yaparla A, Hawdon JM, DM OH, Grayfer L, Eleftherianos I. A putative lysozyme and serine carboxypeptidase from *Heterorhabditis bacteriophora* show differential virulence capacities in *Drosophila melanogaster*. Dev Comp Immunol. 2021;114:103820.

316. Balasubramanian N, Hao YJ, Toubarro D, Nascimento G, Simoes N. Purification, biochemical and molecular analysis of a chymotrypsin protease with prophenoloxidase suppression activity from the entomopathogenic nematode *Steinernema carpocapsae.* Int J Parasitol. 2009;39(9):975-84.

317. Toubarro D, Lucena-Robles M, Nascimento G, Costa G, Montiel R, Coelho AV, et al. An apoptosis-inducing serine protease secreted by the entomopathogenic nematode *Steinernema carpocapsae.* Int J Parasitol. 2009;39(12):1319-30.

318. Toubarro D, Lucena-Robles M, Nascimento G, Santos R, Montiel R, Verissimo P, et al. Serine protease-mediated host invasion by the parasitic nematode *Steinernema carpocapsae*. J Biol Chem. 2010;285(40):30666-75.

319. Rees-Roberts D, Mullen LM, Gounaris K, Selkirk ME. Inactivation of the complement anaphylatoxin C5a by secreted products of parasitic nematodes. Int J Parasitol. 2010;40(5):527-32.

320. Chasseaud LF. The role of glutathione and glutathione S-transferases in the metabolism of chemical carcinogens and other electrophilic agents. Adv Cancer Res. 1979;29:175-274.

321. Singh RR, Reindl KM. Glutathione S-Transferases in Cancer. Antioxidants (Basel). 2021;10(5).

322. Hayes JD, Pulford DJ. The glutathione S-transferase supergene family: regulation of GST and the contribution of the isoenzymes to cancer chemoprotection and drug resistance. Crit Rev Biochem Mol Biol. 1995;30(6):445-600.

323. Hernandez EP, Kusakisako K, Talactac MR, Galay RL, Hatta T, Matsuo T, et al. Characterization and expression analysis of a newly identified glutathione S-transferase of the hard tick *Haemaphysalis longicornis* during blood-feeding. Parasit Vectors. 2018;11(1):91.

324. Huercha, Song R, Li M, Fan X, Hu Z, Wu L, et al. Caracterization of glutathione S-transferase of *Dermacantor marginatus* and effect of the recombinant antigen as a potential anti-tick vaccine. Vet Parasitol. 2020;279:109043.

325. He H, Chen AC, Davey RB, Ivie GW, George JE. Characterization and molecular cloning of a glutathione S-transferase gene from the tick, *Boophilus microplus* (Acari: Ixodidae). Insect Biochem Mol Biol. 1999;29(8):737-43.

326. Rosa de Lima MF, Sanchez Ferreira CA, Joaquim de Freitas DR, Valenzuela JG, Masuda A. Cloning and partial characterization of a *Boophilus microplus* (Acari: Ixodidae) glutathione S-transferase. Insect Biochem Mol Biol. 2002;32(7):747-54.

327. Hernandez EP, Kusakisako K, Talactac MR, Galay RL, Hatta T, Fujisaki K, et al. Glutathione S-transferases play a role in the detoxification of flumethrin and chlorpyrifos in *Haemaphysalis longicornis.* Parasit Vectors. 2018;11(1):460.

328. Enayati AA, Asgarian F, Amouei A, Sharif M, Mortazavi H, Boujhmehrani H, et al. Pyrethroid insecticide resistance in *Rhipicephalus bursa* (Acari, Ixodidae). Pesticide Biochemistry and Physiology. 2010;97(3):243-8.

329. Nandi A, Jyoti, Singh H, Singh NK. Esterase and glutathione S-transferase levels associated with synthetic pyrethroid resistance in *Hyalomma anatolicum* and *Rhipicephalus microplus* ticks from Punjab, India. Exp Appl Acarol. 2015;66(1):141-57.

330. Perner J, Kotal J, Hatalova T, Urbanova V, Bartosova-Sojkova P, Brophy PM, et al. Inducible glutathione S-transferase (IrGST1) from the tick *Ixodes ricinus* is a haem-binding protein. Insect Biochem Mol Biol. 2018;95:44-54.

331. Parizi LF, Utiumi KU, Imamura S, Onuma M, Ohashi K, Masuda A, et al. Cross immunity with *Haemaphysalis longicornis* glutathione S-transferase reduces an experimental *Rhipicephalus (Boophilus) microplus* infestation. Exp Parasitol. 2011;127(1):113-8.

332. Sabadin GA, Parizi LF, Kiio I, Xavier MA, da Silva Matos R, Camargo-Mathias MI, et al. Effect of recombinant glutathione S-transferase as vaccine antigen against *Rhipicephalus appendiculatus* and *Rhipicephalus sanguineus* infestation. Vaccine. 2017;35(48 Pt B):6649-56.

333. Ndawula C, Jr., Sabadin GA, Parizi LF, da Silva Vaz I, Jr. Constituting a glutathione S-transferase-cocktail vaccine against tick infestation. Vaccine. 2019;37(14):1918-27.

334. Parizi LF, Reck J, Jr., Oldiges DP, Guizzo MG, Seixas A, Logullo C, et al. Multi-antigenic vaccine against the cattle tick *Rhipicephalus (Boophilus) microplus:* a field evaluation. Vaccine. 2012;30(48):6912-7.

335. Rudenko N, Golovchenko M, Edwards MJ, Grubhoffer L. Differential expression of *Ixodes ricinus* tick genes induced by blood feeding or *Borrelia burgdorferi* infection. J Med Entomol. 2005;42(1):36-41.

336. Dimopoulos G, Christophides GK, Meister S, Schultz J, White KP, Barillas-Mury C, et al. Genome expression analysis of *Anopheles gambiae:* responses to injury, bacterial challenge, and malaria infection. Proc Natl Acad Sci U S A. 2002;99(13):8814-9.

337. Lehane MJ, Aksoy S, Gibson W, Kerhornou A, Berriman M, Hamilton J, et al. Adult midgut expressed sequence tags from the tsetse fly *Glossina morsitans morsitans* and expression analysis of putative immune response genes. Genome Biol. 2003;4(10):R63.

338. Zivkovic Z, Blouin EF, Manzano-Roman R, Almazan C, Naranjo V, Massung RF, et al. *Anaplasma phagocytophilum* and *Anaplasma marginale* elicit different gene expression responses in cultured tick cells. Comp Funct Genomics. 2009:705034.

339. Dreher-Lesnick SM, Mulenga A, Simser JA, Azad AF. Differential expression of two glutathione S-transferases identified from the American dog tick, *Dermacentor variabilis.* Insect Molecular Biology. 2006;14(4):445–53.

340. de la Fuente J, Blouin EF, Manzano-Roman R, Naranjo V, Almazan C, Perez de la Lastra JM, et al. Functional genomic studies of tick cells in response to infection with the cattle pathogen, *Anaplasma marginale.* Genomics. 2007;90(6):712-22.

341. Devamanoharan PS, Santucci LA, Hong JE, Tian X, Silverman DJ. Infection of human endothelial cells by *Rickettsia rickettsii* causes a significant reduction in the levels of key enzymes involved in protection against oxidative injury. Infect Immun. 1994;62(6):2619-21.

342. Pickart CM, Rose IA. Ubiquitin carboxyl-terminal hydrolase acts on ubiquitin carboxyl-terminal amides. J Biol Chem. 1985;260(13):7903-10.

343. Rodrigues V, Fernandez B, Vercoutere A, Chamayou L, Andersen A, Vigy O, et al. Immunomodulatory Effects of *Amblyomma variegatum* Saliva on Bovine Cells:

Characterization of Cellular Responses and Identification of Molecular Determinants. Front Cell Infect Microbiol. 2017;7:521.

344. Cao Y, Li C, Zhang Q, Wang Y, Xia R. Extracellular ubiquitin enhances the suppressive effects of regulatory T cells on effector T cell responses. Clin Lab. 2014;60(12):1983-91.

345. Majetschak M, Cohn SM, Obertacke U, Proctor KG. Therapeutic potential of exogenous ubiquitin during resuscitation from severe trauma. J Trauma. 2004;56(5):991-9; discussion 9-1000.

346. Sujashvili R. Advantages of Extracellular Ubiquitin in Modulation of Immune Responses. Mediators Inflamm. 2016;2016:4190390.

347. Tran HH, Dang SNA, Nguyen TT, Huynh AM, Dao LM, Kamei K, et al. *Drosophila* Ubiquitin C-Terminal Hydrolase Knockdown Model of Parkinson's Disease. Sci Rep. 2018;8(1):4468.

348. Vancova M, Bily T, Nebesarova J, Grubhoffer L, Bonnet S, Park Y, et al. Ultrastructural mapping of salivary gland innervation in the tick *Ixodes ricinus.* Sci Rep. 2019;9(1):6860.

349. Basseres E, Coppotelli G, Pfirrmann T, Andersen JB, Masucci M, Frisan T. The ubiquitin C-terminal hydrolase UCH-L1 promotes bacterial invasion by altering the dynamics of the actin cytoskeleton. Cell Microbiol. 2010;12(11):1622-33.

350. Edelmann MJ, Kessler BM. Ubiquitin and ubiquitin-like specific proteases targeted by infectious pathogens: Emerging patterns and molecular principles. Biochim Biophys Acta. 2008;1782(12):809-16.

351. Ascenzi P, Bocedi A, Bolognesi M, Spallarossa A, Coletta M, De Cristofaro R, et al. The bovine basic pancreatic trypsin inhibitor (Kunitz inhibitor): a milestone protein. Curr Protein Pept Sci. 2003;4(3):231-51.

352. Corral-Rodriguez MA, Macedo-Ribeiro S, Barbosa Pereira PJ, Fuentes-Prior P. Tick-derived Kunitz-type inhibitors as antihemostatic factors. Insect Biochem Mol Biol. 2009;39(9):579-95.

353. Dai SX, Zhang AD, Huang JF. Evolution, expansion and expression of the Kunitz/BPTI gene family associated with long-term blood feeding in *Ixodes scapularis*. BMC Evol Biol. 2012;12:4.

354. Schwarz A, Cabezas-Cruz A, Kopecky J, Valdes JJ. Understanding the evolutionary structural variability and target specificity of tick salivary Kunitz peptides using next generation transcriptome data. BMC Evol Biol. 2014;14:4.

355. Chmelar J, Kotal J, Langhansova H, Kotsyfakis M. Protease Inhibitors in Tick Saliva: The Role of Serpins and Cystatins in Tick-host-Pathogen Interaction. Front Cell Infect Microbiol. 2017;7:216.

356. Mans BJ, Andersen JF, Schwan TG, Ribeiro JM. Characterization of anti-hemostatic factors in the argasid, *Argas monolakensis:* implications for the evolution of blood-feeding in the soft tick family. Insect Biochem Mol Biol. 2008;38(1):22-41.

357. Alim MA, Islam MK, Anisuzzaman, Miyoshi T, Hatta T, Yamaji K, et al. A hemocyte-derived Kunitz-BPTI-type chymotrypsin inhibitor, HlChI, from the ixodid tick *Haemaphysalis longicornis*, plays regulatory functions in tick blood-feeding processes. Insect Biochem Mol Biol. 2012;42(12):925-34.

358. Fogaca AC, Almeida IC, Eberlin MN, Tanaka AS, Bulet P, Daffre S. Ixodidin, a novel antimicrobial peptide from the hemocytes of the cattle tick *Boophilus microplus* with inhibitory activity against serine proteinases. Peptides. 2006;27(4):667-74.

359. Du W, Gao Z, Wang K, Zhao Y, Zheng P, Yu Z, et al. Expression and function assessment of two serpin-type serine protease inhibitors from *Haemaphysalis doenitzi.* Res Vet Sci. 2020;132:1-9.

360. Oliveira CJ, Anatriello E, de Miranda-Santos IK, Francischetti IM, Sa-Nunes A, Ferreira BR, et al. Proteome of *Rhipicephalus sanguineus* tick saliva induced by the secretagogues pilocarpine and dopamine. Ticks Tick Borne Dis. 2013;4(6):469-77.

361. Sanches GS, Villar M, Couto J, Ferrolho J, Fernandez de Mera IG, Andre MR, et al. Comparative Proteomic Analysis of *Rhipicephalus sanguineus sensu lato* (Acari: Ixodidae) Tropical and Temperate Lineages: Uncovering Differences During *Ehrlichia canis* Infection. Front Cell Infect Microbiol. 2020;10:611113.

362. McClung JK, Jupe ER, Liu XT, Dell'Orco RT. Prohibitin: potential role in senescence, development, and tumor suppression. Exp Gerontol. 1995;30(2):99-124.

363. Mishra S, Murphy LC, Murphy LJ. The Prohibitins: emerging roles in diverse functions. J Cell Mol Med. 2006;10(2):353-63.

364. Theiss AL, Idell RD, Srinivasan S, Klapproth JM, Jones DP, Merlin D, et al. Prohibitin protects against oxidative stress in intestinal epithelial cells. FASEB J. 2007;21(1):197-206.

365. Kuadkitkan A, Wikan N, Fongsaran C, Smith DR. Identification and characterization of prohibitin as a receptor protein mediating DENV-2 entry into insect cells. Virology. 2010;406(1):149-61.

366. Wintachai P, Wikan N, Kuadkitkan A, Jaimipuk T, Ubol S, Pulmanausahakul R, et al. Identification of prohibitin as a Chikungunya virus receptor protein. J Med Virol. 2012;84(11):1757-70.

367. Rachinsky A, Guerrero FD, Scoles GA. Proteomic profiling of *Rhipicephalus (Boophilus) microplus* midgut responses to infection with *Babesia bovis*. Vet Parasitol. 2008;152(3-4):294-313.

368. Li Z, Srivastava P. Heat-shock proteins. Curr Protoc Immunol. 2004;Appendix 1:Appendix 1T.

369. Lindquist S, Craig EA. The heat-shock proteins. Annu Rev Genet. 1988;22:631-77.

370. Kaufmann SH. Heat shock proteins and the immune response. Immunol Today. 1990;11(4):129-36.

371. Schlesinger JM. Heat Shock Proteins. The Journal of Biological Chemistry. 1990;265:121111-4.

372. Pockley AG. Heat shock proteins as regulators of the immune response. Lancet. 2003;362(9382):469-76.

373. Kongsuwan K, Josh P, Zhu Y, Pearson R, Gough J, Colgrave ML. Exploring the midgut proteome of partially fed female cattle tick *Rhipicephalus (Boophilus) microplus*. J Insect Physiol. 2010;56(2):212-26.

374. Busby AT, Ayllon N, Kocan KM, Blouin EF, de la Fuente G, Galindo RC, et al. Expression of heat shock proteins and subolesin affects stress responses, *Anaplasma phagocytophilum* infection and questing behaviour in the tick, *Ixodes scapularis*. Med Vet Entomol. 2012;26(1):92-102.

375. Villar M, Ayllon N, Busby AT, Galindo RC, Blouin EF, Kocan KM, et al. Expression of Heat Shock and Other Stress Response Proteins in Ticks and Cultured Tick Cells in Response to *Anaplasma* spp. Infection and Heat Shock. Int J Proteomics. 2010;2010:657261.

376. Tian Z, Liu G, Zhang L, Yin H, Wang H, Xie J, et al. Identification of the heat shock protein 70 (HLHsp70) in *Haemaphysalis longicornis*. Vet Parasitol. 2011;181(2-4):282-90.

377. Liu L, Cheng TY, Yang Y. Cloning and expression pattern of a heat shock cognate protein 70 gene in ticks (*Haemaphysalis flava*). Parasitol Res. 2017;116(6):1695-703.

378. Trinidad E-G, Cota-Guajardo SC, Sanchez-Paz A, Silva-Hidalgo G, Lopez-Valenzuela M, Carcamo-Arechiga NM. Differential expression of heat shock protein genes in *Rhipicephalus sanguineus* (Acari: Ixodidae) exposed to temperature and humidity variations. Parasitol Res. 2021;120(8):2947-51.

379. Agwunobi DO, Wang T, Zhang M, Wang T, Jia Q, Zhang M, et al. Functional implication of heat shock protein 70/90 and tubulin in cold stress of *Dermacentor silvarum*. Parasit Vectors. 2021;14(1):542.

380. Wang F, Gong H, Zhang H, Zhou Y, Cao J, Zhou J. Molecular characterization, tissue-specific expression, and RNA knockdown of the putative heat shock cognate 70 protein from *Rhipicephalus haemaphysaloides*. Parasitol Res. 2019;118(5):1363-70.

381. Lew-Tabor AE, Moolhuijzen PM, Vance ME, Kurscheid S, Valle MR, Jarrett S, et al. Suppressive subtractive hybridization analysis of *Rhipicephalus (Boophilus) microplus* larval and adult transcript expression during attachment and feeding. Vet Parasitol. 2010;167(2-4):304-20.

382. Flower DR. The lipocalin protein family: structure and function. Biochem J. 1996;318 (Pt 1):1-14.

383. Mans BJ, Louw AI, Neitz AW. The major tick salivary gland proteins and toxins from the soft tick, *Ornithodoros savignyi*, are part of the tick Lipocalin family: implications for the origins of tick toxicoses. Mol Biol Evol. 2003;20(7):1158-67.

384. Mans BJ, Neitz AW. Exon-intron structure of outlier tick lipocalins indicate a monophyletic origin within the larger lipocalin family. Insect Biochem Mol Biol. 2004;34(6):585-94.

385. Paesen GC, Adams PL, Nuttall PA, Stuart DL. Tick histamine-binding proteins: lipocalins with a second binding cavity. Biochim Biophys Acta. 2000;1482(1-2):92-101.

386. Sangamnatdej S, Paesen GC, Slovak M, Nuttall PA. A high affinity serotonin- and histamine-binding lipocalin from tick saliva. Insect Mol Biol. 2002;11(1):79-86.

387. Paesen GC, Adams PL, Harlos K, Nuttall PA, Stuart DI. Tick histamine-binding proteins: isolation, cloning, and three-dimensional structure. Mol Cell. 1999;3(5):661-71.

388. Mans BJ, Ribeiro JM, Andersen JF. Structure, function, and evolution of biogenic amine-binding proteins in soft ticks. J Biol Chem. 2008;283(27):18721-33.

389. Beaufays J, Adam B, Decrem Y, Prevot PP, Santini S, Brasseur R, et al. *Ixodes ricinus* tick lipocalins: identification, cloning, phylogenetic analysis and biochemical characterization. PLoS One. 2008;3(12):e3941.

390. Valdes JJ, Cabezas-Cruz A, Sima R, Butterill PT, Ruzek D, Nuttall PA. Substrate prediction of *Ixodes ricinus* salivary lipocalins differentially expressed during *Borrelia afzelii i*nfection. Sci Rep. 2016;6:32372.

391. Kemp DH, Bourne A. *Boophilus microplus:* the effect of histamine on the attachment of cattle-tick larvae--studies *in vivo* and *in vitro.* Parasitology. 1980;80(3):487-96.

392. Paine SH, Kemp DH, Allen JR. *In vitro* feeding of *Dermacentor andersoni* (Stiles): effects of histamine and other mediators. Parasitology. 1983;86 (Pt 3):419-28.

393. Frischknecht F, Cudmore S, Moreau V, Reckmann I, Rottger S, Way M. Tyrosine phosphorylation is required for actin-based motility of *Vaccinia* but not *Listeria* or *Shigella.* Curr Biol. 1999;9(2):89-92.

394. Ireton K. Molecular mechanisms of cell-cell spread of intracellular bacterial pathogens. Open Biol. 2013;3(7):130079.

395. Sultana H, Neelakanta G, Kantor FS, Malawista SE, Fish D, Montgomery RR, et al. *Anaplasma phagocytophilum* induces actin phosphorylation to selectively regulate gene transcription in *Ixodes scapularis* ticks. J Exp Med. 2010;207(8):1727-43.

396. Castresana J, Saraste M. Does Vav bind to F-actin through a CH domain? FEBS Lett. 1995;374(2):149-51.

397. Ayllon N, Villar M, Busby AT, Kocan KM, Blouin EF, Bonzon-Kulichenko E, et al. *Anaplasma phagocytophilum* inhibits apoptosis and promotes cytoskeleton rearrangement for infection of tick cells. Infect Immun. 2013;81(7):2415-25.

398. Cotte V, Sabatier L, Schnell G, Carmi-Leroy A, Rousselle JC, Arsene-Ploetze F, et al. Differential expression of *Ixodes ricinus* salivary gland proteins in the presence of the *Borrelia burgdorferi sensu lato* complex. J Proteomics. 2014;96:29-43.

399. Shimada O, Ishikawa H, Tosaka-Shimada H, Atsumi S. Rearrangements of actin cytoskeleton during infection with *Escherichia coli* O157 in macrophages. Cell Struct Funct. 1999;24(5):237-46.

400. Elbakri A, Nelson PN, Abu Odeh RO. The state of antibody therapy. Hum Immunol. 2010;71(12):1243-50.

401. Lipman NS, Jackson LR, Trudel LJ, Weis-Garcia F. Monoclonal versus polyclonal antibodies: distinguishing characteristics, applications, and information resources. ILAR J. 2005;46(3):258-68.

Appendix

Supplementary Table 1. Putative genes, primer sequences and PCR or qPCR conditions.

Gene	Primer	Nucleotide sequence (5'-3')	Final concentration (µM)	Annealing temperature (ºC)	Product size (bp)
ferritin	*ferritin_T7_forward* *ferritin_T7_reverse*	T7_ACGCGAGCTACGTCTACACA T7_CTTGATTGCCTTCACCTGCT	-	55	353
	ferritin_forward *ferritin_reverse*	CAGCCGATACAGAAGCCATC CAGCCGATACAGAAGCCATC	0.2	61.7[a] and 58.2[b]	125
psc	*psc_RS_forward* *psc_RS_reverse*	GCGATTTCAGGAGATCCAAC AGCCAGTCAGTTCCTCGAA	0.5	55.5	129
	psc_IDE8_forward *psc_IDE8_ reverse*	CTACAAGTTCGCTGCCACAC GAAGGTCTTGAAGCCTGTCG	0.5	55.5	146
	psc_RS_T7_forward *psc_RS_ T7_reverse*	T7_AGCGATTTCAGGAGATCCA T7_CGTTCCATGTTGACTGATG	-	64.3	400
	psc_IDE8_T7_forward *psc_IDE8_ T7_reverse*	T7_AGCTGAGAGGCGTCATCTGT T7_GTCTTGCTGTGCCAAATTGA	-	55.5	412
imp	*imp_RS_forward* *imp_RS_reverse*	GACGAAATGGTTGCTGGATT CTATGGGTGGGTGTCGTTCT	0.8	55.5	103
prohib	*prohib_RS_forward* *prohib_RS_ reverse*	CAGCAGAAGATCGTGCACTC GAGCTGGCGTTCAGGTAGAC	0.5	61.7	168
	prohib_IDE8_forward *prohib_IDE8_ reverse*				
	prohib_RS_T7_forward *prohib_RS_ T7_reverse*	T7_ACGACATTCGCTCAAGACCT T7_GAGTGCACGATCTTCTGCTG	-	55.5	442

	prohib_IDE8_T7_forward *prohib_IDE8_ T7_reverse*			60	
	phsrp20_RS_forward *phsrp20_RS_reverse*	ACCACCAGCGCTTCTACATC GGAGCGAAGTGCCTAGTGTC	0.5	60	133
	phsrp20_IDE8_forward *phsrp20_IDE8_ reverse*	GCCTAAGAACCAGCAGCAGT TCGACAGTCTTGACGGTGAT	1	62.6	147
	phsrp20_IDE8_T7_forward *phsrp20_IDE8_ T7_reverse*	T7_ACCAGCGCTTCTACATCCAG T7_CTTCGTGCTTCACCTCAAT	-	60	379
	phsrp20_RS_T7_forward *phsrp20_RS_ T7_reverse*				
ß-tubulin §	*ß-tubulin_forward* *ß-tubulin_reverse*	AACATGGTGCCCTTCCCACG GCAGCCATCATGTTCTTTGC	0.4*	58*	140
elf §	*elf_forward* *elf_reverse*	CGTCTACAAGATTGGTGGCATT CTCAGTGGTCAGGTTGGCAG	0.4*	57.2*	109
16s rDNA §§	*16S_tick_forward* *16S_tick_reverse*	GACAAGAAGACCCTA ATCCAACATCGAGGT	0.8*	57.2*	212

T7 promoter sequence: 5'-taatacgactcactatagggaga-3'
§ Nijhof et al. (2009)
§§ Zivkovic et al. (2010)
[a] Annealing temperature used for the samples of the salivary glands.
[b] Annealing temperature used for the samples of the midgut.
* Conditions used in the *ferritin 1* study.

Supplementary Table 2. Real time PCR threshold line values for each gene.

Values were manually defined to use in data analysis in *Rhipicephalus sanguineus* salivary glands and IDE8 cells with the CFX Manager™ Software (Bio-Rad).

Gene	Threshold value
ß-actin	73.99
ß-tubulin	135.27
elf	107.54
16s rDNA	106.5
psc	119.31
prohib	84.30
phsrp20	68.89

Supplementary Table 3. Separation and stacking gel preparation reagents and quantity.

Reagent	12.5% Separation Gel	Stacking Gel
Milli-Q water	2.988 ml	2.825 ml
Acrylamide 30%	3.125 ml	0.625 ml
Tris-HCL 3M; pH = 8.8	0.938 ml	-
Tris-HCL 0.5M; pH = 6.8	-	1.25 ml
SDS 10%	75 µl	50 µl
TEMED	3.75 µl	3.75 µl
APS 10%	37.5 µl	25 µl

Supplementary Table 4. Selected monoclonal antibodies for Western blot for proteomic data validation. Antibodies were acquired from Santa Cruz Biotechnology (Santa Cruz Biotechnology) and the dilution was prepared according to the manufacturer's instructions.

Antibody Designation	Santa Cruz Code	Dilution	MW (kDa)	Epitopes
Prohibitin 2 (A-2)	sc-133094	1:100	37	220-299
MDH2 (1G12)	sc-293474	1:200	36	134-246
PKAα/β/γ cat (B-4)	sc-365615	1:100	40	226-320

Supplementary Table 5. Concentration and purity of RNA extracted from the salivary glands of *Rhipicephalus sanguineus* adult female ticks for RNA-seq.

Parameters measured by spectrophotometry with NanoDrop ND-1000 (ThermoFisher Scientific). Total RNA was extracted from eight salivary glands of ticks fed on a naïve dog (1 to 8) and from ten salivary glands of ticks fed on an *Ehrlichia canis*-infected dog (9 to 18).

	Sample	**RNA Concentration (ηg/µl)**	**A_{260}/A_{280} racio**
Uninfected Samples (Pool 1)	**1**	454.29	2.27
	2	257.07	2.01
	3	394.99	2.16
	4	586.45	1.66
Uninfected Samples (Pool 2)	**5**	138.35	1.84
	6	422.26	2.21
	7	363.87	2.10
	8	164.10	1.83
Infected Samples (Pool 1)	**9**	427.02	2.17
	10	370.82	2.07
	11	341.28	2.07
	12	374.63	2.04
	13	608.82	1.66
Infected Samples (Pool 2)	**14**	740.92	1.68
	15	186.28	1.87
	16	366.62	2.10
	17	370.71	1.97
	18	244.66	1.83

Supplementary Table 6. Double-stranded RNA number of molecules calculation for *ferritin 1*-silencing in *Rhipicephalus sanguineus* adult female ticks.

Gene	Nucleotide repetition in the gene fragment sequence				Molecular weight (g/mol)	Concentration (g/µl)	Number of moles	dsRNA molecules/µl
	Adenine	Uracil	Cytosine	Guanine				
ferritin 1	97	64	106	86	113726.6	$1.69e^{-06}$	$1.49e^{-11}$	$8.95e^{12}$

Supplementary Table 7. Double-stranded RNA number of molecules for gene silencing in IDE8 cells.

Calculations were carried out for *psc*, *prohib* and *phsrp20* dsRNA and for the control *β2m* dsRNA.

Gene	Nucleotide repetition in the gene fragment sequence				Molecular weight (g/mol)	Concentration (g/µL)	Number of moles	dsRNA molecules/µL
	Adenine	Uracil	Cytosine	Guanine				
psc	102	91	119	99	132095.2	$1.69e^{-06}$	$1.28e^{-11}$	$7.71e^{12}$
prohib	90	84	143	119	140230.2	$1.13e^{-06}$	$8.08e^{-12}$	$4.86e^{12}$
phsrp20	90	55	131	102	121819.6	$1.18e^{-06}$	$9.69e^{-12}$	$5.84e^{12}$
β2m	150	139	90	68	143042.4	$4.24e^{-07}$	$2.97e^{-12}$	$1.79e^{12}$

Supplementary Table 8. Double-stranded RNA number of molecules for gene silencing of *Rhipicephalus sanguineus* nymphs.

Calculations were carried out for *psc*, *prohib* and *phsrp20* dsRNA.

Gene	Nucleotide repetition in the gene fragment sequence				Molecular weight (g/mol)	Concentration (g/µL)	Number of moles	dsRNA molecules/µL	dsRNA volume used for soaking (µL)
	Adenine	Thiamine	Cytosine	Guanine					
psc	114	97	97	89	127716.4	$9.12e^{-07}$	$7.12e^{-12}$	$4.28e^{12}$	25
prohib	101	74	145	122	142435.4	$5.60e^{-07}$	$3.93e^{-12}$	$2.37e^{12}$	20
phsrp20	90	55	131	102	121819.6	$5.55e^{-07}$	$4.56e^{-12}$	$2.75e^{12}$	10

Supplementary Table 9. BLAST results of *Rhipicephalus sanguineus ferritin* PCR-amplified ffrom the salivary glands.

The amplicon was obtained with the *ferritin_T7_forward and ferritin_T7_reverse* primers. Data was analised with Blastp (NCBI, https://www.ncbi.nlm.nih.gov).

Description	Max Score	Total Score	Query Cover	E value	Per. Iden.	accession nr.
Rhipicephalus sanguineus isolate Thai ferritin (Fer) mRNA, partial cds	540	540	92%	$2e^{-149}$	96.62%	KP688390.1
Predicted *Rhipicephalus sanguineus* soma ferritin-like (LOC 119382540), mRNA	540	540	92%	$2e^{-149}$	96.62%	XM_037650283.1
Rhipicephalus sanguineus ferritin (Fer) mRNA, complete cds	534	534	92%	$1e^{-147}$	96.31%	AY277907.1

Supplementary Table 10. Concentration and purity of salivary gland RNA extracted of *ferritin 1*-silenced and control *Rhipicephalus sanguineus* adult female ticks.

Parameters measured by spectrophotometry with NanoDrop ND-1000 (ThermoFisher Scientific). Total RNA was extracted from ticks injected with *ferritin 1* dsRNA (*ferritin 1*-silenced 1 to 19) and from the control group (control 1 to 15) with elution buffer.

Sample number	RNA Concentration (ηg/µl)	A_{260}/A_{280} racio
***ferritin 1*-silenced 1**	198.37	1.93
***ferritin 1*-silenced 2**	21.95	2.04
***ferritin 1*-silenced 3**	110.57	1.90
***ferritin 1*-silenced 4**	73.74	1.83
***ferritin 1*-silenced 5**	208.42	1.95
***ferritin 1*-silenced 6**	29.28	1.90
***ferritin 1*-silenced 7**	77.43	1.72
***ferritin 1*-silenced 8**	95.72	1.80
***ferritin 1*-silenced 9**	86.62	1.71
***ferritin 1*-silenced 10**	60.80	1.72
***ferritin 1*-silenced 11**	253.09	1.98
***ferritin 1*-silenced 12**	173.66	1.90
***ferritin 1*-silenced 13**	252.89	2.05
***ferritin 1*-silenced 14**	161.60	1.90
***ferritin 1*-silenced 15**	193.85	1.88
***ferritin 1*-silenced 16**	425.59	2.14
***ferritin 1*-silenced 17**	328.10	2.08
***ferritin 1*-silenced 18**	222.58	1.90
***ferritin 1*-silenced 19**	185.64	1.90
control 1	177.82	1.79
control 2	68.99	1.80
control 3	223.26	1.83
control 4	140.35	1.84
control 5	342.40	2.03
control 6	71.55	1.67
control 7	66.20	1.70
control 8	92.11	1.76
control 9	86.24	1.80
control 10	149.85	1.76
control 11	126.32	1.79
control 12	97.94	1.70
control 13	243.00	1.88
control 14	95.21	1.80

Control 15	82.14	1.92

Supplementary Table 11. Concentration and purity of midgut RNA extracted of *ferritin 1*-silenced and control *Rhipicephalus sanguineus* adult female ticks.

Parameters measured by spectrophotometry with NanoDrop ND-1000 (ThermoFisher Scientific). Total RNA was extracted from ticks injected with *ferritin 1* dsRNA (*ferritin 1*-silenced 1 to 11) and from the control group (control 1 to 13) with elution buffer.

Sample number	RNA Concentration (ηg/µl)	A_{260}/A_{280} racio
***ferritin 1*-silenced 1**	1481.15	1.75
***ferritin 1*-silenced 2**	430.36	2.11
***ferritin 1*-silenced 3**	214.77	1.87
***ferritin 1*-silenced 4**	307.95	1.93
***ferritin 1*-silenced 5**	388.36	2.07
***ferritin 1*-silenced 6**	565.74	1.64
***ferritin 1*-silenced 7**	899.22	1.71
***ferritin 1*-silenced 8**	868.15	1.75
***ferritin 1*-silenced 9**	982.25	1.76
***ferritin 1*-silenced 10**	346.01	2.04
***ferritin 1*-silenced 11**	393.84	1.28
control 1	222.39	2.20
control 2	163.80	1.75
control 3	207.17	1.74
control 4	292.91	1.94
control 5	264.85	1.92
control 6	435.62	1.97
control 7	203.56	1.79
control 8	68.32	1.75
control 9	281.46	1.83
control 10	170.28	1.89
control 11	404.25	1.98
control 12	342.65	1.75
control 13	94.72	1.70

Supplementary Table 12. Concentration and purity of salivary gland DNA extracted of *ferritin 1*-silenced and control *Rhipicephalus sanguineus* adult female ticks.

Parameters measured by spectrophotometry with NanoDrop ND-1000 (ThermoFisher Scientific). Genomic DNA was extracted from ticks injected with *ferritin 1* dsRNA (*ferritin 1*-silenced 1 to 19) and from the control group (control 1 to 15) with elution buffer.

Sample number	DNA Concentration (ηg/µl)	A_{260}/A_{280} racio
***ferritin 1*-silenced 1**	211.34	1.89
***ferritin 1*-silenced 2**	41.71	1.80
***ferritin 1*-silenced 3**	84,47	1.72
***ferritin 1*-silenced 4**	41.53	1.65
***ferritin 1*-silenced 5**	58.00	1.68
***ferritin 1*-silenced 6**	43.54	1.70
***ferritin 1*-silenced 7**	61.41	1.72
***ferritin 1*-silenced 8**	45.01	1.58
***ferritin 1*-silenced 9**	77.53	1.61
***ferritin 1*-silenced 10**	26.16	1.60
***ferritin 1*-silenced 11**	53.11	1.63
***ferritin 1*-silenced 12**	25.01	1.56
***ferritin 1*-silenced 13**	36.42	1.70
***ferritin 1*-silenced 14**	27.53	1.53
***ferritin 1*-silenced 15**	66.24	1.63
***ferritin 1*-silenced 16**	43.86	1.65
***ferritin 1*-silenced 17**	25.22	1.80
***ferritin 1*-silenced 18**	36.06	1.74
***ferritin 1*-silenced 19**	36.72	1.66
control 1	31.53	1.69
control 2	52.52	1.56
control 3	69.74	1.50
control 4	36.77	1.70
control 5	57.42	1.63
control 6	37.93	1.69
control 7	43.56	1.52
control 8	31.11	1.44
control 9	53.85	1.53
control 10	25.48	1.44
control 11	36.45	1.84
control 12	46.39	1.60

control 13	63.59	1.69
control 14	40.02	1.83
control 15	38.45	1.79

Supplementary Table 13. Concentration and purity of midgut DNA extracted of *ferritin 1*-silenced and control *Rhipicephalus sanguineus* adult female ticks.

Parameters measured by spectrophotometry with NanoDrop ND-1000 (ThermoFisher Scientific). Genomic DNA was extracted from ticks injected with *ferritin 1* dsRNA (*ferritin 1*-silenced 1 to 11) and from the control group (control 1 to 13) with elution buffer.

Sample number	DNA Concentration (ηg/µl)	A_{260}/A_{280} racio
***ferritin 1*-silenced 1**	7.93	1.61
***ferritin 1*-silenced 2**	18.62	1.61
***ferritin 1*-silenced 3**	33.74	1.59
***ferritin 1*-silenced 4**	198.22	1.66
***ferritin 1*-silenced 5**	9.13	1.50
***ferritin 1*-silenced 6**	113.44	1.59
***ferritin 1*-silenced 7**	17.35	1.51
***ferritin 1*-silenced 8**	50.19	1.54
***ferritin 1*-silenced 9**	68.81	1.51
***ferritin 1*-silenced 10**	21.09	1.43
***ferritin 1*-silenced 11**	76.38	1.58
control 1	112.30	1.46
control 2	117.98	1.53
control 3	48.64	1.61
control 4	26.72	1.52
control 5	15.33	1.63
control 6	29.58	1.54
control 7	19.82	1.44
control 8	14.37	1.37
control 9	14.71	1.48
control 10	19.71	1.52
control 11	480.62	2.00
control 12	18.98	1.56
control 13	20.27	1.45

Supplementary Table 14. BLAST results of *Rhipicephalus sanguineus ferritin 1* fragments PCR-amplified from the salivary glands and midgut.

The amplicon was obtained with the *ferritin_ forward and ferritin_ reverse* primers. Data was analised with Blastn (NCBI, https://www.ncbi.nlm.nih.gov).

Description	Max Score	Total Score	Query Cover	E value	Per. Iden.	accession nr.
Rhipicephalus sanguineus isolate Thai ferritin (Fer) mRNA, partial cds	134	134	98%	$1e^{-27}$	100.00%	KP688390.1
Predicted *Rhipicephalus sanguineus* soma ferritin-like (LOC 119382540), mRNA	134	134	98%	$1e^{-27}$	100.00%	XM_037650283.1
Rhipicephalus sanguineus ferritin (Fer) mRNA, complete cds	134	134	98%	$1e^{-27}$	100.00%	AY277907.1

Supplementary Table 15. BLAST results of *Rhipicephalus sanguineus β-actin*, *β-tubulin* and *16S* rDNA PCR-amplified.

The amplicons were obtained with the *β-actin_forward* and *β-actin_reverse*, and *β-tubulin_forward* and *β-tubulin_reverse* primers by Nijhof et al. (2009), and *16S_forward* and *16S_reverse* by Zivkovic et al. (2010), with salivary gland and midgut cDNA. Data was analised with Blastp (NCBI, https://www.ncbi.nlm.nih.gov).

Description	Target	Max Score	Total Score	Query Cover	E value	Per. Iden.	accession nr.
Predicted *Rhipicephalus sanguineus* actin, clone 403 (LOC119400476), mRNA	*β-actin*	327	327	83%	$1e^{-88}$	98.39%	XM_037667534.1
Predicted *Rhipicephalus sanguineus* tubulin beta chain (LOC119375769), transcript X2, mRNA	*β-tubulin*	178	178	98%	$1e^{-40}$	100.00%	XM_037645905.1
Rhipicephalus sanguineus isolate 3 *16S* ribosomal RNA gene, partial sequence; mitochondrial	*16S* rDNA	324	324	86%	$4e^{-88}$	100.00%	MH765331.1

Supplementary Table 16. *Rhipicephalus sanguineus* body weights after *ferritin 1*-silencing.
Ticks were injected with *ferritin 1* dsRNA (*ferritin 1*-silenced 1 to 19) or elution buffer (control 1 to 13) and the weight determined after natural drop-off.

Weight after detachment mg/tick		
Sample number	**Control**	***ferritin 1*-silenced**
1	89.1	115.2
2	157.6	98.3
3	54.8	129.6
4	110	61.2
5	101.4	69.2
6	136.3	116.8
7	97	142
8	188.9	81.2
9	85.1	72.6
10	96.5	65.6
11	175.7	95.5
12	175.3	92.8
13	149.2	56.6
14	-	50
15	-	99.1
16	-	37.9
17	-	14.6
18	-	27.2
19		19.6

Supplementary Table 17. Concentration and purity of DNA extracted from the salivary glands of *Rhipicephalus sanguineus* adult female ticks.

Parameters measured by spectrophotometry with NanoDrop ND-1000 (ThermoFisher Scientific). Genomic DNA was extracted from salivary glands of ticks fed on a naïve dog (1 to 8) and from salivary glands of ticks fed on an *Ehrlichia canis*-infected dg (9 to 18).

	Sample number	**A_{260}/A_{280} racio**	**DNA Concentration (ηg/µl)**
Uninfected Samples (Pool 1)	**1**	1.42	28.77
	2	1.60	41.56
	3	1.47	22.10
	4	1.55	17.16
Uninfected Samples (Pool 2)	**5**	1.49	18.38
	6	1.45	25.18
	7	1.57	16.57
	8	1.38	27.83
Infected samples (Pool 1)	**9**	1.71	30.55
	10	1.78	22.27
	11	1.58	31.10
	12	1.55	29.69
	13	1.60	44.80
Infected Samples (Pool 2)	**14**	1.55	41.18
	15	1.76	37.55
	16	1.81	23.25
	17	1.58	37.46
	18	1.64	44.00

Supplementary Table 18. Gene ontology functional annotation of the differentially expressed transcripts obtained by RNA-seq of *Rhipicephalus sanguineus* salivary glands during *Ehrlichia canis* infection.

Statistical analysis was conducted to detect significant differences ($p < 0.05$) using the X^2 to compare the gene expression data between uninfected and *E. canis*-infected salivary glands. Annotation was carried out in different levels: Molecular Function (MF), Biological Process (BP) and Cellular Component (CC) using UniProtKB databse (http://www.UniProt.org/). Expression levels were determined by Log2 fold-change$_{(infected/uninfected)}$ of transcript reads. Highlighted in red are the downregulated transcripts and highlighted in green the upregulated transcripts. NA: not available.

UniProtKB	Description	Gene	Biological Process	GO: BP	Molecular Function	GO: MF	Cellular Component	GO: CC	Domains	Fold Change (i/ni)	Log2 (Fold Change)
Q6JVN0	Glutathione S-transferase	GST (Similar to ISCW022157)	Metabolic process	8152	Glutathione transferase activity	4364	Cytoplasm	5737	Glutathione-S-Trfase_C-like; GST_C;Thioredoxin-like_fold	0.270096463	-1.888453347
L7M3C8	Ubiquitin carboxyl-terminal hydrolase	Unknown	Ubiquitin-dependent protein catabolic process	6511	Omega peptidase activity; ubiquitin-specific protease activity	8242; 4843	Intracellular	5622	Peptidase_C12_UCH; Ubiquitinyl_hydrolase_UCH37	0.736842105	-0.440572591
L7MCD9	Putative trilaris	Unknown	Unknown	NA	Serine-type endopeptidase inhibitor activity	4867	Unknown	*NA*	Kunitz_BPTI	0.848	-0.23786383
G3MH55	Putative uncharacterized protein	Similar to ISCW004923	Protein N-linked glycosylation	6487	Oligosaccharyl transferase activity	4576	Integral component of membrane	16021	OligosaccharylTrfase_OST3/OST6	0.872517617	-0.196743834
B7QAF5	Putative uncharacterized protein	IscW_ISCW013207	Unknown	NA	Unknown	NA	Unknown	*NA*	*NA*	0.877112135	-0.189166798
G3MNA8	Protein kish	Unknown	Unknown	NA	Unknown	NA	Integral component of membrane; Golgi membrane	16022; 139	DUF1242	0.884543762	-0.176994575
L7MF27	Putative mitochondrial import inner membrane	Unknown	Protein import into mitochondrial matrix	30150	Unknown	NA	Integral component of membrane; mitochondrial inner membrane	16021; 5744	Tim21	1.362445415	0.446198431

	translocase subunit tim21						presequence translocase complex				
B7PEW5	Mitochondrial import inner membrane translocase, subunit TIM23, putative	IscW_ISCW004474	Intracellular protein transport	6886	P-P-bond-hydrolysis-driven protein transmembrane transporter activity	15450	Integral component of membrane	16021	Tim17/Tim22/Tim23/PMP24	1.573880597	0.654326094
L7M4M0	Importin subunit α	Unknown	Protein import into nucleus	6606	Protein transporter activity	8565	Cytoplasm; nucleus	5737; 5634	ARM-like; Importin-a_IBB; Importing_su_alpha	1.899320815	0.925483612
L7MH00	Putative serine carboxypeptidase	Unknown	Unknown	NA	Serine-type carboxypeptidase activity	4185	Unknown	*NA*	AB_hydrolase; Peptidase_S10	1.945005945	0.959774565

Supplementary Table 19. BLAST results of *Rhipicephalus sanguineus imp* and *psc* PCR-amplified.

The amplicons were obtained with the primers *imp_RS_forward and imp_RS_reverse* and *psc_RS_forward and psc_RS_reverse* with *R. sanguineus* salivary gland cDNA. Data was analised with Blastp (NCBI, https://www.ncbi.nlm.nih.gov).

Description	Max Score	Total Score	Query Cover	E value	Per. Iden.	accession nr.
PREDICTED: *Rhipicephalus sanguineus* importin subunit α-1-like (LOC119396188), mRNA	730	730	90%	0.0	99.02%	XM_0376633282.1
PREDICTED: *Rhipicephalus microplus* importin subunit α-5-like (LOC119174394), mRNA	597	597	90%	$4e^{-166}$	93.15%	XM_037425276.1
PREDICTED: *Dermacentor silvarum* importin subunit α-5-like (LOC119461449), mRNA	486	486	87%	$8e^{-133}$	89.20%	XM_037733764.1
PREDICTED: *Rhipicephalus sanguineus* probable serine carboxypeptidase CPVL (LOC119372059), mRNA	656	656	56%	0.0	96.95%	XM_037642511.1
PREDICTED: *Rhipicephalus sanguineus* probable serine carboxypeptidase CPVL (LOC119406464), mRNA	656	656	56%	0.0	96.95%	XM_037673211.1

Supplementary Table 20. Concentration and purity of RNA extracted from IDE8 cells for *psc*-silencing gene expression analysis.

Total RNA was extracted at time points (T1) – 48 h, (T2) – 120 h and (T3) – 160 h, from cells inoculated with *psc* dsRNA and or with *β2m* dsRNA, as control. Parameters measured by spectrophotometry with NanoDrop ND-1000 (ThermoFisher Scientific).

	Sample number	**RNA Concentration (ηg/µl)**	**A_{260}/A_{280} racio**
T1	***psc a1 1***	85.64	1.90
	psc a1 2	131.70	1.81
	psc a1 3	82.25	1.71
	psc a1 4	134.61	1.82
	psc b1 1	120.20	1.81
	psc b1 2	84.47	1.86
	psc b1 3	147.73	1.83
	psc b1 4	128.15	1.82
	psc c1 1	56.59	1.74
	psc c1 2	156.74	1.81
	psc c1 3	91.76	1.78
	psc c1 4	98.35	1.72
	β2m a1 1	99.97	1.86
	β2m a1 2	104.98	1.81
	β2m a1 3	76.29	1.79
	β2m a1 4	-0.36*	1.52
	β2m b1 1	99.38	1.95
	β2m b1 2	109.89	1.83
	β2m b1 3	111.13	1.83
	β2m b1 4	88.14	1.85
	β2m c1 1	26.71	1.70

	β2m c1 2	41.06	1.76
	β2m c1 3	15.85	1.82
	β2m c1 4	16.02	2.13
T2	***psc a2 1***	197.17	1.92
	psc a2 2	319.03	1.95
	psc a2 3	237.80	1.95
	psc a2 4	344.44	1.96
	psc b2 1	249.14	1.95
	psc b2 2	106.84	1.81
	psc b2 3	231.60	1.90
	psc b2 4	212.99	1.86
	psc c2 1	244.46	1.89
	psc c2 2	302.06	1.89
	psc c2 3	257.37	1.89
	psc c2 4	210.11	1.87
	β2m a2 1	351.63	2.00
	β2m a2 2	292.08	1.95
	β2m a2 3	202.34	1.96
	β2m a2 4	395.09	2.06
	β2m b2 1	198.61	1.91
	β2m b2 2	278.47	1.98
	β2m b2 3	278.28	2.04
	β2m b2 4	328.88	2.03
	β2m c2 1	308.00	2.01
	β2m c2 2	304.13	1.98
	β2m c2 3	125.75	1.69
	β2m c2 4	185.82	1.91

T3	***psc a3 1***	265.89	2.03
	psc a3 2	180.04	1.88
	psc a3 3	213.42	1.95
	psc a3 4	100.99	1.78
	psc b3 1	13.89	2.17
	psc b3 2	155.05	1.87
	psc b3 3	82.62	1.79
	psc b3 4	83.32	1.80
	psc c3 1	92.04	1.80
	psc c3 2	9.64	1.90
	psc c3 3	352.10	2.11
	psc c3 4	55.89	1.79
	β2m a3 1	379.10	2.06
	β2m a3 2	228.04	1.92
	β2m a3 3	393.33	2.02
	β2m a3 4	128.05	1.85
	β2m b3 1	96.93	1.87
	β2m b3 2	161.78	1.93
	β2m b3 3	164.00	1.97
	β2m b3 4	200.10	1.95
	β2m c3 1	340.21	2.12
	β2m c3 2	115.51	1.94
	β2m c3 3	92.73	1.93
	β2m c3 4	80.44	1.97

* Sample excluded from the study.

Supplementary Table 21. Concentration and purity of RNA extracted from *Rhipicephalus sanguineus* salivary glands for *psc*-silencing gene expression analysis.

Total RNA was extracted from nymphs soaked with *psc* dsRNA (*psc* 1 to 12) and from the control group soaked in PBS (PBS 1 to 12). Parameters measured by spectrophotometry with NanoDrop ND-1000 (ThermoFisher Scientific).

Sample number	RNA Concentration (ηg/µl)
psc 1	2.66
psc 2	9.44
psc 3	3.18
psc 4	6.88
psc 5	15.58
psc 6	8.70
psc 7	4.08
psc 8	5.77
psc 9	6.06
psc 10	7.79
psc 11	0.75
psc 12	0.41
PBS 1	9.87
PBS 2	2.48
PBS 3	7.28
PBS 4	12.78
PBS 5	18.79
PBS 6	4.62
PBS 7	1.94
PBS 8	2.70
PBS 9	2.38
PBS 10	0.15

PBS 11	1.74
PBS 12	9.65

Supplementary Table 22. *Rhipicephalus sanguineus* proteome data of fed uninfected and fed *Ehrlichia canis*-infected salivary glands determined by LC-MS/MS.
A total of 432 tick proteins were found and the Student's *t* test was used to perform two-sample comparisons between the averaged area sums of all the transitions derived for each protein across the replicate runs, in order to identify proteins that were significantly differentially represented between the two groups ($p < 0.05$). Comparison of protein representation was determined by Log2 fold-change$_{(infected/uninfected)}$. Highlighted in blue are the *p* values where $p < 0.05$ for 69 identified proteins; highlighted in green are the Log2 (fold change) values of overexpressed proteins; highlighted in red are the Log2 (fold change) values of those underexpressed.

Peak Name	Group	*t*-value	*p*-value	Mean 1	Mean 2	Median 1	Median 2	Sigma 1	Sigma 2	Delta	Fold Change	Log2 (Fold Change)
tr|A0A023FY19|A0A023FY19_9ACAR	Aconitate hydratase, mitochondrial (Fragment) OS=Amblyomma parvum PE=2 SV=1	11.53001486	0.00032	6752.199917	1419.442656	6836.691015	1593.04914	559.0546556	573.7654754	5332.757262	4.756937443	0.67732744
tr|A0A0C9SC52|A0A0C9SC52_AMBAM	Putative pyruvate dehydrogenase e1 alpha subunit (Fragment) OS=Amblyomma americanum PE=2 SV=1	11.5035526	0.00033	1944.812534	645.302097 2	1959.469937	583.4262862	108.52974	162.8043418	1299.510437	3.013801664	0.479114668
tr|L7M716|L7M716_9ACAR	Putative ribosomal protein s9 OS=Rhipicephalus pulchellus PE=2 SV=1	8.459886565	0.00107	29475.50938	12881.0629	30733.86583	13332.06298	3165.466996	1234.014863	16594.44648	2.288282389	0.359509618
tr|L7MIP5|L7MIP5_9ACAR	Putative dihydroorotase (Fragment) OS=Rhipicephalus pulchellus PE=2 SV=1	7.935840716	0.00137	6103.533612	2425.881212	6212.709789	2305.821743	656.9947269	461.1301453	3677.652401	2.516006795	0.40071181
tr|G3MMG2|G3MMG2_9ACAR	40S ribosomal protein S4 OS=Amblyomma maculatum PE=2 SV=1	7.596226203	0.00161	21057.88116	6520.225754	19629.20376	5900.80937	3090.057175	1199.764351	14537.65541	3.22962455	0.509152038
tr|A0A023FXS2|A0A023FXS2_9ACAR	Putative phosphoglycerate mutase (Fragment) OS=Amblyomma parvum PE=2 SV=1	7.562055297	0.00164	7345.704895	1432.832072	7418.281561	1696.427677	1248.575871	524.6182162	5912.872823	5.126703288	0.709838183
tr|A0A034WYZ2|A0A034WYZ2_RHIMP	Actin-depolymerizing factor 1 OS=Rhipicephalus microplus PE=4 SV=1	-6.50919346	0.00287	13137.78824	99817.38408	7146.190278	101852.6537	10570.511	20500.02063	-86679.59584	0.131618238	-0.880683927
tr|L7M5P4|L7M5P4_9ACAR	Putative prohibitin-like protein OS=Rhipicephalus pulchellus PE=2 SV=1	6.474703816	0.00293	3676.609085	1617.070042	3885.394409	1559.530569	503.7820631	223.0415348	2059.539043	2.273623894	0.356718625
tr|L7MD67|L7MD67_9ACAR	Putative glycine rich protein (Fragment) OS=Rhipicephalus pulchellus PE=2 SV=1	6.460473001	0.00296	9176.669492	1730.039286	9353.661665	2135.232186	1236.750617	1567.23246	7446.630205	5.304312778	0.724629125
tr|A0A023GNW6|A0A023GNW6_9ACAR	Transketolase (Fragment) OS=Amblyomma triste PE=2 SV=1	6.319276394	0.00321	3540.934511	1402.275846	3537.27066	1264.392144	317.2985492	492.8839271	2138.658665	2.525134068	0.402284441
tr|A0A0C9R2A0|A0A0C9R2A0_AMBAM	Putative adp/atp translocase OS=Amblyomma americanum PE=2 SV=1	6.292596405	0.00326	16167.59294	6681.268237	14918.555926	6590.841891	2533.840321	630.6034111	9486.3247	2.419838923	0.383786458

tr|L7M8C7|L7M8C7_9ACAR	Phosphoglycerate kinase OS=Rhipicephalus pulchellus PE=2 SV=1	6.207510296	0.00343	11332.25265	2670.084426	11449.73588	3021.09059	2184.926779	1033.34383	8662.168221	4.244155179	0.627791255
tr|V5GYK8|V5GYK8_IXORI	Putative spectrin beta chain OS=Ixodes ricinus PE=2 SV=1	5.039557469	0.00728	5859.0765	2807.775396	6187.133047	2905.653493	782.6394143	698.0383119	3051.301104	2.086732617	0.319466804
tr|L7M5Q3|L7M5Q3_9ACAR	Putative lateral inhibition OS=Rhipicephalus pulchellus PE=2 SV=1	4.958453842	0.00771	4617.079443	2314.753466	4288.478097	2250.499089	642.6036768	483.5794442	2302.325977	1.994631183	0.299862604
tr|J9P0I1|J9P0I1_CANLF	Keratin, type I cytoskeletal 9 OS=Canis lupus familiaris GN=KRT9 PE=4 SV=1	-4.877949737	0.00817	19161.55404	87182.28415	22816.78278	91736.16909	10430.2168	21784.411	-68020.730011	0.219787245	-0.657997515
tr|G3MKI7|G3MKI7_9ACAR	Putative uncharacterized protein OS=Amblyomma maculatum PE=2 SV=1	4.856967835	0.0083	22267.40966	5190.795942	25161.64377	4117.228798	5575.34641	2449.525067	17076.61372	4.289787137	0.632435743
tr|A0A023FJS3|A0A023FJS3_9ACAR	Putative ribosomal protein (Fragment) OS=Amblyomma cajennense PE=2 SV=1	4.844633947	0.00837	56567.4672	8221.671159	50338.19697	7650.316989	17121.05167	2371.849049	48345.79604	6.880288217	0.837606631
tr|Q4PM27|Q4PM27_IXOSC	Ribosomal protein L11 OS=Ixodes scapularis GN=IscW_ISCW000476 PE=2 SV=1	4.787183345	0.00873	23415.93163	10278.12239	25916.08094	9736.148693	4519.59982	1472.393033	13137.80924	2.278230473	0.357597657
tr|V5IFY7|V5IFY7_IXORI	Putative mitochondrial adp/atp carrier OS=Ixodes ricinus PE=2 SV=1	4.664731116	0.00956	48972.02011	15097.77405	50497.37261	18990.9259	4453.109566	11763.08255	33874.24606	3.2436583	0.511035098
tr|Q4PM40|Q4PM40_IXOSC	Ubiquitin/ribosomal protein S27a fusion protein OS=Ixodes scapularis PE=2 SV=1	4.556804379	0.01036	44541.80016	22435.82021	45813.45734	23466.12443	4359.684232	7183.010866	22105.97995	1.985298498	0.297825814
tr|A0A0A7DS56|A0A0A7DS56_RHIMP	Pyruvate kinase OS=Rhipicephalus microplus PE=2 SV=1	4.495952128	0.01086	30406.3056	7578.368693	31885.79653	7049.906242	7096.263879	5194.641061	22827.9369	4.012249447	0.603387926
tr|L7MHL1|L7MHL1_9ACAR	Putative puromycin-sensitive aminopeptidase (Fragment) OS=Rhipicephalus pulchellus PE=2 SV=1	4.342488276	0.01223	13027.51822	5455.442126	14059.08746	5163.775502	2716.642057	1319.665122	7572.076097	2.38798578	0.378031736
tr|L7M591|L7M591_9ACAR	Putative endocytosis/signaling protein ehd1 OS=Rhipicephalus pulchellus PE=2 SV=1	4.302162847	0.01262	5840.90613	1616.580678	6334.024675	1509.085878	1538.778316	724.2842017	4224.325451	3.613123804	0.557882843
tr|A0A023GNW2|A0A023GNW2_9ACAR	Sodium/potassium-transporting ATPase subunit alpha OS=Amblyomma triste PE=2 SV=1	4.223586878	0.01344	2907.827145	975.025493	3100.924554	877.0397388	729.0528255	311.0187417	1932.801652	2.982308838	0.474552616
tr|B7Q368|B7Q368_IXOSC	High-density lipoprotein-binding protein, putative OS=Ixodes scapularis GN=IscW_ISCW008601 PE=4 SV=1	4.194289029	0.01376	2640.408283	411.3128307	2797.711851	262.2958889	878.8210899	273.9007592	2229.095452	6.419464909	0.807498829
tr|L7M741|L7M741_9ACAR	Putative hydroxyacyl-coenzyme a dehydrogenase/3-ketoacyl-coenzyme a thiolase/enoyl-coenzyme a hydrat OS=Rhipicephalus pulchellus PE=2 SV=1	4.152065264	0.01424	16393.75939	4079.767221	19034.21384	4344.133999	4898.262354	1547.276596	12313.99217	4.018307541	0.604043172
tr|G3MNV3|G3MNV3_9ACAR	Putative uncharacterized protein OS=Amblyomma maculatum PE=2 SV=1	4.065109853	0.01528	10238.16945	2102.969061	9540.794105	1721.330563	2968.021343	1790.406803	8135.200385	4.868435602	0.68738943

tr|L7LQP4|L7LQP4_9ACAR	Putative salivary lipocalin OS=Rhipicephalus pulchellus PE=2 SV=1	4.025060684	0.0158	17908.32615	4923.214069	20226.84254	5481.958803	5412.726349	1387.408429	12985.11208	3.637527416	0.560806275
tr|A0A023FVZ8|A0A023FVZ8_9ACAR	Putative 40s ribosomal protein OS=Amblyomma parvum PE=2 SV=1	4.025144521	0.0158	6079.383701	2568.867842	6304.000802	3100.314338	696.405638	1340.499138	3510.515859	2.366561487	0.374117793
tr|V5HGA0|V5HGA0_IXORI	40S ribosomal protein S24 OS=Ixodes ricinus PE=2 SV=1	4.023968751	0.01581	2555.31251	365.1627065	2041.189749	385.7597011	935.695521	114.8178437	2190.149804	6.997736804	0.844957604
tr|L7MIQ1|L7MIQ1_9ACAR	Putative 26s proteasome regulatory complex subunit (Fragment) OS=Rhipicephalus pulchellus PE=2 SV=1	4.011728934	0.01597	11049.63687	6805.351643	11192.80415	6815.162696	1492.652823	1062.959722	4244.285231	1.623668762	0.210497435
tr|L7MEG0|L7MEG0_9ACAR	Putative heat shock protein (Fragment) OS=Rhipicephalus pulchellus PE=2 SV=1	3.966906814	0.01658	73499.10919	32903.908	67742.47221	27300.30766	13674.11426	11277.85457	40595.20119	2.233750143	0.349034593
tr|E2R8Z5|E2R8Z5_CANLF	Uncharacterized protein OS=Canis lupus familiaris GN=KRT5 PE=3 SV=2	-3.961854423	0.01665	3048.6743	7867.482356	2880.870769	7639.297415	1776.843429	1131.809536	-4818.808055	0.387503163	-0.411724748
tr|Q86G64|Q86G64_DERVA	40S ribosomal protein S5 OS=Dermacentor variabilis PE=2 SV=1	3.936676987	0.01701	2905.494932	1349.154441	2671.653951	1387.753577	640.9997905	240.8510315	1556.340491	2.153567334	0.333158455
tr|L7M653|L7M653_9ACAR	Uncharacterized protein OS=Rhipicephalus pulchellus PE=2 SV=1	3.932854136	0.01706	2203.976751	1275.687353	2271.338454	1079.028554	216.8598422	346.5670417	928.2893982	1.727677825	0.237462759
tr|F1PYU9|F1PYU9_CANLF	Keratin, type I cytoskeletal 10 OS=Canis lupus familiaris GN=KRT10 PE=3 SV=2	-3.856983143	0.01819	77944.84396	27845.3281	95699.49084	304891.5817	37811.64168	81718.07808	-200508.2841	0.279920877	-0.552964709
tr|L7MEH0|L7MEH0_9ACAR	Ribosomal protein L19 (Fragment) OS=Rhipicephalus pulchellus PE=2 SV=1	3.842032553	0.01843	4949.803944	413.1891866	4223.165004	353.65287	2031.417761	236.8589693	4536.614757	11.97950988	1.07843905
tr|A0A0C9SA10|A0A0C9SA10_AMBAM	Putative ribosomal protein l37a OS=Amblyomma americanum PE=2 SV=1	3.832749609	0.01857	1636.432652	876.8806627	1581.553413	885.3553805	336.0381607	69.981174 99	759.5519896	1.866197673	0.270957644
tr|A0A023FNH1|A0A023FNH1_9ACAR	Putative vigilin (Fragment) OS=Amblyomma cajennense PE=2 SV=1	3.813427176	0.01888	3951.24899	1626.258619	4002.14789	1800.584649	545.9498485	903.9287266	2324.990372	2.429655987	0.385544787
tr|G3MKE7|G3MKE7_9ACAR	Putative uncharacterized protein OS=Amblyomma maculatum PE=2 SV=1	3.775931275	0.0195	10439.91352	1840.26766	9563.012342	980.0243323	3630.248019	1543.431863	8599.645858	5.673040801	0.753815907
tr|A0A023FEI8|A0A023FEI8_9ACAR	Putative 60s ribosomal protein l14 OS=Amblyomma cajennense PE=2 SV=1	3.659341697	0.02159	14165.37149	2518.429606	13560.10507	2781.929427	5319.560427	1446.674686	11646.94188	5.624684309	0.750098152
tr|L7M3F2|L7M3F2_9ACAR	Putative ribosomal protein l18 OS=Rhipicephalus pulchellus PE=2 SV=1	3.561332132	0.02356	23344.51982	7436.139027	23036.77013	4585.163154	4372.608617	6382.937001	15908.38079	3.139333428	0.496837444
tr|L7MJY0|L7MJY0_9ACAR	Putative talin (Fragment) OS=Rhipicephalus pulchellus PE=2 SV=1	3.525008967	0.02434	1180.127872	294.5553382	1007.996629	196.9702976	388.0057135	196.9631692	885.5725335	4.006472533	0.60276217

tr|B7Q304|B7Q304_IXOSC	Misexpression suppressor of KSR, putative OS=Ixodes scapularis GN=IscW_ISCW010241 PE=4 SV=1	3.523963066	0.02436	25809.47099	12014.754	26776.61501	12860.0158	4669.521722	4915.952384	13794.71699	2.148148102	0.33206422
tr|L7M642|L7M642_9ACAR	Putative zinc-binding oxidoreductase OS=Rhipicephalus pulchellus PE=2 SV=1	3.487665489	0.02518	12922.62505	6869.49814	13039.1896	7560.039877	2453.660558	1736.743194	6053.126906	1.881159989	0.274425733
tr|O97115|O97115_AMBAM	CAMP-dependent protein kinase catalytic subunit isoform 2 OS=Amblyomma americanum GN=APK-C2 PE=2 SV=1	3.453486779	0.02597	4524.393359	1667.324317	4225.469779	1624.51733	1242.948611	712.9893402	2857.069041	2.713565268	0.433540272
tr|C9W1S4|C9W1S4_RHISA	Signal peptidase (Fragment) OS=Rhipicephalus sanguineus PE=2 SV=1	-3.452510704	0.02599	748.1721403	7916.859807	664.4522477	6994.796051	793.3520424	3507.780283	-7168.687667	0.094503649	-1.024551422
tr|L7MB04|L7MB04_9ACAR	Putative thiol-disulfide isomerase and thioredoxin OS=Rhipicephalus pulchellus PE=2 SV=1	3.424123542	0.02668	25040.91556	13889.2024	27191.97344	13717.26434	5568.740535	899.7361542	11151.71316	1.802905224	0.255972897
tr|C9W1P9|C9W1P9_RHISA	40S ribosomal protein S8 OS=Rhipicephalus sanguineus PE=2 SV=1	3.401621738	0.02724	29182.03302	7492.074825	23249.22219	7569.474979	11043.06709	156.5111789	21689.9582	3.895053601	0.590513438
tr|A0A023FU84|A0A023FU84_9ACAR	Ribosomal protein L15 OS=Amblyomma parvum PE=2 SV=1	3.379532728	0.0278	17592.71805	5619.389675	15580.42137	4054.230784	4503.310267	4168.513382	11973.32837	3.130716868	0.495643793
tr|C9W1D7|C9W1D7_RHISA	Ribosomal protein L22 OS=Rhipicephalus sanguineus PE=2 SV=1	3.361415355	0.02827	17471.60846	5469.730336	16602.52288	6198.59647	3432.573826	5144.170932	12001.87812	3.194235801	0.504366973
tr|G1K265|G1K265_CANLF	Lysozyme OS=Canis lupus familiaris GN=LYZ PE=2 SV=1	-3.347602982	0.02863	788.763183 6	5438.24862	785.74914	6723.213369	44.43284133	2405.23481	-4649.485436	0.145039927	-0.838512427
tr|F1PTS8|F1PTS8_CANLF	Uncharacterized protein (Fragment) OS=Canis lupus familiaris GN=KRT6A PE=3 SV=1	-3.347273923	0.02864	38850.10083	130729.2006	48151.62375	123491.4268	18930.35434	43611.62181	-91879.09975	0.297179977	-0.526980455
tr|L7M9B9|L7M9B9_9ACAR	Putative amblyomma 40-33 family member OS=Rhipicephalus pulchellus PE=2 SV=1	3.333746266	0.029	91828.90969	32713.24973	85692.15064	31012.98978	12651.1178	27987.03315	59115.65995	2.807086133	0.448255739
tr|A0A0C9S201|A0A0C9S201_AMBAM	40S ribosomal protein S6 OS=Amblyomma americanum PE=2 SV=1	3.330684075	0.02909	5403.193426	1960.876867	5143.934089	1392.683373	1469.282755	1022.583262	3442.316559	2.755498581	0.440200192
tr|A0A023FNV6|A0A023FNV6_9ACAR	Putative glycyl-trna synthetase OS=Amblyomma cajennense PE=2 SV=1	3.264111591	0.03096	4306.11899	2046.280804	4088.807654	1716.11673	708.8006614	967.2428729	2259.838186	2.104363674	0.323120796
tr|L7M8Y4|L7M8Y4_9ACAR	Malate dehydrogenase OS=Rhipicephalus pulchellus PE=2 SV=1	3.237046631	0.03176	7517.193617	1406.474765	8322.956403	1507.060698	3190.64673	714.506843	6110.718852	5.344705645	0.727923792
tr|B7P9E4|B7P9E4_IXOSC	Sodium/potassium-transporting ATPase subunit alpha (Fragment) OS=Ixodes scapularis GN=IscW_ISCW002538 PE=3 SV=1	3.212848 34	0.0325	2904.917115	668.4256897	3293.606587	262.3853279	853.5151202	851.5947236	2236.491425	4.345908841	0.638080612
tr|L7M9V8|L7M9V8_9ACAR	Putative proline and glutamine-rich splicing factor sfpq OS=Rhipicephalus pulchellus PE=2 SV=1	3.212662052	0.03251	13738.58395	5888.562987	14510.0132	5603.575661	4198.154528	535.7549386	7850.020963	2.333096204	0.367932647

tr|F1Q0R0|F1Q0R0_CANLF	Uncharacterized protein OS=Canis lupus familiaris GN=KRT14 PE=3 SV=2	-3.189757279	0.03322	1499.708951	6170.179873	1490.103323	7162.250678	1161.479336	2254.481904	-4670.470922	0.243057574	-0.614290841
tr|L7M955|L7M955_9ACAR	Putative vesicle coat complex copii subunit sec31 OS=Rhipicephalus pulchellus PE=2 SV=1	3.170766813	0.03383	4109.790043	2151.182237	4618.010648	1959.098798	987.13726	412.6127637	1958.607807	1.910479723	0.281142433
tr|L7M743|L7M743_9ACAR	Putative glyoxylate/hydroxypyruvate reduct OS=Rhipicephalus pulchellus PE=2 SV=1	3.142355442	0.03477	3083.468677	848.5484644	3287.101755	853.0434345	1130.165949	490.1487972	2234.920213	3.633815635	0.560362889
tr|A0A023G6L8|A0A023G6L8_9ACAR	Putative dihydrolipoamide succinyltransferase 2-oxoglutarate dehydrogenase e2 subunit (Fragment) OS=Amblyomma triste PE=2 SV=1	-3.099649419	0.03623	1910.796766	2792.893	2002.190443	3018.126218	222.0563773	440.0536267	-882.0962345	0.684163971	-0.1648398
tr|G3MMA6|G3MMA6_9ACAR	Putative uncharacterized protein OS=Amblyomma maculatum PE=2 SV=1	3.090494627	0.03656	16315.71175	8421.730679	15929.78082	7779.574764	4209.330276	1361.815025	7893.98107	1.93733478	0.287204675
tr|A0A023FXY9|A0A023FXY9_9ACAR	Putative hydroxyacyl-coa dehydrogenase/enoyl-coa hydratase OS=Amblyomma parvum PE=2 SV=1	3.074164217	0.03714	11896.81591	3463.708804	10759.75218	3434.763877	4556.962894	1345.305988	8433.107103	3.434704411	0.535889368
tr|L7M2Y0|L7M2Y0_9ACAR	Putative igf-ii mrna-binding protein imp OS=Rhipicephalus pulchellus PE=2 SV=1	3.069789807	0.0373	16282.54533	9356.444553	16977.75327	8728.974017	1346.300765	3668.646952	6926.100782	1.74024922	0.240611448
tr|A0A023FXU9|A0A023FXU9_9ACAR	Putative alkyl hydroperoxide reductase thiol specific antioxidant OS=Amblyomma parvum PE=2 SV=1	3.030993098	0.03874	2677.119389	1014.549814	2536.506632	838.0423078	571.9229941	758.6413475	1662.569575	2.638726411	0.421394364
tr|L7LTS0|L7LTS0_9ACAR	Putative tick salivary metalloprotease OS=Rhipicephalus pulchellus PE=2 SV=1	3.009521572	0.03957	5537.481208	2403.293494	4717.663704	2004.444807	1590.127924	851.5776234	3134.187715	2.304121916	0.362505455
tr|L7M2I7|L7M2I7_9ACAR	Aconitate hydratase, mitochondrial OS=Rhipicephalus pulchellus PE=2 SV=1	3.002899652	0.03983	19173.11712	10415.83605	19098.95452	9758.452038	4694.474916	1864.372347	8757.281073	1.840766025	0.26499859
tr|A0A023FWG2|A0A023FWG2_9ACAR	Putative t-complex protein 1 subunit zeta danio rerio chaperonin (Fragment) OS=Amblyomma parvum PE=2 SV=1	2.929870396	0.04282	3315.471359	1695.32802	3302.850105	1754.808296	225.8004569	930.7825915	1620.14334	1.955651839	0.291291541
tr|L7M7P1|L7M7P1_9ACAR	Glutamine synthetase OS=Rhipicephalus pulchellus PE=2 SV=1	2.920543971	0.04322	5936.783788	1335.281468	5371.616033	1375.114954	2727.616009	85.50678805	4601.50232	4.446091652	0.647978411
tr|L7M6Q5|L7M6Q5_9ACAR	Putative heat shock-related protein OS=Rhipicephalus pulchellus PE=2 SV=1	-2.895931188	0.0443	9362.677132	13030.329	9495.514395	12357.68881	822.67483	2033.508014	-3667.651868	0.718529604	-0.143555334
tr|L7LXH5|L7LXH5_9ACAR	Putative emp24/gp25l/p24 family of membrane trafficking OS=Rhipicephalus pulchellus PE=2 SV=1	-2.895040062	0.04434	22283.89533	35744.680288	17905.5507	36226.49039	7605.473187	2648.236671	-13460.78495	0.62341851	-0.205220307
tr|L7MAC8|L7MAC8_9ACAR	Putative dihydrolipoamide succinyltransferase 2-oxoglutarate dehydrogenase e2 subunit (Fragment) OS=Rhipicephalus pulchellus PE=2 SV=1	2.869448671	0.04549	4011.994485	2046.032344	3483.947872	2176.615152	1062.805231	527.9000108	1965.962141	1.960865622	0.292447833

tr|L7MAC6|L7MAC6_9ACAR	Putative glutamate/leucine/phenylalanine/valine dehydrogenase OS=Rhipicephalus pulchellus PE=2 SV=1	2.86550721	0.04568	22942.6028	12435.97816	22027.76832	10860.15224	2645.692821	5773.373161	10506.62464	1.844857116	0.265962736
tr|C9W1T1|C9W1T1_RHISA	Cement-like protein (Fragment) OS=Rhipicephalus sanguineus PE=2 SV=1	2.736933964	0.05207	1235303.714	545103.6073	1325910.323	606054.6383	417802.3957	127379.2395	690200.107	2.266181507	0.355294691
tr|F0J9W5|F0J9W5_AMBVA	RNA-binding protein LARK OS=Amblyomma variegatum PE=2 SV=1	-2.729767119	0.05246	29134.38449	50920.90616	31653.72149	51096.8011	11196.10648	8108.062256	-21786.521667	0.572149765	-0.242490276
tr|L7M7N7|L7M7N7_9ACAR	Aspartate aminotransferase OS=Rhipicephalus pulchellus PE=2 SV=1	2.691614122	0.05457	7925.992688	4051.347593	8216.360795	3893.487353	2380.321272	742.1354287	3874.645095	1.956384266	0.291454161
tr|Q86G67|Q86G67_DERVA	26S proteasome regulatory subunit OS=Dermacentor variabilis PE=2 SV=1	2.690760143	0.05461	5812.803868	2858.938426	6427.532181	3648.730758	1125.900992	1532.226004	2953.865442	2.033203589	0.308180868
tr|L7M562|L7M562_9ACAR	Putative lamin OS=Rhipicephalus pulchellus PE=2 SV=1	2.653782857	0.05676	35455.30834	11747.89432	29597.87253	10514.65678	14944.45941	4010.270097	23707.41402	3.018013898	0.479721235
tr|A0A023FMJ4|A0A023FMJ4_9ACAR	Putative myosin class ii heavy chain (Fragment) OS=Amblyomma cajennense PE=2 SV=1	2.653350697	0.05678	41770.92724	12064.16502	36999.8824	10558.42474	18872.10118	4459.954284	29706.762222	3.462396873	0.539376847
tr|L7M261|L7M261_9ACAR	Putative h+ transporting atp synthase subunit e protein OS=Rhipicephalus pulchellus PE=2 SV=1	-2.622804992	0.05863	4125.401517	7566.670932	4105.871495	7618.812705	1992.39141	1093.094908	-3441.269415	0.545206942	-0.263438623
tr|G3MHR0|G3MHR0_9ACAR	Putative uncharacterized protein (Fragment) OS=Amblyomma maculatum PE=2 SV=1	2.596537919	0.06027	52403.62109	27817.33038	55534.88822	28990.7622	16102.84945	3110.783027	24586.29071	1.88384796	0.275045849
tr|L7MEF8|L7MEF8_9ACAR	Putative leucine-rich ppr-motif protein (Fragment) OS=Rhipicephalus pulchellus PE=2 SV=1	2.479885179	0.06822	2336.766726	1080.522745	1997.943525	1176.842445	693.8409146	537.0612194	1256.24398	2.162626132	0.334981447
tr|A0A023GME7|A0A023GME7_9ACAR	Clathrin heavy chain OS=Amblyomma triste PE=2 SV=1	2.466603444	0.0692	10021.01276	4734.865888	8200.979301	3897.97842	3296.26727	1706.778686	5286.146875	2.116430117	0.325603933
tr|L7LSB9|L7LSB9_9ACAR	Uncharacterized protein OS=Rhipicephalus pulchellus PE=2 SV=1	2.441932751	0.07106	2779.927734	1947.092583	2858.340468	1957.447909	254.5118442	533.0860617	832.8351513	1.427732692	0.154646904
tr|L7LXX6|L7LXX6_9ACAR	Putative rna-binding protein hnrnp-m OS=Rhipicephalus pulchellus PE=2 SV=1	2.419691047	0.07279	10616.15112	3930.377946	11807.26657	4159.095842	4757.038183	523.6769824	6685.77317	2.701050958	0.431532778
tr|A0A0C9S283|A0A0C9S283_AMBAM	40S ribosomal protein S3a OS=Amblyomma americanum PE=2 SV=1	2.37618504	0.07631	36893.24416	17436.71431	38057.40963	22026.63528	2873.381996	13888.14111	19456.529855	2.115836935	0.325482194
tr|L7M7C2|L7M7C2_9ACAR	Putative ap-2 complex subunit alpha OS=Rhipicephalus pulchellus PE=2 SV=1	2.329397301	0.08031	6434.564326	3983.844924	6759.215849	4199.423345	1034.324067	1500.269947	2450.719402	1.615164357	0.208216722
tr|L7LZ33|L7LZ33_9ACAR	Coatomer subunit beta OS=Rhipicephalus pulchellus PE=2 SV=1	2.316143787	0.08148	6621.097832	3637.06239	6607.474185	3780.965142	309.5426033	2209.938007	2984.035443	1.820452091	0.260179254

tr|A0A0C9RRZ5|A0A0C9RRZ5_AMBAM	Putative ribosomal protein OS=Amblyomma americanum PE=2 SV=1	-2.308592834	0.08216	5651.670345	10278.45857	6229.029585	11609.61473	1823.065068	2954.047982	-4626.788226	0.549855828	-0.259751168
tr|B7PNL8|B7PNL8_IXOSC	Cysteine proteinase, putative (Fragment) OS=Ixodes scapularis GN=IscW_ISCW005779 PE=3 SV=1	2.248375669	0.0878	3019.463076	1660.655787	2742.560717	1417.645153	901.6235937	531.7837967	1358.807289	1.818235362	0.2596501
tr|A0A023FZ65|A0A023FZ65_9ACAR	Putative metallopeptidase OS=Amblyomma parvum PE=2 SV=1	2.211492475	0.09147	11490.74798	5338.15422	11195.89627	5237.240086	3975.810479	2722.71489	6152.593757	2.152569503	0.332957183
tr|L7M803|L7M803_9ACAR	Putative 4-aminobutyrate aminotransferase OS=Rhipicephalus pulchellus PE=2 SV=1	2.156881766	0.09723	7956.683598	2420.503635	8115.895091	2195.859966	4415.329839	519.1391406	5536.179963	3.287201673	0.516826349
tr|L7M9E8|L7M9E8_9ACAR	Putative molecular chaperones grp170/sil1 hsp70 superfamily OS=Rhipicephalus pulchellus PE=2 SV=1	2.145975686	0.09843	10189.4489	5699.649879	10291.43542	5130.515159	753.5018192	3544.583388	4489.799025	1.787732426	0.252302517
tr|V5IK57|V5IK57_IXORI	Putative alpha-catenin OS=Ixodes ricinus PE=2 SV=1	2.124939071	0.10078	3944.118737	2137.919641	4634.502608	2007.612237	1413.092848	413.1231389	1806.199096	1.844839563	0.265958604
tr|V5HUX3|V5HUX3_IXORI	Putative 60s ribosomal protein l38 OS=Ixodes ricinus PE=2 SV=1	-2.12370352	0.10092	1443.451617	3477.751785	1333.453607	3056.387115	292.3290978	1633.17889	-2034.300168	0.415053088	-0.381896351
tr|L7M4H1|L7M4H1_9ACAR	Proteasome subunit alpha type OS=Rhipicephalus pulchellus PE=2 SV=1	2.114008217	0.10203	15241.52767	4458.655196	12890.52388	3896.021049	8678.205048	1655.133179	10782.87248	3.418413626	0.533824611
tr|L7M7D4|L7M7D4_9ACAR	Putative nadh:ubiquinone oxidoreductase ndufv2/24 kd subunit OS=Rhipicephalus pulchellus PE=2 SV=1	2.110416085	0.10244	17956.37606	13832.14861	18879.96662	14433.47596	3069.322644	1426.969598	4124.227455	1.29816246	0.113329046
tr|L7N0P4|L7N0P4_CANLF	Uncharacterized protein OS=Canis lupus familiaris GN=KRT71 PE=3 SV=1	-2.091153428	0.10469	7995.565356	22928.6563	11005.28461	28609.40601	5253.888427	11197.39551	-14933.09095	0.348714955	-0.457529427
tr|L7MLF4|L7MLF4_9ACAR	Putative 97 kDa heat shock protein (Fragment) OS=Rhipicephalus pulchellus PE=2 SV=1	2.079433462	0.10609	7457.095825	5131.510162	8064.441205	4361.651548	1075.478301	1611.096513	2325.585663	1.453197127	0.162324531
tr|L7MII0|L7MII0_9ACAR	Putative dolichyl-diphosphooligosaccharide--protein glycosyltransferase subunit 2 (Fragment) OS=Rhipicephalus pulchellus PE=2 SV=1	2.073985726	0.10675	23046.9199	15420.29083	21941.4393	14520.83274	2405.415674	5897.556295	7626.62907	1.494583997	0.174520328
tr|V5I4B8|V5I4B8_IXORI	Putative myosin class i heavy chain OS=Ixodes ricinus PE=2 SV=1	2.056673632	0.10886	25412.98944	6747.2853	26507.57964	7253.726485	15681.3235	1095.351079	18665.70414	3.766402087	0.575926682
tr|L7MDL8|L7MDL8_9ACAR	Uncharacterized protein (Fragment) OS=Rhipicephalus pulchellus PE=2 SV=1	2.015946962	0.11402	27468.48876	10520.25172	32069.95612	6651.539188	11891.27829	8404.446716	16948.23704	2.611010599	0.416808635
tr|L7MAW2|L7MAW2_9ACAR	Uncharacterized protein OS=Rhipicephalus pulchellus PE=2 SV=1	1.978571808	0.119	2834.293192	1681.670373	2681.821815	2089.517882	314.1430066	958.86284	1152.622818	1.685403535	0.2267039
tr|L7MGA3|L7MGA3_9ACAR	Putative signal peptidase complex subunit spc25 (Fragment) OS=Rhipicephalus pulchellus PE=2 SV=1	-1.969822743	0.12019	4697.404107	6262.348562	4281.815459	5905.457092	1073.236661	861.1973724	-1564.	0.750102627	-0.124879314

										944455		
tr|G3MRE3|G3MRE3_9ACAR	Putative uncharacterized protein OS=Amblyomma maculatum PE=2 SV=1	1.952402706	0.12262	17948.99254	12520.66494	15247.29311	12831.94085	4737.135957	866.1870484	5428.327601	1.433549466	0.156412683
tr|G3MM77|G3MM77_9ACAR	Putative uncharacterized protein OS=Amblyomma maculatum PE=2 SV=1	1.945882941	0.12354	55141.62541	22796.35699	42916.57299	20552.23282	28280.95612	5394.560922	32345.268422	2.418878834	0.383614114
tr|L7M4K4|L7M4K4_9ACAR	Uncharacterized protein OS=Rhipicephalus pulchellus PE=2 SV=1	1.910305951	0.1287	3245.584845	1878.166634	3158.029562	1784.597211	272.6682017	1209.46627	1367.418211	1.728060113	0.237558846
tr|L7M7R7|L7M7R7_9ACAR	Putative atp synthase subunit b OS=Rhipicephalus pulchellus PE=2 SV=1	1.888638438	0.13196	17147.76203	10821.00416	16089.05241	10778.15936	5800.382397	145.3921383	6326.75787	1.584673823	0.199939884
tr|A0A023FY35|A0A023FY35_9ACAR	Putative elongation factor 2-like isoform 1 OS=Amblyomma parvum PE=2 SV=1	1.865774881	0.13549	113531.5324	39808.3653	86265.15165	30627.35303	65444.6623	20023.23339	73723.16709	2.851951632	0.455142156
tr|G3MNI4|G3MNI4_9ACAR	Putative uncharacterized protein OS=Amblyomma maculatum PE=2 SV=1	-1.848942138	0.13816	2207.307988	3229.365132	2444.150806	3143.860363	883.449133	369.0702606	-1022.057144	0.683511433	-0.165254217
tr|L7MD20|L7MD20_9ACAR	Putative m13 family peptidase (Fragment) OS=Rhipicephalus pulchellus PE=2 SV=1	-1.843978036	0.13896	1138.282647	2307.957631	1254.222278	2036.891623	249.1257823	1070.059711	-1169.674984	0.493199109	-0.306977717
tr|L7M679|L7M679_9ACAR	Putative f0f1-type atp synthase gamma subunit OS=Rhipicephalus pulchellus PE=2 SV=1	1.832007979	0.1409	3625.329815	1902.855917	2967.776328	2337.564356	1323.646107	948.6573027	1722.473898	1.905204584	0.279941618
tr|L7M6I3|L7M6I3_9ACAR	Putative prolyl endopeptidase prolyl oligopeptidase prolyl endopeptidase prolyl oligopeptidase OS=Rhipicephalus pulchellus PE=2 SV=1	1.826472455	0.14181	2674.013125	1453.296211	3128.855829	1470.9643	1148.220368	147.146484	1220.716914	1.839964286	0.264809393
tr|L7LX53|L7LX53_9ACAR	Putative low-density lipoprotein receptor domain class a OS=Rhipicephalus pulchellus PE=2 SV=1	1.822727143	0.14243	13779.87715	7321.794601	14065.91608	5810.860303	5131.748304	3365.349271	6458.082551	1.882035471	0.274627804
tr|L7M4E8|L7M4E8_9ACAR	Putative ras-related protein rab-11a OS=Rhipicephalus pulchellus PE=2 SV=1	-1.815645594	0.1436	8939.056488	14068.4642	7596.070639	14069.05944	4434.527992	2068.522846	-5129.407707	0.635396754	-0.196955008
tr|G3MH39|G3MH39_9ACAR	Putative uncharacterized protein (Fragment) OS=Amblyomma maculatum PE=2 SV=1	1.806220988	0.14518	8102.258041	1959.349999	8550.084298	1816.519092	5858.42424	615.3931944	6142.908042	4.135176484	0.616494049
tr|L7M942|L7M942_9ACAR	Putative beta-spectrin OS=Rhipicephalus pulchellus PE=2 SV=1	1.801953976	0.14591	27974.18335	16041.14482	25781.33658	16599.63422	9892.846717	5804.760562	11933.03852	1.743901926	0.241522057
tr|L7M619|L7M619_9ACAR	Kinesin-like protein OS=Rhipicephalus pulchellus PE=2 SV=1	1.793807946	0.1473	2571.021477	2050.257435	2294.751087	2004.95422	493.0243154	98.8446456	520.764042	1.253999343	0.098297309
tr|L7M8C0|L7M8C0_9ACAR	Putative microtubule associated complex OS=Rhipicephalus pulchellus PE=2 SV=1	1.789336685	0.14806	4649.300582	2234.043761	5224.789564	1425.539672	1239.444907	1982.347456	2415.256821	2.081114374	0.318295949

tr|L7MAA0|L7MAA0_9ACAR	ATP synthase subunit alpha OS=Rhipicephalus pulchellus PE=2 SV=1	1.73328998	0.15807	64990.12758	48203.5654	58334.14591	47056.37115	15708.89332	5883.584699	16786.562167	1.348243165	0.129768227
tr|L7MAZ4|L7MAZ4_9ACAR	Putative enoyl-coa hydratase OS=Rhipicephalus pulchellus PE=2 SV=1	1.720340058	0.16049	28606.92461	16124.71647	31206.47784	13604.15859	10442.35439	6992.222997	12482.208814	1.774104039	0.248979085
sp|Q6EIZ1|K22E_CANLF	Keratin, type II cytoskeletal 2 epidermal OS=Canis lupus familiaris GN=KRT2 PE=2 SV=1	-1.716456223	0.16156	3023.020059	11690.15334	3023.625272	15498.78638	104.5454761	8754.434083	-8667.133281	0.258595415	-0.587379179
tr|L7M501|L7M501_9ACAR	Putative 26s proteasome regulatory complex subunit rpn1/psmd2 OS=Rhipicephalus pulchellus PE=2 SV=1	1.707469103	0.16292	1666.510607	842.2981057	2008.645265	765.0485318	663.3133472	508.9620716	824.2125017	1.978528262	0.296342258
tr|A0A023GBN3|A0A023GBN3_9ACAR	Putative quinone oxidoreductase OS=Amblyomma triste PE=2 SV=1	1.695182571	0.16529	71610.45865	37049.20557	66524.13387	37199.01081	29860.17969	18851.3124	34561.253039	1.932847346	0.286197555
tr|L7M5S1|L7M5S1_9ACAR	Putative phosphatidylinositol transfer protein OS=Rhipicephalus pulchellus PE=2 SV=1	1.685752423	0.16712	1804.123956	672.3022373	1426.870033	714.7236803	1060.123376	478.0066197	1131.821718	2.683501342	0.428701817
tr|L7MEL9|L7MEL9_9ACAR	Putative signal recognition particle subunit srp68 (Fragment) OS=Rhipicephalus pulchellus PE=2 SV=1	1.684240435	0.16742	8125.387576	2652.896208	7137.928101	2658.541389	5325.667727	1819.293538	5472.491369	3.062836591	0.486123827
tr|A0A0C9S1J0|A0A0C9S1J0_AMBAM	Putative ras-related protein rab-1a OS=Amblyomma americanum PE=2 SV=1	1.677150153	0.16882	34882.42702	21258.19925	31849.47546	27253.01275	6793.968215	12321.23382	13624.227777	1.640892844	0.215080221
tr|L7M0M1|L7M0M1_9ACAR	Putative lethal 2 35di OS=Rhipicephalus pulchellus PE=2 SV=1	1.675452726	0.16916	3472.260406	1965.305783	3725.968303	2344.838955	1065.156671	1136.825077	1506.954623	1.766778705	0.247182156
tr|A0A023FSGs7|A0A023FSGs7_9ACAR	Putative chaperonin complex component tcp-1 delta subunit (Fragment) OS=Amblyomma parvum PE=2 SV=1	1.661969273	0.17185	7156.346969	3720.919117	6934.08097	2095.42419	1038.791713	3426.281344	3435.427853	1.923273994	0.284041159
tr|A0A023FNA0|A0A023FNA0_9ACAR	Putative calpain-b OS=Amblyomma cajennense PE=2 SV=1	1.660063792	0.17224	21186.92996	14446.16979	21818.83759	13222.08024	5967.036725	3722.700301	6740.760168	1.466612276	0.166315316
tr|F1PRB0|F1PRB0_CANLF	Uncharacterized protein (Fragment) OS=Canis lupus familiaris GN=KRT7 PE=3 SV=2	-1.648453557	0.1746	4619.574029	65808.06147	121.2435895	32761.20704	7896.569599	63804.72165	-61188.48744	0.070197692	-1.153677167
sp|Q86RN8|MYSP_RHIMP	Paramyosin OS=Rhipicephalus microplus GN=PRM PE=1 SV=1	1.643676186	0.17559	163134.0246	31404.61368	97354.81127	29433.28899	138582.9877	7970.943227	131729.4109	5.194587847	0.715551095
tr|A0A023FWX3|A0A023FWX3_9ACAR	Succinate dehydrogenase (ubiquinone) flavoprotein subunit, mitochondrial OS=Amblyomma parvum PE=2 SV=1	1.637136021	0.17694	19515.06242	11903.720774	18722.71217	11775.29834	7237.648588	3530.027589	7611.341683	1.639408623	0.214687215
tr|L7M8R8|L7M8R8_9ACAR	Adenosylhomocysteinase OS=Rhipicephalus pulchellus PE=2 SV=1	1.62888127	0.17867	22789.68382	14381.77294	25897.662443	14492.30379	8833.218681	1380.530321	8407.910875	1.584622696	0.199925872
sp|O97162|TPM_RHIMP	Tropomyosin OS=Rhipicephalus microplus PE=2 SV=1	-1.627777275	0.1789	107254.147	283292.6381	111033.4562	345731.0287	15815.64388	186646.4361	-176038.4911	0.378598426	-0.421821195

tr|L7M3V3|L7M3V3_9ACAR	Putative glutathione s-transferase OS=Rhipicephalus pulchellus PE=2 SV=1	1.613372673	0.18196	14457.4206	7923.94858	16276.3215	7064.649261	5962.317996	3694.308163	6533.472025	1.824522264	0.261149167
tr|L7M5J9|L7M5J9_9ACAR	Putative electron transfer flavoprotein alpha subunit OS=Rhipicephalus pulchellus PE=2 SV=1	1.607631268	0.1832	48306.42412	28015.42318	46344.89516	23422.05504	13992.63427	16796.61571	20291.00095	1.724279652	0.236607703
tr|A0A023GM86|A0A023GM86_9ACAR	Putative lysine-ketoglutarate reductase/saccharopine dehydrogenase OS=Amblyomma triste PE=2 SV=1	1.593965035	0.18617	2240.849583	790.6162358	2353.344326	192.3291496	1094.142432	1134.112429	1450.233347	2.834307571	0.452446977
tr|L7LXD4|L7LXD4_9ACAR	Putative er-golgi vesicle-tethering protein OS=Rhipicephalus pulchellus PE=2 SV=1	-1.590376006	0.18696	2086.972648	6789.404143	1993.950765	3897.999782	305.0025868	5112.245911	-4702.431495	0.307386717	-0.512314904
tr|L7M4P3|L7M4P3_9ACAR	Putative dorsal switch protein 1 OS=Rhipicephalus pulchellus PE=2 SV=1	1.582281214	0.18875	6510.040314	3950.152707	6204.943262	4555.840984	1254.856154	2505.516863	2559.887607	1.648047758	0.216969793
tr|G3MGL5|G3MGL5_9ACAR	Putative uncharacterized protein (Fragment) OS=Amblyomma maculatum PE=2 SV=1	1.568865424	0.19176	24719.77049	18661.646332	26118.01068	20246.12628	5443.048699	3886.648194	6058.124172	1.324629675	0.12209448
tr|G3MP43|G3MP43_9ACAR	Putative uncharacterized protein OS=Amblyomma maculatum PE=2 SV=1	-1.566480955	0.1923	1726.149089	4693.169275	1834.54504	5612.70485	424.7304549	3253.010244	-2967.020186	0.367800305	-0.434387915
tr|L7M5T3|L7M5T3_9ACAR	Proteasome subunit alpha type OS=Rhipicephalus pulchellus PE=2 SV=1	1.565159905	0.1926	4877.463375	3361.110757	5068.831925	2901.396106	673.0990384	1537.126064	1516.352618	1.451146281	0.161711193
tr|L7M7W1|L7M7W1_9ACAR	Putative medium subunit of clathrin adaptor complex OS=Rhipicephalus pulchellus PE=2 SV=1	1.553430836	0.19528	4194.921647	1562.904677	3421.841638	309.3151372	1829.841756	2294.299261	2632.01697	2.684054702	0.428791363
tr|L7LW75|L7LW75_9ACAR	Putative laminin a OS=Rhipicephalus pulchellus PE=2 SV=1	1.543910823	0.19749	4071.256962	1905.258455	3853.339272	1487.75015	2243.375053	933.7582461	2165.998506	2.136852851	0.329774617
tr|L7MGY9|L7MGY9_9ACAR	Putative heteroproteinous nuclear ribonucleoprotein l (Fragment) OS=Rhipicephalus pulchellus PE=2 SV=1	1.542058813	0.19792	1994.597479	1021.423683	1411.105009	1226.956944	1026.368643	376.0067917	973.1737966	1.952762123	0.290649343
tr|A0A0C9SBZ9|A0A0C9SBZ9_AMBAM	60S ribosomal protein L6 OS=Amblyomma americanum PE=2 SV=1	1.541128462	0.19814	10493.10338	4763.782935	7952.909982	2735.004173	5127.797706	3894.566461	5729.320447	2.202682936	0.342951987
tr|L7MG42|L7MG42_9ACAR	Putative alkyl hydroperoxide reductase thiol specific antioxidant (Fragment) OS=Rhipicephalus pulchellus PE=2 SV=1	-1.534214832	0.19976	2985.808509	21254.36512	3023.491799	11671.15526	1532.107015	20567.28853	-18268.55661	0.140479779	-0.852386186
tr|L7M4P7|L7M4P7_9ACAR	Putative vesicle coat complex copii gtpase subunit sar1 OS=Rhipicephalus pulchellus PE=2 SV=1	1.525276088	0.20188	2411.817597	1479.064545	2327.105205	1313.88157	334.091115	1005.132963	932.7530521	1.630637152	0.212357333
tr|L7N0L3|L7N0L3_CANLF	Histone H4 (Fragment) OS=Canis lupus familiaris PE=3 SV=1	1.516771546	0.20392	425222.1323	220446.3556	511978.7633	241622.8829	214808.344	92404.43637	204775.7767	1.928914321	0.285312937
tr|L7M9U7|L7M9U7_9ACAR	Putative cytosolic ca2+-dependent cysteine prote OS=Rhipicephalus pulchellus PE=2 SV=1	1.511762644	0.20513	5122.018792	1562.762884	5793.388612	2003.879368	3952.503241	1003.474238	3559.255908	3.277540594	0.515548079

tr|L7M7Z9|L7M7Z9_9ACAR	Putative cytochrome c1 OS=Rhipicephalus pulchellus PE=2 SV=1	1.496542907	0.20885	10472.64188	5575.305288	9969.175069	7464.632289	3889.408824	4122.97888	4897.336595	1.878397925	0.2737876
tr|L7M6W4|L7M6W4_9ACAR	Putative 60 kDa heat shock protein OS=Rhipicephalus pulchellus PE=2 SV=1	1.49231403	0.2099	129660.9489	77842.76682	122563.1931	48503.08398	27734.97587	53365.8108	51818.18209	1.665677547	0.221590932
tr|L7MFS4|L7MFS4_9ACAR	Putative heat shock protein (Fragment) OS=Rhipicephalus pulchellus PE=2 SV=1	1.479067912	0.21321	7945.102716	4089.599924	6960.264633	2321.530603	2034.192329	4030.74315	3855.502792	1.942757938	0.288418692
tr|L7MF21|L7MF21_9ACAR	Putative f-actin capping protein alpha subunit (Fragment) OS=Rhipicephalus pulchellus PE=2 SV=1	1.473066583	0.21473	1380.633759	866.12278	1444.352369	871.7753564	463.0458559	389.3271721	514.5109786	1.59403931	0.202499027
tr|J9NVC6|J9NVC6_CANLF	Uncharacterized protein OS=Canis lupus familiaris PE=4 SV=1	1.470982843	0.21526	8296.256587	2513.352186	9369.973407	1506.248402	6139.445599	2945.002659	5782.904401	3.300873086	0.518628827
tr|A0A023FPG2|A0A023FPG2_9ACAR	Putative acetyl-coa acetyltransferase (Fragment) OS=Amblyomma cajennense PE=2 SV=1	-1.45537264	0.21927	20590.17098	45382.23779	9624.770483	53851.6174	20772.10165	20954.21181	-24792.066801	0.453705502	-0.343225954
tr|J9NXL3|J9NXL3_CANLF	Uncharacterized protein OS=Canis lupus familiaris GN=LOC100855558 PE=3 SV=1	-1.421804439	0.22814	1280.081113	15456.78772	448.8690418	6846.195125	1587.397568	17197.04204	-14176.706661	0.082816762	-1.081881753
tr|V5H2W8|V5H2W8_IXORI	Putative myosin class ii heavy chain OS=Ixodes ricinus PE=2 SV=1	1.408311257	0.23181	12611.25194	5046.462328	10303.61343	1744.055291	7287.745073	5783.498439	7564.789611	2.499028253	0.397771166
tr|L7M6I8|L7M6I8_9ACAR	Putative ribosomal protein s13 OS=Rhipicephalus pulchellus PE=2 SV=1	1.380709068	0.2395	29452.86633	17663.51239	28320.08595	15516.65669	12871.51818	7283.423547	11789.35395	1.667441089	0.222050499
tr|L7M575|L7M575_9ACAR	Putative flotillin OS=Rhipicephalus pulchellus PE=2 SV=1	1.380119349	0.23967	2747.268106	1744.573406	2199.980902	1754.329389	1243.847406	190.710198	1002.694699	1.57475065	0.197211796
tr|L7MAE8|L7MAE8_9ACAR	Putative mannose lectin ergic-53 involved in glycoprotein traffic OS=Rhipicephalus pulchellus PE=2 SV=1	1.357581198	0.24614	2040.313476	1449.297292	1754.178223	1417.352923	730.9014792	185.3613475	591.0161839	1.407794996	0.148539417
tr|J9JHF7|J9JHF7_CANLF	Uncharacterized protein OS=Canis lupus familiaris GN=LOC100855540 PE=3 SV=1	-1.352892153	0.2475	4679.168569	20294.4984	1618.312665	19837.30928	5586.49075	19195.2374	-15615.329833	0.230563401	-0.637209631
tr|E2J6V5|E2J6V5_9ACAR	Protein disulfide isomerase (Fragment) OS=Hyalomma marginatum rufipes PE=2 SV=1	1.351941087	0.24778	6224.455617	3723.636428	5797.033774	4276.002389	2189.499534	2339.093872	2500.819189	1.671606704	0.223134104
tr|G3MKG0|G3MKG0_9ACAR	Putative uncharacterized protein OS=Amblyomma maculatum PE=2 SV=1	-1.332695157	0.25348	1311.910329	19214.03855	1059.866056	6905.37774	551.445372	23260.14707	-17902.128222	0.068278739	-1.165714506
tr|L7M3R3|L7M3R3_9ACAR	Putative cargo transport protein OS=Rhipicephalus pulchellus PE=2 SV=1	-1.325551181	0.25563	22571.19416	40511.31173	24805.89174	28845.27876	4302.579742	23043.47815	-17940.117557	0.557157821	-0.254021769

tr|L7M2D4|L7M2D4_9ACAR	Putative sirtuin 5 OS=Rhipicephalus pulchellus PE=2 SV=1	-1.324390198	0.25598	399.141017	2858.309726	542.2934168	1066.864653	350.2401564	3196.997865	-2459.168708	0.139642326	-0.854982927
tr|V5HEV5|V5HEV5_IXORI	Putative g-protein alpha subunit OS=Ixodes ricinus PE=2 SV=1	1.31469371	0.25892	12577.4603	5289.369591	12228.53812	3428.503907	8612.222151	4245.34868	7288.090711	2.377875111	0.376189041
tr|L7M2A4|L7M2A4_9ACAR	Putative alpha actinin OS=Rhipicephalus pulchellus PE=2 SV=1	1.31291092	0.25947	76136.32176	35898.95252	50473.28282	38175.97062	52707.61709	6301.157082	40237.36924	2.120850788	0.326510115
tr|L7M551|L7M551_9ACAR	Peptidyl-prolyl cis-trans isomerase OS=Rhipicephalus pulchellus PE=2 SV=1	1.30343 9472	0.26238	1198.778276	748.528182 1	1218.406062	857.5824352	168.1634533	574.1876634	450.2500937	1.601513884	0.204530708
tr|L7LZV6|L7LZV6_9ACAR	Putative vesicle-fusing atpase 2 OS=Rhipicephalus pulchellus PE=2 SV=1	1.28587 7424	0.26788	9973.806287	5803.067655	8100.294131	5212.361629	4714.420855	3055.329799	4170.738631	1.718712736	0.235203295
tr|L7M7H8|L7M7H8_9ACAR	Putative glyoxalase OS=Rhipicephalus pulchellus PE=2 SV=1	-1.284927096	0.26818	476.587561 7	2336.509796	426.9979818	1647.493862	243.572606	2495.27059	-1859.922235	0.203974134	-0.690424903
tr|A0A034WXE0|A0A034WXE0_RHIMP	Heat shock protein 70 1 OS=Rhipicephalus microplus PE=3 SV=1	1.28017515	0.26968	3031.928125	2152.568	2572.27229	2130.788553	1148.760729	309.6268312	879.3601248	1.408516769	0.148762022
tr|A0A034WYY9|A0A034WYY9_RHIMP	Elongation factor 1-alpha OS=Rhipicephalus microplus PE=3 SV=1	1.27565 1488	0.27112	122598.9938	66701.0549	102678.7354	37056.41883	45432.55758	60796.63871	55897.93889	1.838036804	0.264354203
tr|V5I1L1|V5I1L1_IXORI	Putative ribosomal protein l30 (Fragment) OS=Ixodes ricinus PE=2 SV=1	-1.274317225	0.27155	3100.809969	5082.770127	3284.905751	5044.493934	420.990658	2660.779565	-1981.960158	0.610062996	-0.214625317
tr|L7M4F5|L7M4F5_9ACAR	Putative glyoxylate/hydroxypyruvate reduct OS=Rhipicephalus pulchellus PE=2 SV=1	1.26719 2285	0.27384	8195.57706	4156.589228	9749.208032	3600.627902	4798.849841	2729.226636	4038.987833	1.971707237	0.29484243
tr|L7M3S2|L7M3S2_9ACAR	Putative elongation factor 1 beta OS=Rhipicephalus pulchellus PE=2 SV=1	-1.266371715	0.2741	916.4548415	8636.133099	1186.42502	3010.188838	815.6947324	10526.85694	-7719.678257	0.106118656	-0.974208257
tr|A0A023FUW9|A0A023FUW9_9ACAR	Putative alpha-d-galactosidase melibiase OS=Amblyomma cajennense PE=2 SV=1	-1.261789452	0.27559	12371.65906	62932.16028	12419.0782	40674.10973	1769.750986	69381.52927	-50560.50122	0.19658723	-0.706444697
tr|L7M7P8|L7M7P8_9ACAR	Proteasome subunit alpha type OS=Rhipicephalus pulchellus PE=2 SV=1	-1.247208838	0.28036	3572.331859	8053.999161	3110.271773	6049.734354	1414.787187	6060.945571	-4481.667302	0.443547583	-0.353059783
tr|L7M0L6|L7M0L6_9ACAR	Putative rna-binding protein elav/hu rrm superfamily OS=Rhipicephalus pulchellus PE=2 SV=1	-1.231668969	0.28553	3030.106785	6243.030705	3180.422429	4486.562054	1154.207108	4368.305084	-3212.92392	0.485358302	-0.313937537
tr|L7M1K6|L7M1K6_9ACAR	Putative glycine rich protein OS=Rhipicephalus pulchellus PE=2 SV=1	1.22690 0968	0.28714	10935.9014	7424.223123	11024.16893	7000.87182	1942.681892	4561.046599	3511.67828	1.473002794	0.168203571

tr|V5I1T0|V5I1T0_IXORI	Histone H2B OS=Ixodes ricinus PE=2 SV=1	1.218549549	0.28997	54480.51308	26647.7792	42014.00999	18150.15025	35297.5514	17866.14456	27832.73388	2.044467296	0.310580168
tr|B7P4J5|B7P4J5_IXOSC	Putative uncharacterized protein OS=Ixodes scapularis GN=IscW_ISCW001432 PE=4 SV=1	1.216766416	0.29058	5198.372381	2113.876926	4490.518833	1907.851598	4159.419333	1406.347471	3084.495455	2.459165109	0.390787688
tr|L7MFR3|L7MFR3_9ACAR	Putative carbonic anhydrase (Fragment) OS=Rhipicephalus pulchellus PE=2 SV=1	-1.212473804	0.29204	3509.802984	28073.77885	3745.978411	9400.252931	584.1145049	35085.42546	-24563.97586	0.125020682	-0.903018135
tr|L7MI50|L7MI50_9ACAR	Putative glycine rich protein (Fragment) OS=Rhipicephalus pulchellus PE=2 SV=1	-1.210758761	0.29263	954.4910293	3480.414	630.6728576	2338.303679	1151.083348	3425.214119	-2525.922971	0.274246406	-0.561859056
tr|L7M2C1|L7M2C1_9ACAR	Putative prohibitin OS=Rhipicephalus pulchellus PE=2 SV=1	1.204965888	0.29463	71739.69694	53857.23195	61481.99357	53837.70144	20180.66959	15920.87825	17882.465	1.33203461	0.124515509
tr|L7LZK9|L7LZK9_9ACAR	Putative translocon-associated complex trap delta subunit OS=Rhipicephalus pulchellus PE=2 SV=1	-1.198357983	0.29692	2735.899046	12678.31118	2954.982702	7343.353539	1031.700588	14333.2166	-9942.412137	0.21579365	-0.665961339
tr|G3MMF8|G3MMF8_9ACAR	Putative uncharacterized protein OS=Amblyomma maculatum PE=2 SV=1	-1.192585014	0.29894	10716.93174	14308.41783	10065.64632	14718.13361	4450.347707	2720.670759	-3591.486094	0.748994883	-0.125521149
tr|C9W1T4|C9W1T4_RHISA	Putative cement protein (Fragment) OS=Rhipicephalus sanguineus PE=2 SV=1	1.178024786	0.30409	1422148.902	886088.008	1516461.839	785142.081	210464.0608	759551.2125	536060.8939	1.604974776	0.205468211
tr|A8B3A8|A8B3A8_RHIMP	Triosephosphate isomerase OS=Rhipicephalus microplus GN=TIM PE=1 SV=1	1.172440028	0.30608	1502.001942	775.5864557	1026.408119	800.6618605	1063.913184	140.3969691	726.4154858	1.936601562	0.287040278
tr|A0A023GMF4|A0A023GMF4_9ACAR	Putative beta-spectrin (Fragment) OS=Amblyomma triste PE=2 SV=1	1.163137391	0.30943	9792.299051	6753.853379	8394.195751	5288.536268	3107.238258	3288.945107	3038.445672	1.449883274	0.16133304
tr|G3MKF8|G3MKF8_9ACAR	Putative uncharacterized protein OS=Amblyomma maculatum PE=2 SV=1	-1.162111592	0.3098	10597.57693	61284.33348	1369.002564	22813.1894	16937.57201	73622.05475	-50686.756555	0.172924732	-0.762142889
RRRRRtr|E2RIM4|E2RIM4_CANLF	REVERSED Uncharacterized protein (Fragment) OS=Canis lupus familiaris GN=FZD2 PE=4 SV=2	1.148476227	0.31478	64406.97288	21798.99549	92669.84011	3364.729439	55388.97093	32576.01579	42607.97739	2.95458444	0.470496406
tr|L7M7V3|L7M7V3_9ACAR	Putative gtpase ran/tc4/gsp1 nuclear protein OS=Rhipicephalus pulchellus PE=2 SV=1	-1.147852225	0.31501	4172.09374	16226.11069	4381.97327	6829.987647	1671.831545	18111.90389	-12054.016955	0.257122229	-0.589860376
tr|A0A0C9SCJ0|A0A0C9SCJ0_AMBAM	Putative 60 kDa chaperonin (Fragment) OS=Amblyomma americanum PE=2 SV=1	1.145455022	0.31589	76749.93668	39523.90663	77585.95322	17260.80545	39668.42924	39936.84432	37226.03004	1.941861097	0.288218161
tr|L7LXU7|L7LXU7_9ACAR	Putative transcription factor nfat subunit nf90 OS=Rhipicephalus pulchellus PE=2 SV=1	1.144017232	0.31643	2395.14331	1651.936202	2180.28359	1619.9028	898.5183532	677.3385962	743.207107	1.449900612	0.161338233

tr|A0A023FM62|A0A023FM62_9ACAR	Putative troponin t skeletal muscle OS=Amblyomma cajennense PE=2 SV=1	1.14185916	0.31722	100790.9634	47984.72311	67842.50227	45966.67576	79693.80334	8058.032538	52806.24024	2.100480253	0.322318603
tr|A0A023G8A1|A0A023G8A1_9ACAR	Putative spermidine synthase (Fragment) OS=Amblyomma triste PE=2 SV=1	-1.133029536	0.32051	1546.70462	5835.595699	1486.594575	2057.292128	380.139179	6545.354958	-4288.891079	0.265046569	-0.576677813
tr|B7QIP4|B7QIP4_IXOSC	4SNc-Tudor domain protein, putative OS=Ixodes scapularis GN=IscW_ISCW014289 PE=4 SV=1	1.126026359	0.32314	6415.855947	3299.776249	5706.153988	1900.472094	3011.816805	3728.700159	3116.079698	1.944330604	0.288770112
tr|Q64K72|Q64K72_RHISA	Calreticulin OS=Rhipicephalus sanguineus PE=3 SV=1	-1.116093235	0.3269	10521.31454	56182.30942	9263.994668	17288.29269	2352.504945	70821.65239	-45660.99488	0.187270951	-0.727529583
tr|G3MF42|G3MF42_9ACAR	Putative uncharacterized protein OS=Amblyomma maculatum PE=2 SV=1	1.114639714	0.32746	44588.13924	20854.82354	26071.0009	17471.35874	35122.02503	11248.90166	23733.31571	2.138025247	0.330012829
tr|L7M2X4|L7M2X4_9ACAR	Putative ca2+ calmodulin dependent protein kinase ef-hand protein superfamily OS=Rhipicephalus pulchellus PE=2 SV=1	1.108012506	0.32999	5359.231016	2951.128312	6229.260176	2201.379256	2335.55038	2952.219321	2408.102704	1.815993901	0.259114386
tr|A0A023FX57|A0A023FX57_9ACAR	Annexin (Fragment) OS=Amblyomma parvum PE=2 SV=1	-1.104636607	0.33129	443.0656294	8767.279473	508.6370607	1611.361276	117.5732045	13051.69162	-8324.213843	0.050536273	-1.29639679
tr|L7M5R1|L7M5R1_9ACAR	Proteasome subunit alpha type OS=Rhipicephalus pulchellus PE=2 SV=1	-1.102153102	0.33225	3272.300889	7009.006703	3224.501532	3948.260528	144.5473033	5870.512231	-3736.705813	0.466870846	-0.330803245
tr|V5HMU2|V5HMU2_IXORI	Putative 14-3-3 logues OS=Ixodes ricinus PE=2 SV=1	-1.090819476	0.33666	14961.37045	38481.26392	14459.93357	20973.34786	5208.897794	36980.86919	-23519.89347	0.388796233	-0.410277952
tr|L7M463|L7M463_9ACAR	Uncharacterized protein OS=Rhipicephalus pulchellus PE=2 SV=1	-1.088054948	0.33774	2534.201558	7645.573643	2485.515763	2977.889268	497.6552952	8121.448133	-5111.372085	0.331459963	-0.479568922
tr|V5HJX3|V5HJX3_IXORI	Histone H2A OS=Ixodes ricinus PE=2 SV=1	1.087474231	0.33797	32521.03212	18909.651066	38136.89538	21078.61378	21291.92684	4079.564711	13611.381066	1.719811329	0.235480805
tr|G3MTL2|G3MTL2_9ACAR	Putative uncharacterized protein OS=Amblyomma maculatum PE=2 SV=1	-1.087285232	0.33804	978.5537969	13356.150662	495.8905453	3910.437323	904.1453761	19696.83299	-12377.596833	0.073266155	-1.135096602
tr|G3MPV4|G3MPV4_9ACAR	Nucleoside diphosphate kinase OS=Amblyomma maculatum PE=2 SV=1	-1.086077439	0.33852	11151.64477	39243.712666	11170.85837	14677.59816	139.8415256	44800.35225	-28092.067889	0.284163857	-0.54643116
tr|L7M502|L7M502_9ACAR	Putative cytochrome b5 domain-containing protein OS=Rhipicephalus pulchellus PE=2 SV=1	1.074783141	0.34298	813.166247 1	497.171175	666.8074335	567.7463849	400.31742	314.7514154	315.995072 1	1.635586068	0.213673402

tr|L7MHC3|L7MHC3_9ACAR	Putative cytosolic sulfotransferase (Fragment) OS=Rhipicephalus pulchellus PE=2 SV=1	1.071270931	0.34438	1977.565831	1359.184284	1861.194524	1110.725248	782.335675	622.5532491	618.381547	1.454965198	0.162852605
tr|M9ZBR2|M9ZBR2_RHISA	Glutathione S-transferase OS=Rhipicephalus sanguineus PE=2 SV=1	-1.058195228	0.34964	2108.56141	14228.98934	2153.284079	3909.873927	1334.224541	19793.76384	-12120.42793	0.148187715	-0.8291878
tr|L7MAJ1|L7MAJ1_9ACAR	Putative fumarase OS=Rhipicephalus pulchellus PE=2 SV=1	-1.053207447	0.35166	625.362959 1	1689.862906	656.684299	741.2732415	82.16708974	1748.692514	-1064.499947	0.370067274	-0.431719319
tr|G3MJY2|G3MJY2_9ACAR	Putative uncharacterized protein OS=Amblyomma maculatum PE=2 SV=1	-1.053052427	0.35172	1521.974323	2481.364466	1926.891723	2211.844766	1065.006057	1164.402566	-959.3901422	0.61336186	-0.212283233
tr|L7MB25|L7MB25_9ACAR	Isocitrate dehydrogenase (NAD) subunit, mitochondrial OS=Rhipicephalus pulchellus PE=2 SV=1	-1.050944118	0.35258	2738.9751	5188.939432	2603.544085	2895.834003	396.6361603	4018.234114	-2449.964332	0.527848732	-0.277490517
tr|A0A034WWK3|A0A034WWK3_RHIMP	Peptidyl-prolyl cis-trans isomerase 1 OS=Rhipicephalus microplus PE=3 SV=1	-1.050643833	0.3527	7378.99922	20238.83428	8265.549697	9471.582684	2949.299167	20994.07671	-12859.83506	0.364596059	-0.43818803
tr|A0A0K8RQ45|A0A0K8RQ45_IXORI	Putative f0f1-type atp synthase gamma subunit (Fragment) OS=Ixodes ricinus PE=2 SV=1	-1.042725118	0.35595	1547.033063	5241.744494	2239.809283	1892.753314	1234.887078	6011.693447	-3694.711431	0.295137061	-0.529976252
tr|L7M6U9|L7M6U9_9ACAR	Uncharacterized protein OS=Rhipicephalus pulchellus PE=2 SV=1	-1.041097781	0.35662	1208.6541	3826.122202	1338.96261	1397.247309	411.3602551	4335.149266	-2617.468102	0.315895321	-0.500456807
tr|Q19V51|Q19V51_DERVA	Hemelipoglycoprotein OS=Dermacentor variabilis PE=2 SV=1	-1.039333181	0.35734	5658.486653	6989.135134	5142.682195	6682.096493	1911.277229	1124.478216	-1330.648481	0.809611854	-0.091723142
tr|L7MBL5|L7MBL5_9ACAR	Putative amblyomma 40-33 family member OS=Rhipicephalus pulchellus PE=2 SV=1	-1.036297462	0.3586	1654.660615	5648.399061	1677.253893	2091.186746	775.0297873	6629.923508	-3993.738446	0.292943292	-0.533216442
tr|L7M2W1|L7M2W1_9ACAR	Putative der and-48 ribosomal protein l32 OS=Rhipicephalus pulchellus PE=2 SV=1	1.028589282	0.3618	11475.55548	7499.954514	10549.98216	5490.553705	5258.203373	4143.465118	3975.600962	1.530083343	0.184715087
tr|V9R842|V9R842_9RICK	Elongation factor Tu OS=Ehrlichia muris AS145 GN=tuf PE=3 SV=1	-1.028447634	0.36186	1576.823863	2460.728885	1524.938736	2558.475176	295.7821654	1458.939482	-883.9050218	0.640795446	-0.193280583
tr|L7LZM3|L7LZM3_9ACAR	Putative cytochrome c OS=Rhipicephalus pulchellus PE=2 SV=1	-1.023791405	0.36381	3806.342729	7061.30235	2478.355322	4890.185685	2391.075553	4960.541154	-3254.959622	0.539042593	-0.268376917

tr|C9W1R6|C9W1R6_RHISA	Hematopoietic stem/progenitor cells protein-like protein OS=Rhipicephalus sanguineus PE=2 SV=1	-1.015404371	0.36734	3719.830196	5549.149356	3256.835367	5665.450663	1550.573375	2707.887517	-1829.31916	0.670342418	-0.173703299
tr|V5HR13|V5HR13_IXORI	Putative sarcomere (Fragment) OS=Ixodes ricinus PE=2 SV=1	-1.014299401	0.36781	5088.627194	15707.16555	5103.226331	5586.623082	789.224853	18115.37938	-10618.53835	0.323968521	-0.489497187
tr|L7LWU5|L7LWU5_9ACAR	Putative microtubule associated complex OS=Rhipicephalus pulchellus PE=2 SV=1	1.010220389	0.36954	16028.29904	12045.32781	17678.24587	9191.886324	3535.785712	5842.28472	3982.971224	1.330665241	0.124068813
tr|L7MAX7|L7MAX7_9ACAR	Putative eukaryotic translation initiation factor 4a2 OS=Rhipicephalus pulchellus PE=2 SV=1	1.006409862	0.37116	22324.77601	14907.60317	19257.25543	8961.295174	6295.937899	11104.45339	7417.172843	1.497542949	0.175379287
tr|C9W1T0|C9W1T0_RHISA	Secreted protein (Fragment) OS=Rhipicephalus sanguineus PE=2 SV=1	-1.004241786	0.37208	1337.085351	10825.85194	665.6166469	2168.613833	1391.309107	16306.35866	-9488.766589	0.123508557	-0.908302952
tr|G3MKN2|G3MKN2_9ACAR	Putative uncharacterized protein OS=Amblyomma maculatum PE=2 SV=1	-1.000729988	0.37359	4449.850635	9641.111573	3920.710089	9216.075211	3554.222171	8252.100868	-5191.260938	0.461549542	-0.335781675
tr|G3MLS3|G3MLS3_9ACAR	Dolichyl-diphosphooligosaccharide--protein glycosyltransferase subunit 1 OS=Amblyomma maculatum PE=2 SV=1	0.995725979	0.37574	6506.330504	4278.156003	5937.777007	5071.079571	2028.03618	3302.952003	2228.1745	1.520825912	0.182079503
tr|L7M046|L7M046_9ACAR	Putative cuticular protein OS=Rhipicephalus pulchellus PE=2 SV=1	-0.987944794	0.37911	1226.342037	21112.67414	994.2974478	1059.527932	486.7026053	34861.03823	-19886.33211	0.058085585	-1.235931629
tr|L7M3F0|L7M3F0_9ACAR	Uncharacterized protein OS=Rhipicephalus pulchellus PE=2 SV=1	-0.973453779	0.38545	5209.53792	17121.36909	4044.873603	5250.302571	2912.137956	20993.51372	-11911.83117	0.304271107	-0.516739286
tr|V9VL04|V9VL04_RHIMP	Serine protease inhibitor 6 RmS6 OS=Rhipicephalus microplus GN=RmS-6 PE=2 SV=1	-0.972810303	0.38573	3893.317679	14855.44975	4017.765794	5278.190629	630.1623629	19507.4731	-10962.13207	0.262080095	-0.581565963
tr|A0A023FLK6|A0A023FLK6_9ACAR	Putative neural cell adhesion molecule l1 (Fragment) OS=Amblyomma cajennense PE=2 SV=1	0.964738347	0.38931	1492.744446	906.2953332	1409.183459	550.8183188	766.8242149	721.491442	586.4491125	1.647083893	0.21671572
tr|G3MMU1|G3MMU1_9ACAR	Putative uncharacterized protein OS=Amblyomma maculatum PE=2 SV=1	0.963264157	0.38996	6485.020953	3905.294359	5868.440341	3930.543982	4223.773076	1917.432541	2579.726594	1.660571613	0.22025761
tr|L7M3Y9|L7M3Y9_9ACAR	Putative fatty acid-binding protein fabp OS=Rhipicephalus pulchellus PE=2 SV=1	-0.957984966	0.39232	1494.820167	18232.84609	1209.64879	968.8012236	689.8332432	30254.73191	-16738.02592	0.081985015	-1.086265518
tr|L7M897|L7M897_9ACAR	Putative mitochondrial inner membrane protein mitofilin OS=Rhipicephalus pulchellus PE=2 SV=1	0.954378892	0.39394	7596.705716	5470.963806	7718.803643	4864.4263	2275.721807	3115.1948	2125.74191	1.388549803	0.142561461

tr|A0A0C9SEI9|A0A0C9SEI9_AMBAM	Protein disulfide-isomerase OS=Amblyomma americanum PE=2 SV=1	-0.953914632	0.39415	764.934040 9	3406.639112	807.0366374	889.9830767	290.1059651	4787.840438	-2641.705071	0.224542141	-0.64870214
tr|A0A023GCL4|A0A023GCL4_9ACAR	Putative 40s ribosomal protein s19 (Fragment) OS=Amblyomma triste PE=2 SV=1	0.953827272	0.39418	3532.051586	2099.056607	3331.882766	2055.115747	2497.158283	731.7690486	1432.999499	1.682685247	0.226002887
tr|L7MIS7|L7MIS7_9ACAR	Putative reticulocalbin calumenin dna supercoiling factor (Fragment) OS=Rhipicephalus pulchellus PE=2 SV=1	-0.950817315	0.39554	727.369189 1	2209.802828	614.7505963	1031.110759	268.9434644	2687.040967	-1482.433639	0.329155697	-0.482598624
tr|M4PPE7|M4PPE7_AMBAM	AV422 OS=Amblyomma americanum PE=2 SV=1	-0.949372376	0.39619	3927.400553	25778.94989	2410.268677	3019.510008	3636.2583	39700.1511	-21851.54933	0.152349129	-0.817160025
tr|L7M921|L7M921_9ACAR	Putative lysosomal & prostatic acid phosphatase OS=Rhipicephalus pulchellus PE=2 SV=1	0.948893054	0.39641	18728.79536	15539.83733	20581.0367	13727.05594	3427.050863	4705.158344	3188.958025	1.205211802	0.081063376
tr|L7M7M2|L7M7M2_9ACAR	Uncharacterized protein OS=Rhipicephalus pulchellus PE=2 SV=1	-0.938661836	0.40105	2505.94054	10519.37055	2339.21547	2156.283216	1004.197373	14752.51599	-8013.430011	0.238221529	-0.623018992
tr|L7M8L6|L7M8L6_9ACAR	Putative branched chain alpha-keto acid dehydrogenase e1 beta subunit OS=Rhipicephalus pulchellus PE=2 SV=1	-0.938342982	0.40119	465.527705 3	1738.306007	417.3911279	500.2910835	106.0207778	2346.978522	-1272.778302	0.267805383	-0.572180698
tr|L7M8A8|L7M8A8_9ACAR	Putative chaperonin OS=Rhipicephalus pulchellus PE=2 SV=1	0.937798333	0.40144	7996.382701	6756.970887	8032.301679	7143.303441	2119.071509	865.7735853	1239.411814	1.183427135	0.073141523
tr|L7MGW5|L7MGW5_9ACAR	Uncharacterized protein (Fragment) OS=Rhipicephalus pulchellus PE=2 SV=1	-0.936707848	0.40194	1481.999654	18065.42198	1383.121782	576.7474112	542.6591307	30659.32667	-16583.42233	0.082035153	-1.086000008
tr|E4W3Z1|E4W3Z1_9ACAR	Protein disulfide isomerase 3 (Fragment) OS=Haemaphysalis qinghaiensis PE=2 SV=1	-0.932119547	0.40404	969.6756356	4745.423704	1206.649946	876.8956103	734.6334873	6977.472524	-3775.748068	0.204339106	-0.689648512
sp|P49822|ALBU_CANLF	Serum albumin OS=Canis lupus familiaris GN=ALB PE=1 SV=3	-0.930373123	0.40484	1974.678489	9290.896546	1978.864552	1558.610181	40.06126637	13620.34894	-7316.218057	0.212539068	-0.672561229
tr|L7M7U4|L7M7U4_9ACAR	Proteasome subunit alpha type OS=Rhipicephalus pulchellus PE=2 SV=1	0.930210435	0.40492	7884.983265	4691.350386	6499.575697	4986.377278	5921.749183	542.4346727	3193.632878	1.680749169	0.225502905
tr|A0A023FXR2|A0A023FXR2_9ACAR	Putative glutathione s-transferase ixodes scapularis glutathione s-transferase OS=Amblyomma parvum PE=2 SV=1	-0.929862129	0.40508	1755.619926	6245.661402	1903.637126	2768.841655	381.9613885	8354.857373	-4490.041476	0.281094317	-0.551147935
tr|G3MHT9|G3MHT9_9ACAR	Putative uncharacterized protein (Fragment) OS=Amblyomma maculatum PE=2 SV=1	-0.926711415	0.40653	3439.839592	5472.689642	1584.348731	4501.094598	3242.137978	1981.012341	-2032.	0.62854644	-0.201662629

										850049		
tr|C9W1Q2|C9W1Q2_RHISA	Protein disulfide isomerase OS=Rhipicephalus sanguineus PE=2 SV=1	-0.924144577	0.40771	5786.591105	35866.84847	6386.787704	4394.579587	1041.424147	56367.41849	-30080.25737	0.161335365	-0.792270423
tr|C9W1U0|C9W1U0_RHISA	Putative cement protein (Fragment) OS=Rhipicephalus sanguineus PE=2 SV=1	-0.919388881	0.40992	1257314.29	1897296.269	1659769.49	2073256.874	868963.1776	835791.622	-639981.9792	0.662687378	-0.178691301
tr|L7MIL3|L7MIL3_9ACAR	Putative aldehyde dehydrogenase (Fragment) OS=Rhipicephalus pulchellus PE=2 SV=1	-0.915716187	0.41163	3222.125131	15203.96619	3574.260443	2697.579163	1240.270651	22629.34453	-11981.84106	0.211926618	-0.673814493
tr|E2J6W6|E2J6W6_9ACAR	40S ribosomal protein SA (P40)/laminin receptor 1 (Fragment) OS=Hyalomma marginatum rufipes PE=2 SV=1	-0.915100247	0.41191	1176.929104	9445.902355	1160.871027	548.5971129	61.90555406	15650.92984	-8268.973251	0.124596789	-0.904493149
tr|E7CF11|E7CF11_RHIMP	Mitochondrial volatge dependent anion-selective channel (Fragment) OS=Rhipicephalus microplus GN=VDAC PE=4 SV=1	0.914971395	0.41197	22224.27637	16432.782988	20877.70336	20545.36692	5019.465715	9746.805963	5791.493387	1.352435336	0.131116509
tr|A0A023G9I9|A0A023G9I9_9ACAR	Putative ribosomal protein l35a OS=Amblyomma triste PE=2 SV=1	0.911912029	0.4134	13593.80276	6599.497776	16950.29514	9221.687098	12264.99161	5104.276514	6994.304979	2.059823825	0.313830077
tr|L7LPR5|L7LPR5_9ACAR	Putative tick salivary cystatin OS=Rhipicephalus pulchellus PE=2 SV=1	-0.911525811	0.41358	628.0529185	1600.996501	792.4720569	671.2719313	286.2188215	1826.464643	-972.9435823	0.392288752	-0.406394145
tr|B7SP58|B7SP58_DERVA	Guanine nucleotide-binding protein OS=Dermacentor variabilis PE=2 SV=1	-0.893454787	0.42211	3745.287135	14277.98172	1066.440169	5004.294508	5140.895699	19760.907	-10532.69458	0.262312084	-0.581181703
tr|B1B544|B1B544_HAELO	Vitellogenin-2 OS=Haemaphysalis longicornis GN=HlVg-2 PE=2 SV=1	-0.887839464	0.42479	1822.11532	4716.217475	2041.316679	1538.700042	1024.162369	5552.322474	-2894.102154	0.386350996	-0.413017963
tr|A0A023GP35|A0A023GP35_9ACAR	Putative elongation factor 1 beta/delta chain ixodes scapularis elongation factor 1 beta/delta chain OS=Amblyomma triste PE=2 SV=1	-0.863226896	0.4367	6568.50794	13966.89264	6870.367055	5507.698608	762.7489355	14825.13062	-7398.384696	0.470291289	-0.327633066
tr|L7M8Y1|L7M8Y1_9ACAR	Putative yippee OS=Rhipicephalus pulchellus PE=2 SV=1	-0.859734073	0.43841	4692.493343	9984.232519	3801.199776	5891.452722	4880.975785	9477.943508	-5291.739177	0.469990391	-0.327911021
tr|L7M911|L7M911_9ACAR	Putative zn2+-binding dehydrogenase nuclear receptor binding factor-1 OS=Rhipicephalus pulchellus PE=2 SV=1	0.857260436	0.43963	2624.646894	1628.348189	2780.990339	903.3730234	1552.68132	1281.10538	996.2987053	1.611846233	0.207323609
tr|L7LXL4|L7LXL4_9ACAR	Inosine-5'-monophosphate dehydrogenase OS=Rhipicephalus pulchellus PE=2 SV=1	-0.855492431	0.4405	4114.667195	8321.098446	3281.212625	4760.685568	1956.241869	8288.722551	-4206.431252	0.494486061	-0.305845946

tr|L7M877|L7M877_9ACAR	Putative malectin OS=Rhipicephalus pulchellus PE=2 SV=1	-0.855464517	0.44051	3912.231388	7770.237041	4844.052598	3856.628712	2063.288277	7533.839307	-3858.005653	0.503489323	-0.298009735
tr|L7MJK0|L7MJK0_9ACAR	Putative seryl-trna synthetase (Fragment) OS=Rhipicephalus pulchellus PE=2 SV=1	0.854947365	0.44077	3574.495356	2729.704804	3767.574482	2106.423043	1011.270953	1380.751316	844.7905523	1.309480553	0.117099053
tr|V5HYK0|V5HYK0_IXORI	Putative conserved protein mo25 OS=Ixodes ricinus PE=2 SV=1	0.851883684	0.44228	3905.346384	2200.798523	4523.757579	869.5336946	2471.642237	2429.399418	1704.547861	1.774513361	0.249079274
tr|L7M420|L7M420_9ACAR	Putative ribosomal protein s10b OS=Rhipicephalus pulchellus PE=2 SV=1	-0.850744637	0.44284	11632.7696	26382.93615	14194.20391	10217.2706	5462.385077	29529.23476	-14750.16655	0.440920204	-0.35564
tr|C9W1A7|C9W1A7_RHISA	Putative cement protein (Fragment) OS=Rhipicephalus sanguineus PE=2 SV=1	0.850463488	0.44298	21163.32415	15013.04093	19272.6849	12454.58806	5337.223267	11331.62871	6150.283223	1.409662723	0.149115215
tr|A0A023GBX7|A0A023GBX7_9ACAR	Putative moesin/ezrin/radixin protein 1 OS=Amblyomma triste PE=2 SV=1	0.850038305	0.44319	9069.856577	6389.555442	9019.287329	4179.326557	1087.004336	5352.15168	2680.300136	1.419481409	0.152129709
tr|L7ME67|L7ME67_9ACAR	Putative glycine rich protein (Fragment) OS=Rhipicephalus pulchellus PE=2 SV=1	-0.848241622	0.44408	72139.96001	216730.8882	76000.119585	51800.53106	10364.25554	295062.7197	-144590.9282	0.332855001	-0.477744914
tr|C9W1H9|C9W1H9_RHISA	NADH dehydrogenase 1 alpha subcomplex OS=Rhipicephalus sanguineus PE=2 SV=1	-0.845728233	0.44533	1506.567097	4022.960575	1256.087398	1187.742208	625.3144125	5115.494737	-2516.393478	0.374492136	-0.426557298
tr|A0A0C9SB67|A0A0C9SB67_AMBAM	Calponin OS=Amblyomma americanum PE=2 SV=1	-0.842591854	0.44689	2616.177013	4129.388062	2594.905035	4574.084321	587.4389933	3054.617846	-1513.211048	0.633550777	-0.198218572
tr|L7M8A4|L7M8A4_9ACAR	Aspartate aminotransferase OS=Rhipicephalus pulchellus PE=2 SV=1	-0.840710421	0.44783	27164.45458	56409.603777	25893.27931	32035.85189	2770.396203	60187.79836	-29245.14919	0.481557266	-0.31735206
tr|B7SP52|B7SP52_DERVA	Ribosomal protein S17 OS=Dermacentor variabilis PE=2 SV=1	0.839295195	0.44854	11501.58056	7147.048274	13774.37379	3553.937438	5661.814023	6978.528801	4354.532287	1.609277022	0.20663081
tr|L7M2B2|L7M2B2_9ACAR	Translocon-associated protein subunit beta OS=Rhipicephalus pulchellus PE=2 SV=1	0.830865122	0.45277	4549.572763	3613.441844	5015.098791	3468.10516	1101.111916	1611.171018	936.1309186	1.259069042	0.100049546
tr|A0A023FMI0|A0A023FMI0_9ACAR	Putative acetyl-coa hydrolase OS=Amblyomma cajennense PE=2 SV=1	0.830820231	0.45279	18040.71435	12080.929665	16262.34874	5971.110972	5753.760036	11012.09119	5959.784698	1.493321695	0.174153375
tr|L7M2B5|L7M2B5_9ACAR	Proteasome subunit alpha type OS=Rhipicephalus pulchellus PE=2 SV=1	-0.828211559	0.45411	5160.446579	9020.060575	4694.316851	5024.212699	1524.766954	7926.341316	-3859.613996	0.572107752	-0.242522168

tr|L7LYB7|L7LYB7_9ACAR	Putative conserved secreted protein OS=Rhipicephalus pulchellus PE=2 SV=1	0.824495	0.45598	33172.68423	20418.88206	36838.55323	22200.30451	25805.15002	7206.185395	12753.80217	1.624608249	0.210748654
tr|F2Z4Q6|F2Z4Q6_CANLF	Serum albumin OS=Canis lupus familiaris GN=ALB PE=4 SV=1	-0.824117474	0.45618	1265.741454	5261.55734	1390.952694	474.9095748	513.5662812	8382.303505	-3995.815886	0.240564033	-0.618769304
tr|L7M2X3|L7M2X3_9ACAR	Putative mitochondrial electron transport nadh to ubiquinone OS=Rhipicephalus pulchellus PE=2 SV=1	0.823140511	0.45667	3587.803793	2552.970177	3509.851452	2781.487438	1556.176969	1523.088311	1034.833616	1.405344969	0.147782943
tr|A0A023FM97|A0A023FM97_9ACAR	Putative puromycin-sensitive aminopeptidase (Fragment) OS=Amblyomma cajennense PE=2 SV=1	0.820031806	0.45825	10026.92256	6093.007799	9938.074718	6509.554172	7905.606417	2557.892292	3933.914763	1.645644137	0.216335927
tr|B7PLC7|B7PLC7_IXOSC	Cuticular protein, putative OS=Ixodes scapularis GN=IscW_ISCW006422 PE=4 SV=1	0.818962947	0.45879	9737.977546	6633.515011	10009.66036	3175.420915	2164.658057	6198.630647	3104.462535	1.46799661	0.166725053
tr|L7M8D8|L7M8D8_9ACAR	Succinate dehydrogenase (ubiquinone) iron-sulfur subunit, mitochondrial OS=Rhipicephalus pulchellus PE=2 SV=1	-0.805685831	0.46559	1561.242917	3179.863526	1560.060826	1243.864391	146.3075627	3476.608088	-1618.620609	0.490977963	-0.308938
tr|L7MHC5|L7MHC5_9ACAR	Putative glutamine synthetase (Fragment) OS=Rhipicephalus pulchellus PE=2 SV=1	0.80318459	0.46688	6230.748083	3228.1346	5994.312068	1576.989746	5683.179773	3102.908668	3002.613484	1.930138875	0.285588558
tr|G3MKR0|G3MKR0_9ACAR	40S ribosomal protein SA OS=Amblyomma maculatum PE=2 SV=1	0.802219519	0.46738	10170.68884	7710.267067	10339.83901	6408.761705	2733.126044	4555.197244	2460.421777	1.319109799	0.120280947
tr|L7M982|L7M982_9ACAR	Putative tick thioester protein OS=Rhipicephalus pulchellus PE=2 SV=1	0.79627357	0.47046	9427.313378	6272.921099	8719.591856	5116.210041	6302.93638	2711.472384	3154.392279	1.502858593	0.176918119
tr|A0A023FNJ0|A0A023FNJ0_9ACAR	T-complex protein 1 subunit gamma (Fragment) OS=Amblyomma cajennense PE=2 SV=1	0.794805529	0.47122	7310.787878	5228.104101	7564.553456	3529.695782	1102.688583	4402.621846	2082.683776	1.398363104	0.145619956
tr|L7MM52|L7MM52_9ACAR	Putative emp24/gp25l/p24 family of membrane trafficking (Fragment) OS=Rhipicephalus pulchellus PE=2 SV=1	-0.794011155	0.47163	5558.500257	6188.392211	6013.984473	6532.721372	1027.413748	912.365715	-629.8919545	0.898213957	-0.046620201
tr|G3MMT9|G3MMT9_9ACAR	Putative uncharacterized protein OS=Amblyomma maculatum PE=2 SV=1	0.790815851	0.4733	7306.157323	5510.47602	7015.409872	7670.44592	1187.648922	3749.307637	1795.681304	1.325866821	0.122499903
tr|L7M6S1|L7M6S1_9ACAR	Putative heat shock-related protein OS=Rhipicephalus pulchellus PE=2 SV=1	0.782242615	0.47779	50406.04407	40986.02196	51132.34586	36243.74961	17814.9671	10848.03827	9420.022109	1.229834994	0.089846846
tr|L7M7Q3|L7M7Q3_9ACAR	Putative flotillin OS=Rhipicephalus pulchellus PE=2 SV=1	0.779577785	0.47919	4935.903706	4242.709027	4961.852065	3395.951862	56.40103295	1539.093418	693.1946786	1.163384921	0.06572343
tr|L7M5K4|L7M5K4_9ACAR	Putative chloride intracellular channel 6-like protein OS=Rhipicephalus pulchellus PE=2 SV=1	-0.773795301	0.48224	1869.188298	5269.830865	1965.306233	1100.209825	492.4296876	7595.998216	-3400.642568	0.35469607	-0.450143623

tr|L7M7J5|L7M7J5_9ACAR	Putative 20s proteasome regulatory subunit beta type psmb1/pre7 OS=Rhipicephalus pulchellus PE=2 SV=1	-0.758605269	0.49033	7297.667344	11119.70261	7514.540667	6598.677509	1290.43491	8630.547999	-3822.035264	0.6562826	-0.18290911
tr|J9P430|J9P430_CANLF	Uncharacterized protein OS=Canis lupus familiaris GN=TF PE=3 SV=1	-0.751394179	0.49421	3858.352185	6334.12508	4347.725963	3289.998849	1112.006426	5597.557563	-2475.772895	0.609137353	-0.215284768
tr|L7M4W5|L7M4W5_9ACAR	60S ribosomal protein L13 OS=Rhipicephalus pulchellus PE=2 SV=1	0.746638704	0.49678	7740.650948	4000.677215	5120.047646	2547.322446	8237.724251	2722.604625	3739.973733	1.934835162	0.286643971
tr|L7MGG4|L7MGG4_9ACAR	Putative g-protein alpha subunit (Fragment) OS=Rhipicephalus pulchellus PE=2 SV=1	0.745871761	0.49719	4283.706325	2640.409716	2661.017954	3162.786252	3580.263575	1320.545616	1643.29661	1.622364249	0.210148367
tr|L7LY48|L7LY48_9ACAR	Putative transcriptional regulator dj-1 OS=Rhipicephalus pulchellus PE=2 SV=1	-0.744171091	0.49811	7087.886983	11638.96099	7980.276634	6746.431404	2584.477083	10272.44945	-4551.074007	0.608979357	-0.215397428
tr|L7M7W2|L7M7W2_9ACAR	Fructose-bisphosphate aldolase OS=Rhipicephalus pulchellus PE=2 SV=1	-0.740644789	0.50003	15594.83651	29409.76594	15917.44859	13973.9917	4226.632087	32029.52986	-13814.92943	0.530260477	-0.275510742
tr|L7M7G4|L7M7G4_9ACAR	Putative actin-binding cytoskeleton protein filamin OS=Rhipicephalus pulchellus PE=2 SV=1	0.739729463	0.50053	9488.432055	5663.658201	5463.789096	5327.810417	8615.189475	2445.574135	3824.773854	1.675318622	0.224097416
tr|L7MIW9|L7MIW9_9ACAR	Putative eukaryotic translation initiation factor 3 subunit m (Fragment) OS=Rhipicephalus pulchellus PE=2 SV=1	-0.737271494	0.50187	1184.931658	1435.427164	1268.343701	1232.98827	236.0688434	539.0570195	-250.4955059	0.825490619	-0.083287858
tr|L7M3T4|L7M3T4_9ACAR	Putative cdc42 OS=Rhipicephalus pulchellus PE=2 SV=1	-0.737255137	0.50187	1193.437876	3129.70479	1388.366248	754.7160869	912.0616774	4456.544897	-1936.266914	0.381326021	-0.418703558
tr|A0A023GME3|A0A023GME3_9ACAR	Putative vitellogenin-1 (Fragment) OS=Amblyomma triste PE=2 SV=1	-0.735507053	0.50283	1631.057314	1916.885453	1654.505228	2112.110724	55.96193285	670.7683335	-285.828139 7	0.850889296	-0.07012694
tr|L7M1M5|L7M1M5_9ACAR	Putative tfiif-interacting ctd phosphat OS=Rhipicephalus pulchellus PE=2 SV=1	0.734527277	0.50336	2374.476865	1478.246077	1553.285146	1840.037951	1855.201363	1012.17556	896.230788	1.606279835	0.205821207
tr|V5HZY4|V5HZY4_IXORI	Putative transcriptional activator protein (Fragment) OS=Ixodes ricinus PE=2 SV=1	0.731408571	0.50507	1986.73311	1458.226012	1698.538918	1130.924215	1109.077436	579.9549508	528.5070987	1.36243154	0.134314689
tr|L7M840|L7M840_9ACAR	Putative multifunctional chaperone 14-3-3 family OS=Rhipicephalus pulchellus PE=2 SV=1	-0.731180521	0.5052	14295.38369	20797.62035	15696.56781	13966.95854	7100.750325	13668.38032	-6502.236658	0.6873567	-0.16281783
tr|B7PZZ8|B7PZZ8_IXOSC	Putative uncharacterized protein (Fragment) OS=Ixodes scapularis GN=IscW_ISCW010302 PE=4 SV=1	0.729495182	0.50612	3035.4553	2077.5394	1908.33458	2353.224426	2155.797163	724.8474459	957.9159001	1.461081942	0.164674573

tr|L7M861|L7M861_9ACAR	Putative tropomodulin OS=Rhipicephalus pulchellus PE=2 SV=1	0.725160649	0.5085	12283.67014	9775.713902	9316.237526	9009.50675	5554.051457	2244.067674	2507.956241	1.256549677	0.099179663
tr|A0A0N6VM48|A0A0N6VM48_9ACAR	Muscle LIM protein OS=Hyalomma marginatum rufipes GN=MLP PE=2 SV=1	-0.724364823	0.50894	3141.413906	5122.896818	2413.463468	7060.053234	2599.758961	3961.028591	-1981.482912	0.613210458	-0.212390447
tr|A0A023GJ99|A0A023GJ99_9ACAR	Putative lysophosphatidic acid acyltransfer OS=Amblyomma triste PE=2 SV=1	-0.715150209	0.51404	633.557541	1501.301943	426.3168723	329.9153643	454.2825544	2051.939089	-867.7444014	0.42200541	-0.374681982
tr|A0A023FI34|A0A023FI34_9ACAR	Putative myosin alkali light chain protein OS=Amblyomma cajennense PE=2 SV=1	-0.711560048	0.51603	9872.995247	12419.88361	9291.467619	13853.73005	1224.108819	6077.48039	-2546.888365	0.794934603	-0.099668598
tr|B7Q730|B7Q730_IXOSC	Cuticular protein, putative OS=Ixodes scapularis GN=IscW_ISCW021519 PE=4 SV=1	-0.704112065	0.52019	6202.604311	8775.411352	2624.514206	8490.13244	6219.872796	1169.511061	-2572.807041	0.70681636	-0.150693407
tr|A0A023FJI0|A0A023FJI0_9ACAR	Ribosomal protein OS=Amblyomma cajennense PE=2 SV=1	0.701313337	0.52176	13609.21166	10142.61924	11862.19837	7048.856663	3895.730347	7623.84793	3466.592422	1.341784734	0.127682847
tr|L7M4Z0|L7M4Z0_9ACAR	Putative phosphoenolpyruvate carboxykinase OS=Rhipicephalus pulchellus PE=2 SV=1	0.69765495	0.52382	8691.627549	6395.804526	7761.742869	3342.944962	1920.620301	5366.446567	2295.823022	1.358957659	0.133205926
tr|R4IKG1|R4IKG1_RHISA	Cytochrome c oxidase subunit 2 OS=Rhipicephalus sanguineus GN=cox2 PE=3 SV=1	-0.695708923	0.52491	4427.471392	6466.368268	3942.25862	4041.560177	1532.155511	4839.325426	-2038.896877	0.684692119	-0.164504671
tr|F1PCE8|F1PCE8_CANLF	Uncharacterized protein OS=Canis lupus familiaris GN=LOC475521 PE=3 SV=1	-0.676834427	0.53563	1084133.551	1640522.176	1193909.494	2353412.358	271756.5685	1397649.552	-556388.6255	0.66084663	-0.179899321
tr|L7MF58|L7MF58_9ACAR	Putative emp24/gp25l/p24 family of membrane trafficking (Fragment) OS=Rhipicephalus pulchellus PE=2 SV=1	-0.667322022	0.54109	2082.352861	3302.456861	2031.570844	1715.115524	1245.48331	2911.607382	-1220.104001	0.630546574	-0.200282829
RRRRRtr|F1PQ54|F1PQ54_CANLF	REVERSED Uncharacterized protein OS=Canis lupus familiaris GN=TOX2 PE=4 SV=2	-0.665691296	0.54203	2613.099687	7347.199587	1549.679457	563.1685086	1946.673231	12162.7745	-4734.099899	0.355659276	-0.44896586
tr|A0A023FWU0|A0A023FWU0_9ACAR	Putative mitochondrial phosphate carrier protein OS=Amblyomma parvum PE=2 SV=1	-0.665249928	0.54229	67514.45957	119443.1896	66826.97436	92134.85711	2323.272566	135182.1545	-51928.72999	0.565243274	-0.247764596
tr|L7M1R8|L7M1R8_9ACAR	Putative ribosome bioproteinsis protein OS=Rhipicephalus pulchellus PE=2 SV=1	-0.664995414	0.54243	7797.38461	10533.67136	9281.694733	10406.48272	6396.841234	3142.261742	-2736.286752	0.740234277	-0.130630808

tr|L7MIJ5|L7MIJ5_9ACAR	Putative ubiquitin activating enzyme uba1 (Fragment) OS=Rhipicephalus pulchellus PE=2 SV=1	-0.664451774	0.54275	1026.445135	1973.966326	1003.831013	780.8974314	270.5982334	2455.070567	-947.521190 4	0.519991209	-0.284003999
tr|Q26229|Q26229_RHIAP	Autoantigen OS=Rhipicephalus appendiculatus PE=2 SV=1	-0.663025614	0.54357	4030.418972	6443.512811	4572.70777	4750.09728	1335.098	6160.827313	-2413.09384	0.625500265	-0.203772502
tr|L7LZP0|L7LZP0_9ACAR	Uncharacterized protein OS=Rhipicephalus pulchellus PE=2 SV=1	0.659170605	0.5458	19966.3996 9	13177.16956	13615.56529	14602.02657	15374.13724	9049.011724	6789.230133	1.515226741	0.180477626
tr|L7MAC0|L7MAC0_9ACAR	Putative chaperonin chaperonin OS=Rhipicephalus pulchellus PE=2 SV=1	-0.649944795	0.55117	1236.656629	1800.870795	1205.248207	1803.361575	75.66345539	1501.680574	-564.2141664	0.686699252	-0.163233425
tr|L7MKU0|L7MKU0_9ACAR	Uncharacterized protein (Fragment) OS=Rhipicephalus pulchellus PE=2 SV=1	0.644512432	0.55434	12685.62004	9398.831385	13113.09571	8367.225279	8601.936681	2006.493257	3286.788655	1.349701843	0.130237841
tr|L7MDQ8|L7MDQ8_9ACAR	ATP synthase subunit beta (Fragment) OS=Rhipicephalus pulchellus PE=2 SV=1	-0.639756517	0.55713	346575.0577	419752.0476	332590.5377	337833.7803	80466.01837	181039.5863	-73176.98994	0.825666151	-0.083195519
tr|L7M4S8|L7M4S8_9ACAR	Signal peptidase complex catalytic subunit SEC11 OS=Rhipicephalus pulchellus PE=2 SV=1	-0.635285012	0.55977	6916.860454	10903.06258	6895.869456	5358.209299	321.6384717	10863.28219	-3986.202123	0.634396107	-0.197639491
tr|S5FVY5|S5FVY5_RHIMP	60S acidic ribosomal protein P0 OS=Rhipicephalus microplus PE=2 SV=1	-0.626137803	0.56518	47080.35509	76944.2861	47137.9729	32395.86344	11487.11615	81808.41698	-29863.93101	0.61187591	-0.213336645
tr|L7M621|L7M621_9ACAR	Putative translocon-associated protein OS=Rhipicephalus pulchellus PE=2 SV=1	0.625915001	0.56531	4076.375772	2900.113373	4157.063357	3258.08701	2967.835603	1336.750949	1176.262399	1.405591867	0.147859236
tr|A0A023FLK4|A0A023FLK4_9ACAR	Putative medium-chain acyl-coa dehydrogenase OS=Amblyomma cajennense PE=2 SV=1	-0.625284706	0.56569	5903.06559	8739.491563	6905.994872	4941.395165	2043.066009	7586.674222	-2836.425973	0.675447255	-0.170408559
tr|L7M253|L7M253_9ACAR	Putative host cell transcription factor hcfc1 OS=Rhipicephalus pulchellus PE=2 SV=1	0.624451751	0.56618	854.3528744	630.3751627	721.2897577	453.7598155	271.4328551	558.8166233	223.9777116	1.355308592	0.132038192
tr|G3MJC1|G3MJC1_9ACAR	Putative uncharacterized protein (Fragment) OS=Amblyomma maculatum PE=2 SV=1	-0.622155627	0.56755	3522.143504	4385.846602	3318.663072	4659.281678	2352.707409	496.4095505	-863.7030985	0.803070381	-0.095246391
tr|L7M6Z0|L7M6Z0_9ACAR	Putative rap1a member of ras oncoprotein family OS=Rhipicephalus pulchellus PE=2 SV=1	0.621940128	0.56768	5569.208672	4780.667391	4752.479861	4560.280319	1488.231517	1614.829725	788.5412809	1.164943765	0.066304961
tr|G3MKS0|G3MKS0_9ACAR	Putative uncharacterized protein OS=Amblyomma maculatum PE=2 SV=1	0.621742223	0.56779	9921.635779	7805.648396	9978.753722	5296.486727	2948.540184	5104.298112	2115.987383	1.271084127	0.104174295

tr|L7M880|L7M880_9ACAR	Putative rab geranylgeranyltransferase component a rab escort protein OS=Rhipicephalus pulchellus PE=2 SV=1	0.600382261	0.58061	3065.49514	2269.098963	2917.015006	1031.224381	429.0057961	2257.125693	796.3961772	1.350974634	0.130647195
tr|A0A023FXZ4|A0A023FXZ4_9ACAR	Putative heat shock protein 90 (Fragment) OS=Amblyomma parvum PE=2 SV=1	0.596579375	0.58291	3136.594994	2309.638797	3075.30935	1370.016766	770.2358246	2274.000777	826.9561973	1.358045682	0.132914379
tr|L7M7J9|L7M7J9_9ACAR	Putative phosphoribosylamidoimidazole-succinocarboxamide synthase OS=Rhipicephalus pulchellus PE=2 SV=1	-0.584715411	0.59013	4853.178906	6109.248777	4997.177232	4978.825861	426.5304252	3696.216142	-1256.069871	0.794398638	-0.099961509
tr|L7MAA3|L7MAA3_9ACAR	Putative chaperonin chaperonin OS=Rhipicephalus pulchellus PE=2 SV=1	0.579239645	0.59348	2851.09001	2033.068396	2844.522293	893.4881941	668.5525243	2352.923214	818.0216143	1.402358138	0.146858939
tr|L7M7X5|L7M7X5_9ACAR	Catalase OS=Rhipicephalus pulchellus PE=2 SV=1	-0.572520008	0.59761	5393.472479	8434.452215	5318.43513	3462.619793	645.9501568	9177.203051	-3040.979736	0.639457352	-0.194188415
tr|V5GXZ5|V5GXZ5_IXORI	Putative elongation factor-1 gamma (Fragment) OS=Ixodes ricinus PE=2 SV=1	-0.569174484	0.59968	1407.410339	2067.031566	1507.094386	942.9052624	187.206466	1998.539825	-659.6212266	0.680884783	-0.166926372
tr|L7ME31|L7ME31_9ACAR	Putative laminin a (Fragment) OS=Rhipicephalus pulchellus PE=2 SV=1	0.560529613	0.60503	37063.00376	31261.97628	33210.87386	28694.92407	11827.14459	13469.81268	5801.027483	1.185561765	0.073924184
tr|E2J6V2|E2J6V2_9ACAR	40S ribosomal protein S7 (Fragment) OS=Hyalomma marginatum rufipes PE=2 SV=1	0.554585546	0.60872	3393.743085	2923.275161	3426.771973	2245.002128	135.4110646	1463.08642	470.467923 8	1.160938638	0.064809266
tr|L7M7R5|L7M7R5_9ACAR	Putative cathepsin d isoform 1 protein OS=Rhipicephalus pulchellus PE=2 SV=1	-0.554215198	0.60896	7151.869829	11889.80146	7070.079519	4773.102381	784.8636955	14786.31752	-4737.931633	0.601512973	-0.220755001
tr|L7LXA9|L7LXA9_9ACAR	Putative splicing factor proline-and glutamine-rich OS=Rhipicephalus pulchellus PE=2 SV=1	-0.547889731	0.61291	2095.405633	3135.952283	1799.575656	1464.387959	1265.563222	3036.299838	-1040.546651	0.668187984	-0.175101339
tr|L7MGQ3|L7MGQ3_9ACAR	Putative maltase glucoamylase (Fragment) OS=Rhipicephalus pulchellus PE=2 SV=1	-0.544399588	0.61509	1154.949946	1458.964652	1096.942907	1288.048395	420.1575042	871.2259202	-304.014706	0.79162298	-0.101481607
tr|A0A023G859|A0A023G859_9ACAR	Putative cysteine proteinase ixodes scapularis cysteine proteinase OS=Amblyomma triste PE=2 SV=1	0.538165263	0.61901	32653.27029	25571.65722	28444.46268	22123.89417	20984.23399	8895.198984	7081.613074	1.276932113	0.106167809
tr|L7LYQ1|L7LYQ1_9ACAR	Putative camp-dependent protein kinase r2 OS=Rhipicephalus pulchellus PE=2 SV=1	0.53794287	0.61915	14395.14455	11061.29064	13325.90945	5597.759008	4556.947672	9718.950367	3333.853913	1.301398274	0.114410227
tr|L7M587|L7M587_9ACAR	Superoxide dismutase OS=Rhipicephalus pulchellus PE=2 SV=1	-0.531750835	0.62306	5014.234296	9300.298131	4081.652745	3549.222827	5518.547733	12823.81629	-4286.063835	0.539147695	-0.268292248
tr|G3MHB6|G3MHB6_9ACAR	Putative uncharacterized protein (Fragment) OS=Amblyomma maculatum PE=2 SV=1	-0.518185511	0.63167	6233.937202	7883.626197	6480.858577	5973.042485	2019.899651	5130.857284	-1649.	0.790744899	-0.101963601

										688996		
tr|A0A0E9Y2V9|A0A0E9Y2V9_AMBAM	Serine protease inhibitor OS=Amblyomma americanum PE=3 SV=1	-0.516931882	0.63247	4020.191668	5616.815281	5557.27943	4059.096764	3030.095789	4408.839541	-1596.623613	0.71574219	-0.145243382
tr|A0A023GBG2|A0A023GBG2_9ACAR	Putative creatine kinase OS=Amblyomma triste PE=2 SV=1	0.503091885	0.64134	5951.405738	4654.800309	6075.21424	4824.333514	3743.18385	2432.199039	1296.60543	1.278552321	0.106718505
tr|L7M520|L7M520_9ACAR	Malic enzyme OS=Rhipicephalus pulchellus PE=2 SV=1	0.494155498	0.6471	5000.342535	4241.752936	5478.077584	3198.500724	1612.53959	2114.125432	758.589599	1.178838704	0.071454386
tr|A0A023GNU4|A0A023GNU4_9ACAR	Alpha-1,4 glucan phosphorylase OS=Amblyomma triste PE=2 SV=1	0.490314899	0.64959	4505.021053	3135.247565	4004.89171	1120.070138	2523.760759	4128.468578	1369.773488	1.436894841	0.157424986
tr|L7M8A9|L7M8A9_9ACAR	Putative nucleoside-diphosphate sugar epimerase OS=Rhipicephalus pulchellus PE=2 SV=1	-0.484826712	0.65315	1848.068008	2627.157974	2028.84953	1145.425598	658.0845055	2704.393381	-779.089658	0.703447614	-0.152768239
tr|L7MD37|L7MD37_9ACAR	Putative tubulin alpha 1c (Fragment) OS=Rhipicephalus pulchellus PE=2 SV=1	-0.482286268	0.65481	6525.839968	7796.245562	6119.288827	8378.460969	3742.634792	2609.336265	-1270.405593	0.837049054	-0.07724909
tr|L7M579|L7M579_9ACAR	Dolichyl-diphosphooligosaccharide--protein glycosyltransferase 48 kDa subunit OS=Rhipicephalus pulchellus PE=2 SV=1	0.481397253	0.65538	13744.12447	12392.61111	13145.77801	13193.22517	2497.226701	4172.492945	1351.513351	1.109057997	0.044954258
tr|L7LVA0|L7LVA0_9ACAR	Putative cytosolic ca2+-dependent cysteine prote OS=Rhipicephalus pulchellus PE=2 SV=1	-0.481031973	0.65562	1082.055567	1841.995494	1261.152095	405.8206163	610.0916029	2667.433793	-759.9399275	0.587436598	-0.231039
tr|L7MG30|L7MG30_9ACAR	Uncharacterized protein (Fragment) OS=Rhipicephalus pulchellus PE=2 SV=1	0.480241273	0.65614	13832.9304	8786.151077	9562.709151	801.7264409	11749.00825	13902.0877	5046.779327	1.57440161	0.197115525
tr|Q8MTY1|Q8MTY1_RHIAP	Putative cement protein RIM36 OS=Rhipicephalus appendiculatus GN=RIM36 PE=2 SV=1	-0.474803881	0.65969	10387.62939	13448.60703	11258.55997	14431.9422	4375.226856	10273.36641	-3060.977646	0.772394447	-0.112160857
tr|L7MGQ7|L7MGQ7_9ACAR	Putative ribose 5-phosphate isomerase (Fragment) OS=Rhipicephalus pulchellus PE=2 SV=1	-0.470942953	0.66222	2984.212943	3777.493542	2864.447364	3394.4105	1322.79712	2600.44979	-793.2805985	0.789998159	-0.102373921
tr|L7M437|L7M437_9ACAR	Proteasome subunit beta type OS=Rhipicephalus pulchellus PE=2 SV=1	-0.466308697	0.66526	4124.900371	5927.637744	3778.368596	2359.469469	644.8942175	6664.936611	-1802.737373	0.69587592	-0.157468191
tr|L7LXY6|L7LXY6_9ACAR	Putative nadh:ubiquinone oxidoreductase ndufa9/39kda subunit OS=Rhipicephalus pulchellus PE=2 SV=1	-0.455183671	0.67259	4165.183909	6205.155146	3550.471952	1960.51953	1175.620157	7672.89515	-2039.971236	0.671245732	-0.173118463

tr|F1PTY1|F1PTY1_CANLF	Keratin, type II cytoskeletal 1 OS=Canis lupus familiaris GN=KRT1 PE=3 SV=1	-0.451982343	0.67471	152270.2968	200046.338	114799.5057	271130.5399	71443.24682	168568.8218	-47776.04114	0.761175128	-0.118515411
tr|L7M4A5|L7M4A5_9ACAR	Peptidyl-prolyl cis-trans isomerase OS=Rhipicephalus pulchellus PE=2 SV=1	-0.448058823	0.67731	53482.06997	66337.61222	44013.13556	56571.03348	25222.31399	42818.98431	-12855.54225	0.806210356	-0.093551627
tr|L7M7S5|L7M7S5_9ACAR	Putative dihydropteridine reductase dhpr/qdpr OS=Rhipicephalus pulchellus PE=2 SV=1	-0.445835299	0.67878	1407.443519	1796.73687	1717.792269	1827.749695	565.4802808	1402.693436	-389.293350 6	0.783333132	-0.106053504
tr|L7LXM2|L7LXM2_9ACAR	Uncharacterized protein OS=Rhipicephalus pulchellus PE=2 SV=1	-0.445314273	0.67913	4570.301894	6108.780327	2854.920521	4444.576562	5083.081897	3157.454456	-1538.478433	0.748152929	-0.12600962
tr|A0A034WXH7|A0A034WXH7_RHIMP	Vitellogenin 4 (Fragment) OS=Rhipicephalus microplus PE=4 SV=1	0.43015886	0.68924	1373.104319	1161.100201	1224.588046	1463.172663	575.2195629	630.7361159	212.0041181	1.182588994	0.072833833
tr|L7M0V0|L7M0V0_9ACAR	Putative heat shock-related protein OS=Rhipicephalus pulchellus PE=2 SV=1	0.428132928	0.6906	9440.295766	8312.993866	9568.699454	8068.126043	3051.929671	3388.926353	1127.301899	1.135607209	0.055228141
tr|A0A023FP13|A0A023FP13_9ACAR	Putative transcriptional coactivator OS=Amblyomma cajennense PE=2 SV=1	0.409748612	0.70298	3997.434425	3227.90909	3790.732166	2135.536119	2260.411085	2339.160821	769.5253342	1.238397462	0.092860053
tr|L7M7D6|L7M7D6_9ACAR	Putative biosynthetic process OS=Rhipicephalus pulchellus PE=2 SV=1	0.403892828	0.70695	21337.74779	17180.178554	21096.83856	10316.22642	4092.619592	17353.21132	4157.569256	1.241998024	0.094120905
tr|A0A023FPQ7|A0A023FPQ7_9ACAR	Putative calnexin OS=Amblyomma cajennense PE=2 SV=1	0.396246161	0.71215	2861.4957	2286.478221	3322.308728	1975.510425	2268.947755	1081.430487	575.017479	1.251486095	0.097426029
tr|L7MAE4|L7MAE4_9ACAR	Putative chaperonin protein OS=Rhipicephalus pulchellus PE=2 SV=1	-0.37952039	0.72359	8338.27067	9845.639008	8217.5645	6803.525489	4414.609643	5275.995891	-1507.368338	0.846899898	-0.07216792
tr|L7M4U7|L7M4U7_9ACAR	Eukaryotic translation initiation factor 3 subunit F OS=Rhipicephalus pulchellus PE=2 SV=1	-0.375262088	0.72652	3146.61911	4228.039457	3298.605767	1941.260805	2944.190712	4030.582687	-1081.420346	0.744226524	-0.128294856
tr|A0A034WZ79|A0A034WZ79_RHIMP	Glycine-rich protein 3 (Fragment) OS=Rhipicephalus microplus PE=4 SV=1	-0.375168972	0.72658	19929.74029	23570.359866	19136.86759	14915.84551	4761.39409	16119.20748	-3640.619574	0.84554247	-0.072864574
tr|F1PYZ1|F1PYZ1_CANLF	Uncharacterized protein (Fragment) OS=Canis lupus familiaris GN=LOC485255 PE=3 SV=2	-0.374409366	0.7271	243975.3756	303617.1721	196715.4445	323156.9023	208521.115	180677.3103	-59641.796 51	0.803562506	-0.094980336
tr|A0A023FYS2|A0A023FYS2_9ACAR	Putative rna-binding protein musashi/mrna cleavage and polyadenylation factor i complex subunit hrp1 (Fragment) OS=Amblyomma parvum PE=2 SV=1	-0.362279303	0.73547	6871.760409	8795.233914	7687.310884	4809.659007	2133.256003	8945.240557	-1923.473504	0.78130502	-0.107179385

tr|G3MGQ1|G3MGQ1_9ACAR	Putative uncharacterized protein (Fragment) OS=Amblyomma maculatum PE=2 SV=1	0.362223149	0.73551	148976.669	134419.8921	133942.7253	138413.2304	45744.91914	52463.93034	14556.77694	1.108293324	0.044654717
tr|L7M801|L7M801_9ACAR	Putative translocase of outer membrane 40 OS=Rhipicephalus pulchellus PE=2 SV=1	0.359205058	0.7376	903.300266 9	727.270487	719.3849482	565.821608	393.3525261	752.1514319	176.029799	1.242041693	0.094136175
tr|L7M870|L7M870_9ACAR	Putative 3-hydroxyacyl-coa dehydrogenase OS=Rhipicephalus pulchellus PE=2 SV=1	0.358143845	0.73834	4972.204057	3983.387508	5212.600153	1718.280797	677.1080814	4733.923008	988.8165498	1.248235088	0.096296387
tr|B7PRW2|B7PRW2_IXOSC	Putative uncharacterized protein OS=Ixodes scapularis GN=IscW_ISCW019899 PE=4 SV=1	0.352844684	0.74201	3777.985715	3093.13249	2582.653617	3575.426467	2428.037402	2325.182392	684.8532249	1.221410892	0.086861789
tr|L7M3S7|L7M3S7_9ACAR	Putative thioredoxin/protein disulfide isomerase OS=Rhipicephalus pulchellus PE=2 SV=1	-0.352772402	0.74206	6098.295873	6823.60476	5631.949099	8326.456558	1093.465434	3389.107566	-725.308886 9	0.893705906	-0.048805372
tr|L7LXJ2|L7LXJ2_9ACAR	Putative golgi reassembly stacking protein grasp65 OS=Rhipicephalus pulchellus PE=2 SV=1	-0.348238377	0.74522	42040.68908	50247.02186	43573.23743	67319.44071	9751.64904	39634.22464	-8206.332774	0.836680216	-0.0774405
tr|C9W1E7|C9W1E7_RHISA	Cement-like antigen OS=Rhipicephalus sanguineus PE=2 SV=1	-0.347062147	0.74604	3017.797688	3622.430366	3910.034682	4369.997504	2629.768616	1479.705187	-604.632673	0.83308646	-0.079309924
tr|A0A023GEZ4|A0A023GEZ4_9ACAR	Putative myosin regulatory light chain ixodes scapularis myosin regulatory light chain (Fragment) OS=Amblyomma triste PE=2 SV=1	0.334290146	0.75495	57789.33685	46383.2522	29752.80243	64483.9074	49246.14363	32671.16095	11406.08466	1.24590955	0.095486515
tr|G3MH96|G3MH96_9ACAR	Putative uncharacterized protein (Fragment) OS=Amblyomma maculatum PE=2 SV=1	0.333852678	0.75526	2093.528471	1723.365674	2536.826416	1091.815313	1549.074207	1135.086485	370.1627968	1.214790629	0.084501433
tr|L7M4T9|L7M4T9_9ACAR	Putative rab-protein 10 OS=Rhipicephalus pulchellus PE=2 SV=1	-0.329757936	0.75813	1903.784624	2187.046012	1759.104999	2510.219235	1330.533948	665.816645	-283.261388	0.8704822	-0.060240105
tr|A0A023G0Q8|A0A023G0Q8_9ACAR	Putative secreted protein OS=Amblyomma parvum PE=2 SV=1	0.328363929	0.75911	17610.72756	16219.07743	17049.27712	15352.18248	6613.724822	3184.95959	1391.65013	1.085803285	0.035751151
tr|L7M834|L7M834_9ACAR	Putative phenylalanyl-trna synthetase beta subunit OS=Rhipicephalus pulchellus PE=2 SV=1	-0.324809444	0.7616	2854.650868	3592.345689	2543.134488	1703.070329	878.0228177	3834.527942	-737.694821	0.794648153	-0.099825122
tr|L7M7Y5|L7M7Y5_9ACAR	Proliferating cell nuclear antigen OS=Rhipicephalus pulchellus PE=2 SV=1	0.324240352	0.762	3521.555163	2927.941505	2373.583493	1697.432848	2323.745811	2157.661306	593.6136576	1.202740955	0.0801721
tr|G3ML11|G3ML11_9ACAR	Putative uncharacterized protein OS=Amblyomma maculatum PE=2 SV=1	-0.3211825	0.76415	115113.917	144307.0174	162519.9423	201179.095	97088.2104	123928.4198	-29193.10046	0.797701449	-0.098159619
tr|L7M0S5|L7M0S5_9ACAR	Glycerol-3-phosphate dehydrogenase OS=Rhipicephalus pulchellus PE=2 SV=1	0.319715477	0.76519	4072.519999	3342.004291	3652.250747	2366.681099	3570.070438	1707.866322	730.5157074	1.218586107	0.085856222

tr|L7M706|L7M706_9ACAR	Putative oligomycin sensitivity-conferring protein OS=Rhipicephalus pulchellus PE=2 SV=1	-0.3171057	0.76702	25361.5794	31258.80546	25978.71463	15586.20037	2798.659803	32089.19957	-5897.226061	0.811341925	-0.090796082
tr|L7M7K0|L7M7K0_9ACAR	Putative rab2a member ras oncoprotein family OS=Rhipicephalus pulchellus PE=2 SV=1	0.312737157	0.77011	5521.998478	4734.642633	4886.838425	6282.993415	2246.909426	3737.211705	787.355846	1.166296785	0.066809078
tr|L7MB37|L7MB37_9ACAR	Putative actin OS=Rhipicephalus pulchellus PE=2 SV=1	0.311686537	0.77085	2956.754655	2531.671808	3446.55187	3179.611207	1157.868963	2058.959799	425.0828475	1.167905985	0.067407884
tr|L7LWG4|L7LWG4_9ACAR	Putative hu li tai shao OS=Rhipicephalus pulchellus PE=2 SV=1	0.295170848	0.78255	2117.4946	1782.197135	1845.991494	947.1135082	784.5636031	1804.318213	335.2974645	1.188137136	0.07486657
tr|L7MFA9|L7MFA9_9ACAR	Putative 40s ribosomal protein s2 (Fragment) OS=Rhipicephalus pulchellus PE=2 SV=1	-0.293913528	0.78344	19811.34754	22071.894662	19821.44197	16303.35556	4242.588891	12627.906	-2260.54708	0.897582554	-0.046925597
tr|A0A023FT23|A0A023FT23_9ACAR	Putative myosin regulatory light chain ef-hand protein superfamily (Fragment) OS=Amblyomma parvum PE=2 SV=1	0.274901203	0.79701	36717.718111	31226.167655	20556.12457	39000.38457	28001.80402	20324.24109	5491.55046	1.175863735	0.070356996
tr|L7MAF1|L7MAF1_9ACAR	T-complex protein 1 subunit delta OS=Rhipicephalus pulchellus PE=2 SV=1	0.262017379	0.80625	5875.471089	5534.861418	6147.917761	5281.049709	1400.776578	1762.793328	340.6096706	1.06153897	0.025935942
tr|A0A0D5W3J6|A0A0D5W3J6_HYAAA	Histamine release factor OS=Hyalomma anatolicum anatolicum PE=2 SV=1	-0.260679862	0.80721	500.4611318	542.9607022	548.1623074	544.3777443	203.1726573	196.1140312	-42.499570339	0.92172625	-0.035398044
tr|L7MG70|L7MG70_9ACAR	Eukaryotic translation initiation factor 5A (Fragment) OS=Rhipicephalus pulchellus PE=2 SV=1	-0.258290355	0.80893	11828.3793	14721.139488	11893.6461	3902.161902	4698.664782	18820.69784	-2892.760183	0.803496177	-0.095016185
tr|G3MM98|G3MM98_9ACAR	Putative uncharacterized protein OS=Amblyomma maculatum PE=2 SV=1	-0.249670324	0.81514	6050.936146	7111.126021	4663.948044	8011.207684	5177.408228	5223.901151	-1060.189875	0.850911111	-0.070115805
tr|L7LXM0|L7LXM0_9ACAR	Uncharacterized protein OS=Rhipicephalus pulchellus PE=2 SV=1	0.244333535	0.81899	1951.420009	1728.108028	1969.2217	1892.465141	149.7209262	1575.935451	223.3119807	1.129223392	0.052779866
tr|A0A023FKR8|A0A023FKR8_9ACAR	Putative mitochondrial volatge dependent anion-selective channel OS=Amblyomma cajennense PE=2 SV=1	0.243550311	0.81956	1979.337867	1746.825384	2104.094969	1185.263609	347.4411635	1616.639519	232.5124831	1.133105739	0.054270439
tr|L7M1I4|L7M1I4_9ACAR	Putative karyopherin importin beta 1 OS=Rhipicephalus pulchellus PE=2 SV=1	-0.24154723	0.82101	3399.511157	3764.709446	3548.034632	3523.605124	1213.726195	2320.454137	-365.1982892	0.902994296	-0.044314993
tr|L7M8W3|L7M8W3_9ACAR	Putative molecular chaperone dnaj superfamily OS=Rhipicephalus pulchellus PE=2 SV=1	0.231489942	0.82829	3786.444933	3438.114905	4723.407163	2790.6121	2220.538852	1364.496561	348.3300273	1.101314248	0.041911258
tr|L7MI37|L7MI37_9ACAR	Putative transglutaminase/protease-like logues (Fragment) OS=Rhipicephalus pulchellus PE=2 SV=1	0.2240757	0.83368	2886.009875	2469.17194	2304.146195	2191.154446	2840.802629	1520.357237	416.837935	1.168816893	0.06774648

tr|G3MQM7|G3MQM7_9ACAR	Putative uncharacterized protein OS=Amblyomma maculatum PE=2 SV=1	0.221976857	0.8352	1647.876834	1484.860735	1238.195659	1854.444989	1001.87041	783.7169336	163.0160994	1.109785447	0.045239025
tr|L7MGF8|L7MGF8_9ACAR	Putative glycine rich protein (Fragment) OS=Rhipicephalus pulchellus PE=2 SV=1	0.219827854	0.83677	1868.96792	1768.947165	1938.560725	1761.571869	723.4109853	312.6341852	100.020754 6	1.056542534	0.023886985
tr|A0A023GFY8|A0A023GFY8_9ACAR	Putative actin-binding cytoskeleton protein filamin (Fragment) OS=Amblyomma triste PE=2 SV=1	-0.211147837	0.84309	5305.295682	5954.325067	2475.518172	6491.052135	5054.380226	1672.798927	-649.029385 1	0.890998664	-0.050122947
tr|Q2V829|Q2V829_9ACAR	Troponin I protein OS=Rhipicephalus haemaphysaloides haemaphysaloides PE=2 SV=1	0.211036392	0.84317	10478.27779	9496.395688	7950.037292	9773.258862	7880.721973	1684.089581	981.8821024	1.103395239	0.042731106
tr|L7M958|L7M958_9ACAR	Putative g protein beta-subunit 13f OS=Rhipicephalus pulchellus PE=2 SV=1	0.206294379	0.84664	4056.385614	3298.420192	1843.060612	3015.324864	5507.374284	3188.717166	757.9654215	1.229796502	0.089833253
tr|L7M755|L7M755_9ACAR	Putative nadh-ubiquinone oxidoreductase ndufs1/75 kDa subunit OS=Rhipicephalus pulchellus PE=2 SV=1	-0.204289088	0.8481	11434.45021	12434.97092	10388.5606	9536.179794	2506.653522	8104.033022	-1000.520714	0.919539762	-0.036429486
tr|L7M3S8|L7M3S8_9ACAR	Putative ribosomal protein s16 OS=Rhipicephalus pulchellus PE=2 SV=1	-0.199526319	0.85158	22442.49664	23249.67497	22064.89354	20975.23629	4823.150079	5082.79232	-807.1783306	0.965282167	-0.015345717
tr|A0A023GIK7|A0A023GIK7_9ACAR	Putative grp-3 321 glycine rich family (Fragment) OS=Amblyomma triste PE=2 SV=1	-0.194210045	0.85548	19384.49038	23075.62175	23698.56248	5300.027587	8660.357514	31759.53064	-3691.131364	0.840041954	-0.075699024
tr|G3MQN1|G3MQN1_9ACAR	Putative uncharacterized protein OS=Amblyomma maculatum PE=2 SV=1	0.189598474	0.85886	2512.547742	2351.994414	2776.813393	1955.228125	908.0766789	1151.800061	160.5533277	1.068262631	0.028678037
tr|L7MBE1|L7MBE1_9ACAR	Putative ixoderin OS=Rhipicephalus pulchellus PE=2 SV=1	0.179681776	0.86614	3822.170846	3568.060398	3628.601252	2826.998184	972.7966137	2248.057654	254.1104477	1.07121809	0.029877898
tr|L7MMB5|L7MMB5_9ACAR	6-phosphogluconate dehydrogenase, decarboxylating (Fragment) OS=Rhipicephalus pulchellus PE=2 SV=1	0.175682282	0.86908	4019.868061	3749.034083	4657.297921	2822.320504	1208.437684	2381.046915	270.8339785	1.072241002	0.03029241
tr|L7MBU1|L7MBU1_9ACAR	Putative amblyomma 40-33 family member OS=Rhipicephalus pulchellus PE=2 SV=1	-0.165542105	0.87655	4630.282716	4982.936087	5007.43654	4533.237987	2130.211143	3012.749494	-352.6533711	0.929227796	-0.031877808
sp|P60526|HBB_CHRBR	Hemoglobin subunit beta OS=Chrysocyon brachyurus GN=HBB PE=1 SV=1	-0.162153868	0.87905	115801.922	130641.5943	90480.42996	157465.382	105644.5158	118172.6187	-14839.67239	0.886409283	-0.052365704
tr|L7M0N6|L7M0N6_9ACAR	Uncharacterized protein OS=Rhipicephalus pulchellus PE=2 SV=1	0.153890416	0.88515	1658.348368	1522.813209	2259.463781	1088.645934	1268.87655	846.748293	135.5351593	1.089003141	0.037029133
tr|L7ME84|L7ME84_9ACAR	Putative nucleoside diphosphate-sugar hydrolase of the mutt nudix family (Fragment) OS=Rhipicephalus pulchellus PE=2 SV=1	0.150283935	0.88781	94397.44626	85098.79043	53876.76765	121433.4454	81227.7411	69908.50572	9298.655825	1.109268954	0.045036858

tr|L7LZD0|L7LZD0_9ACAR	Putative microtubule binding protein OS=Rhipicephalus pulchellus PE=2 SV=1	-0.146782287	0.8904	4239.593626	4674.88177	4496.117206	2359.634238	720.9833253	5085.606433	-435.288144	0.906887882	-0.042446401
tr|C9W1B4|C9W1B4_RHISA	Hypothetical secreted protein (Fragment) OS=Rhipicephalus sanguineus PE=2 SV=1	0.144740303	0.89192	3074.250634	2963.369057	2475.449254	2892.38458	1319.622499	138.5570972	110.8815776	1.037417404	0.01595353
tr|V5GR07|V5GR07_IXORI	Putative laminin alpha 5 (Fragment) OS=Ixodes ricinus PE=2 SV=1	0.143074788	0.89315	1409.974617	1304.836094	1187.656557	794.7485869	502.7317599	1169.305269	105.138523	1.080576038	0.033655333
tr|E4W3Z2|E4W3Z2_HAELO	Heat shock 70 kDa protein 5 OS=Haemaphysalis longicornis PE=2 SV=1	0.140128071	0.89533	18426.03158	16719.23197	18632.29365	8275.192345	5726.158817	20304.90129	1706.799615	1.102086006	0.042215488
tr|A0A0K8RH49|A0A0K8RH49_IXORI	Putative cuticle protein OS=Ixodes ricinus PE=2 SV=1	-0.140035657	0.8954	6634.153226	7596.435626	8896.518916	1460.947183	4550.194422	10998.01482	-962.2824006	0.873324484	-0.058824364
tr|A0A023FJS2|A0A023FJS2_9ACAR	Putative glycine c-acetyltransferase/2-amino-3-ketobutyrate-coa ligase OS=Amblyomma cajennense PE=2 SV=1	-0.135772829	0.89856	5311.129776	5746.504917	5424.898942	2867.23233	1680.347882	5293.782201	-435.3751402	0.924236532	-0.034216869
tr|L7MK84|L7MK84_9ACAR	Uncharacterized protein (Fragment) OS=Rhipicephalus pulchellus PE=2 SV=1	0.127249117	0.90488	2751.25256	2481.165741	839.5232679	2868.413568	3580.942171	831.8225172	270.0868192	1.108854808	0.044874684
tr|L7M832|L7M832_9ACAR	Elongation factor Tu OS=Rhipicephalus pulchellus PE=2 SV=1	-0.119482423	0.91065	5412.008632	5826.949708	4011.097612	3009.208022	2534.029149	5455.286892	-414.9410758	0.928789316	-0.032082789
tr|L7LTQ8|L7LTQ8_9ACAR	Putative heteroproteinous nuclear ribonucleoprotein at 87f OS=Rhipicephalus pulchellus PE=2 SV=1	0.110003512	0.9177	81264.99579	75899.252	69175.02642	34024.63015	28769.18167	79436.73007	5365.743794	1.070695608	0.029666021
tr|L7LYM2|L7LYM2_9ACAR	Uncharacterized protein OS=Rhipicephalus pulchellus PE=2 SV=1	-0.107382975	0.91966	7058.715973	7281.365772	5372.128192	7024.476035	3423.990099	1083.272477	-222.6499796	0.969421973	-0.013487141
tr|A0A023FUF0|A0A023FUF0_9ACAR	Putative cytochrome b5 ixodes scapularis cytochrome b5 ixodes pacificus cytochrome b5 OS=Amblyomma parvum PE=2 SV=1	-0.105027167	0.92141	8580.237184	8949.125344	6479.523799	10110.205	3809.268423	4743.255972	-368.8881595	0.958779418	-0.018281298
tr|L7MGB9|L7MGB9_9ACAR	Putative aicar transformylase/imp cyclohydrolase/methylglyoxal synthase (Fragment) OS=Rhipicephalus pulchellus PE=2 SV=1	-0.102973059	0.92294	4508.635512	4826.665949	6530.478446	3858.138269	3653.291323	3907.636782	-318.0304372	0.934109706	-0.029602115
tr|A0A023FMW6|A0A023FMW6_9ACAR	Putative amino acid transporter ixodes scapularis amino acid transporter (Fragment) OS=Amblyomma cajennense PE=2 SV=1	-0.099692621	0.92538	2912.993935	3118.082727	1310.958529	2536.88844	3331.793485	1263.134129	-205.088792	0.934225994	-0.029548053
tr|A0A023GME5|A0A023GME5_9ACAR	Putative actin-binding cytoskeleton protein filamin (Fragment) OS=Amblyomma triste PE=2 SV=1	0.097592779	0.92695	7321.490547	6924.82406	3761.803206	5517.650067	6422.883919	2882.221746	396.6664874	1.057281815	0.024190762
tr|L7M9A4|L7M9A4_9ACAR	Putative 2-oxoglutarate dehydrogenase e1 subunit OS=Rhipicephalus pulchellus PE=2 SV=1	0.082740178	0.93803	2418.563689	2286.164433	1788.001812	1806.539256	1439.662472	2368.355782	132.3992562	1.057913269	0.024450064

tr|L7MHT4|L7MHT4_9ACAR	Putative glycine rich protein (Fragment) OS=Rhipicephalus pulchellus PE=2 SV=1	-0.081023807	0.93932	4033.623158	4219.023152	5263.247646	5182.922668	2620.91439	2972.979826	-185.3999938	0.95605618	-0.019516587
tr|L7M720|L7M720_9ACAR	Putative heat shock protein OS=Rhipicephalus pulchellus PE=2 SV=1	-0.059319818	0.95554	8608.443319	8746.766965	8132.509524	6635.924457	1101.325192	3885.788959	-138.3236455	0.98418574	-0.006922932
tr|C9W1L7|C9W1L7_RHISA	60S ribosomal protein L9 OS=Rhipicephalus sanguineus PE=2 SV=1	-0.05389153	0.95961	15709.64831	16046.64117	16258.51505	11904.61985	1128.710197	10771.8334	-336.9928656	0.978999165	-0.009217679
tr|A0A023FSH0|A0A023FSH0_9ACAR	Putative differentiation-related protein OS=Amblyomma cajennense PE=2 SV=1	-0.053066199	0.96022	19236.21543	19424.09973	19530.7838	16936.62354	866.246802	6070.947683	-187.8842969	0.990327258	-0.004221267
tr|A0A0C9R303|A0A0C9R303_AMBAM	Putative hnrnp-l/ptb/hephaestus splicing factor family (Fragment) OS=Amblyomma americanum PE=2 SV=1	0.048004077	0.96401	2928.402566	2828.995636	3212.359479	1247.226311	574.147507	3540.482331	99.40692968	1.035138594	0.014998501
tr|L7M1L5|L7M1L5_9ACAR	Citrate synthase OS=Rhipicephalus pulchellus PE=2 SV=1	-0.044919411	0.96632	54845.08865	56454.90622	59249.86167	24853.7686	19003.56972	59092.55915	-1609.817569	0.971484895	-0.012563948
tr|L7M602|L7M602_9ACAR	Putative 26s proteasome regulatory complex subunit rpn2/psmd1 OS=Rhipicephalus pulchellus PE=2 SV=1	0.041159673	0.96914	14103.71659	13822.43696	15252.70478	8175.56783	2682.451296	11528.64107	281.2796245	1.020349496	0.008748954
tr|L7MB29|L7MB29_9ACAR	Putative transcription factor nfat subunit nf45 OS=Rhipicephalus pulchellus PE=2 SV=1	-0.032631485	0.97553	3778.217172	3859.139777	4021.305255	2506.933237	738.0355291	4231.420309	-80.92260506	0.979030921	-0.009203591
tr|L7M5K3|L7M5K3_9ACAR	Putative succinyl-coa synthetase alpha subunit OS=Rhipicephalus pulchellus PE=2 SV=1	-0.02966292	0.97776	3785.669852	3854.755363	4274.064587	1864.137683	899.6887374	3932.372263	-69.0855112 1	0.982077848	-0.007854085
tr|A0A0C9RU44|A0A0C9RU44_AMBAM	Putative 40s ribosomal protein s3 OS=Amblyomma americanum PE=2 SV=1	-0.017031821	0.98723	30497.35558	30587.74517	30821.8913	26243.46961	2294.202852	8901.268469	-90.389587 13	0.997044908	-0.00128528
tr|L7M817|L7M817_9ACAR	Putative peptid OS=Rhipicephalus pulchellus PE=2 SV=1	0.015447628	0.98841	1874.522268	1864.267394	1605.716918	1372.690023	679.7246881	927.3921022	10.25487388	1.005500753	0.0023824
tr|G3MNX9|G3MNX9_9ACAR	Putative uncharacterized protein OS=Amblyomma maculatum PE=2 SV=1	0.012716683	0.99046	14845.82608	14727.92053	8427.129478	18872.35829	11800.42395	10892.40425	117.9055436	1.00800558	0.003462936
tr|L7MJ61|L7MJ61_9ACAR	Putative heparan sulfate proteoglycan 2 (Fragment) OS=Rhipicephalus pulchellus PE=2 SV=1	-0.011517287	0.99136	1172.59895	1179.907157	835.9002678	1173.986928	833.9990116	715.8059154	-7.30820749 2	0.993806116	-0.002698335
tr|L7M3E5|L7M3E5_9ACAR	Putative cytochrome c oxidase subunit iv/cox5b OS=Rhipicephalus pulchellus PE=2 SV=1	0.006325807	0.99526	15907.47957	15866.0178	15204.49343	21546.68132	5119.772137	10132.51062	41.4617684 7	1.002613244	0.001133437

Supplementary Table 23. Gene ontology functional annotation of the differentially represented proteins obtained by LC-MS/MS.

Statistical analysis was conducted to determine significant differences ($p < 0.05$) using the student's *t*-test to compare the protein representation data between uninfected and *E. canis*-infected *Rhipicephalus sanguineus* salivary glands. Annotation was carried out in different levels: Molecular Function (MF), Biological Process (BP) and Cellular Component (CC) using UniProtKB (http://www.UniProt.org/). Representation levels were determined by Log2 fold-change$_{(infected/uninfected)}$ of protein hits. Highlighted in red are the under represented proteins and highlighted in green the over represented proteins. NA: not available.

UniProt KB	Description	Gene	Biological Process	GO: BP	Molecular Function	GO: MF	Cellular Component	GO: CC	Domains	Fold Change i/ni	Log10 (Fold Change)	Log2 (Fold Change)
C9W1S4	Signal peptidase	Similar to ISCW016779	Signal peptide processing	6465	Peptidase activity	8233	Integral component of membrane; sigUnknownl peptidase complex	16021; 5787	SPC22	10.58160199	1.024551422	3.403486154
A0A034WYZ2	Actin-depolymerizing factor 1	Unknown	Actin filament depolymerization	30042	Actin binding	3779	Actin cytoskeleton; intracellular	15629; 5622	ADF-H/Gelsolin-like_dom; ADF/Cofilin/Destrin	7.597731234	0.880683927	2.925568678
L7LXH5	Putative emp24/gp25l/p24 family of membrane trafficking	Similar to ISCW001550	Transport	6810	Unknown	NA	Integral component of membrane	16021	EMP24/GP25L family; GOLD domain	1.604058885	0.205220307	0.681727104
A0A023G6L8	Putative dihydrolipoamide succinyltransferase 2-oxoglutarate dehydrogenase e2 subunit (Fragment)	Similar to ISCW008731	Tricarboxylic acid cycle	6099	Dihydrolipoylly sine-residue succinyltransfer ase activity	4149	Oxoglutarate dehydrogeUn knownse complex	45252	2-oxoA_DH_lipoyl-BS; 2-oxoacid_DH_actylT frase; Biotin_lipoyl; CAT-like_dom	1.461637915	0.1648398	0.547585963
L7M6Q5	Putative heat shock-related protein	Unknown	Response to (a)biotic stress	6950	Unknown	NA	Unknown	NA	A-crystallin/Hsp20_dom; Alpha-crystallin/HSP	1.391731106	0.143555334	0.476880497
L7MIQ1	Putative 26s proteasome regulatory complex subunit	Similar to ISCW012119	Regulation of proteolysis	30162	Protein binding	5515	Proteasome complex	502	PAM; PCI_dom; TPR-like_helical_dom; WHTH_DNA-bd_dom	0.615889166	-0.210497435	-0.699257344
L7M653	Uncharacterized protein	Unknown	Unknown	NA	Unknown	NA	Unknown	NA	Thioredoxin-like_fold	0.57881162	-0.237462759	-0.78883421
L7M2Y0	Putative igf-ii mrna-binding protein imp	Unknown	RNA processing	6396	Nucleotide binding; RNA binding	166; 3723	Nucleus	5634	KH_dom; Nucleotide-	0.574630339	-0.240611448	-0.799293928

									bd_a/b_plait; RRM_dom			
L7MB04	Putative thiol-disulfide isomerase and thioredoxin	Unknown	Cell redox homeostasis	45454	Isomerase activity	16853	Cell	5623	Thioredoxin-like_fold	0.554660326	-0.255972897	-0.850323558
L7M2I7	Aconitate hydratase, mitochondrial	Similar to ISCW010818	Tricarboxylic acid cycle	6099	4 iron, 4 sulfur cluster binding; aconitate hydratase activity; metal ion binding	51539; 3994; 46872	Mitochondrion	5739	Acnase/IPM_dHydase_lsu_aba_1/3; Aconitase_4Fe-4S_BS	0.543252095	-0.26499859	-0.880306261
L7MAC6	Putative glutamate/leucine/phenylalanine/valine dehydrogenase	Similar to ISCW000393	Cellular amino acid metabolic process	6520	Oxidoreductase activity	16491	Unknown	NA	Glu/Leu/Phe/Val dehydrogenases family	0.542047398	-0.265962736	-0.883509084
A0A0C9SA10	Putative ribosomal protein l37a	Similar to ISCW023173 and ISCW024187	Translation	6412	Structural constituent of ribosome	3735	Ribosome	5840	Ribosomal_L37ae	0.535848916	-0.270957644	-0.900101809
L7M642	Putative zinc-binding oxidoreductase	Unknown	Oxidation-reduction	55114	Oxiredutase F activity; zinc ion binding	16491; 8270	Unknown	NA	ADH_SF_Zn-type; GroES-like; NAD(P)-bd_dom	0.531586896	-0.274425733	-0.911622553
L7M955	Putative vesicle coat complex copii subunit sec31	Similar to ISCW017083	Regulation of COPII vesicle coating	3400	Protein binding	5515	Integral component of Golgi membrane	30173	ACE1_Sec16_Sec31; SRA1-protein/COPII_Sec31; WD40/YVTN_repeat-like_dom	0.523428743	-0.281142433	-0.933934946
G3MMA6	Ribosomal protein L3	Similar to ISCW023076	Translation	6412	Structural constituent of ribosome	3735	Ribosome	5840	Ribosomal_L3_CS; Transl_B-barrel	0.516173049	-0.287204675	-0.954073279
A0A023FWG2	Putative t-complex protein 1 subunit zeta danio rerio chaperonin	Similar to ISCW008709	Protein folding; cellular protein metabolic process	6457; 44267	ATP binding; nucleotide binding	5524; 166	Cytoplasm	5737	TCP-1 chaperonin family	0.51133846	-0.291291541	-0.967649553
L7MAC8	Putative dihydrolipoamide succinyltransferase 2-oxoglutarate dehydrogenase e2 subunit	Unknown	Tricarboxylic acid cycle	6099	Dihydrolipoylly sine-residue succinyltransferase activity	4149	Oxoglutarate dehydrogeUnknownse complex	45252	2-oxoA_DH_lipoyl-BS; 2-oxoacid_DH_actylTfrase; Biotin_lipoyl; CAT-like_dom	0.509978853	-0.292447833	-0.971490671
Q4PM40	Ubiquitin/ribosomal protein S27a fusion protein	Similar to ISCW000125 and ISCW010407	Translation	6412	Structural constituent of ribosome	3735	Ribosome	5840	Ribosomal_S27a; Ribosomal_zn-bd; Ubiquitin-rel_dom	0.503702592	-0.297825814	-0.989355939
L7M5Q3	Putative lateral inhibition	Unknown	Metabolic process; ion transport	8152; 6811	Cation transmembrane transporter activity	8324	Integral component of membrane	16021	F1F0-ATPsyn_F_prd	0.501345817	-0.299862604	-0.996122009

V5GYK8	Putative spectrin beta chain	Similar to ISCW021585	Metabolic process; peptidyl-tyrosine dephosphorylation	8152; 35335	Phospholipid binding; structural constituent of cytoskeleton; actin binding_F	5543; 5200; 3779	Spectrin	8091	Actinin_actin-bd_CS; CH-domain; PH_dom-like; Spectrin/alpha-actinin	0.479218081	-0.319466804	-1.061245753
A0A023FNV6	Putative glycyl-trna synthetase	Unknown	Glycyl-tRNA aminoacylation	6426	ATP binding; glycine-tRNA ligase activity	5524; 4820	Cytoplasm	5737	aa-tRNA-synt_Iib; Anticodon-bd; Gly-tRNA_synthase/POLG2; S15_NS1_RNA-bd; WHEP-TRS_dom	0.475203033	-0.323120796	-1.073384051
B7Q304	Misexpression suppressor of KSR, putative	IscW_ISCW010241	Unknown	NA	Unknown	NA	Unknown	NA	AB_hydrolase; NDRG	0.465517251	-0.33206422	-1.103093462
Q86G64	40S ribosomal protein S5	Similar to ISCW012831 and ISCW021155	Translation	6412	RNA binding; Structural constituent of ribosome	3723; 3735	Small ribosomal subunit	15935	Ribosomal_S5/S7_euk/arc	0.464345825	-0.333158455	-1.106728432
L7MEG0	Putative heat shock protein	Similar to ISCW014265	Protein folding; response to (a)biotic stress	6457; 6950	ATP binding	5524	Unknown	NA	HATPase_C; Heat_shock_protein_90_CS; Hsp90_fam; Ribosomal_S5_D2-typ_fold	0.447677643	-0.349034593	-1.159467821
L7M5P4	Putative prohibitin-like protein	Unknown	Negative regulation of cell proliferation	8285	Unknown	NA	Membrane	16020	Band_7; Prohibitin	0.439826483	-0.356718625	-1.184993621
Q4PM27	Ribosomal protein L11	IscW_ISCW000476	Translation	6412	Structural constituent of ribosome	3735	Ribosome	5840	Ribosomal_L5	0.438937154	-0.357597657	-1.187913702
L7M716	Putative ribosomal protein s9	Similar to ISCW023083	Translation	6412	rRNA binding; structural constituent of ribosome	19843; 3735	Small ribosomal subunit	15935	Ribosomal_S4/S9	0.437009001	-0.359509618	-1.194265101
L7LTS0	Putative tick salivary metalloprotease	Unknown	Proteolysis	6508	Metalloendopeptidase activity; peptidase activity	4222; 8233	Unknown	NA	MetalloPept_cat_dom; ADAM_MEPRO. 1 hit	0.434004813	-0.362505455	-1.204217055
L7M9V8	Putative proline and glutamine-rich splicing factor sfpq	Unknown	Unknown	NA	Nucleic acid binding; nucleotide binding	3676; 166	Unknown	NA	NOPS; Nucleotide-bd_a/b_plait; RRM_dom	0.428614987	-0.367932647	-1.222245797
A0A023FVZ8	Putative 40s ribosomal protein	Similar to ISCW003489	Translation	6412	RNA binding; Structural	3723; 3735	Small ribosomal subunit	15935	dsRBD_dom; Ribosomal_S5_D2-typ_fold_subgr	0.42255399	-0.374117793	-1.242792406

					constituent of ribosome							
L7MHL1	Putative puromycin-sensitive aminopeptidase	Unknown	Proteolysis	6508	Aminopeptidase activity; metallopeptidase activity; zinc ion binding	4177; 8237; 8270	Integral component of membrane; membrane	16021; 16020	ERAP1-like_C_dom; Peptidase_M1	0.418762963	-0.378031736	-1.255794246
A0A0C9R2A0	Putative adp/atp translocase	Similar to ISCW021754 and ISCW021753	Transmembrane transport	55085	Transporter activity	5215	Integral component of membrane; mitochondrial inner membrane	16021; 5743	Aden_trnslctor; Mit_carrier; Mitochondrial_sb/sol_carrier	0.413250647	-0.383786458	-1.274911018
A0A023FNH1	Putative vigilin	Similar to ISCW008601 (high-density lipoprotein-binding protein)	Metabolic process	8152	RNA binding; nucleic acid binding;hydrolase activity	3723; 3676; 16787	Unknown	NA	KH_dom	0.411580901	-0.385544787	-1.280752059
L7MIP5	Putative dihydroorotase	Unknown	Metabolic process	8152	Hydrolase activity, acting on carbon-nitrogen (but not peptide) bonds	16810	Cytoplasm	5737	Amidohydro-rel; Dihydropyrimidinase; Hydantoinase/dihydroPyrase; Metal_Hydrolase	0.397455206	-0.40071181	-1.331135818
A0A023GNW6	Transketolase	Unknown	Metabolic process	8152	Metal ion binding; transketolase activity; catalytic activity; transferase activity	46872; 4802; 3824; 16740	Unknown	NA	THDP-binding; Transketo_C/Pyr-ferredox_oxred	0.396018577	-0.402284441	-1.336359987
A0A023FXU9	Putative alkyl hydroperoxide reductase thiol specific antioxidant	Unknown	Oxidation-reduction process	55114	Peroxiredoxin activity; antioxidant activity; oxidoreductase activity	51920; 16209; 16491	Unknown	NA	AhpC/TSA; Peroxiredoxin_C; Thioredoxin-like_fold	0.378970702	-0.421394364	-1.399841776
O97115	CAMP-dependent protein kinase catalytic subunit isoform 2	APK-C2	Protein phosphorylation	6468	ATP binding; protein serine/threonine kinase activity	5524; 4674	Unknown	NA	AGC-kinase_C; Protein_kinase_ATP_BS	0.368518868	-0.433540272	-1.44018961
A0A0C9S201	40S ribosomal protein S6	Similar to ISCW024315	Translation	6412	Structural constituent of ribosome	3735	Ribosome	5840	Ribosomal_S6_euk	0.362910729	-0.440200192	-1.462313384

L7M9B9	Putative amblyomma 40-33 family member	Unknown	Unknown	NA	Unknown	NA	Unknown	NA	NA	0.356241295	-0.448255739	-1.489073332
A0A023GNW2	Sodium/potassium-transporting ATPase subunit alpha	Similar to ISCW002538	Ion transport	6811	ATP binding; metal ion binding; sodium:potassium-exchanging ATPase activity	5524; 46872; 5391	Integral component of membrane	16021	ATPase_P-typ_cation-transptr_C;	0.335310678	-0.474552616	-1.576429666
A0A0C9SC52	Putative pyruvate dehydrogenase e1 alpha subunit	Similar to ISCW019126	Oxidation-reduction	55114	Oxidoreductase activity, acting on the aldehyde or oxo group of donors, disulfide as acceptor	16624	Intracellular membrane-bounded organelle	43231	DH_E1; THDP-binding	0.331806838	-0.479114668	-1.591584477
A0A023FU84	Ribosomal protein L15	Similar to ISCW008173	Translation	6412	Structural constituent of ribosome	3735	Ribosome	5840	Rbsml_L15e_core_dom; Ribosomal_L23/L15e_core_dom	0.319415662	-0.495643793	-1.646493042
L7M3F2	Putative ribosomal protein l18	Similar to ISCW021924	Translation	6412	Structural constituent of ribosome	3735	Ribosome	5840	Ribosomal_L18e/L15P	0.318538958	-0.496837444	-1.650458265
C9W1D7	Ribosomal protein L22	Similar to ISCW011505	Translation	6412	Structural constituent of ribosome	3735	Ribosome	5840	Ribosomal_L22e	0.313063926	-0.504366973	-1.675470817
G3MMG2	40S ribosomal protein S4	ISCW024787	Translation	6412	rRNA binding; structural constituent of ribosome	19843; 3735	Ribosome	5840	40S_S4_C; KOW; Ribosomal_S4e_central_region	0.309633515	-0.509152038	-1.691366458
V5IFY7	Putative mitochondrial adp/atp carrier	Similar to ISCW021754 and ISCW021753	Transmembrane transport	55085	Transporter activity	5215	Integral component of membrane; mitochondrial inner membrane	16021; 5743	Aden_trnslctor; Mit_carrier; Mitochondrial_sb/sol_carrier	0.308293879	-0.511035098	-1.697621848
A0A023FXY9	Putative hydroxyacyl-coa dehydrogenase/enoyl-coa hydratase	Unknown	Fatty acid beta-oxidation	6635	3-hydroxyacyl-CoA dehydrogenase activity; enoyl-CoA hydratase activity	3857; 4300	Mitochondrial fatty acid beta-oxidation multienzyme complex	16507	3-OHacyl-CoA_DH_CS; 6-PGluconate_DH_C-like	0.291145869	-0.535889368	-1.780185947
L7M591	Putative endocytosis/signaling protein ehd1	Similar to ISCW024633 and ISCW021581	Endocytic recycling	32456	Calcium ion binding; GTP binding; protein binding	5509; 5525; 5515	Intracellular	5622	Dynamin_SF; EF-hand-dom_pair; EHD_N;	0.276768817	-0.557882843	-1.85324669

									G_DYNAMIN_dom ; P-loop_NTPase			
L7M743	Putative glyoxylate/hydroxypyruvate reduct	Unknown	L-serine biosynthetic process	6564	NAD binding; phosphoglycerate dehydrogenase activity	51287; 4617	Unknown	NA	D-isomer specific 2-hydroxyacid dehydrogenase family	0.275192828	-0.560362889	-1.861485225
L7LQP4	Putative salivary lipocalin	Unknown	Unknown	NA	Unknown	NA	Unknown	NA	Calycin-like; signal domain	0.274912017	-0.560806275	-1.862958121
C9W1P9	40S ribosomal protein S8	Similar to ISCW015393	Translation	6412	Structural constituent of ribosome	3735	Ribosome	5840	Ribosomal_S8e/biogenesis_NSA2	0.256735876	-0.590513438	-1.961643182
L7MJY0	Putative talin	Unknown	Cell adhesion; cytoskeletal anchoring at plasma membrane	7155; 7016	Structural constituent of cytoskeleton	5200	Cytoskeleton; focal adhesion; ruffle	5856; 5925; 1726	Band_41_domain; FERM/acyl-CoA-bd_prot_3-hlx; ILWEQ_dom; Talin_cent; Vinculin-bd_dom	0.24959612	-0.60276217	-2.002332586
A0A0A7DS56	Pyruvate kinase	Unknown	Glycolytic process; phosphorylation	6096; 16310	Kinase activity; magnesium ion binding; potassium ion binding; pyrovate kinase activity; catalytic activity; transferase activity	16301; 287; 30955; 4743; 3824;	Unknown	NA	Pyrv/PenolPyrv_Kinase-like_dom	0.249236747	-0.603387926	-2.004411303
L7M741	Putative hydroxyacyl-coenzyme a dehydrogenase/3-ketoacyl-coenzyme a thiolase/enoyl-coenzyme a hydrat	Unknown	Fatty acid beta-oxidation	6635	3-hydroxyacyl-CoA dehydrogenase activity; enoyl-CoA hydratase activity	3857; 4300	Mitochondrial fatty acid beta-oxidation multienzyme complex	16507	3-OHacyl-CoA_DH_CS; 6-PGluconate_DH_C-like	0.248860992	-0.604043172	-2.006587985
L7M8C7	Phosphoglycerate kinase	Unknown	Glycolytic process	6096	ATP binding; phosphoglycerate kinase activity	5524; 4618	Unknown	NA	Phosphoglycerate_kinase	0.235618152	-0.627791255	-2.085477407
G3MKI7	Putative uncharacterized protein	Similar to ISCW017610	Translation	6412	5S rRNA binding; structural constituent of ribosome	8097; 3735	Ribosome	5840	Rbsml_L5_euk/L18_arc; Rbsml_L5e/L18P_C	0.2331118	-0.632435743	-2.100906062

B7P9E4	Sodium/potassium-transporting ATPase subunit alpha (Fragment)	IscW_ISCW002538	Ion transport	6811	ATP binding; metal ion binding; sodium:potassium-exchanging ATPase activity	5524; 46872; 5391	Integral component of membrane	16021	ATPase_P-typ_cation-transptr_C	0.230101467	-0.638080612	-2.119657913
L7M7P1	Glutamine synthetase	Unknown	Glutamine biosynthetic process	6542	ATP binding; glutamate-ammonia ligase activity	5524; 4356	Unknown	NA	glutamine synthetase family	0.224916641	-0.647978411	-2.152537688
A0A023FY19	Aconitate hydratase, mitochondrial	Similar to ISCW010818	Tricarboxylic acid cycle	6099	4 iron, 4 sulfur cluster binding; aconitate hydratase activity; metal ion binding	51539; 3994; 46872	Mitochondrion	5739	Acnase/IPM_dHydase_lsu_aba_1/3; Aconitase_4Fe-4S_BS	0.210219288	-0.67732744	-2.250033053
G3MNV3	Putative uncharacterized protein	Similar to ISCW017543	Translation	6412	Structural constituent of ribosome	3735	Ribosome	5840	Ribosomal_L10e/L16	0.205404792	-0.68738943	-2.283458259
A0A023FXS2	Putative phosphoglycerate mutase	Unknown	Glucose catabolic process	6007	Manganase ion binding; phosphoglycerate mutase activity	30145; 4619	Cytoplasm	5737	Alkaline_Pase-like_a/b/a; BPG-indep_PGM_N; Metalloenzyme; Pgm_bpd_ind	0.195057124	-0.709838183	-2.358031403
L7MD67	Putative glycine rich protein	Unknown	Unknown	NA	Unknown	NA	Unknown	NA	Mite_allergen_group-7	0.188525836	-0.724629125	-2.407165849
L7M8Y4	Malate dehydrogenase	Similar to ISCW003528	Carbohydrate metabolic process; malate metabolic process; tricarboxylic acid cycle	5975; 6108; 6099	L-malate dehydrogenase activity	30060	Unknown	NA	L-lactate/malate_DH	0.187101043	-0.727923792	-2.418110495
A0A023FEI8	Putative 60s ribosomal protein l14	Unknown	Translation	6412	Structural constituent of ribosome	3735	Ribosome	5840	Rib_L2_dom2	0.177787756	-0.750098152	-2.491772126
G3MKE7	Putative uncharacterized protein	Similar to ISCW014825, ISCW024529, ISCW024616, ISCW024039	Ribosome biogenesis	42254	Unknown	NA	Ribonucleoprotein complex	30529	L30e-like; Ribosomal_L7Ae/L30e/S12e/Gad45	0.176272309	-0.753815907	-2.50412224
B7Q368	High-density lipoprotein-binding protein, putative	IscW_ISCW008601	Metabolic process	8152	Hydrolase activity; RNA binding	16787; 3723	Unknown	NA	KH_dom	0.155776223	-0.807498829	-2.682453047

A0A023FJS3	Putative ribosomal protein	Similar to ISCW007478	Translation	6412	Structural constituent of ribosome	3735	Ribosome	5840	Ribos_L4_C_dom	0.145342749	-0.837606631	-2.782469001
V5HGA0	40S ribosomal protein S24	Similar to ISCW006068	Translation	6412	Nucleotide binding; Structural constituent of ribosome	166; 3735	Ribosome	5840	Nucleotide-bd_a/b_plait; Ribosomal_L23/L15e_core_dom	0.142903345	-0.844957604	-2.806888403
L7MEH0	Ribosomal protein L19	Similar to ISCW013810	Translation	6412	Structural constituent of ribosome	3735	Ribosome	5840	Ribosomal_L19/L19e	0.083475869	-1.07843905	-3.582496979

Supplementary Table 24. BLAST alignment of tick proteins against the human protein sequence used to produce polyclonal antibodies in mice.

The UniProtKB references for human proteins were retrieved from the Santa Cruz Biotechnology technical sheets of antibodies (Santa Cruz Biotechnology; https://www.scbt.com/). Data was analised with Blastp (NCBI, https://www.ncbi.nlm.nih.gov).

Putative tick protein and UniProtKB	Max Score	Total Score	Query Cover	E value	Per. Iden.	UniProtKB Human Proteins
Putative prohibitin-like protein (UniProtKB L7M5P4)	421	421	97%	$2e^{-154}$	63.99%	Q99623
cAMP-dependent protein kinase catalytic subunit isoform 2 (UniProtKB O97115)	609	609	96%	0.0	82.99%	P17612
Malate desidrogenase (UniProtKB L7M8Y4)	504	504	94%	0.0	73.60%	P40926

Supplementary Table 25. Concentration and purity of salivary gland DNA and protein extracted from *Rhipicephalus sanguineus* salivary glands during *Ehrlichia canis* infection.

Parameters measured by spectrophotometry with NanoDrop ND-1000 (ThermoFisher Scientific). Genomic DNA and protein was extracted from from three pools of ten SGs of ticks fed on a naïve dog (NI_1, NI_2 and NI_3) and from three pools of ten SGs of ticks fed on an *E. canis*-infected dog (I_1, I_2 and I_3).

Sample	**DNA Concentration (ηg/µl)**	**A_{260}/A_{280} racio**	**Protein Concentration (ηg/µl)**
NI_1	73.04	18.2	3.62
NI_2	105.94	1.87	3.22
NI_3	350.44	2.02	6.63
I_1	162.04	1.93	*
I_2	167.55	1.91	8.58
I_3	223.33	1.94	6.64

* Excluded sample because it was negative for the presence of *E. canis* DNA.

Supplementary Table 26. Concentration and purity of RNA extracted from IDE8 cells for *prohib* and *phsrp20* gene expression analysis.

Total RNA was extracted at time points (T1) – 48 h, (T2) – 120 h and (T3) – 160 h from cells inoculated with *prohib* or *phsrp20* dsRNA and with *β2m* dsRNA, as control. Parameters measured by spectrophotometry with NanoDrop ND-1000 (ThermoFisher Scientific).

	Sample number	**RNA Concentration (ηg/µl)**	**A_{260}/A_{280} racio**
T1	***prohib A1 1***	132.6	1.95
	prohib A1 2	132.55	1.82
	prohib A1 3	209.7	1.84
	prohib A1 4	51.72	2.06
	prohib B1 1	196.02	1.87
	prohib B1 2	86.37	1.84
	prohib B1 3	77.52	1.88
	prohib B1 4	101.04	1.75
	prohib C1 1	143.82	1.82
	prohib C1 2	151.92	1.78
	prohib C1 3	67.44	1.72
	prohib C1 4	58.77	1.79
	phsrp20 A1 1	253.61	1.92
	phsrp20 A1 2	102.5	1.78
	phsrp20 A1 3	215.96	1.98
	phsrp20 A1 4	81.25	1.82
	phsrp20 B1 1	85.28	1.83
	phsrp20 B1 2	173.86	1.89
	phsrp20 B1 3	97.5	1.91
	phsrp20 B1 4	85.17	1.79
	phsrp20 C1 1	102.06	1.82
	phsrp20 C1 2	37.7	1.82

	phsrp20 C1 3	85.45	1.88
	phsrp20 C1 4	107.92	1.86
T2	***prohib A2 1***	325.23	1.83
	prohib A2 2	138.21	1.81
	prohib A2 3	300.97	1.89
	prohib A2 4	308.21	1.89
	prohib B2 1	99.8	1.74
	prohib B2 2	209.86	1.8
	prohib B2 3	135.78	1.77
	prohib B2 4	304.33	1.96
	prohib C2 1	129.46	1.78
	prohib C2 2	134.78	1.77
	prohib C2 3	386.21	1.98
	prohib C2 4	169.31	1.77
	phsrp20 A2 1	280.11	1.96
	phsrp20 A2 2	226.02	2.03
	phsrp20 A2 3	363.92	2.03
	phsrp20 A2 4	402.87	2.04
	phsrp20 B2 1	177.89	1.92
	phsrp20 B2 2	198.92	1.93
	phsrp20 B2 3	362.65	2.12
	phsrp20 B2 4	163.87	1.87
	phsrp20 C2 1	411.46	2.06
	phsrp20 C2 2	215.06	1.93
	phsrp20 C2 3	155.06	1.93
	phsrp20 C2 4	385.28	2.06
T3	***prohib A3 1***	265.66	2.05

	prohib A3 2	137.68	1.82
	prohib A3 3	135.33	1.84
	prohib A3 4	142.95	1.85
	prohib B3 1	109.75	1.86
	prohib B3 2	30.88	1.72
	prohib B3 3	146.27	1.89
	prohib B3 4	6.96	2.39
	prohib C3 1	219.43	2
	prohib C3 2	25.27	1.72
	prohib C3 3	213.05	1.92
	prohib C3 4	76.13	1.82
	phsrp20 A3 1	312.61	2.03
	phsrp20 A3 2	59.96	1.79
	phsrp20 A3 3	126.27	1.9
	phsrp20 A3 4	187.61	1.9
	phsrp20 B3 1	277.07	2.05
	phsrp20 B3 2	101.05	1.83
	phsrp20 B3 3	186.63	1.92
	phsrp20 B3 4	231.18	1.97
	phsrp20 C3 1	48.24	1.81
	phsrp20 C3 2	273.35	2.01
	phsrp20 C3 3	213.94	1.97
	phsrp20 C3 4	237.58	1.97

Supplementary Table 27. Concentration of RNA extracted from *Rhipicephalus sanguineus* salivary glands for *prohib* and *phsrp20* gene expression analysis.

Total RNA was extracted from nymphs soaked in *prohib* or *phsrp20* dsRNA (*prohib* 1 to 12; *phsrp20* 1 to 12) and from nymphs soaked in PBS, as control (PBS 1 to 12). Parameters measured by spectrophotometry with NanoDrop ND-1000 (ThermoFisher Scientific).

Sample number	RNA Concentration (ηg/µl)
prohib 1	2.42
prohib 2	6.66
prohib 3	7.67
prohib 4	4.99
prohib 5	5.40
prohib 6	2.93
prohib 7	3.39
prohib 8	2.74
prohib 9	4.20
prohib 10	7.76
prohib 11	1.09
prohib 12	11.2
phsrp20 1	3.37
phsrp20 2	2.10
phsrp20 3	5.98
phsrp20 4	12.65
phsrp20 5	2.31
phsrp20 6	9.66
phsrp20 7	8.78
phsrp20 8	5.18
phsrp20 9	2.81
phsrp20 10	6.74

phsrp20 11	1.74
phsrp20 12	3.04
PBS 1	3.56
PBS 2	3.61
PBS 3	2.48
PBS 4	1.90
PBS 5	4.02
PBS 6	4.06
PBS 7	2.52
PBS 8	3.76
PBS 9	0.93
PBS 10	3.65
PBS 11	4.80
PBS 12	2.09